Iver Bakken Sperstad

Dissipative quantum phase transitions and high-temperature superconductors

Thesis for the degree of Philosophiae Doctor

Trondheim, September 2012

Norwegian University of Science and Technology
Faculty of Natural Sciences and Technology
Department of Physics

NTNU – Trondheim
Norwegian University of
Science and Technology

NTNU
Norwegian University of Science and Technology

Thesis for the degree of Philosophiae Doctor

Faculty of Natural Sciences and Technology
Department of Physics

ISBN 978-82-471-3760-4 (printed ver.)
ISBN 978-82-471-3761-1 (electronic ver.)
ISSN 1503-8181

Doctoral theses at NTNU, 2012:229

Printed by NTNU-trykk

Abstract

This thesis presents seven research papers on topics in condensed-matter theory. Five of the papers report on Monte Carlo studies of quantum phase transitions in various (d+1)-dimensional statistical mechanics models featuring Caldeira-Leggett-like dissipation. The principal motivation for these studies was to investigate a particular bond-dissipative (2+1)-dimensional XY model of circulating currents in cuprate high-temperature superconductors. It has been proposed that quantum critical fluctuations associated with a local quantum critical point described by this model can explain the marginal-Fermi-liquid behaviour of the normal state of these compounds. We present simulation results for this model for both compact and noncompact phase variables and show unambiguously that the quantum critical point in the compact case is not local. If the phases are taken to be noncompact variables, the model is also a model of resistively shunted Josephson junction arrays. The results in this case reveal a more complicated phase diagram, but we have not been able to establish critical behaviour consistent with the scenario of local quantum criticality.

The study of extended quantum dissipative models is also motivated by the general effect on condensed-matter systems of the coupling to environmental degrees of freedom. Their influence on quantum critical phenomena is characterized by the dynamical critical exponent z, a measure of spatiotemporal anisotropy, the value of which can be estimated by naive scaling arguments. We confirm by numerical means that such scaling estimates give correct results to a good approximations (with a few reservations), irrespective of system dimensionality, order parameter symmetry, or whether the variables are compact or noncompact. Corrections to the naive scaling estimates have to be invoked for strongly super-Ohmic dissipation for $d = 1$ due to relatively large values of the anomalous scaling dimension η.

The two last research papers are concerned with the superconducting pairing state of the recently discovered class of iron-based high-temperature superconductors. Here, we calculate possible signatures of the proposed $s_{\pm}$-wave pairing state in conductance-spectroscopy and Josephson-effect experiments.

Preface

This thesis is submitted as part of the requirements for the degree philosophiae doctor at the Norwegian University of Science and Technology (NTNU). The work has been performed at the Department of Physics, NTNU, under the supervision of Professor Asle Sudbø.

It is the conclusion of four years of work, starting August 2008, of which the equivalent of one year of full-time work was devoted to teaching duties and the equivalent of a half year of full-time study was devoted to coursework. The research has been funded by NTNU. All papers except paper VI and VII have also required extensive use of the supercomputing facilities at the University of Tromsø (`stallo`), supported through the Norwegian consortium for high-performance computing (NOTUR). Paper I to V were co-authored by Einar B. Stiansen and Asle Sudbø, and paper VI and VII were co-authored by Jacob Linder and Asle Sudbø.

Iver Bakken Sperstad,
Trondheim, May 2012

Acknowledgements

First and foremost, I would like to thank Professor Asle Sudbø for his supervision during these four years of PhD studies. Among his many qualities as a supervisor, I wish to point out his readiness to take off time to guide his students when lost and his tireless and enthusiastic pursuit of solutions to our problems.

I would also like to express my sincere gratitude to Professor Chandra M. Varma, Dr Flavio S. Nogueira, and Professor Jon Andreas Støvneng for their willingness to serve on the evaluation committee for this thesis as well as on my defence 12 September 2012.

Furthermore, I am grateful to Professor Jacob Linder for very fruitful collaboration and co-supervision on parts of this thesis work. The person I have worked most closely with these years is fellow PhD student Einar B. Stiansen, and I thank him for a most enjoyable collaboration and for sharing all his crazy ideas and listening to mine. Egil V. Herland is thanked for a great number of very useful discussions on physical problems in general and simulation techniques in particular. Einar and Egil are also acknowledged for providing feedback on parts of this thesis. Steinar Kragset gave me a much needed crash course in the practical aspects of Monte Carlo simulations the first month of my study, and I have also profited from continued use of some of his scripts. Lab tutoring has provided some variation from simulational labour, and I would like to thank fellow tutors, Professor Thor Bernt Melø, and all our undergraduate students for years of rewarding teaching duties. At the same time, I may also use this opportunity to thank all the great teachers I have been exposed to during some twenty years of schooling.

Finally, special mention must go to my parents and my sisters, and also to my grandparents, my uncle, and my aunts.

Iver Bakken Sperstad

List of papers

Paper I:
Iver Bakken Sperstad, Einar B. Stiansen, and Asle Sudbø:
Monte Carlo simulations of dissipative quantum Ising models,
Physical Review B **81**, 104302 (2010) [arXiv:1002.3369]

Paper II:
Iver Bakken Sperstad, Einar B. Stiansen, and Asle Sudbø:
Quantum criticality in spin chains with non-Ohmic dissipation,
Physical Review B **85**, 214302 (2012) [arXiv:1204.2538]

Paper III:
Einar B. Stiansen, Iver Bakken Sperstad, and Asle Sudbø:
Criticality of compact and noncompact quantum dissipative Z_4 models in (1+1) dimensions,
Physical Review B **83**, 115134 (2011) [arXiv:1105.0935]

Paper IV:
Iver Bakken Sperstad, Einar B. Stiansen, and Asle Sudbø:
Quantum criticality in a dissipative (2+1)-dimensional XY model of circulating currents in high-T_c cuprates,
Physical Review B **84**, 180503(R) (2011) [arXiv:1111.0629]

Paper V:
Einar B. Stiansen, Iver Bakken Sperstad, and Asle Sudbø:
Three distinct types of quantum phase transitions in a (2+1)-dimensional array of dissipative Josephson junctions,
Physical Review B **85**, 224531 (2012) [arXiv:1206.2928]

Paper VI:
Jacob Linder, Iver Bakken Sperstad, and Asle Sudbø:
0–π phase shifts in Josephson junctions as a signature for the $s_\pm$-wave pairing state,
Physical Review B **80**, 020503(R) (2009) [arXiv:0901.1895]

Paper VII:
Iver Bakken Sperstad, Jacob Linder, and Asle Sudbø:
Quantum transport in ballistic $s_\pm$-wave superconductors with interband coupling: conductance spectra, Josephson current, and crossed Andreev reflection,
Physical Review B **80**, 144507 (2009) [arXiv:0908.1384]

My contributions to the papers

In those papers where I am listed as the first author, namely paper I, II, IV, and VII, I have contributed substantially to all parts of the paper. That is, I wrote simulation code, carried out the majority of the simulations or calculations, wrote code for analysing the data and generating figures, was involved in interpreting the results, and contributed to all parts of the text.

I am listed as the second author in the remaining papers III, V, and VI. In paper III, I was responsible for the simulations for the compact model, corresponding to Sec. V. In paper VI, I was responsible for the calculations for the ballistic case, corresponding to Fig. 3. In all these papers, I was also involved in interpreting the results and writing the paper.

Contents

1 Introduction

To begin with a lofty and somewhat debatable assertion, the grand ambition of physics is to unify the multitude of apparently different phenomena observable in nature by a handful of basic principles. Although there is of course more to the science than this, this point of view may be particularly recognizable to those physicists doing research on *phase transitions*. Phases of various kinds abound in nature, from the more prosaic liquid and solid phases of water to highly abstract phases of elementary particle fields. A system passes a phase transition when tuned from one (disordered) phase to another (ordered) phase by decreasing (for instance) the temperature. If this passage from disorder to order happens smoothly, we call the transition point a *critical* point.[1] At the critical point, the system fluctuates wildly at all length scales, from the smallest to the very largest. One of the great insights of 20th century physics was that all critical points, although arising in very diverse systems, can be characterized by one of a small number of *universality classes*. The properties of each class describe the essence of how the phase transition happens when viewed on a macroscopic scale. Which universality class a particular transition belongs to does not depend on the microscopic description, the nature of the adjoining phases or whether the transition happens at high or low temperatures and so on, but only on a few key attributes such as the symmetry and dimensionality of the system. One way to understand this is to realize that the characteristic length scale of the fluctuations of the system has to grow to infinity at the transition point, effectively averaging out all the microscopic details.

Several other parameters than temperature may determine where in the phase diagram a system is found, and tuning these other parameters may drive down the critical temperature to lower values, as illustrated in Fig. 1.1. The point in the phase diagram where such a line of critical points hits zero temperature is called a *quantum critical point* (QCP). This name comes from the fact that there can be no thermal fluctuations at $T = 0$, and so only quantum fluctuations can drive a zero-temperature phase transition (which unsurprisingly also goes by the name of a *quantum phase transition*). Although this QCP may itself be inaccessible to experiments, it makes its presence felt in a *quantum critical region* spreading like a fan

[1] This – and most of what else is written in this chapter – could certainly be put in more precise and technical terms. We have, however, chosen to keep this introductory chapter at a very basic level, hoping to make it (almost) comprehensible also for the occasional non-physicist. Neither do we want to overburden it with the required footnotes and references, so we simply have to refer to later chapters for the details.

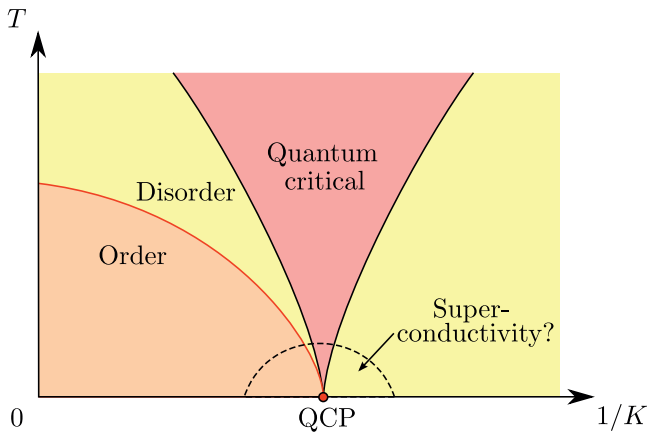

Figure 1.1: The anatomy of a quantum phase transition: A critical line (red curve) separating an ordered from a disordered phase at finite temperatures terminates in a quantum critical point (QCP) at zero temperature, $T = 0$. Going to the right along the x axis corresponds to increasing the strength of quantum fluctuations, and increasing the coupling parameter K suppresses these fluctuations. The quantum critical region is found at finite temperatures above the QCP. The dashed dome around the QCP speculatively indicates the possibility of a phase with superconducting pairing arising from the quantum critical fluctuations.

at higher temperatures above the QCP. This is the region where finite-temperature remnants of quantum critical fluctuations determine the frequency-dependent properties of the system. Precisely this kind of behaviour seems to be in force in several classes of unconventional superconductors, above the transition temperature below which superconductivity sets in. A quantum critical point hiding inside the superconducting part of the phase diagram may thus serve as a unifying concept across a wide range of different superconducting materials, and might also hint towards a common pairing mechanism responsible for these superconducting states.

One of the non-thermal coupling parameters that may drive the system through a quantum phase transition by suppressing quantum fluctuations is the coupling between the system and its environment. A quantum system is never in complete isolation, and the environment may induce *dissipation*, or damping, of the quantum motion. In popular terms, those parts of the universe that are left out when defining the system reduce the quantumness of the system by continuously measuring it. The general effect of this is to reduce the critical fluctuations in time relative to those in space. This destroys the symmetry between space and time that might otherwise be present at the quantum critical point, and this space-time anisotropy changes the universality class of the phase transition. It has been argued that dissipation in some cases even may lead to *local quantum criticality*, meaning that the anisotropy is infinite and spatial sites fluctuate in time as if they were completely decoupled from their neighbours. Such curious fluctuations may actually be relevant to the problem of unconventional superconductors. In fact, precisely this kind of dissipation-driven local quantum phase transition has been proposed as a prerequisite for explaining

the phase diagram of high-temperature cuprate superconductors [1], which is the class of superconductors that can attain the highest transition temperatures. To be a little more concrete, this is a model of microscopic current loops circulating inside each unit cell of these materials, and a particular form of dissipation of bond variables is an essential ingredient to the model.

In papers I to V of this thesis, we study models in quantum statistical mechanics with dissipation. The motivation for this study is twofold: We will try to detect local quantum criticality in models of superconducting systems where this phenomenon has been proposed to occur, and we also aim to increase our understanding of how dissipation affects quantum criticality in general. In paper I, we first show as a proof of principle that space-time anisotropy essentially does not depend on dimensionality but does depend on whether the environment couples to sites or bonds in the system. In paper II, this study is extended to determine how the universality class depends on the effectiveness of the dissipation and on system symmetry. We take a step closer to the model of Ref. [1] in paper III by investigating how criticality in a related model depends on whether the system variables are defined on a circle or along a line. The actual model believed to represent the one proposed in Ref. [1] is studied in paper IV, and it is shown *not* to exhibit local quantum criticality. In paper V, we turn to a model of arrays of weak links between superconducting elements (Josephson junctions) shunted by normal-metal resistors. This can also be regarded as an alternative interpretation of the model of circulating currents in cuprates in the case that one does not allow the system variables to be defined on a circle.

The topic of papers VI and VII is somewhat less strongly related to the themes presented above, as these papers deal with ways of probing the nature of the superconducting state in the recently discovered class of iron-based high-temperature superconductors.

The above seven papers form the second part of the thesis, whereas the first part is an introduction intended to provide the background necessary to understand topics covered in the papers. In Ch. 2 we give a brief survey of the physics of the superconducting systems that have motivated this thesis work. Here, we also mention concepts relevant to papers VI and VII for describing charge transport in such systems. In Ch. 3 we turn from concrete physical systems to more general theory of phase transitions in classical and quantum systems, and we also describe some of the basic building blocks of the models encountered later in the thesis. Dissipation is introduced and added to these models in Ch. 4, and we describe the dissipative model of circulating currents in cuprate superconductors.[2] The Monte Carlo simulation techniques used to investigate dissipative quantum phase transitions are described in Ch. 5. Finally, in Ch. 6 we state precisely the models we have studied, summarize our results, and discuss some central issues.

[2]Here we formulate this part of the motivation for our work in more precise – but also more technical – terms, and the reader that needs no introduction to the basic concepts involved may skip to Sec. 4.5.

2 Superconducting systems

The work reported in this thesis has to a large extent been motivated by physical properties of superconducting systems, and it is therefore appropriate to start by introducing the systems in question. In particular, we are interested in high-temperature cuprate and iron-based superconductors, and will in this chapter highlight those aspects of the phenomenology of these compounds that will be relevant in the later parts of the thesis. We also provide some background to the question of how to characterize the superconducting state of iron-based superconductors that is addressed in papers VI and VII. Most concepts will be treated relatively superficially and from a physical point of view, focusing on relevant experiments.

2.1 Superconductors

The variation in material properties we observe in everyday life, at comparably elevated temperatures, is nothing compared to the exotica found as one reduces the temperature and allows quantum effects to take hold. Superconductivity has a unique and senior position among these exciting quantum states of matter, as the centenary of its discovery was celebrated last year. This phenomenon can be described in several ways, depending on the point of view one chooses. For our purposes, we will first describe it as electrons collectively forming a single, coherent quantum state, characterized by a macroscopic quantum wave function $\psi(\mathbf{r}) = |\psi(\mathbf{r})|e^{i\theta(\mathbf{r})}$. The quantum phase of this wave function forms a *compact* phase field $\theta(\mathbf{r})$, meaning that the phase is only defined on the interval $\theta \in [0, 2\pi\rangle$; a quantum state described by the phase field $\theta(\mathbf{r})$ is indistinguishable from a state with phase field $\theta(\mathbf{r}) + 2\pi$. At the transition to a superconducting state of matter, the $U(1)$ rotational symmetry of the phase θ is broken, establishing coherence of the phase field. Phase coherence does not necessarily mean that $\theta(\mathbf{r})$ is everywhere constant, and smooth variations over macroscopic length scales are allowed. Following such variations are electric currents that do not dissipate energy – supercurrents – with direction and magnitude given by the phase gradient $\nabla\theta$.

Superconductors can also be described as a phase coherent condensate of Cooper pairs, that is, of electron pairs in momentum space. This pairing is typically viewed as being mediated by some fluctuating bosonic field, and a *conventional* superconductor can be defined as one where the pairing is mediated by phonons [2]. In the

conventional picture, the superconducting state arises from a *Fermi liquid*. This is a system of interacting electrons (fermions) with well-defined quasiparticles, meaning that the low-energy excitations of the system retain some of their electron-like character [3]. Well-defined quasiparticle peaks at the Fermi level in the single-particle excitation spectrum lead to a distinct Fermi surface, and the sharpness of these features are quantified by the *quasiparticle weight*. At the onset of superconductivity, an energy gap Δ in the single-particle excitation spectrum opens at the Fermi surface due to Cooper pairing. This gives yet another way to describe superconductivity, and the *gap function* $\Delta(\mathbf{k})$ along the Fermi surface can be used to characterize the pairing state. Conventional superconductors have an s-wave pairing state, meaning that the gap function is invariant under $\pi/2$ rotations in momentum space and therefore essentially isotropic, assuming an underlying square lattice. A d-wave state, on the other hand, is symmetric with respect to π rotations but antisymmetric with respect to $\pi/2$ rotations.

2.2 High-temperature superconductors

By high-temperature superconductors we mean the classes of unconventional superconductors with higher values of the critical temperature T_c than what is (usually) allowed by conventional, phonon-based pairing mechanisms. For the first two decades after their discovery in 1986, the term was synonymous with the cuprates, compounds distinguished by their CuO_2 layers containing one copper atom and two oxygen atom per unit cell. In early 2008, however, a different class of high-temperature superconductors was discovered, this time based around iron atoms. Also these are layered compounds, with the iron atoms residing in puckered layers shared typically by arsenic atoms. Upon *doping* these material classes, in other words introducing additional charge carriers,[1] a superconducting phase will eventually arise, and it is widely believed in both cases that the mechanism of this superconductivity is intrinsically linked to the copper- [4] or iron-based [5] layers. The maximal temperature for onset of superconductivity does however depend on the composition of the interstitial layers, as well as other details, with the record at present lying at $T_c \approx 135$ K for cuprates and $T_c = 56$ K for iron-based superconductors [6]. It is well established that the pairing symmetry of this superconducting state is d wave in the cuprates. Despite the commonality of the two material classes, this pairing symmetry is not a universal property of high-T_c superconductors, and a form of s-wave pairing now seems to be favoured for the iron-based materials. The nature of this pairing state is the main concern of this thesis work for the iron-based case, as will be explained in Sec. 2.4. For the cuprate case, what we are interested in is the phase diagram, which is described below.

[1] This is a simplification, especially for the iron-based materials, but we will not enter into the details of how the various materials are doped.

2.2.1 Cuprate high-T_c superconductors

Figure 2.1 shows the universal topology of the phase diagram of hole-doped cuprates [2, 7, 8, 9]. Starting at zero doping and low temperatures, the system is a strongly correlated insulating antiferromagnet (AF) where neighbouring Cu spins are oppositely aligned. Doping the system leads to destruction of the AF order, and, for sufficiently low temperatures, the subsequent onset of the superconducting state.

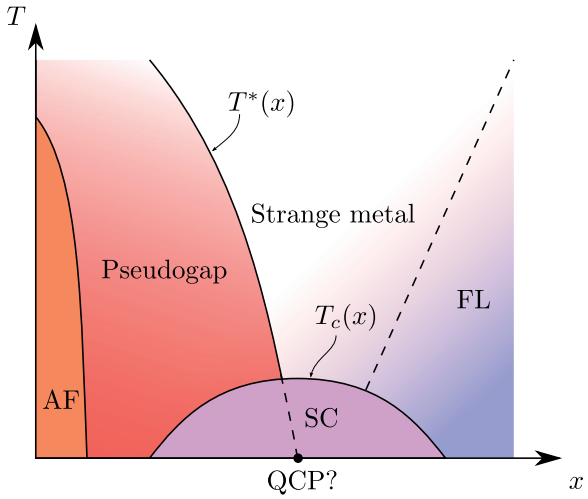

Figure 2.1: Schematic phase diagram of cuprate superconductors in the space of hole doping x and temperature T. AF denotes the antiferromagnetic phase, and SC and FL are abbreviations of supercondictivity and Fermi liquid, respectively. (The above cartoon is what appears to be the canonical version of the phase diagram. If we had considered it expedient – which we certainly do not – we could also include in the phase diagram almost any other kind of transition and crossover line imaginable for a condensed-matter system [10].)

The critical temperature reaches a maximum as a function of doping at the so-called *optimal* doping, and the regions to the left and to the right in the phase diagram are referred to as *underdoped* and *overdoped*, respectively. When taking the system further to the overdoped side, the superconducting state eventually gives way to a normal state well described by Landau's Fermi-liquid theory. For higher temperatures there is a crossover from this FL region – with the resistivity characteristically going as T^2 – to a region with the resistivity being linear in T. This normal-state region above optimal doping is often called the *strange metal* phase, and the name is justified by the observation of anomalous behaviour in all transport properties. The thermodynamic properties, on the other hand, are more similar to those of a Fermi liquid. This metallic state also seems to have a Fermi surface, but it turns out to be "marginal" in the sense that the quasiparticle weight goes to zero logarithmically – in other words as slowly as it possibly can – as the excitation energy approaches zero. It was against this backdrop that Varma et al. in 1989 characterized the strange metal phase as a *marginal Fermi liquid* (MFL) [11], postulating a fluctuation spectrum that could explain the transport experiments and possibly

also superconductivity at lower temperatures. The possible origin of the bosonic excitations giving rise to such a spectrum is discussed in Sec. 2.2.2 and Sec. 4.5, but here we will just state – for later reference – the postulated MFL fluctuation spectrum as a function of momentum $\mathbf{q}$, frequency $\omega(>0)$ and temperature T:

$$\text{Im}\,\chi(\mathbf{q},\omega,T) \propto \begin{cases} \omega/T & \text{for } \omega \ll T, \\ \text{const.} & \text{for } \omega \gg T. \end{cases} \tag{2.1}$$

Moving towards the underdoped side and decreasing temperature from the strange metal phase, the material loses its last remnants of Fermi-liquid-like properties. However, it does so long before reaching a superconducting or antiferromagnetic state. The *pseudogap* phase below a temperature $T^*(x)$ was first discovered as a loss of low-energy density of states in the spin susceptibility [12], and it was later verified that this was caused by a genuine energy gap at the Fermi level [7]. There are traditionally two lines of thought regarding the origin of this gap. One is that it is associated with a precursor state of superconductivity where Cooper pairs are formed but do not have global phase coherence. Alternatively, it could be associated with another form of order that is distinct from (and possibly competing with) superconductivity. Within this second approach, there is a number of different subclasses of theories and scenarios. To avoid the risk of getting lost in this zoo of prospective competing, hidden or fluctuating forms of order, we will here restrict ourselves to the one proposal that has direct relevance to our work.

Doing so, we first take for granted that there is a pseudogap energy scale $\propto T^*(x)$ that crosses the superconducting dome $T_c(x)$ and goes to zero somewhere around optimal doping. There is ample evidence to support such a supposition [7, 13], and it indicates that something else than superconducting fluctuations is (also) at play. If the pseudogap line $T^*(x)$ also is a genuine phase transition line, it is likely that it terminates at $T = 0$ in a quantum critical point around optimal doping, just as in the phase diagram in Fig. 1.1. This is a very attractive scenario from the point of view of the strange metal phase, which bears many of the hallmarks of a quantum critical region above a quantum critical point [9, 14]. This could also explain the superconducting pairing in terms of quantum critical fluctuations, and such an explanation may at least be very plausible in other unconventional superconductors [2].

If the pseudogap line marks the onset of some sort of long-range order, it has to be of a rather subtle kind. One reason is that none of the usual telltale signs of a phase transition, such as a peak in the specific heat, is visible at the transition point. Another is that most candidates for the hidden pseudogap order have ordering wave vectors $\mathbf{q} \neq (0,0)$. This would result in a reconstruction of the Fermi surface and the appearance of additional Fermi pockets. This has not been unambiguously demonstrated in the pseudogap phase.[2]

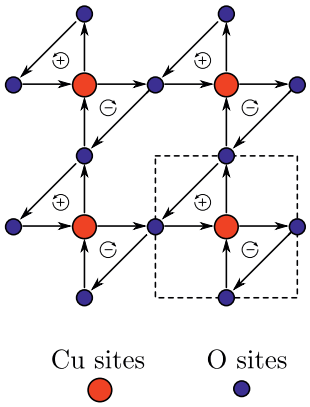

Figure 2.2: Illustration of the circulating-current pattern described in the text. One CuO_2 unit cell is indicated by the dashed square, and the plus and minus signs indicate the magnetic moments due to the current loops. The figure shows one of four possible ordered states, and the three other are obtained through $\pi/2$ rotations of the pattern of each unit cell.

2.2.2 Circulating currents in high-T_c cuprates

One proposal of a hidden pseudogap order conforming with the considerations above is the theory of circulating currents by Varma [9, 18]. These currents – also referred to as orbital currents or loop currents – are currents flowing within each unit cell of the CuO_2 layers. Figure 2.2 illustrates one of four possible ordered states within the pseudogap phase, and the quantum critical fluctuations in the strange metal phase are assumed to be fluctuations within each unit cell between the four possible patterns. Each ordered state respects translational symmetry, the ordering wave vector being $\mathbf{q} = (0, 0)$, but breaks time-reversal symmetry and fourfold rotational symmetry.

What sets the circulating-current order of Varma apart from other candidates for a hidden order are the direct experimental signatures of the onset of similar magnetic order for temperatures consistent with T^* [19]. The first indications were given by the detection by angle-resolved photoemission spectroscopy of spontaneous breaking of time-reversal symmetry as the temperature was lowered below T^* [20]. These results are, however, somewhat controversial, and other studies have reached the opposite conclusion [21, 22]. More direct evidence appeared in 2006, when polarized neutron diffraction was used to demonstrate magnetic long-range order respecting the symmetries of the model. Later studies confirmed the finding in the same [23] and other [24, 25] cuprate compounds, and collective magnetic modes agreeing with circulating-current order have also been discovered [26, 27]. Other recent experiments measuring the magneto-optic Kerr effect [28, 29] and the magnetic susceptibility [30] also substantiate this picture of spontaneously broken symmetries in the pseudogap phase. We should nevertheless mention that there are studies using muon

[2]See, however, Refs. [15, 16, 17] for a different point of view.

spin relaxation [31, 32, 33] and nuclear magnetic resonance [34, 35] that find no evidence of magnetic order consistent with circulating currents. Finally, also numerical experiments disagree on the presence or absence of circulating currents in cuprates; a variational Monte Carlo investigation supports that similar states can be stable in these materials [36], whereas exact-diagonalization studies do not [37, 38].

The circulating-current model will be discussed from a more theoretical point of view in Sec. 4.5, where we also introduce the concrete statistical mechanics model we have been studying and explain its possible connection to a QCP at optimal doping and the MFL fluctuation spectrum (2.1).

2.2.3 Iron-based high-T_c superconductors

Describing the phase diagram of iron-based superconductors is done most easily by comparing it to the cuprate phase diagram described in Sec. 2.2.1. We have to say from the start, however, that the degree of universality in the iron-based case is less than for the cuprate phase diagram. What follows will therefore be valid for a large portion of the iron-based superconductors, but not for all.

Just as for the cuprates, the undoped parent compounds of iron-based superconductors have a form of antiferromagnetic order. Although these materials are certainly not good metals, the ground state in this case is not insulating, and correlations are weaker than in the cuprates [39]. Magnetic order is again suppressed for increasing doping, but not as abruptly as in the cuprates, and when superconductivity arises, the two orders in several cases coexist before the magnetic ordering temperature is at last driven to zero [6]. The possible existence of a quantum critical point also beneath the superconducting dome of iron-based materials makes it plausible that quantum criticality is somehow responsible for superconductivity [5]. The potential importance of quantum criticality is also underlined by the observation of linear-in-T resistivity in the normal-state region at optimal doping [40]. There have been observations of a pseudogap also for underdoped iron-based superconductors [41, 42], although there does not seem to be a prominent pseudogap phase such as in the cuprates [43].

When discussing the nature of the pairing state of iron-based superconductors, it is necessary to describe the Fermi surface. In contrast to the single, large, hole-like Fermi surface of the cuprates, the iron-based materials usually have four smaller, distinct Fermi pockets. Their position in the Brillouin zone is illustrated in Fig. 2.3. The two pockets around the zone centre are hole-like and the two along the edges are electron-like, and all are gapped in the superconducting phase. Although all gaps close at the same critical temperature, their magnitudes are in general different [44]. The favoured pairing state is called $s_\pm$ wave, which means that, while the overall symmetry of the state is s wave, the gap function has opposite signs on the electron- and hole-like Fermi surfaces.[3] Other candidate states that have been investigated are d wave and non-sign-changing s wave (which we will refer to as s_{++} wave). In

[3] Interestingly, the same kind of sign-shifted s-wave order parameter has previously also been proposed for the cuprates [45].

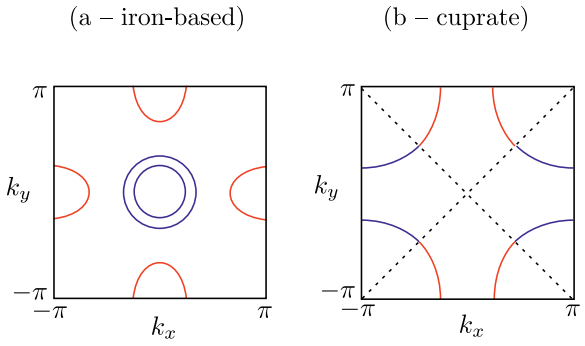

Figure 2.3: Schematic of the Fermi surface of iron-based (a) and cuprate (b) superconductors. The relative sign of the gap function is also illustrated, with blue indicating plus and red indicating minus. An $s_{\pm}$-wave state is assumed for the iron-based case and a d-wave gap in the cuprate case (with the line nodes indicated by dashed lines). The representation in (a) corresponds to a unit cell containing a single iron atom, and the hole-like Fermi pockets are found at the zone centre and the electron-like pockets at the edges.

contrast to d wave, an s-wave symmetry does not enforce nodes on the Fermi surface where the gap function goes to zero. We return to the issue of possible pairing states in Sec. 2.4.[4]

2.3 Josephson junctions

When a superconducting system is separated in two distinct parts by a so-called weak link, we call the system a *Josephson junction*. On each side of junction, we will assume that the superconducting phase takes the constant values θ_1 and θ_2, respectively. Given that this weak link is strong enough to allow tunnelling of Cooper pairs, there may still exist phase coherence across the composite superconducting system even though the phase in the junction region itself is not well defined. Introducing discreteness to the system in this manner implies that the gradient expression $I \propto \nabla\theta$ valid for a continuous superconductor may no longer apply. On the other

[4]This thesis is not really concerned with what pairing mechanisms could possibly bring about candidate pairing states of iron-based superconductors, but we want to mention that a scenario based on AF spin fluctuations is popular [46, 47, 43]. At wave vectors $\mathbf{q} = (0,\pi),(\pi,0)$, these fluctuations connect hole and electron pockets (see Fig. 2.3) and may generate a gap function with opposite sign, in accordance with the $s_{\pm}$-wave state. A similar effect may also take place for the cuprate Fermi surface if one instead assumes a spin-fluctuation wave vector $\mathbf{q} = (\pi,\pi)$. The wave vectors in both cases are the ordering wave vectors of the corresponding AF phase. Due to the proximity to these AF phases, such a spin-fluctuation scenario for superconducting pairing is often pointed out as a possible unifying feature of unconventional superconductors [43, 48]. We should hasten to emphasize that there are by no means consensus on the pairing mechanism in cuprate superconductors, and the theories we are concerned with in this thesis have a very different starting point.

hand, approximating the gradient with the discrete phase difference $\Delta\theta = \theta_1 - \theta_2$ would not work either: Because each of the phases $\theta_{1,2}$ is defined modulo 2π, it only makes physical sense to consider phase differences $\Delta\theta$ defined on the interval $[-\pi, \pi\rangle$. The natural solution [49] then is to introduce a 2π-periodic function so that the current across the junction is given by

$$I = I_c \sin(\Delta\theta), \tag{2.2}$$

for which the gradient expression is a good approximation for small $\Delta\theta$. Equation (2.2) is the sinusoidal current-phase relation usually associated with Josephson junctions. As we force an increasing current I through the junction, the phase difference $\Delta\theta$ adjusts to accommodate it. There is no voltage drop across the junction until the critical current $I = I_c$ is reached at $\Delta\theta = \pi/2$. Increasing the current further at this point, a voltage difference V appears, and the current is no longer dissipationless. Equation (2.2) is called the first Josephson relation; the second Josephson relation relates the voltage drop V to the time evolution of the phase difference:

$$\frac{\partial \Delta\theta}{\partial t} = 2eV. \tag{2.3}$$

(Here and in the rest of the thesis, we are using units such that $\hbar = 1$.)

The sinusoidal current-phase relation (2.2) is often a very good approximation, but it is far from being the only possibility [50]. A slightly less heuristic approach to the general current-phase relation starts by finding the energy E associated with the junction as a function of the phase difference across it. We again assume that this energy has to be invariant under 2π translations of the phase difference, and also that it is invariant when interchanging θ_1 and θ_2 [51]. Under these conditions, an arbitrary energy function can be expanded as the Fourier series

$$E(\Delta\theta) = \sum_{n=1}^{\infty} E_n \cos(n\Delta\theta). \tag{2.4}$$

Assuming that higher-order components $n > 1$ can be neglected, we have the *Josephson potential* on the form [50]

$$E(\Delta\theta) = \frac{I_c}{2e}\left[1 - \cos(\Delta\theta)\right]. \tag{2.5}$$

Note that the ground-state phase difference is $\Delta\theta = 0$. Using next that the number of Cooper pairs and the phase of their wave function are canonical conjugate variables, the (Cooper pair) current can be found through the Hamiltonian equations as [49]

$$I = 2e\frac{\partial E}{\partial(\Delta\theta)}. \tag{2.6}$$

Inserting the standard Josephson potential of Eq. (2.5) then results in the standard sinusoidal current-phase relation (2.2).

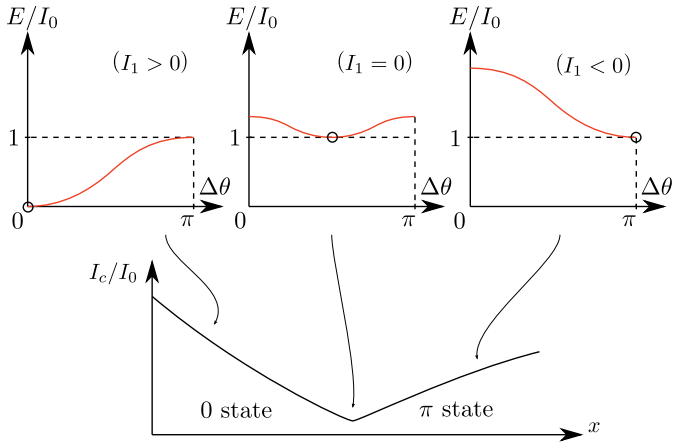

Figure 2.4: Illustration of a 0–π transition of the Josephson current as a function of some parameter x (below). The energy dispersion of the junction as a function of the phase difference, Eq. (2.7), is sketched (above) for three values of x. For small x, the first-harmonic component to the Josephson current is positive and dominant, and the ground state of the junction is at $\Delta\theta = 0$. (We have used $I_1 = I_0$, $I_2 = 0$ for simplicity.) For a certain value of x, I_1 goes to zero, and the second-harmonic component is dominant. Around this point, the ground-state phase difference may take some arbitrary value φ. For large values of x, the first-harmonic component is negative and dominant, and the ground-state phase difference is $\Delta\theta = \pi$. (Here, $I_1 = -I_0$, $I_2 = 0$.) The ground state is indicated by a black circle for each of the cases.

2.3.1 0–π transitions

We now expand the Josephson energy potential (2.4) to higher orders and write the result as

$$E(\Delta\theta) = \frac{1}{2e}\left[I_0 - I_1\cos(\Delta\theta) + \frac{I_2}{2}\cos(2\Delta\theta)\right]. \tag{2.7}$$

The current-phase relation then becomes

$$I(\Delta\theta) = I_1\sin(\Delta\theta) - I_2\sin(2\Delta\theta), \tag{2.8}$$

including a second-harmonic component $\propto I_2$ to the Josephson current. The prefactors I_1 and I_2 in general depend on various junction parameters, and the conventional case is that $I_1 > 0$ and $I_1 \gg I_2$. If we assume that there is a junction parameter x such that I_1 decreases and I_2 remains largely unchanged as x is increased, we can make the second-harmonic component dominate by tuning x. Imagining that we drive a current through the junction and measure the critical current I_c as we tune x, I_c will decrease until we reach the point where $I_1 = 0$. Increasing x further drives I_1 negative, and the critical current begins to increase again.[5] This is the signature of a *0–π transition*. This name follows from the change in the ground-state phase difference of the Josephson junction; for small x the junction is in the conventional

[5]Recall that we are imagining a current-biased experiment, so $\Delta\theta$ always adjusts to the value sustaining the largest current $I > 0$ as $I \to I_c$. In general, this value does not equal $\pi/2$ when $I_2 \neq 0$ or $I_1 < 0$.

0 state with equilibrium phase difference $\Delta\theta = 0$, whereas for large x the junction is in a π state with equilibrium phase difference $\Delta\theta = \pi$. For a small region around the transition point, the junction may be in a φ state corresponding to some intermediate ground-state phase difference $\Delta\theta = \varphi$. The transition is illustrated in Fig. 2.4.

The phenomenon of 0–π transitions is well known both theoretically [52] and experimentally [53] for Josephson junctions containing a ferromagnetic interlayer [52], where the transition point can be accessed both by tuning the temperature and the width of the interlayer. We discuss in paper VI and VII how it may also be relevant in the context of iron-based superconductors as a possible signature of an $s_{\pm}$-wave pairing state.

2.3.2 Josephson junction arrays

Arrays of Josephson junctions occur naturally for instance in granular superconducting systems, and they can also be manufactured artificially. Putting identical Josephson junctions in sequence on a regular 1D or 2D grid allows experimental control over the relative effect of quantum fluctuations in superconducting systems. One can also add metallic shunts in parallel to the junctions, thus coupling the system to a metallic environment and introducing dissipation. We will introduce models of such dissipative systems in Sec. 4.4.2, but mention here that resistively shunted Josephson junction arrays have been studied experimentally both in one [54, 55] and two [56, 57] dimensions. Experiments have also considered dissipative quantum phase transitions in a single Josephson junction [58].

2.3.3 Other superconducting heterostructures

If one replaces one of the superconductors (S) in a Josephson junction by a normal metal (N), one gets an NS junction. Conductance spectroscopy experiments can then be performed on such heterostructures by applying a voltage difference and measuring the current. In the case of a strong barrier, the tunnelling spectra essentially measure the superconducting density of states. For weaker tunnelling barriers, the technique is often referred to as (point-contact) Andreev reflection (PCAR) spectroscopy [44]. An *Andreev reflection* is a process by which an electron from the N side is reflected *as a hole* at the NS interface, creating a Cooper pair inside the S region. Such reflection processes can give rise to resonant surface states, so-called Andreev bound states (ABS), for certain electron energies [59].

Another important superconducting structure is the superconducting quantum interference device, or SQUID [49]. A SQUID is formed by inserting either one or two Josephson junctions in a superconducting loop. The magnetic flux allowed through the loop is quantized, making it possible to trap a number of flux quanta and study it as a macroscopic (quantum) variable. For more practical purposes, we mention that in the case of two Josephson junctions, the energy and critical current of the composite system will be periodic functions of the applied magnetic flux.

2.4 Probing the pairing state of iron-based superconductors

In this thesis, we emphatically do not take any position on the issue of what the pairing mechanism might possibly be in iron-based superconductors, only how one may identify whatever pairing state it is this mechanism produces. To be specific, we define the problem as how to distinguish an $s_{\pm}$-wave state from an s_{++}-wave state.

Early experiments on iron-based superconductors painted a rather confused picture of the gap structure. Thermal measurements that essentially probe the existence of nodes in the gap function produced results both in agreement and disagreement with nodal gaps [60, 5]. Nodal behaviour would be consistent with d-wave symmetry, but can also be explained by s-wave symmetry if the gap function has deep minima or accidental nodes not enforced by the pairing symmetry [61]. Results were similarly inconsistent in the case of PCAR experiments [44]. In some cases zero-bias conductance peaks were observed that would indicate resonant transport through an Andreev bound state at zero energy. Such an ABS is typically taken as a signature of d-wave symmetry [62, 59]. To complicate matters further, there were also predictions of ABSs for the $s_{\pm}$-wave state both at zero and finite (sub-gap) energies. (See Ref. [10] in paper VI for references.) A possibly very important requirement for such signatures is a significant value of the interband coupling between Fermi pockets hosting gaps with opposite signs.

We do not consider the possibility of a d-wave pairing state in this thesis. Although one cannot say that d-wave symmetry in iron-based superconductors is universally ruled out by experiments, there is now good evidence for s-wave symmetry as a general rule. For instance, recent PCAR experiments mostly point to nodeless gaps [44], and d-wave symmetry would be unable to explain the observation of a z-axis Josephson effect [63]. Apart from being theoretically well supported [46, 47, 61], also experimental support has been accumulating the last years for an s-wave order parameter with sign shifts. In particular, Ref. [64] inferred the existence of π junctions among the many grain-boundary Josephson junctions of a polycrystalline sample. The $s_{\pm}$-wave pairing state also seems to be supported by neutron scattering experiments [65] and in quasiparticle interference studies of scanning tunnelling spectra [66].

Although it is now well established that cuprate superconductors universally have d-wave pairing symmetry, this was not demonstrated explicitly by a *phase-sensitive* experiment until the mid-nineties [67]. A phase-sensitive probe of the gap function is an experimental technique that is able to measure the phase of the gap function, that is, its sign if it has no imaginary component. In contrast, most of the experiments mentioned above measure only the magnitude of the gap function. A directly phase-sensitive experiment was possible for the d-wave symmetry of the cuprates because the gap function changes sign when probed at angles shifted by $\pi/2$ in momentum space, as can be seen from the right panel of Fig. 2.3. This was utilized in a corner SQUID setup formed by a cuprate (d-wave) superconductor and an s-wave superconductor. To perform a similar experiment to probe directly the phase of the gap function of iron-based superconductors would be highly desirable. The left

panel shows why such an experiment would unfortunately not differentiate an $s_{\pm}$-wave state from an s_{++}-wave state: The phase of the gap function is essentially isotropic in momentum space for both cases.

A substantial number of possible alternative phase-sensitive probes of the pairing state had already been proposed at the time of writing papers VI and VII, and for these we simply refer to the references of paper VII. An overview of selected suggestions can also be found in Refs. [60] and [61], and Ref. [68] reviews both proposed and performed experiments on iron-based superconductors involving the Josephson effect.

2.4.1 Theoretical approaches to quantum transport

We end this chapter with a very short introduction to the methods used in papers VI and VII to study the effect of the sign structure of the superconducting order parameter. In these papers, we consider conductance spectroscopy and the Josephson effect as possible order parameter probes.

When studying quantum transport, it is useful to first make the distinction between clean and dirty systems, or equivalently, between ballistic and diffusive transport. In ballistic transport theory, one may assume that the particles travel along straight lines, scattered only at the interfaces of the heterostructure in question. Diffusive transport theory, on the other hand, takes into account an (assumed) large density of impurities within the material, the scattering on which makes the particle paths appear as biased random walks. The theoretical tool of choice for this latter limit is the Usadel equation [69], but we will focus on a popular approach for the ballistic case, namely the *BTK* formalism [70]. Named after Blonder, Tinkham and Klapwijk, this theory essentially reduces the transport problem in superconducting heterostructures to a matter of calculating reflection and transmission coefficients at the interfaces for electron- and hole-like plane waves. Applied to an NS junction, one finds the conductance as the sum of contributions from Andreev reflection and electron tunnelling. Applied to a Josephson junction, one calculates the resonance energies corresponding to Andreev bound states carrying the current across the weak link. Approximating the energy $E(\Delta\theta)$ of the junction with the sum of ABS energies, one can then find the current-phase relation $I(\Delta\theta)$ by differentiation as in Eq. (2.6) [71].

3 Phase transitions and quantum criticality

The phase transitions that are the primary motivation of our work are invariably *quantum* phase transitions. Large portions of this chapter will nevertheless deal with principles and concrete examples of classical phase transitions, before introducing their quantum counterparts. The reason for this is that most quantum phase transitions we are interested in can be reformulated as a classical phase transition by the use of the so-called quantum-to-classical mapping. This allows us to recycle the entire apparatus of concepts developed to describe the classical transitions. For the more basic concepts covered in this chapter, we refer to textbooks such as Refs. [72], [73] and [74].

3.1 Statistical mechanics

In order to establish notation and terminology used later in this thesis, we will recapitulate some basic concepts of classical statistical mechanics. Most systems we will consider in this thesis will be described by such degrees of freedom that they can be regarded as spin models defined on d-dimensional hypercubic lattices. A general spin degree of freedom will be denoted by $\mathbf{s}$. This spin can for the most part be viewed as a unit vector living in a two-dimensional space, so we write $\mathbf{s} = (s_x, s_y) = (\cos\theta, \sin\theta)$. The allowed values of the angle (or phase[1]) variables θ define the symmetry of the system, or more precisely, of its degrees of freedom. The degree of order in the field of spins $\mathbf{s_r}$ on lattice sites $\mathbf{r}$ can be measured by the *order parameter*

$$m = \frac{1}{L^d} \sum_{\mathbf{r}} (\mathbf{s_r} \cdot \hat{\mathbf{e}}) = \mathbf{m} \cdot \hat{\mathbf{e}}, \tag{3.1}$$

where the sum is over all L^d lattice sites and $\hat{\mathbf{e}}$ is an appropriately chosen unit vector. For this reason, the field of $\mathbf{s_r}$ is called the *order parameter field*. The *order parameter symmetry* refers to the symmetry of the constituent degrees of freedom, and *order parameter space* is the space in which the vectors $\mathbf{s_r}$ and $\mathbf{m}$ lives. We will refer to the dimensionality of the order parameter (space) as n, corresponding to n-components spins. In spin language, the order parameter m is a measure of

[1] In the introductory part of this thesis, we will consistently refer to θ as a phase; in the papers, the term used depends on the most appropriate interpretation for the given model.

uniform ferromagnetic (corresponding to $\mathbf{q} = \mathbf{0}$ order) magnetization in the system. Alternatively, one could also consider the order parameter to be the (magnetization) vector

$$\mathbf{m} = \frac{1}{L^d}\left(\sum_{\mathbf{r}} \cos\theta_{\mathbf{r}}, \sum_{\mathbf{r}} \sin\theta_{\mathbf{r}}\right) \equiv |m|(\cos\varphi, \sin\varphi) \tag{3.2}$$

instead of its length $|m|$.[2]

We will write the partition function in terms of these classical spin degrees of freedom on the form

$$\mathcal{Z} = \sum_{\{\mathbf{s}\}} \mathrm{e}^{-S[\mathbf{s}]}, \tag{3.3}$$

where the action defining the model in general is on the form[3]

$$S = \sum_i K_i E_i[\mathbf{s}] = K_1 E_1[\mathbf{s}] + K_2 E_2[\mathbf{s}] + \ldots. \tag{3.4}$$

For classical systems, one conventionally has the action $S = \beta H$, with H being the classical Hamiltonian and the thermal coupling $\beta = 1/T$ being the inverse temperature, setting $k_B = 1$. In this thesis, we will instead use the notation of Eq. (3.4), speaking of general couplings K_i and general energy terms E_i also for classical systems. This is done in anticipation of the usual notation for quantum models that will be necessary from Sec. 3.6.1 onwards.

The thermal average[4] of a general observable A is defined as

$$\langle A \rangle = \frac{1}{\mathcal{Z}} \sum_{\{\mathbf{s}\}} A[\mathbf{s}]\ \mathrm{e}^{-S[\mathbf{s}]}. \tag{3.5}$$

The perhaps most important thermal average is that of the order parameter, $\langle m \rangle$. Assuming uniform ferromagnetic order, this is equivalent to the thermal average $\langle \mathbf{s}_{\mathbf{r}} \rangle$ for an arbitrary lattice site $\mathbf{r}$. This illustrates why the order parameter is referred to as a *local* order parameter.

Finally, we will also need to define the general two-point correlation function of the order parameter field,

$$g(r) = \langle \mathbf{s}_{\mathbf{r}} \cdot \mathbf{s}_{\mathbf{r}'} \rangle, \tag{3.6}$$

where $r = |\mathbf{r} - \mathbf{r}'|$. The correlation function will in general measure short-range order $g(r) > 0$ at small distances r for all finite coupling values, but will only measure *long-range order* $g(r \to \infty) = \langle m^2 \rangle > 0$ in an ordered phase.

[2] We are in general not interested in the sign of m, and therefore use m interchangeably with the more practical definition $|m|$. Note also that we by the magnetization m always really refer to the magnetization *density*.

[3] Where $\mathbf{s}$ appears as an argument of a functional, as in $S[\mathbf{s}]$, it should be interpreted as a configuration of the spin field and not as a single spin variable.

[4] We will use terms such as "thermal" average, "thermal" equilibrium or "thermodynamics" also when the "classical" action strictly speaking represents a quantum model at zero temperature.

3.2 Phase transitions and critical phenomena

We will denote the general coupling that tunes the system through a phase transition by K and the location of the transition point by K_c. Assuming that the transition can be described by a local order parameter m, the phase at $K > K_c$ will be one where one measures order with respect to this order parameter, $m \neq 0$. As the system enters this ordered phase from the disordered phase at $K < K_c$ where $m = 0$, the order parameter experiences a non-analyticity that defines the transition point $K = K_c$. This non-analytic behaviour can be traced back to a singularity associated with the free-energy density $f \propto -\ln \mathcal{Z}$ of the system at the transition point.[5] The phase transition can be characterized by the strength of this non-analyticity. If it gives rise to a discontinuity in m, it signifies a *first-order* phase transition. In this case the system transitions abruptly from one phase to another, with phase coexistence at the transition point itself. For a *continuous* phase transition, on the other hand, the order parameter is a continuous (but still non-analytic) function at $K = K_c$.

One can also characterize a phase transition from disorder to order by the symmetry that is *spontaneously broken* in the ordered phase. As the transition point is crossed, the spins – on their own account – all agree on one preferred direction in order parameter space. The symmetry being broken is therefore usually identified with the order parameter symmetry. Spontaneous symmetry breaking should be distinguished from *explicit* symmetry breaking, which means that the appearance of order is caused by some external field acting on the variables in question.

For continuous phase transitions, the transition point is called a *critical point*, and we say that the system is critical at the critical point. To define more precisely what criticality entails, we list below the behaviour of the correlation function at and away from criticality:

$$g(r) \sim \quad \mathrm{e}^{-r/\xi} \quad \text{for } K < K_c, \tag{3.7}$$

$$g(r) \sim \quad 1/r^{d-2+\eta} \quad \text{for } K = K_c, \tag{3.8}$$

$$g(r) - \langle m^2 \rangle \sim \quad \mathrm{e}^{-r/\xi} \quad \text{for } K > K_c. \tag{3.9}$$

The characteristic length scale ξ introduced above is the *correlation length*. For the critical system, one notices that there is no characteristic length scale, or formally, $\xi = \infty$. The decay exponent of the power-law correlations at criticality defines the *anomalous scaling dimension* η, our first example of a *critical exponent*.

The expressions for $K \neq K_c$ are strictly speaking only valid for large $r \gg \xi$. As one gets close to the critical point, the correlation length diverges as $\xi \sim |K - K_c|^{-\nu}$, with the correlation length exponent ν being another critical exponent. This definition is also listed together with the definition of all the other relevant critical exponents in Table 3.1. The value of each of them (except for η) characterizes the non-analyticity

[5] When considering the free-energy density f in relation to phase transitions, we will implicitly neglect any constant or analytic terms. Also, when discussing general properties of phase transitions we will implicitly assume that the system is infinite, as thermodynamic quantities cannot be truly non-analytic unless the thermodynamic limit is taken.

of a quantity of interest as the reduced coupling $t \equiv |K - K_c|$ goes to zero at the transition point. If the values of all critical exponents for two critical points coincide, we say that these phase transitions belong to the same *universality class*. In Table 3.1 we also defined the correlation time ξ_τ, although this quantity does not enter in the description of (the thermodynamics of) classical phase transitions. It will feature prominently from Sec. 3.6.3 onwards as a correlation length in imaginary time, and also makes an appearance in Sec. 5.1.2 in the context of Monte Carlo simulations.

Table 3.1: Definition of critical exponents, with $t \equiv |K - K_c|$ for an arbitrary coupling parameter K close to the critical coupling K_c. We will assume that there is no external magnetic field. All definitions carry over also to quantum phase transitions, but for the correlation function, d will have to be replaced with an effective dimensionality.

Exponent	Quantity	Definition	Condition
β	Magnetization	$\langle m \rangle \sim t^\beta$	$K \to K_c^+$
γ	Susceptibility	$\chi \sim t^{-\gamma}$	$K \to K_c$
α	Specific heat	$C \sim t^{-\alpha}$	$K \to K_c$
η	Correlation function	$g(r) \sim 1/r^{d-2+\eta}$	$K = K_c$
ν	Correlation length	$\xi \sim t^{-\nu}$	$K \to K_c$
z	Correlation time	$\xi_\tau \sim \xi^z$	$K \to K_c$

3.2.1 The renormalization group idea

The exponents of Table 3.1 are defined from quantities that can be derived either from the correlation function or from the free energy of the system. For this reason, the critical exponents are not independent, but are related by scaling laws that can be derived using ideas of the *renormalization group* (RG). The actual application of these scaling ideas to the free-energy density and the correlation function will be deferred till we have generalized these quantities to the quantum case in Sec. 3.6. It is nevertheless expedient to introduce some basic RG concepts already now.

In essence, the renormalization group as it is employed here amounts to rescaling the system, $r \to r' = r/b$, where $b > 1$ is a scale factor. One then observes how the parameters of the system, h_i, have to be scaled if one requires the description of the system in terms of the rescaled parameters to remain the same, $h_i \to h_i' = h_i b^{y_i}$. The parameters are called the *scaling fields*, and their *flow* in parameter space refers to how the set of scaling fields evolves under rescaling. In this simplified picture, the flow tells you what the system tends to look like when viewed on larger and larger length scales. An *irrelevant* scaling field is associated with a *scaling dimension* y_i that is negative. This means that the scaling fields flows to zero under renormalization, and the parameter then plays a negligible role in the description of the large-scale physics of the system. This in turn means that the perturbation of a finite h_i leaves the universality class of the system unchanged. A positive scaling dimension $y_i > 0$, on the other hand, characterizes a *relevant* scaling field, whereas the borderline case $y_i = 0$ is termed *marginal*. A relevant scaling field may constitute a singular perturbation, altering the universality class for infinitesimal values of h_i.

The marginal case is more subtle, but in general leads to a gradual change of the universality class.

The flow in parameter space terminates in *fixed points* where all scaling fields remain invariant under renormalization and the system can be said to look the same on all length scales. This is exactly the distinguishing characteristic of a continuous phase transition, and some of the fixed points in an RG flow diagram are in general associated with possible phase transitions of the system. More precisely, each such fixed point is associated with a certain universality class, and when the RG flow of a system is governed by this fixed point, one would measure critical exponents in accordance with the corresponding universality class.

Scaling dimensions can also be defined for quantities that are not regarded as scaling fields. A general quantity A has an associated scaling dimension y_A if its renormalized value is given by $A' = Ab^{y_A}$. The value of y_A in some cases follows from simple dimensional analysis. If A can be expressed as some power of some length scale, y_A equals minus the exponent of this power. This is most easily seen if considering the most simple example of the linear size of the system, $A = L$. Then, $L' = L/b$, and so $y_L = -1$.

3.3 Classical models and universality classes

Here follows a brief overview of properties of simple models of classical statistical mechanics that will be relevant for the more complicated models studied in this thesis. For later reference we also list critical-exponent values for these models in Table 3.2.

Table 3.2: Values of critical exponents, as defined in Table 3.1, for some important universality classes. The infinite values for the 2D XY case are to be understood as formal limits of the power-law definitions, as explained in Sec. 3.3.4. The values are exactly known in the 2D and mean-field cases, whereas the numerically estimated 3D values are from Ref. [75], with uncertainties in the last digit omitted.

	ν	η	β	γ	α
2D Ising	1	0.25	0.125	1.75	0
2D XY	∞	0.25	∞	∞	$-\infty$
3D Ising	0.6301	0.0364	0.3265	1.2372	0.110
3D XY	0.6716	0.0380	0.3485	1.3177	−0.007
Mean field	0.5	0	0.5	1	0

3.3.1 The Ising model

With Ising models we mean a class of one-component spin models with binary degrees of freedom, $\sigma \in \{-1, 1\}$. For the simplest realizations of these models, namely those on a hypercubic lattice with isotropic nearest-neighbour interactions in the absence

of an external magnetic field, the action is simply

$$S = -K \sum_{\langle \mathbf{r},\mathbf{r}' \rangle} \sigma_{\mathbf{r}} \sigma_{\mathbf{r}'}. \tag{3.10}$$

We will assume that the interactions are ferromagnetic, $K > 0$.

An order-disorder phase transition of this model is associated with spontaneous breaking of the Z_2 symmetry that is evident in the above action from the transformation $\sigma_{\mathbf{r}} \to -\sigma_{\mathbf{r}}$ for all $\mathbf{r}$. The one-dimensional Ising chain, however, is disordered for all finite temperatures (corresponding to $K < \infty$). Since the action (3.10) gives rise to a continuous phase transition to long-range order for all higher dimensions, the *lower critical dimension* is $d_l = 1$. The two-dimensional case is exactly solvable, with exactly known critical exponents as presented in Table 3.2. This is not the case in three dimensions, but the exponents are known to a very good accuracy from numerical computations.

From the exact solution of the 2D nearest-neighbour Ising model, not only do we know the exponents, but we also have an expression for the (non-universal) critical coupling K_c. In fact, this result also applies if Eq. (3.10) is generalized to anisotropic interactions. In the parameter space of the couplings in the two directions, K_x and K_y, the critical line is given by the expression [76]

$$\sinh(2K_x)\sinh(2K_y) = 1. \tag{3.11}$$

This means that if we choose to fix one of the couplings, say K_y, the critical value K_c of the other coupling K_x can be calculated as

$$K_c = -\frac{1}{2}\ln(\tanh K_y). \tag{3.12}$$

In the case of isotropic couplings $K_y = K_x \equiv K$, as assumed in Eq. (3.10), the critical coupling has the value

$$K_c = \frac{1}{2}\ln(1+\sqrt{2}) \approx 0.44068. \tag{3.13}$$

3.3.2 The q-state clock model

The two-state Ising model can be generalized to a q-state model by introducing angular degrees of freedom θ that can take on a discrete set of q values, $\theta \in \{\pi/q, 3\pi/q, \ldots, (2q-1)\pi/q\}$. The action for the resulting q-state clock model becomes

$$S = -K \sum_{\langle \mathbf{r},\mathbf{r}' \rangle} \cos(\theta_{\mathbf{r}} - \theta_{\mathbf{r}'}), \tag{3.14}$$

where we again have assumed ferromagnetic, isotropic nearest-neighbour interactions. Analogously to the Ising model, a disorder-order transition described by this action is associated with the spontaneous breaking of the cyclic Z_q symmetry. In

fact, that the Z_2 clock model is equivalent to the Ising model is easily shown by rewriting Eq. (3.14) as

$$S = -K \sum_{\langle \mathbf{r},\mathbf{r}' \rangle} (\cos\theta_{\mathbf{r}} \cos\theta_{\mathbf{r}'} + \sin\theta_{\mathbf{r}} \sin\theta_{\mathbf{r}'}) \tag{3.15}$$

and considering the y projection of the clock spin in order parameter space, $\sin\theta \equiv \sigma \in \{-1, 1\}$. Perhaps more remarkably, the four-state clock model can be shown to be equivalent to two decoupled Ising models. Introducing two species of Ising spins σ and μ defined by $\cos\theta \equiv (\sigma + \mu)/2$ and $\sin\theta \equiv (\sigma - \mu)/2$, the action can be rewritten as

$$S = -K/2 \sum_{\langle \mathbf{r},\mathbf{r}' \rangle} (\sigma_{\mathbf{r}}\sigma_{\mathbf{r}'} + \mu_{\mathbf{r}}\mu_{\mathbf{r}'}) \,. \tag{3.16}$$

Note that the coupling of each of these Ising models is reduced by a factor of two with respect to Eq. (3.10). To find the critical coupling of the 2D four-state clock model, one therefore has to modify the condition (3.11) to read $\sinh(K_x)\sinh(K_y) = 1$ in the anisotropic case. Nevertheless, the d-dimensional q-state clock model belongs to the universality class of the corresponding Ising model for both $q = 2$ and $q = 4$, and it has critical exponents as given in Table 3.2.

For the cases $q \geq 5$, the behaviour of the q-state clock model suddenly diverges from the relatively simple behaviour of the Ising models. Exactly how this happens is a somewhat convoluted story, and we postpone these cases to Sec. 3.4.

3.3.3 The Ashkin-Teller model

Generalizing the two-dimensional four-state clock model in the Ising representation to also include a four-spin coupling term between the two species of Ising spins, we obtain the Ashkin-Teller model. Using the same mapping between the Ising variables and the phase variables as in Sec. 3.3.2, we can write the action in both the Ising-spin and the phase representation as follows:

$$S = -\sum_{\langle \mathbf{r},\mathbf{r}' \rangle} [K(\sigma_{\mathbf{r}}\sigma_{\mathbf{r}'} + \mu_{\mathbf{r}}\mu_{\mathbf{r}'}) + K_4 \sigma_{\mathbf{r}}\sigma_{\mathbf{r}'}\mu_{\mathbf{r}}\mu_{\mathbf{r}'}] \tag{3.17}$$

$$= -\sum_{\langle \mathbf{r},\mathbf{r}' \rangle} [2K\cos(\theta_{\mathbf{r}} - \theta_{\mathbf{r}'}) + K_4 \cos(2\theta_{\mathbf{r}} - 2\theta_{\mathbf{r}'})) \,. \tag{3.18}$$

The Ashkin-Teller model has a number of unusual features, but the only one we are interested in here is that its critical exponents may vary continuously [76]. In particular, the specific heat exponent α decreases monotonously from its Ising value $\alpha = 0$ at $K_4 = 0$ as the interspecies coupling K_4 is lowered to negative values. This means that a system described by the Ashkin-Teller model may have a phase transition without the usual divergence of the specific heat.

3.3.4 The XY model

In the limit of $q \to \infty$, the discrete Z_q symmetry of the clock model is elevated to a continuous $U(1)$ symmetry, and the action (3.14) becomes that of the XY model. We repeat the action

$$S = -K \sum_{\langle \mathbf{r},\mathbf{r}' \rangle} \mathbf{s}_{\mathbf{r}} \cdot \mathbf{s}_{\mathbf{r}'} = -K \sum_{\langle \mathbf{r},\mathbf{r}' \rangle} \cos\left(\theta_{\mathbf{r}} - \theta_{\mathbf{r}'}\right), \tag{3.19}$$

where we also have expressed it in terms of planar spins $\mathbf{s}_{\mathbf{r}}$. Among the many applications of the XY model, it is appropriate to point out here that the phases $\theta_{\mathbf{r}}$ can describe the $U(1)$-symmetric order parameter phase of a superconducting system.

For $d > 2$, the phase transition from a disordered state resembles those of the discrete models considered above: The continuous $U(1)$ symmetry associated with arbitrary phase translations $\theta_{\mathbf{r}} \to \theta_{\mathbf{r}} + \varphi$ for all $\mathbf{r}$ is spontaneously broken for $K > K_c$. The case $d = 2$ is, however, very different, and there is no transition to a state with long-range order (LRO) for any finite value of K. The crucial difference from models with discrete symmetry is that the spin gap $\propto 1 - \cos(2\pi/q)$ in the excitation spectrum vanishes for the XY model. Due to the Mermin-Wagner theorem [77], there can therefore be no LRO phase for $K < \infty$, and the lower critical dimension is increased with respect to the discrete case to $d_l = 2$. What one gets instead is a so-called Kosterlitz-Thouless (KT) transition [78] at a coupling K_c, above which *quasi-long-range order* (QLRO) develops. This means that there are (critical) power-law correlations $g(r) \sim 1/r^{\eta(K)}$ for all $K > K_c$ so that $g(r) \to 0$ as $r \to \infty$.[6] The anomalous dimension $\eta(K)$ varies continuously with the coupling strength in this critical phase and takes the value $\eta(K) = 1/4$ at the critical endpoint, which is at $K_c \approx 1.1199$ [79] for the isotropic 2D XY model. The remaining exponents are not well-defined, and their values are formally infinite. For the correlation length exponent ν, this means that the correlation length diverges faster than any power law upon approaching $K = K_c$ from below. To be more specific, it diverges exponentially on the form

$$\xi \sim \mathrm{e}^{b/\sqrt{t}} \tag{3.20}$$

for $K \lesssim K_c$. For all $K \geq K_c$, the system is critical and the correlation length ξ remains infinite. The extreme form of the divergence in Eq. (3.20) means [74] that the singularity associated with the free-energy density f is an *essential* singularity in the case of a KT transition.

Although there exists no local order parameter to mark the onset of this critical QLRO phase, it is possible to define a *global* order parameter that describes the KT transition. For now, we will merely say that this order parameter is related to the stiffness of the order parameter field with respect to twisting the direction of the spins. We will postpone a more detailed discussion of this spin stiffness till Sec. 3.8.2, where we will be in a position to describe the scaling behaviour and physical origin of this quantity.

[6] We might instead write K_{KT} to distinguish this transition point from that of an ordinary continuous phase transition, but since both are critical points, we will use K_c also for the critical endpoint of the 2D XY model.

3.3.5 Mean field theory

Whereas fluctuations at or below the lower critical dimension d_l are so effective that any long-range order is inhibited, they are rendered irrelevant above an upper critical dimension d_u. The result is that for all $d > d_u$, the universality class is influenced neither by order parameter symmetry nor by dimensionality, and all critical exponents take their *mean-field* values as listed in Table 3.2. For all models considered above, the upper critical dimension is $d_u = 4$.

3.4 Anisotropy and intermediate critical phases

Section 3.3.2 described the behaviour of 2D q-state clock models as Ising-like for $q = 2$, 4. This description may also be valid for higher $q < \infty$, but only in the sense that the Z_q symmetry is spontaneously broken in a long-range-ordered phase for sufficiently high $K > K_{c,2}$. The behaviour at lower K, however, turns out to have more in common with that of the continuous ($q \to \infty$) 2D XY model if $q \geq 5$. As shown by Ref. [80], the 2D q-state clock model features an intermediate phase with the same kind of QLRO also for $q_c \leq q < \infty$, where most probably $q_c = 5$. In this phase, it is as if the spin gap is an irrelevant scaling field that flows to zero under renormalization.[7] For large length scales, the discreteness of the phase variable is hence washed out for $K \lesssim K_{c,2}$ and plays no role in the large-scale description of the system. Instead, the behaviour is dictated by an *emergent* $U(1)$ symmetry [81, 82].

The critical power-law correlations and associated QLR order allowed for such an emergent $U(1)$ symmetry are destroyed below an even lower coupling $K = K_{c,1}$ in much the same manner as for the 2D XY model. The resulting phase structure is illustrated in Fig. 3.1. Although the value of $K_{c,1}$ seems to be almost independent of q for $q \geq q_c$, the value of $K_{c,2}$ diverges as q^2 for increasing q [81, 83], reproducing the XY phase diagram with no LRO phase in the limit $q \to \infty$.

We should also mention that there has been a fair amount of controversy surrounding the exact value of q above which the intermediate phase appears, and also surrounding the nature of the adjoining phase transitions. However, very recent numerical computations [83] support the original [80] result $q_c = 5$ with two KT transitions for all $q \geq q_c$, and the same conclusion was also reached in a very recent analytical work [82].

Turning briefly to the corresponding results for 3D clock models, the phase diagram contains only two phases irrespective of the value of q: One fully ordered and one fully disordered. The discreteness is rendered irrelevant at the transition for all $q \geq 5$ [84], and the critical point of these clock models therefore exhibits 3D XY exponents.

[7] The spin gap is relevant for $K > K_{c,2}$ in the sense that the order here is Z_q order.

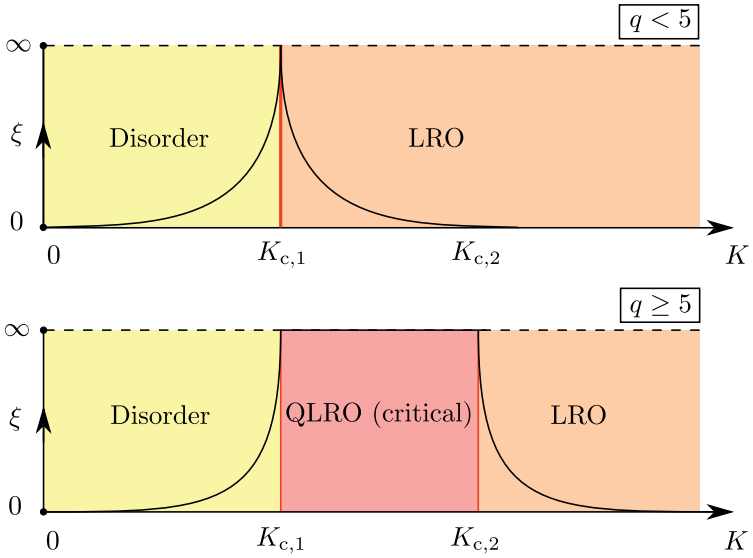

Figure 3.1: Schematic phase diagram for the 2D q-state clock model and related models featuring intermediate phases. The intermediate critical phase for $q \geq q_c$ emerges from a single critical point $K = K_c$ for $q < q_c$, and we assume here that $q_c = 5$. $K_{c,2}$ moves towards higher coupling for increasing q, and the region with long-range order (LRO) vanishes as $q \to \infty$. The evolution of the correlation length ξ is shown schematically along the y axis. It diverges upon approaching criticality and remains infinite within the intermediate critical phase.

3.4.1 Symmetry-breaking fields

One may relax the *hard constraint* of the clock model – the constraint of only allowing a discrete set of phase values – and instead introduce a *soft constraint* favouring the same set of values. Letting θ now be a continuous phase field as in Eq. (3.19), one has an XY model with q-fold anisotropy, with the action given by

$$S = -K \sum_{\langle \mathbf{r},\mathbf{r}' \rangle} \cos\left(\theta_{\mathbf{r}} - \theta_{\mathbf{r}'}\right) - h_q \sum_{\mathbf{r}} \cos\left(q\theta_{\mathbf{r}}\right). \tag{3.21}$$

The coupling h_q appears as an external field breaking the underlying $U(1)$ symmetry. The resulting phase diagram is essentially the same as for the hard-constraint clock models, and an intermediate critical phase appears for $q \geq 5$ in 2D systems [85].

The limit $h_q = \infty$ reproduces the q-state clock model with a finite spin gap, but for any finite value of h_q, the spin gap is still zero and the second term of the action may be regarded as a perturbation. One consequence of this is that whereas the anisotropy of a q-state clock model may be either relevant or irrelevant to the universality class, one must for the symmetry-breaking field h_q distinguish between irrelevance and *perturbative* irrelevance. For instance, it is known [86, 87] that a fourfold anisotropy field h_4 is perturbatively irrelevant to the 3D XY model at the critical point, but driving h_4 to infinity evidently changes the universality class to that of the 3D Ising model.

In principle, it is also possible that the phase transition of a model may change its universality class at some finite value of h_q even though the $h_q = 0$ fixed point of this model is stable to (infinitesimal) h_q perturbations. For the 2D XY model, it is known that h_4 is marginally relevant [85], so that $h_4 > 0$ results in a continuous phase transition with continuously varying critical exponents that approach those of the 2D Ising model as $h_4 \to \infty$.[8]

3.5 Models with long-range interactions

For the models with short-range interactions discussed in Sec. 3.3, no (finite-temperature) phase transition was possible in one dimension, $d = 1$ being at or below the lower critical dimension d_l. When the models are generalized to have long-range interactions, this result no longer needs to be valid. We will parametrize such classical, long-range-interacting spin models by the action

$$S = -K \sum_{\mathbf{r}' \neq \mathbf{r}} \frac{\mathbf{s}_\mathbf{r} \cdot \mathbf{s}_{\mathbf{r}'}}{|\mathbf{r} - \mathbf{r}'|^{d+s}}, \tag{3.22}$$

where all spins interact with each other with an interaction strength that decays as $1/r^{d+s}$ with distance r. A lower value of s means that the interaction decays more slowly with distance, and it appears as if the number of "nearest neighbours" interacting with each spin is increased. This increases the effective dimensionality of the system, rendering a phase transition possible even for $d = 1$ if s becomes sufficiently low. From our point of view, this is very important in the context of zero-dimensional dissipative quantum systems. As we will treat in more detail in Ch. 4, many of these are equivalent to one-dimensional classical systems with long-range interactions, and can therefore demonstrate a quantum phase transition despite their low dimensionality.

The discussion of absence or presence of long-range order in classical 1D models with various long-range interactions has a long history, and we refer to Ref. [88] for a survey of early works. To summarize, it turns out that the criterion for a long-range-interacting Ising chain to have a phase transition is $s \leq 1$. To understand this, we first turn our attention to RG study of Fisher et al. [89], who showed that for arbitrary dimensionality of the system and the order parameter, long-range interactions reduce the upper critical dimension from the short-range result $d_u = 4$ to $d_u = 2s$. This can be viewed as a change in the effective dimensionality of the system from d to $d_{\text{eff}} = 2d/s$ in the long-range case [90]. It follows from this argument that the case $d = 1$, $s = 1$ gives effective dimensionality $d_{\text{eff}} = 2$, which is just above the lower critical dimension of the Ising model. Fisher et al. also determined the decay exponent $s = s^*$ above which the long-range nature of the interaction was irrelevant to be $s^* = 2$. This result was soon contested by Sak [91], who found $s^* = 2 - \eta_{\text{SR}}$, with η_{SR} denoting the anomalous dimension of the underlying short-range model. The value of s^* remained controversial for decades, but it was eventually confirmed numerically for a 2D Ising model [92] that $s^* = 2 - \eta_{\text{SR}}$.

[8] For $K > K_c$, the h_4 perturbation is relevant in the sense that the symmetry being spontaneously broken here is the Z_4 symmetry and not the $U(1)$ order parameter symmetry.

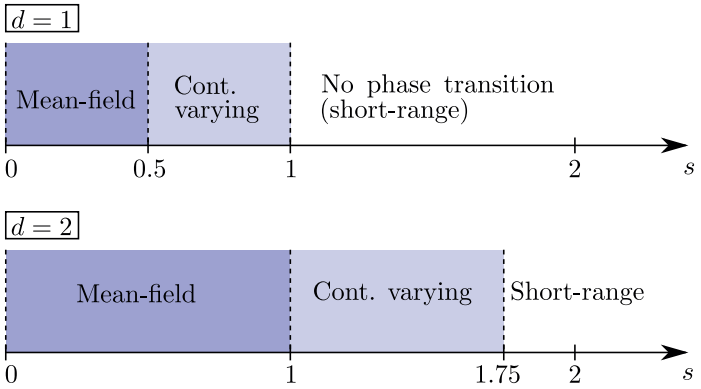

Figure 3.2: Different regimes of the criticality of spin systems with long-range interactions decaying with distance as $1/r^{d+\sigma}$. The labels indicate the behaviour of the critical exponents, which are continuously varying in the intermediate region. For the region with short-range behaviour, the 2D model has a phase with long-range order only for Ising-symmetric order parameter, while no long-range order is possible in 1D models with short-range interactions.

For values of s below the "upper" critical decay exponent $s_u = d/2$, the critical exponents take the values predicted by mean-field theory. It is, however, important to note that not all these mean-field exponents equal those for short-range models; whereas α, β and γ take the values listed in Table 3.2, ν and η do not. Most notably, $\eta = 2 - s$ is an exact result, not only in the mean-field region, but for all $s \in \langle 0, s^*]$ [92]. (For $s > 2 - \eta_{\mathrm{SR}}$, η assumes its short-range value η_{SR}.) Figure 3.2 illustrates three different regimes of s showing different criticality. In the intermediate regime below $s = s^*$ and above the "upper" critical decay exponent $s = d/2$, the critical exponents are varying continuously with s. It follows that in this region, one can effectively tune the dimensionality and the resulting nature of the critical point by varying the decay exponent s. Although it has proved very useful to do this to infer the behaviour of higher-dimensional systems from their lower-dimensional counterparts with long-range interactions [88], one must keep in mind that they still belong to different universality classes, as implied by the discussion of the exponent values above.

The most interesting decay exponent value for 1D systems is the borderline case $s = 1$. Not only does this case represent the most relevant classical analogue of dissipative quantum systems, but it is also a very unconventional kind of phase transition, and we will briefly review some of its properties. The phase transition is KT-like in the sense that it is associated with an essential singularity, as for the 2D XY model.[9] Thus, the correlation length diverges exponentially upon approaching the critical point from the disordered side. But in contrast to the XY model, the transition in the inverse-square Ising chain is to long-range order.[10]

[9] Recall that both the 2D XY model and the inverse-square Ising chain have effective dimensionality two, although the order parameter symmetry is different.

[10] More remarkably, this order sets in discontinuously at the transition point [93], which is followed by an intermediate phase with continuously varying anomalous dimension [94, 95].

3.6 Quantum criticality

The concept of quantum criticality has already been introduced and motivated in Ch. 1 and Sec. 2.2, and we will here put the distinction from classical phase transitions on a more formal basis. In brief, a quantum phase transition (QPT) is a phase transition happening at zero temperature, and if this phase transition is continuous, we call its locus in the phase diagram a quantum critical point (QCP). There is a number of good general reviews available on quantum critical phenomena, and for the presentation given in this chapter, we refer to Refs. [96], [97] and [98].

Quite remarkably, it turns out that many QPTs can be described as transitions of a classical model with one additional time-like dimension, and we will for the most part limit ourselves to QPTs where such a quantum–to–classical mapping is possible. We can treat the resulting (d+1)-dimensional models on the same footing as d-dimensional classical models, and will refer to the dimensionality d of the original (quantum) model as the *spatial* dimensionality. How this mapping is carried out is best illustrated by the following concrete example.

3.6.1 Quantum-to-classical mapping

The archetypal example of a quantum model having a phase transition at zero temperature is the transverse-field Ising chain. The mapping of this 1D quantum model onto a (1+1)D classical model [99], equivalent with the 2D Ising model, also serves as an introduction to the methods used in paper III and alluded to in Sec. 4.4.1 for mapping quantum rotor models to classical models.

The quantum Hamiltonian of a chain of $SU(2)$ spins $\hat{\boldsymbol{\sigma}} = [\hat{\sigma}^x, \hat{\sigma}^y, \hat{\sigma}^z]$ in an external transverse field h_x is

$$\hat{H} = -J \sum_{r=1}^{L} \hat{\sigma}_r^z \hat{\sigma}_{r+1}^z - h_x \sum_{r=1}^{L} \hat{\sigma}_r^x = -J\hat{E}_0 - h_x \hat{E}_1. \tag{3.23}$$

The spins are coupled by interactions with Ising symmetry, and we will choose the z-axis eigenstates $|\sigma = -1\rangle, |\sigma = 1\rangle$ as our basis. In this basis, the operator $\hat{\sigma}^x$ due to the field along the x axis acts as a spin-flip operator, so that the field h_x promotes quantum fluctuations between the states $|-1\rangle$ and $|1\rangle$. Although the system described by $\hat{E}_0$ is fully ordered at $T = 0$, increasing h_x will suppress this order, eventually destroying it completely at a quantum critical point.

The quantum partition function is in general given by

$$\mathcal{Z} = \mathrm{Tr}\left\{ \mathrm{e}^{-\beta \hat{H}} \right\}. \tag{3.24}$$

Using a complete set of states $\{|\nu\rangle\}$, in the present case this can be written as

$$\mathcal{Z} = \sum_{\nu} \langle \nu | \mathrm{e}^{\beta(J\hat{E}_0 + h_x \hat{E}_1)} | \nu \rangle. \tag{3.25}$$

The essence of the mapping to a classical system lies in the next step, where we use the path-integral idea [100] to decompose the inverse temperature β in L_τ *Trotter slices*. Each Trotter slice has the same width $\Delta\tau = \beta/L_\tau$. This allows us to rewrite the partition function as

$$\mathcal{Z} = \lim_{L_\tau\to\infty} \sum_{\nu} \langle\nu| \prod_{\tau=1}^{L_\tau} \mathrm{e}^{(J\Delta\tau)\hat{E}_0}\ \mathrm{e}^{(h_x\Delta\tau)\hat{E}_1)} |\nu\rangle. \tag{3.26}$$

In effect, we are introducing a second, *imaginary-time* dimension to the problem, indexed by $\tau = 1, 2, \ldots, L_\tau$.[11]

Next, we insert the completeness relation $\mathbb{1} = \sum_{\nu_\tau} |\nu_\tau\rangle\langle\nu_\tau|$ between factors for different Trotter slice and get

$$\sum_{\nu} \langle\nu| \prod_{\tau=1}^{L_\tau} \mathrm{e}^{-\Delta\tau\hat{H}} |\nu\rangle = \sum_{\{\nu_\tau\}} \prod_{\tau=1}^{L_\tau} \langle\nu_{\tau-1}|\mathrm{e}^{(J\Delta\tau)\hat{E}_0}\mathrm{e}^{(h_x\Delta\tau)\hat{E}_1}|\nu_\tau\rangle. \tag{3.27}$$

Here we get periodic boundary conditions also for the Trotter slices, $|\nu\rangle \equiv |\nu_0\rangle = |\nu_{L_\tau}\rangle$, since the trace operation is cyclic.

In the z basis, the states $|\nu_\tau\rangle$ are eigenstates of the $\hat{E}_0$ operator, and we can deal with the first part of the Hamiltonian as follows:

$$\langle\nu_{\tau-1}|\mathrm{e}^{(J\Delta\tau)\sum_{r=1}^{L}\hat{\sigma}_r^z\hat{\sigma}_{r+1}^z} = \mathrm{e}^{-(J\Delta\tau)\sum_{r=1}^{L}\sigma_{r,\tau}\sigma_{r+1,\tau}}\langle\nu_{\tau-1}|. \tag{3.28}$$

For the second term of the Hamiltonian, one then gets transfer matrices on the form

$$\langle\nu_{\tau-1}|\mathrm{e}^{(h_x\Delta\tau)\sum_{r=1}^{L}\hat{\sigma}_r^x}|\nu_\tau\rangle = \prod_{r=1}^{L}\sum_{n=0}^{\infty}\frac{1}{n!}(h_x\Delta\tau)^n\langle\sigma_{r,\tau-1}|(\hat{\sigma}_r^x)^n|\sigma_{r,\tau}\rangle. \tag{3.29}$$

Here we have used that the basis states $|\nu_\tau\rangle$ are products of z-projection states $|\sigma_{r,\tau}\rangle$ for all spatial sites r on Trotter slice τ. By some manipulation,[12] the transfer matrix may be evaluated and re-exponentiated to yield

$$\langle\nu_{\tau-1}|\mathrm{e}^{(h_x\Delta\tau)\sum_{r=1}^{L}\hat{\sigma}_r^x}|\nu_\tau\rangle \propto \prod_{r=1}^{L}\mathrm{e}^{\frac{1}{2}\ln\coth(h_x\Delta\tau)\sigma_{r,\tau-1}\sigma_{r,\tau}}. \tag{3.31}$$

[11] Strictly speaking, it would probably be more correct to assign to the Trotter slices a different index k so that $\tau = k\Delta\tau \in \langle 0, \beta]$ remains a genuine imaginary-time coordinate. However, we choose to follow the same notation as for the spatial direction, where r is an index and the lattice spacing is not included explicitly. Since we are not interested in finite-temperature behaviour ($\beta \ll \infty$) in this thesis, one can for all practical purposes regard $\Delta\tau = 1$ as fixed.

[12] The sum over n has contributions only from even n when $\sigma = \sigma'$ and from odd n when $\sigma = -\sigma'$ ($\sigma = \sigma_{r,\tau}$, $\sigma' = \sigma_{r,\tau-1}$), resulting in the series expansion of a cosh and a sinh function, respectively. We next want to write this transfer matrix expression on a re-exponentiated form

$$\delta_{\sigma,\sigma'}\cosh(h_x\Delta\tau) + \delta_{\sigma,-\sigma'}\sinh(h_x\Delta\tau) = C\mathrm{e}^{K_\tau\sigma\sigma'}, \tag{3.30}$$

where C and K_τ are constants to be determined. One finds that the equation holds for both $\sigma = \sigma'$ and for $\sigma = -\sigma'$ given that $C = \left[\frac{1}{2}\sinh(h_x\Delta\tau)\right]^{1/2}$ and $K_\tau = \frac{1}{2}\ln\coth(h_x\Delta\tau)$.

Inserting these factors into Eq. (3.27) along with the factors (3.28) from the Ising term of the Hamiltonian, we can write the partition function (3.25) as

$$\mathcal{Z} \propto \lim_{L_\tau \to \infty} \sum_{\{\sigma_{r,\tau}\}} \mathrm{e}^{-S}, \tag{3.32}$$

where the effective action is given by

$$S = -\sum_{\tau=1}^{L_\tau} \sum_{r=1}^{L} \left(K \sigma_{r,\tau} \sigma_{r+1,\tau} + K_\tau \sigma_{r,\tau} \sigma_{r,\tau+1} \right). \tag{3.33}$$

This is the action of a classical, anisotropic (1+1)D Ising model with coupling $K = J\Delta\tau$ in the (spatial) r direction and coupling $K_\tau = \frac{1}{2} \ln \coth (h_x \Delta\tau)$ in the (temporal) τ direction. The procedure is the same also for $d \neq 1$.

We will use the same notation also in other models, referring to K as the spatial coupling and to the imaginary-time coupling K_τ as the kinetic or quantum coupling. Note that increasing the strength of the transverse field h_x decreases the quantum coupling K_τ, thus intensifying the (quantum) fluctuations of σ along the imaginary-time direction, as expected.[13]

Even though the spatial and temporal interactions of Eq. (3.33) are anisotropic, this is only a quantitative anisotropy in the sense that the two interaction terms themselves are qualitatively equivalent. This can be seen by considering the correlation length ξ_τ in the imaginary-time direction. It will in general be different from the spatial correlation length ξ, but will nevertheless scale in the same way as one approaches criticality, $\xi_\tau \sim \xi$. In the RG picture of Sec. 3.2.1, one can therefore perform a spatial rescaling $r \to r/b$ and a temporal rescaling $\tau \to \tau/b$ with the same scale factor b and still obtain an equivalently anisotropic system. Alternatively, one can just redefine the coordinate system in advance so that the description of the system remains isotropic during the rescaling [73]. The (very important) cases where this is not possible will be treated in the next section.

3.6.2 Free energy and effective dimensionality

The last step in explaining how a QPT can be in the same universality class as a classical phase transition of higher dimensionality is to show how their free-energy densities relate. We will use the result of the preceding section to equate the partition function $\mathcal{Z}$ [Eq. (3.24)] of an arbitrary d-dimensional quantum system to the partition function $\mathcal{Z}_{d+1}$ of a $(d+1)$-dimensional classical system. (To generalize the results for the quantum Ising model, we have to assume there actually exists a quantum-to-classical mapping for the given model.) This can be expressed as

$$\mathrm{e}^{-\beta F} = \mathcal{Z} \propto \mathcal{Z}_{d+1} = \mathrm{e}^{-Vf}, \tag{3.34}$$

[13] In order to reduce the quantum fluctuations to drive the system through a QPT to an ordered phase, one could increase either K or K_τ, and we will therefore still use K as the generic coupling symbol. Also, in our simulations, we will predominantly be varying K with K_τ fixed.

where $\beta = L_\tau \Delta\tau$ and F is the inverse temperature and the free energy, respectively, of the quantum system; $V = (L_\tau \Delta\tau) L^d$ and f is the space-time volume and the (reduced) free-energy density, respectively, of the $(d+1)$-dimensional classical system. Just as all thermodynamic quantities of a finite-temperature phase transitions can be derived from the free energy F, the corresponding quantities for a zero-temperature phase transition of a quantum system are determined by the ground-state energy $E_0 = \lim_{T\to 0} F$. Using the result (3.34) from the quantum-to-classical mapping, this ground-state energy is written as [101]

$$E_0/L^d = -\lim_{T\to 0} \frac{T}{L^d} \ln \mathrm{Tr}\left\{ \mathrm{e}^{-\hat{H}/T} \right\} \sim -\lim_{L_\tau \to 0} \frac{1}{\Delta\tau L_\tau L^d} \ln \mathcal{Z}_{d+1} = \lim_{V\to\infty} f. \qquad (3.35)$$

Implicit in the above equation is the limit $L \to \infty$, as we are interested in genuine phase transitions. The limit $V \to \infty$ above therefore means that one takes the zero-temperature limit $L_\tau \to \infty$ for the imaginary-time dimension simultaneously with taking the thermodynamic limit for the spatial dimensions.[14]

The scaling dimension of the critical free-energy density (3.35) is that of the inverse of the space-time volume V, $y_f = -y_V$. For the Ising models in Sec. 3.6.1, the rescaled volume is $V' = (L')^d (\Delta\tau L'_\tau) = (L/b)^d \Delta\tau L_\tau / b = V b^{-(d+1)}$, giving $y_f = d+1$. In contrast, for a classical d-dimensional system, f will have scaling dimension d. Since thermodynamic quantities are determined by the free energy, the critical thermodynamics of a d-dimensional quantum model at $T = 0$ indeed is that of a corresponding classical model with *effective* dimensionality $d_{\mathrm{eff}} = d + 1$. This rests on the assumption that the temporal length L_τ has the same scaling dimension as the spatial length L, and, crucially, this needs not always be the case. If the temporal interaction term(s) were not (qualitatively) equivalent to the spatial, it would not be natural to rescale the temporal length scale by the same scale factor b. Instead, one would have to adopt a generalized, anisotropic rescaling procedure, where $r \to r/b$ as before, but $\tau \to \tau/b^z$, introducing the *dynamical critical exponent* z not necessarily identical to unity [102]. The rescaled imaginary-time extent of the system then becomes $L'_\tau = L_\tau / b^z$, and the space-time volume is rescaled to $V' = V b^{-(d+z)}$. This implies an effective dimensionality $d_{\mathrm{eff}} = d + z$. The scaling dimension of the free-energy density changes accordingly, changing the scaling properties of all thermodynamic quantities.

Since the effective dimensionality of the system is larger than d, this also means that the upper critical dimension (with respect to spatial dimensionality) is lowered to $d_u = 4 - z$. A quantum system at zero temperature should hence exhibit mean-field behaviour for $d_{\mathrm{eff}} = d + z > 4$.

3.6.3 Dynamical scaling and the dynamical critical exponent

The anisotropic scaling of space and imaginary time also translates into anisotropic divergence of the correlation volume upon approaching criticality, meaning that the

[14] This interpretation of the thermodynamic limit is important from the point of view of Monte Carlo simulations on such quantum systems: Although carried out at finite system sizes for finite temperatures, increasing both L and L_τ (at appropriate rates) allows such simulations to probe the critical behaviour of an infinite system at zero temperature.

relative scaling of the temporal and spatial correlation lengths is given by $\xi_\tau \sim \xi^z$. In other words, the temporal correlation length $\xi_\tau \sim t^{-\nu_\tau}$ diverges as $t \to 0$ with a correlation length exponent $\nu_\tau = z\nu$ that may differ from the spatial correlation length exponent ν. In Fourier space, one equivalently has a characteristic frequency[15] $\omega \sim 1/\xi_\tau$ scaling with a characteristic momentum $q \sim 1/\xi$ as $\omega \sim q^z$. Note that these scaling forms also apply in the case of a KT-type transition with ξ diverging exponentially as $t \to 0$, but only if ξ_τ diverges exponentially in the same manner.

An alternative to the above *conventional* dynamical scaling is *activated* dynamical scaling. This means that the spatiotemporal scaling relation is $\ln \xi_\tau \sim \xi^\psi$, or, equivalently, $\ln \omega \sim q^\psi \implies \omega \sim \exp\left[\text{const.} \times q^\psi\right]$. Such an extreme form of dynamical scaling can formally be seen as the limit $z \to \infty$ of the conventional form $\omega \sim q^z$. Activated dynamical scaling is therefore an example of *local quantum criticality*, which we define as any quantum critical phenomenon with an associated dynamical critical exponent that is in some sense infinite. We will have more to say on different possible realizations of local quantum criticality in Sec. 4.5.3 and Sec. 6.1.4.

A major part of this thesis work revolves around the question of finding the dynamical critical exponent. Why this exponent is important is illustrated in the next section, where we show how it permeates the scaling theory of quantum critical phenomena.

3.7 Scaling theory of quantum criticality

Since the scaling expressions relevant for quantum criticality are usually not exposed in any detail in the literature, we choose to spend some time on this topic. This scaling theory also lies at the foundations of the techniques we use to extract critical exponents from numerical simulations. In cases where the imaginary-time dimension does not feature explicitly, the well-known expressions for classical criticality are recovered if the effective dimensionality $d + z$ is replaced by d.

3.7.1 Scaling of the free-energy density

We first apply the RG ideas of Sec. 3.2.1 to the free-energy density (3.35) at criticality. Viewed at rescaled lengths $r' = r/b$ and imaginary times $\tau' = \tau/b^z$, the rescaled free-energy density can be written as $f' = fb^{d+z}$. Expressing f as a function of the relevant scaling fields t and h, where h is a (magnetic) field coupling linearly to the order parameter, f' takes the same form, only evaluated at rescaled scaling fields t' and h'. This gives us the scaling equation

$$f(t, h) = b^{-(d+z)} f(tb^{y_t}, hb^{y_h}) \tag{3.36}$$

for the free-energy density.

[15] Although ξ_τ would be more correctly described as a time scale, we will consistently treat is as an (imaginary-time) length scale.

To extract information about the thermodynamics, we must make a convenient choice of the scaling factor, namely $b = t^{-1/y_t}$. This sets the first argument of the left-hand-side function to unity, and we can express the free-energy density by a new, single-argument scaling function $\mathcal{F}_1(x)$ as

$$f(t,h) = t^{(d+z)/y_t}\mathcal{F}_1(ht^{-y_h/y_t}). \tag{3.37}$$

Which scaling fields that are included explicitly in the scaling equations above depends on the physics we are interested in studying. For instance, here we have implicitly set the physical temperature to $T = 0$.[16] In that case, the quantum analogue of the specific heat is found by differentiating $f(t, h = 0)$ twice with respect to the temperature-like scaling field t. The physical order parameter (magnetization) and susceptibility, on the other hand, is found by the appropriate first and second derivatives with respect to the magnetic field, respectively. Comparing with the definitions of C, m and χ from Table 3.1, we can write the associated critical exponents in terms of the scaling dimensions y_t and y_h:

$$\alpha = 2 - \frac{d+z}{y_t}, \tag{3.38}$$

$$\beta = \frac{d+z-y_h}{y_t}, \tag{3.39}$$

$$\gamma = \frac{2y_h - d - z}{y_t}. \tag{3.40}$$

Since these three exponents are expressed by only two scaling dimensions, they are not independent, but are related by the scaling relation

$$\alpha + 2\beta + \gamma = 2. \tag{3.41}$$

The correlation length exponent ν can be found separately by considering the scaling of the correlation length $\xi \sim t^{-\nu}$, and one can show that [73]

$$\nu = \frac{1}{y_t}. \tag{3.42}$$

Combining with Eq. (3.38) yields the so-called hyperscaling relation

$$2 - \alpha = (d+z)\nu. \tag{3.43}$$

Hyperscaling is known to break down in certain cases, typically in the mean-field regime above the upper critical dimension, $d > d_u$.

3.7.2 Scaling of correlation functions

To relate the anomalous dimension η to the other exponents, we next consider the spatiotemporal correlation function $g(r, \tau - \tau') = \langle \mathbf{s}_{\mathbf{r},\tau} \cdot \mathbf{s}_{\mathbf{r}',\tau'} \rangle$. Generalizing the

[16] We have also set to zero the interaction term of the ϕ^4-type field theory assumed to describe the critical point, which means that we will assume that hyperscaling is valid in all that follows.

classical critical correlation function (3.8) to the quantum case gives the scaling equation

$$g(r,\tau) = b^{-(d+z-2+\eta)} g(r/b, \tau/b^z). \tag{3.44}$$

As for the classical case, the anomalous scaling dimension η can be regarded as defined by the scaling dimension of g. Choosing the scaling factor as $b = r$ and $b = \tau^{1/z}$, respectively, we get the expressions

$$g(r,\tau) = 1/r^{d+z-2+\eta} \mathcal{G}_1(\tau/r^z), \tag{3.45}$$

$$g(r,\tau) = 1/\tau^{(d+z-2+\eta)/z} \mathcal{G}_2(r/\tau^{1/z}). \tag{3.46}$$

Equation (3.45) is convenient when considering purely spatial correlations [$g(r) \equiv g(r, \tau = 0)$], whereas Eq. (3.46) is the appropriate expression for purely temporal correlations [$g(\tau) \equiv g(r = 0, \tau)$].

Next, the correlation function can be related to the susceptibility through

$$\chi = \int_0^{L_\tau} \mathrm{d}\tau \int_0^{L} \mathrm{d}r\, r^{d-1} g(r,\tau). \tag{3.47}$$

Close to criticality, we can use the expression (3.45) for $r \ll \xi$ since the majority of the contribution to the integral comes from this regime, and

$$\chi \sim \int_0^{L_\tau} \mathrm{d}\tau \int_0^{L} \mathrm{d}r\, r^{d-1} 1/r^{d+z-2+\eta} \mathcal{G}_1(\tau/r^z). \tag{3.48}$$

By choosing the infinitesimal space-time shells we are integrating over in such a way that $\tau \propto r^z$, the scaling function $\mathcal{G}_1(\tau/r^z)$ is constant, and the space-time integral is simplified to an integral over r:

$$\chi \sim \int_0^{\xi} \mathrm{d}r\, r^z r^{d-1} 1/r^{d+z-2+\eta} = \xi^{2-\eta}. \tag{3.49}$$

Using $\xi \sim t^{-\nu}$ gives the expression $\chi \sim t^{-(2-\eta)\nu}$ for $t \to 0$, and identification with the definition $\chi \sim t^{-\gamma}$ from Table 3.1 gives us the scaling law

$$\gamma = (2-\eta)\nu. \tag{3.50}$$

Thus we can finally write also the anomalous dimension in terms of the scaling dimensions as

$$\eta = 2 + d + z - 2y_h. \tag{3.51}$$

A possible additional scaling relation relating the dynamical critical exponent and the anomalous dimension will be discussed in Sec. 4.3.2.

Here we will also make the observation that η is independent of y_t, ignoring any possible dependence via z, and only depends on (effective) dimensionality and the magnetic scaling dimension y_h. Using the scaling relations obtained in the previous section, we see that this is also the case for the exponent combinations β/ν and γ/ν. For the 2D XY model, this means that because the exponent η is well defined, so is y_h and thereby the combinations β/ν and γ/ν. The fact that the exponents β and γ themselves are formally infinite for the 2D XY model can be traced back to the thermal scaling dimension $y_t = 1/\nu$ being formally given by the limit $y_t \to 0$.

3.7.3 Finite-size scaling

We will now consider a general quantity A that in principle can be derived from the free-energy density and that scales as $A \sim t^{-\rho}$ as $t \to 0$. We will furthermore restrict ourselves to zero external field, but will include finite-size scaling fields L^{-1} and L_τ^{-1} in order to infer how the observable is influenced by the system dimensions. The thermodynamic limit of the (d+1)-dimensional system then corresponds to setting both these scaling fields to zero. The scaling equation is

$$A(t, L^{-1}, L_\tau^{-1}) = b^{\rho/\nu} A(tb^{y_t}, L^{-1}b, L_\tau^{-1}b^z). \tag{3.52}$$

The scaling dimension ρ/ν can be shown to be consistent with the stated behaviour for $t \to 0$ by setting the scaling factor to $b = t^{-1/y_t}$. Here we will instead choose $b = L$ to put Eq. (3.52) on the *finite-size scaling* (FSS) form

$$A(t, L, L_\tau) = L^{\rho/\nu} \mathcal{A}_1(tL^{1/\nu}, L_\tau/L^z). \tag{3.53}$$

Here we have inserted $\nu = 1/y_t$. Often we wish to extract ρ/ν by measuring A for increasing L at criticality. The above equation illustrates that it matters which aspect ratio we let the system have as it approaches the thermodynamic limit.

Assuming for simplicity that we can fix the second argument L_τ/L^z, we consider the influence of the only remaining argument of $\mathcal{A}_1$, namely $tL^{1/\nu}$. The behaviour of the scaling function will be that of a critical system for $t \to 0$, or, rather, for $t \ll L^{-1/\nu}$ in the case of a finite system. Rewriting the scaling argument in terms of the infinite-system correlation length $\xi = t^{-\nu}$, an equivalent condition is $\xi \gg L$. For values of $t \approx 0$ where a system appears to have a divergent correlation length due to its restricted extent and L is the only remaining length scale, we say that it is *pseudocritical*.

The finite-size scaling form can also be generalized to take into account irrelevant scaling fields that were implicitly set to zero in Eq. (3.53). Although these do not affect the exponent of the power law in the thermodynamic limit, they do in general influence the scaling behaviour and the extracted (effective) exponent for finite L. Assuming again that A derives from the free energy (or the correlation length), we can add to the scaling equation (3.36) a new scaling field h_i. It appears on the right hand side as an argument $h_i b^{y_i}$ with scaling dimension $y_i < 0$. One can show [103] that expanding the free-energy density around $h_i = 0$, calculating A and taking $t \to 0$, one generically gets a scaling form

$$A(t, L^{-1}, h_i) \approx L^{\rho/\nu}(1 + cL^{-\omega})\mathcal{A}_2(tL^{1/\nu}). \tag{3.54}$$

The exponent $\omega = -y_i > 0$ quantifies the corrections to scaling and c is a non-universal constant.

Finally, we include a concrete example of a finite-size scaling form that also will be useful later. Considering the magnetization m (with the exponent $\rho = -\beta$), neglecting any irrelevant scaling fields and again assuming that the second argument of Eq. (3.53) is constant, we have

$$\langle |m(t, L)| \rangle = L^{-\beta/\nu} \mathcal{M}(tL^{1/\nu}). \tag{3.55}$$

Setting $t = 0$ and fitting $\langle |m| \rangle$ as a function of L in logarithmic coordinates, we can find β/ν from the slope of the curve. A couple of more involved finite-size scaling techniques will be reviewed in Sec. 5.4.

3.7.4 Dynamical critical scaling

In order to describe more precisely the properties of the quantum critical region alluded to in the introduction, we will briefly discuss the scaling of dynamical quantities depending on momentum k and frequency ω. Assuming an infinite system and including a scaling field to also describe finite temperatures, the scaling equation is

$$A(t, k, \omega, T) = b^{\rho/\nu} A(tb^{y_t}, kb, \omega b^z, Tb^z). \tag{3.56}$$

If we first assume that we are not interested in the momentum argument, we can choose the scaling factor $b = T^{-1/z}$ to obtain

$$A(t, \omega, T) = T^{-\rho/z\nu} \mathcal{A}_3(L_\tau/\xi_\tau, \omega/T). \tag{3.57}$$

Here we have rewritten the first scaling argument using $\xi_\tau \sim t^{-\nu z}$ and $T \propto L_\tau^{-1}$. Sufficiently close to $K = K_c$, the zero-temperature temporal correlation length satisfies $\xi_\tau \gg L_\tau$, and the first scaling argument vanishes. One way to understand this is that the quantum critical region is a pseudocritical region with respect to imaginary time. One is then left with L_τ as the only imaginary-time length scale and T as the only energy scale.

Now including scaling with momentum, we assume that we are directly above the quantum critical point, $t = 0$, and choose a new scaling factor $b = \omega^{-1/z}$. The scaling form then can be written as

$$A(k, \omega, T) = \omega^{-\rho/z\nu} \mathcal{A}_4(k^z/\omega, \omega/T). \tag{3.58}$$

If the quantum critical point is a local quantum critical point, this would imply $z \to \infty$ so that the first argument of this scaling function vanishes for small k. The scaling function would then only depend on frequency and not on momentum,[17] in accordance with the MFL hypothesis.

3.8 Topological defects

When a system is subject to thermal or quantum fluctuations, one can often identify distinct features in the order parameter field – *topological defects* – that contribute to making it less ordered. The destruction of a phase with spontaneously broken symmetry can then be characterized as the *proliferation* of topological defects associated with this symmetry. For example, the disordering of the long-range-ordered phase of Z_q clock models can be explained as the proliferation of *domain walls* separating different domains of the q distinct states. One can often gain considerable physical insight if one is able to describe the phase transition in terms of such defect degrees of freedom instead of the original degrees of freedom.

[17] Assuming hyperscaling [104], the scaling function would only depend on ω/T.

3.8.1 Vortices

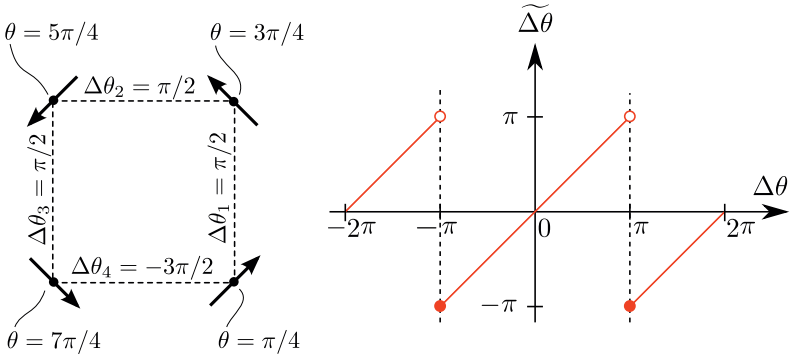

Figure 3.3: Cartoon of a vortex configuration, illustrating also how it is identified by calculating the vorticity of the plaquette it is situated in. Using Eq. (3.60) for a noncompact phase field, the phase differences $\Delta\theta_i$ sum up to $(\pi/2) + (\pi/2) + (\pi/2) + (-3\pi/2) = 0$. For a compact phase field, using compactified phase differences $\widetilde{\Delta\theta}$, the last phase difference $\Delta\theta_{i=4} = -3\pi/2$ has to be put back into the primary interval $[-\pi, \pi\rangle$, so that the sum over $\widetilde{\Delta\theta}_i$ becomes $4 \times (\pi/2) = 2\pi \neq 0$.

Topological defects can describe the phase transition even when there is no broken-symmetry phase to destroy, as is the case for the KT transition of the 2D XY model. In this case the topological defects are *vortices* associated with 2π phase windings of the compact $U(1)$ order parameter field $\theta(\mathbf{r})$. In the QLRO phase the vortices are bound in pairs of opposite vorticity, and these pairs unbind when the coupling is lowered beneath the critical endpoint K_c of this phase. Figure 3.3 shows a cartoon of a possible vortex configuration and illustrates how this topological defect is inherently connected to the compactness of the phase field. The vorticity of a region of the phase field is defined as the curve integral

$$\oint_C \nabla\theta \cdot \mathrm{d}\mathbf{r} = 2\pi m, \tag{3.59}$$

where m is an integer-valued vortex charge that is $m = 1$ when the curve C encircles a vortex and $m = -1$ when C encircles an anti-vortex. Were the phase field noncompact instead of compact, one would always get $m = 0$, and there would be no vortices. This can be seen on a square lattice, as illustrated in Fig. 3.3, by calculating Eq. (3.59) as a sum of the discrete (noncompact) phase differences $\Delta\theta$ of the four links. This gives

$$\oint_C \nabla\theta \cdot \mathrm{d}\mathbf{r} = \sum_{i=1}^{4} \Delta\theta_i = 0, \tag{3.60}$$

as the contributions inevitably cancel. For a compact field, on the other hand, phase differences are only defined in a meaningful way modulo 2π, so we replace $\Delta\theta$ in Eq. (3.60) by the *compactified* phase difference $\widetilde{\Delta\theta}$ restricted to the *primary interval*

$[-\pi, \pi\rangle$. The compactification mapping $\Delta\theta \to \widetilde{\Delta\theta}$ is shown in Fig. 3.3. This way to think about compactness has major implications for the treatment of certain dissipative models in Sec. 4.4.3.

We mention in passing that in three dimensions, the relevant topological defects are the higher-dimensional counterparts of point vortices of the 2D XY models, namely vortex loops.

3.8.2 The helicity modulus

As the coupling is lowered and vortices or vortex loops proliferate, the stiffness of the phase field is reduced dramatically. In the language of superconducting systems, this is equivalent with a loss of superconducting phase coherence, or one may instead speak of spin stiffness if the physical context is a system of planar spins. As a generic term, we will refer to the phase stiffness as the *helicity modulus*, Υ. It is defined by the free-energy cost of a phase twist $\Theta = L\delta\theta$ across the system [105],

$$\Upsilon = \frac{\partial^2 f}{\partial(\delta\theta)^2}, \tag{3.61}$$

in the limit of $\delta\theta \to 0$. In contrast to magnetization, this quantity is a global order parameter, as alluded to in Sec. 3.3.4. This means that it also takes finite values in the QLRO phase of the 2D XY model, as well as in the LRO phase of the 3D XY model.

A scaling equation analogous to Eq. (3.52) can be constructed for this quantity by noting that the phase twist $\delta\theta$ one differentiates with respect to scales as the inverse of the system size and therefore has scaling dimension $y_{\delta\theta} = 1$ [72]. As before, we also assume the scaling dimension $d+z$ for the free-energy density, and the finite-size scaling form is therefore

$$\Upsilon(t, L, L_\tau) = L^{-\kappa}\mathcal{Y}(tL^{y_t}, L_\tau/L^z), \tag{3.62}$$

with $\kappa = d + z - 2$.[18] This means that when the effective dimensionality of the system is $d+z > 2$, $\kappa > 0$, and the helicity modulus vanishes at the critical point in the thermodynamic limit. This is the case for the 3D XY model. For $d+z = 2$, on the other hand, the helicity modulus does not vanish, which is to say that there is a discontinuous jump at the transition point. This is regarded as one of the hallmarks of the KT transition in the 2D XY model.

Although Eq. (3.62) indicates that Υ does not scale with the system size at $K = K_c$, a scaling dimension $\kappa = 0$ is in this case an expression of a logarithmic dependence of Υ on L. To be concrete, the finite-size scaling function for the helicity modulus of a classical system has been shown to be [106]

$$\Upsilon(K = K_c, L) = \Upsilon(K = K_c, L = \infty)\left(1 + \frac{1}{2}\frac{1}{\ln L + C}\right), \tag{3.63}$$

[18] Since hyperscaling was already assumed for the scaling of f, we could equivalently write $\kappa = 2\beta/\nu - \eta$, using Eqs. (3.41), (3.43), and (3.50).

where C is a constant. Curve fitting to this functional form has proved useful in locating the transition point $K = K_c$ of such a transition.

3.8.3 Other topological defects

We will now mention some other topological defects that will make appearances throughout this thesis. All these examples are illustrated in Fig. 3.4.

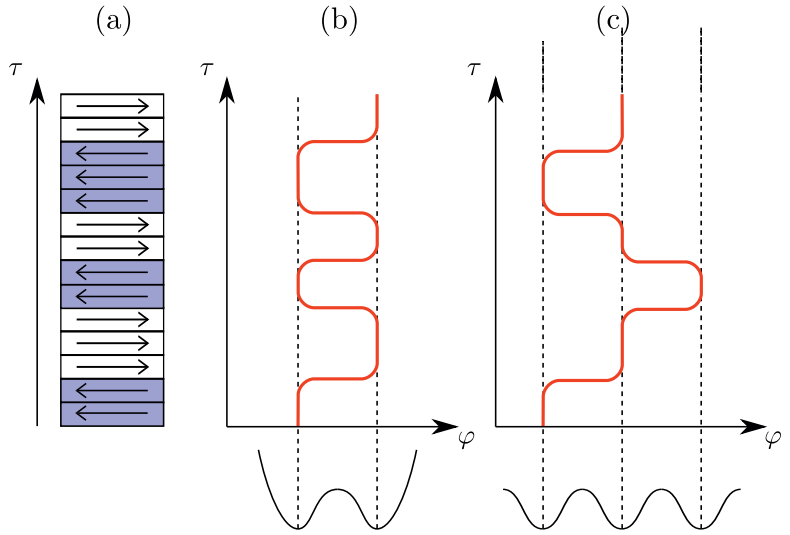

Figure 3.4: Cartoon of three different topological defects: a) Kinks and anti-kinks associated with the reversal of spin direction for a Z_2 spin chain. b) Instantons and anti-instantons in a two-well potential $V_1(\varphi)$. c) Instantons and anti-instantons in an extended periodic potential $V_2(\varphi)$. All the models are defined in one space-time dimension, which is here taken to be imaginary time, τ. The shape of the potentials $V_1(\varphi)$ and $V_2(\varphi)$ are indicated below configuration (b) and (c), respectively.

Just as the transition of the 2D XY model can be understood from the binding of vortices and anti-vortices, the inverse-square Ising chain is described analogously by interacting kinks and anti-kinks [107]. These are topological defects located at the points along the chain where the Ising spins flip from pointing in one direction to the other, and their proliferation restores the Ising symmetry of the model. If one generalizes the Z_2 field to a continuous field with a two-well potential, one gets the continuum version of the kinks, which are the *instantons*. Generalizing further to a periodic potential, one gets instanton configurations along the chain where an instanton can be followed by another instanton and not necessarily an anti-instanton. In the two-well potential, proliferation of instantons destroys the localization of the configuration to one well or the other, which is again associated with the Z_2 symmetry. The same localization picture applies to the periodic potential, but in this case proliferation of instantons is more loosely associated with the restoration of the translational symmetry of the potential.

4 Quantum models with damping and dissipation

When studying a physical phenomenon, it is usually desirable to separate the system of interest from the rest of the universe – the environment – and base the description solely on the system degrees of freedom. Very rarely is the system truly in isolation, and often it is subject to frictional effects that dissipate energy from the system to the environment. In quantum mechanics, such damping generally suppresses quantum tunnelling effects and reduces quantum coherence for the system degrees of freedom. These degrees of freedom may be virtually any set of variables describing a condensed-matter system, and concrete examples of environments are metallic electrons, normal quasiparticles, electromagnetic modes, phonon modes or magnetic fluctuations.

A theory in terms of system degrees of freedom only may still be possible if one is able to integrate out the environmental degrees of freedom, which is the approach we will follow below.

4.1 The Caldeira-Leggett model

What is commonly called the Caldeira-Leggett model [108, 109] is a phenomenological framework for emulating the effect of damping on a quantum system by coupling it to an infinite number of harmonic oscillators. This reservoir can be taken to represent the environment of the system, and is also referred to as a bosonic bath or a heat bath. The result is that a new term appears in the quasiclassical equation of motion for the system that may, depending on the details of the bath, be interpreted as a friction term. In this sense, dissipation has been introduced in the system.

Since the model was originally motivated by quantum phenomena of macroscopic systems, we will define φ as some (in principle) observable generalized coordinate describing an (in principle) distinguishable state of such a system. If we think of the system as a quantum particle with mass M living in a potential $V(\varphi)$, our starting point will be the following action:

$$S_{\mathrm{S}}[\varphi] = \int_0^\beta \mathrm{d}\tau \left[\frac{1}{2} M \left(\frac{\partial \varphi}{\partial \tau} \right)^2 + V[\varphi] \right]. \tag{4.1}$$

In the Caldeira-Leggett model, one then adds to this system a bath of harmonic oscillators,

$$S_{\mathrm{B}}[x_\nu] = \int_0^\beta \mathrm{d}\tau \sum_\nu \left[\frac{1}{2} m_\nu \left(\frac{\partial x_\nu}{\partial \tau} \right)^2 + \frac{1}{2} m_\nu \omega_\nu^2 x_\nu^2 \right], \tag{4.2}$$

each of which is coupled linearly to the system coordinate by the interaction term

$$S_{\mathrm{SB}}[\varphi, x_\nu] = \int_0^\beta \mathrm{d}\tau \sum_\nu \left[-c_\nu x_\nu \varphi + \frac{c_\nu^2 \varphi^2}{2 m_\nu \omega_\nu^2} \right]. \tag{4.3}$$

Above, m_ν, ω_ν and c_ν is the mass, frequency and coupling strength of the bosonic mode ν, respectively. The distributions of these parameters are in general left undetermined, but with regard to their effect on the system coordinate, the bath parameters are characterized uniquely by the spectral density [110]

$$J(\omega) = \frac{\pi}{2} \sum_\nu \frac{c_\nu^2}{m_\nu \omega_\nu^2} \delta(\omega - \omega_\nu). \tag{4.4}$$

The case that is most commonly studied – and also most widespread in nature – is that of *Ohmic* dissipation. This is the case where m_ν, ω_ν and c_ν are chosen such that $J(\omega) \sim \omega$ for small ω, which introduces a friction term in the equation of motion that is proportional to the rate of change of the coordinate φ. Generalizing the low-frequency spectral density to a power law with an arbitrary bath exponent s, we define

$$J(\omega) = 2\pi\alpha\omega^s \omega_c^{1-s} \tag{4.5}$$

below a cutoff frequency ω_c, while $J(\omega) = 0$ for $\omega > \omega_c$. The Ohmic case then corresponds to a bath exponent $s = 1$, and the cases $s < 1$ and $s > 1$ are referred to as *sub-Ohmic* and *super-Ohmic* dissipation, respectively.

The next step in the procedure is to generate an effective action for the system by integrating out the bosonic modes. Since the harmonic oscillator bath is represented by a Gaussian theory, this can be done exactly, and we refer to Refs. [109, 111, 112] for details of the calculations. The end result is that the bath gives rise to a non-local term

$$S_{\mathrm{diss}}[\varphi] = \frac{1}{2} \int_0^\beta \mathrm{d}\tau \int_0^\beta \mathrm{d}\tau' \, K(\tau - \tau') \left[\varphi(\tau) - \varphi(\tau') \right]^2 \tag{4.6}$$

in the action. This additional interaction in imaginary time is characterized by the dissipation kernel

$$K(\tau - \tau') = \frac{1}{\pi} \int_0^\infty \mathrm{d}\omega \, \frac{J(\omega)}{\omega} \frac{1}{\beta} \sum_n \left[1 - \frac{\omega_n^2}{\omega_n^2 + \omega^2} \right] \mathrm{e}^{-\mathrm{i}\omega_n(\tau - \tau')}. \tag{4.7}$$

When we insert the spectral density (4.5), the effective action becomes

$$\begin{aligned} S[\varphi] = &\int_0^\beta \mathrm{d}\tau \left[\frac{1}{2} M \left(\frac{\partial \varphi}{\partial \tau} \right)^2 + V[\varphi] \right] \\ &+ \frac{\alpha}{2} \int_0^\beta \mathrm{d}\tau \int_0^\beta \mathrm{d}\tau' \left(\frac{\pi}{\beta} \right)^{1+s} \frac{[\varphi(\tau) - \varphi(\tau')]^2}{\sin^{1+s}(\pi/\beta|\tau - \tau'|)}. \end{aligned} \tag{4.8}$$

We see that in the imaginary-time representation, dissipation appears in the form of a memory effect, and the system interacts with all "past" and "future" instances of itself.

4.2 The spin-boson model

If the damped quantum particle described in the previous section lives in a double-well potential, the description can be reduced to that of the dissipative two-state system, also called a *spin-boson model* [110]. As the name suggests, this model can be expressed as a quantum spin $\hat{\boldsymbol{\sigma}}$ in a transverse magnetic field $\mathbf{h} = h_x\hat{\mathbf{x}}$ (see Sec. 3.6.1) where the generalized coordinate φ that is coupled to a bath of harmonic oscillators (bosons) is the Ising spin $\sigma \equiv \sigma^z \in \{-1, 1\}$:

$$\hat{H} = -h_x\hat{\sigma}^x + \sum_\nu \left(\frac{\hat{p}_\nu^2}{2m_\nu} + \frac{1}{2}m_\nu\omega_\nu^2\hat{x}_\nu^2 \right) + \hat{\sigma}^z \sum_\nu c_\nu\hat{x}_\nu. \tag{4.9}$$

Here $\hat{x}_\nu$ and $\hat{p}_\nu$ are the coordinate operator and its canonical conjugate (momentum operator), respectively.

The spin-boson model is paradigmatic in the sense that it provides a very simple representation of dissipation that nevertheless exhibits very rich behaviour and that is applicable to a wide range of subfields of physics [113]. We will regard several of the dissipative models considered in this thesis as generalizations of the simple spin-boson model where either the dimensionality is increased from $d = 0$ or the symmetry is elevated from Z_2.

We now apply the quantum-to-classical mapping of Sec. 3.6.1 to the $L = 1$ transverse-field Ising model of Eq. (4.9). Adopting the representation (4.8) of the effect of dissipation, we obtain the action of a classical Ising chain with long-range interactions [114]:

$$S[\sigma] = -K_\tau \sum_{\tau=1}^{L_\tau} \sigma_\tau\sigma_{\tau+1} + \frac{\alpha}{2} \sum_{\tau\neq\tau'}^{L_\tau} \left(\frac{\pi}{L_\tau} \right)^{1+s} \frac{(\sigma_\tau - \sigma_{\tau'})^2}{\sin^{1+s}(\frac{\pi}{L_\tau}|\tau - \tau'|)}. \tag{4.10}$$

These interactions decay as $\sim 1/\tau^{1+s}$ in imaginary time τ in the limit $L_\tau \to \infty$. Accordingly, the results presented for the inverse-square Ising chain in Sec. 3.5 can to a large extent be carried directly over to the spin-boson model. In particular, for $s = 1$ it undergoes a KT-like QPT from a delocalized to a localized phase when increasing dissipation across a threshold value α_c.

From the discussion of Sec. 3.5, we would expect a sub-Ohmic spin-boson model to have mean-field behaviour for $s < 1/2$, since the equivalent long-range-interacting Ising chain then would be above its upper critical dimension. It was therefore a cause of much surprise when non-mean-field exponents were reported for the $s < 0.5$ spin-boson model in 2005 [115], and the years that followed have seen an intensi-

fied interest in similar models.[1] For super-Ohmic dissipation, $s > 1$, the spin-boson model does not undergo a transition to a localized state when increasing the dissipation strength, and the reasons are the same as for the classical analogue discussed in Sec. 3.5.

4.3 Spatially extended dissipative systems

For a (0+1)D dissipative system such as the spin-boson model of Eq. (4.10), there is no sense in introducing an independent dynamical critical exponent. The question of how dissipation affects the exponent z becomes relevant first when considering spatially extended systems. In this thesis, we will consider (d+1)D generalizations of actions similar to Eq. (4.10) where one can view each spin as coupled to its own bosonic bath. To make the discussion as general as possible, we will assume that we can describe such a system by a ϕ^4-type order parameter field theory with quadratic part of the critical action on the form [102]

$$S_0 = \frac{1}{2}\sum_{\mathbf{q},\omega}(q^2 + \omega^2 + |\omega|^s)|\phi_{\mathbf{q},\omega}|^2 \equiv \frac{1}{2}\sum_{\mathbf{q},\omega} G_0^{-1}(\mathbf{q},\omega)|\phi_{\mathbf{q},\omega}|^2. \tag{4.11}$$

This is the usual Landau-Ginzburg-Wilson representation, with G_0 being the bare propagator and $\phi_{\mathbf{q},\omega}$ being the fields representing the local order parameter. We assume spatial isotropy, and we define $q = |\mathbf{q}|$. Fourier transformation of spatial nearest-neighbour interactions gives the q^2 term, the assumed equivalent kinetic term gives ω^2, and $|\omega|^s$ arises from the Fourier transform of the $\sim 1/\tau^{1+s}$ damping term, or, equivalently, from a bosonic spectral density $J(\omega)$. We omit all prefactors in the propagator and also a possible constant term representing the distance from criticality.

4.3.1 Estimates of the dynamical critical exponent

We are interested in a transition to a state with spatiotemporally uniform order of the field $\phi_{\mathbf{q},\omega}$, and to study the contributions from long-range fluctuations that are dominant at criticality, we consider the limit $q \to 0$. At the same time, we need to take the limit $\omega \to 0$ to consider only modes with appropriately low energies corresponding to low momenta q. To ensure that $(q,\omega) = (0,0)$ is approached uniformly for all (the dominant) terms in the action, we fix $\omega \sim q^z$. Introducing a non-trivial dynamical critical exponent z in this manner in a scaling analysis of a damped quantum field theory was first done in the pioneering work of Hertz [102]. In terms of momentum, the propagator then takes the form

$$G_0^{-1}(q) = q^2 + q^{2z} + q^{sz}, \tag{4.12}$$

[1] The original claim was later retracted [116], but it is still controversial whether or not quantum-to-classical mapping can be applied to the spin-boson model and related quantum models for all values of $s \leq 1$ [117].

and the behaviour of the various terms as $q \to 0$ is illustrated in Fig. 4.1. We observe that for all $s < 2$, the kinetic term q^{2z} will always scale to zero faster than both the spatial term q^2 and the dissipation term q^{sz}. This means that the kinetic term is subdominant and cannot influence the behaviour of the critical singularity $q \to 0$ of the propagator, hence it will be neglected.[2] For the two remaining terms, one then asks what value of z makes them balance so that they approach zero uniformly at the singularity. Requiring $q^2 \sim q^{sz}$ readily leads us to the scaling estimate $z = 2/s$ for the dynamical critical exponent. The corresponding balance of terms for $s > 2$ would be $q^2 \sim q^{2z}$, giving $z = 1$, and a formula valid for all s would be

$$z = \max\left\{\frac{2}{s}, 1\right\}. \tag{4.13}$$

We will refer to this formula as the *naive scaling estimate* for the dynamical critical exponent. Note that this estimate makes no reference to the dimensionality or the order parameter symmetry of the system.

For such *site-dissipative* (having q-independent damping, that is) models as Eq. (4.11), a more careful field-theoretical study [118] found dynamical critical scaling $z = 2 - \eta$ in the Ohmic case $s = 1$. This was also confirmed by large-scale Monte Carlo studies of (1+1)D spin chains, with the anomalous dimension being $\eta \approx 0.015$ both in the case of Ising spins [119] and XY spins [120]. This means that the naive scaling estimate is a good approximation, and one of the aims of this thesis is to see how general this result is.

Next, we generalize the dissipation term to also include spatial dependence given by a momentum-dependent factor $\Gamma_{\mathbf{q}}$. Restricting ourselves to Ohmic dissipation, we have the inverse propagator

$$G_0^{-1}(\mathbf{q}, \omega) = q^2 + \omega^2 + \Gamma_{\mathbf{q}}|\omega|. \tag{4.14}$$

Dissipation of *bond* variables instead of site variables gives an additional factor $\Gamma_{\mathbf{q}} \propto q^2$, so that the dissipation term scales as $q^2|\omega| \sim q^{2+z}$ when we require $\omega \sim q^z$. The exponent $2 + z$ is larger than those of the spatial and kinetic terms for all $z > 0$, making the dissipation term subdominant as $q \to 0$. Therefore, a naive scaling estimate would predict that bond dissipation is irrelevant, so that $z = 1$.[3] This is illustrated in the last panel of Fig. 4.1.

4.3.2 Scaling relations for non-Ohmic dissipation

The naive scaling estimate (4.13) can be regarded as a mean-field scaling relation, assuming $\eta = 0$. Reducing the effective dimensionality of the system to $d + z \ll 4$ by

[2] As we will discuss in Sec. 4.3.2 and paper II, it turns out that the kinetic term may actually dominate the dissipation term even for $s < 2$ if the distance $|2 - s|$ is sufficiently small,.

[3] Another prevalent case in condensed-matter systems is $\Gamma_{\mathbf{q}} \propto 1/q$, or a damping term $\propto |\omega|/q$. This is often referred to as Landau damping and arises generically from the coupling of a bosonic $q = 0$ order parameter field to particle-hole excitations on the Fermi surface [102, 121]. The naive scaling estimate in this case is $z = 3$.

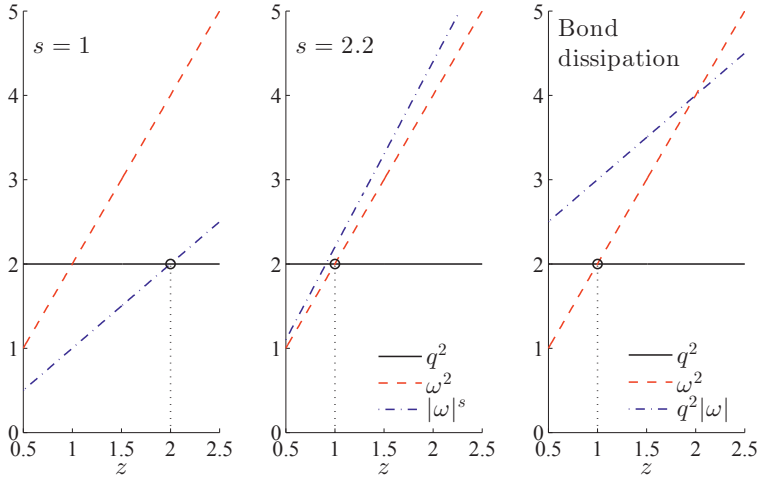

Figure 4.1: Naive scaling of the three terms of the inverse bare propagator appearing in Eq. (4.12). The exponents of the terms are plotted for possible values of the dynamical critical exponent z, and the (naive estimate of the) actual value of z is indicated by the vertical dotted line, which marks the crossing of the two lowest curves. The two first panels (with shared legends) are for site dissipation with two illustrative values of the bath exponent s, whereas the rightmost panel is for bond dissipation.

increasing s, η might be expected to increase, eventually making Eq. (4.13) a bad approximation in the super-Ohmic regime.

Naive scaling also predicts that the long-range-interacting dissipation term is rendered irrelevant at $s = 2$. In analogy to the isotropic long-range-interacting systems discussed in Sec. 3.5, one might however expect that long-range interactions instead become irrelevant already at $s = s^* \equiv 2 - \eta_{\mathrm{SR}}$.[4] If this is the case, one also expects the anomalous dimension to take its short-range value $\eta = 2 - \eta_{\mathrm{SR}}$ for $s \geq s^*$.

A scaling relation between z and η that is consistent with this behaviour for large s, and that is also consistent with the relation $z = 2 - \eta$ for $s = 1$, is the scaling ansatz

$$z = \max\left\{\frac{2-\eta}{s}, 1\right\}. \tag{4.15}$$

This relation is compared with naive scaling in Fig. 4.2. If valid, this would be yet another scaling law relating the various critical exponents, and it would imply that the dynamical critical exponent – like the anomalous dimension – is independent of the thermal scaling dimension y_t. Numerical results and heuristic arguments substantiating the above ansatz are presented in paper II and will also be discussed in Sec. 6.1.3.

[4] This is not entirely obvious due to the anisotropy of the interactions in the dissipative case, which is why we investigated the issue numerically in paper II.

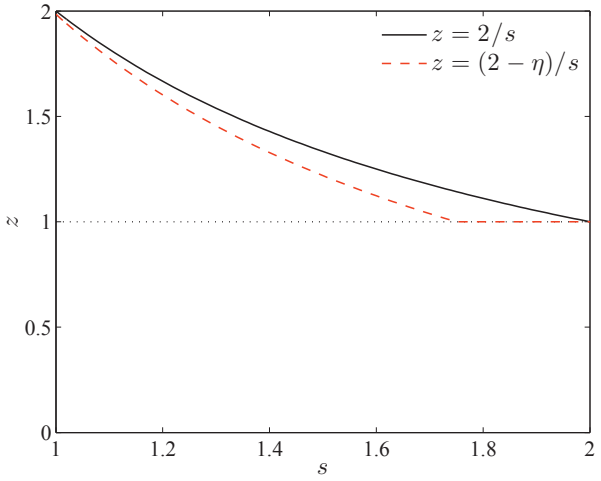

Figure 4.2: Comparison of naive scaling estimate for the dynamical critical exponent, $z = 2/s$, with a scaling ansatz including corrections due to a finite anomalous dimension η. The values of η are assumed to follow a linear function interpolating between $\eta(s = 1) \approx 0.015$ and $\eta(s \geq 1.75) = 0.25$, assuming a (1+1)D model. (Such an approximate functional form seems to be supported by the numerical data shown in Fig. 2 of paper II.) For both formulas, $z \geq 1$ is implicit.

4.4 Resistively shunted Josephson junctions

The original motivation of the Caldeira-Leggett model was the macroscopic quantum tunnelling of a magnetic flux out of a SQUID where the Josephson junction is resistively shunted. The model was applied to a double-well potential – which reduces to the two-state model discussed above – soon thereafter [114, 122], followed by the case of a periodic (cosine) potential [123, 124]. This latter case can be interpreted as the energy potential of a Josephson junction, with the phase difference $\Delta\theta$ itself taking the role of the dissipative variable φ.

We are interested in systems that can be modelled as arrays of superconducting elements connected by resistively shunted Josephson junctions. Looking at each of these superconducting islands or grains in isolation, they can be described as quantum rotors where the superconducting phase is analogous to a particle living on a ring. Although the model we study in paper V is precisely that of a Josephson junction array, the very similar models investigated in papers III and IV are instead regarded as generalized quantum rotor systems. For this reason, we will begin by introducing quantum rotors and their relation to superconducting systems.

4.4.1 Quantum rotors and superconducting islands

A quantum particle rotating on a ring with an angular coordinate θ is described by the Hamiltonian

$$\hat{H} = \frac{\hat{L}_z^2}{2I} = -\frac{1}{2I}\frac{\partial^2}{\partial\theta^2} \tag{4.16}$$

in the absence of an energy potential. Here I is the inertia of the system, and we have used the form

$$\hat{L}_z = \frac{1}{\mathrm{i}}\frac{\partial}{\partial\theta} \tag{4.17}$$

of the angular momentum operator in the angle representation.

The partition function of this quantum Hamiltonian can be recast in the form of an imaginary-time path integral through a quantum-to-classical mapping similar to that of the spin chain in Sec. 3.6.1. The details can be found in Refs. [96, 101] and are also reproduced in the appendix of paper III. The central point is that the indistinguishability of θ and $\theta + 2\pi$ restricts which basis states we are allowed to insert to form the transfer matrices, and this leads to a periodic imaginary-time interaction term

$$S[\theta] = -\sum_{\tau=1}^{L_\tau}\left[\frac{I}{\Delta\tau}\,\cos\left(\theta_{\tau+1} - \theta_\tau\right)\right] \tag{4.18}$$

between the (discrete) Trotter slices. This result of the compactness of the phase field is analogous to how the discreteness of a Josephson junction enforces a periodic supercurrent $\propto \sin(\Delta\theta)$ instead of $\propto \Delta\theta$. In effect, the quantum rotor has in Eq. (4.18) been mapped to a (classical) (0+1)D XY model. The shorthand continuum expression for this kinetic term is

$$S[\theta] = \int_0^\beta \mathrm{d}\tau\left[\frac{I}{2}\left(\frac{\partial\theta}{\partial\tau}\right)^2\right], \tag{4.19}$$

where one has to keep in mind that the differentiation has to be defined on a ring.

Consider next a small superconducting island containing N charges. We will now show how this system can be treated analogously to the above quantum rotor. A Hamiltonian that includes only the electrostatic energy associated with the capacitance C with respect to ground is

$$\hat{H} = \frac{\hat{Q}^2}{2C}. \tag{4.20}$$

The charge operator is written as $\hat{Q} = Q_0\hat{N}$, where Q_0 is the charge of a single particle; $Q_0 = 2e$ in the case of Cooper pairs. The charge number operator is denoted $\hat{N}$, and, being conjugate to the phase operator, it takes the same form as the angular momentum operator (4.17). Thus we get

$$\hat{H} = -\frac{Q_0^2}{2C} = \frac{E_C}{2}\frac{\partial^2}{\partial\theta^2}, \tag{4.21}$$

where we have introduced an energy scale $E_C = Q_0^2/C$. This quantity represents twice the charging energy associated with moving an additional charge Q_0 onto the

island. The quantum-to-classical mapping goes through just as before, yielding the standard kinetic term of the action,

$$S[\theta] = \int_0^\beta \mathrm{d}\tau \left[\frac{1}{2E_C} \left(\frac{\partial \theta}{\partial \tau} \right)^2 \right]. \tag{4.22}$$

4.4.2 The resistively shunted Josephson junction

The quantum rotor action is conventionally applied to a Josephson junction by replacing the phase θ (for a single superconducting island) by the phase difference $\Delta\theta$ (between two islands) as the dynamical variable. This comes about if one assumes that the dominating contribution to the electrostatic energy is from mutual capacitance and not self-capacitance as assumed above. Including the Josephson potential $V(\Delta\theta) \propto \cos(\Delta\theta)$, the model could in principle describe both a pendulum realization of the quantum rotor and a quantum particle in a periodic potential [125]; $\Delta\theta$ will be compact in the first case, whereas in the second case it can reasonably be regarded as an extended (noncompact) variable. We here take the second point of view for the phase difference of the Josephson junction and explain the interpretation in more detail in Sec. 4.4.3.

Before adding dissipation, we comment on the nature of the quantum fluctuations in this system. In analogy with the transverse magnetic field h_x for the case of Ising degrees of freedom, the parameter that induces quantum fluctuations in the phase degree of freedom is the charging energy E_C. Decreasing the intergrain capacitance C increases the energy barrier $\propto E_C$ for charge transfer between the superconducting grains, effectively localizing the charges. This means that the conjugate phase variables are subject to large quantum fluctuations, which also manifests as a small quantum coupling $K_\tau \propto 1/E_C$ of the kinetic term. Particularly violent phase fluctuations come in the form of *phase slips*, where the imaginary-time path of $\Delta\theta$ makes abrupt jumps, of the order of a multiple of 2π, from one minimum of the Josephson potential to another. Such configurations are related to the instanton topological defects introduced in Sec. 3.8.3.

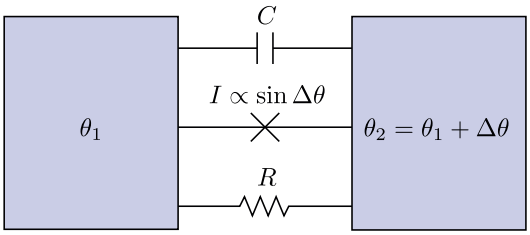

Figure 4.3: Schematic of a resistively shunted Josephson junction, with circuit elements from top to bottom being a capacitor, a Josephson junction, and a resistor.

Coupling a metallic shunt with resistance R in parallel to the junction as shown in Fig. 4.3, we can write the Caldeira-Leggett action of this resistively shunted Josephson junction (RSJJ) as [126]

$$S[\Delta\theta] = \int_0^\beta \mathrm{d}\tau \left[\frac{1}{2E_c} \left(\frac{\partial \Delta\theta}{\partial \tau} \right)^2 - K \cos\left(\Delta\theta\right) \right] + \frac{1}{8\pi^2} \frac{R_Q}{R} \int_0^\beta \mathrm{d}\tau \int_0^\beta \mathrm{d}\tau' \left(\frac{\pi}{\beta} \right)^2 \frac{\left[\Delta\theta(\tau) - \Delta\theta(\tau')\right]^2}{\sin^2\left(\pi/\beta|\tau - \tau'|\right)}. \tag{4.23}$$

Here $R_Q = \pi/2e^2$ is the resistance quantum, and the dimensionless dissipative coupling is usually defined as $\alpha = R_Q/R$. Assuming that a junction experiences strong quantum phase fluctuations, shunting it in this manner may stabilize superconductivity by the following mechanism. At the occurrence of a quantum phase slip, the second Josephson relation (2.3) dictates that a voltage difference V develops across the junction. Given a finite shunt resistance $R < \infty$, a dissipative current V/R goes through the shunt, and the corresponding resistive energy cost $\propto V^2/R$ enforces damping of the phase dynamics. In this way, decreasing the resistance R amounts to strengthening the dissipation, which in turn increases the phase coherence across the junction.

Lowering the resistance below $R = R_Q$ so that the dissipation strength increases beyond $\alpha = \alpha_c = 1$, the RSJJ model is known to undergo a dissipation-driven quantum phase transition where phase slips are suppressed and the phase difference $\Delta\theta$ localizes in one of the minima of the periodic potential [123]. This localization transition is different from the disorder-to-order transition associated with localization in the spin-boson-model, where a Z_2 symmetry was spontaneously broken. For an RSJJ, the $U(1)$ symmetry associated with the primary interval of $\Delta\theta$ is already broken explicitly by the Josephson potential, and one must characterize the localization transition with some other observable than the usual order parameter. This has been done in Monte Carlo studies in Refs. [127, 128, 129], confirming the theoretical picture.

4.4.3 Decompactification of the phase variable

That the initially compact phase difference $\Delta\theta$ was treated as a noncompact variable in Eq. (4.23) can be justified on several levels. One is to simply observe that the dissipation term is not a 2π-periodic function of $\Delta\theta$ in the same way as the Josephson potential [or the kinetic term (4.18)], and so it no longer makes any sense to assert that $\Delta\theta$ only is defined modulo 2π [126].

A more physical argument is based on the assumption that the dissipative variable φ introduced in Sec. 4.1 should describe distinguishable states. A phase slip event $\Delta\theta \to \Delta\theta + 2\pi$, the argument goes [130], results in a voltage drop across the junction due to the second Josephson relation, Eq. (2.3). In the presence of resistive shunting, this leads to a measurable, dissipative current through the shunt. (In the absence of a shunt, the voltage difference would not be measurable.) Therefore, $\Delta\theta$ and $\Delta\theta + 2\pi$

are distinguishable states and $\Delta\theta$ cannot be treated as a compact variable.[5]

If one is to take the noncompactness of the phase difference seriously, one should reconsider the quantum-to-classical mapping outlined in Sec. 4.4.1. We take as our starting point the rotor Hamiltonian (4.16), but assume that the Hamiltonian also contains other terms coupling the rotor phase θ linearly to harmonic oscillators. The variable θ then should be treated as noncompact from the outset, and the restriction on the basis states for the compact case no longer applies. The mapping then proceeds somewhat differently, as explained in more detail in the appendix of paper III, and one ends up with a kinetic term in the classical action on the form

$$S[\theta] = \sum_{\tau=1}^{L_\tau} \left[\frac{I}{2\Delta\tau} \ (\theta_{\tau+1} - \theta_\tau)^2 \right] . \tag{4.24}$$

This interaction between (discrete) Trotter slices clearly differs from the compact expression (4.18).

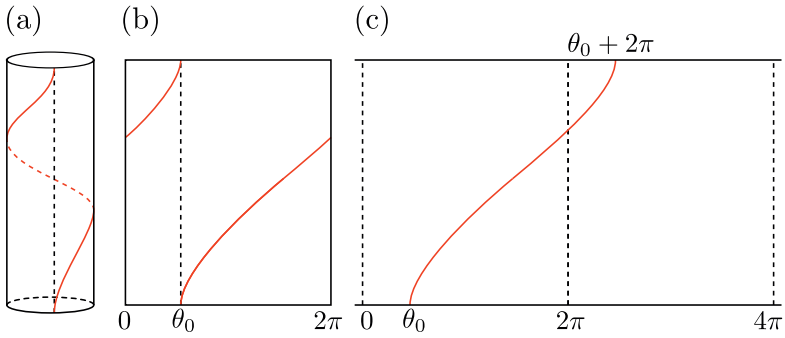

Figure 4.4: Decompactification of the phase variable θ: Figure (a) shows the (continuous) imaginary-time path of a phase variable defined on a ring, and in figure (b) this ring is "unwrapped" onto the interval $[0, 2\pi\rangle$. In figure (c) the phase variable has been decompactified and is thus defined on a line instead of on a ring.

An intuitive way to understand the distinction is to consider the difference between the imaginary-time path $\theta(\tau)$ for compact and noncompact phases as illustrated in Fig. 4.4. For the compact case shown in panel (b), it is natural to define the discretized imaginary-time derivative of $\theta(\tau)$ by finite differences that are periodic under translations of 2π. For the noncompact case in panel (c), this is no longer necessary in order to have a smooth derivative along the path, and the derivative can be defined by ordinary finite differences.

[5] It now seems to be universally recognized that noncompact variables are appropriate for the RSJJ, but the early literature presents some alternative views. Whereas Ref. [125] argues for a noncompact $\Delta\theta$ for a current-biased junction even in the absence of dissipation, Refs. [109, 124] regard the minima of the Josephson potential as fundamentally indistinguishable. In [131] it is also argued that for such compact phase variables, one can only allow a dissipative variable φ that is itself a 2π-periodic function of the phase to couple to the bosonic bath.

4.4.4 Dissipative Josephson junction arrays

Stringing together terms as in Eq. (4.23) for a number of superconducting islands connected to their neighbours by resistively shunted Josephson junctions, one obtains an action for a dissipative Josephson junction array [132, 133]. There are, however, a few subtleties to take into account. First, one must decide whether one includes self-capacitance, mutual capacitance, or both. Second, assuming that self-capacitance is not neglected altogether, one should realize that one now has a system with genuine *bond dissipation*, and not site dissipation. This means that the dissipation term only couples bond variables $\Delta\theta_{\mathbf{r},\mathbf{r}'}$ in imaginary time whereas the kinetic term couples site variables $\theta_{\mathbf{r}}$. (For the single junction with mutual capacitance only, both terms couple the bond variable $\Delta\theta$, making the system effectively site dissipative.) Although it is appreciated that the mutual capacitance may dominate in experimentally realistic systems [55, 56], it is believed that the results are essentially unaffected if one restricts the model to self-capacitance only [133]. Since most theoretical formulations we are interested in make this assumption, we will neglect mutual capacitance in what follows. Furthermore, phases and not phase differences are the fundamental degrees of freedom, and the phases $\theta_{\mathbf{r}}$ themselves are treated as noncompact variables.

Experimental work on Josephson junction arrays where dissipation was believed to be important was reviewed briefly in Sec. 2.3.2. The theoretical literature is far more extensive, and we will only cite those works that are most relevant to our work. In the simplest scenario, one gets two phases: metallic (disordered) and superconducting (ordered). However, there are several predictions of a phase diagram that contains additional, unconventional phases that are in some sense partially ordered [134, 135, 136, 137]. In addition, there are also predictions that the metallic phase itself is an unconventional "*floating*" phase [138, 139], meaning that the superconducting elements are in essence spatially decoupled. Turning finally to numerical work, we mention that a 2D array of resistively shunted Josephson junctions has previously been studied by Monte Carlo methods in Refs. [140, 141], focusing primarily on finite-temperature behaviour for dominating mutual capacitance. A very early numerical study was also made in Ref. [135], although on a dual representation in 1+1 dimensions.

4.5 A dissipative model for circulating currents in high-T_c cuprates

We finally arrive at the model that has been the main motivation for this thesis work: A quantum XY model in two spatial dimensions with bond dissipation that has been proposed to explain a quantum critical point of circulating-current order in cuprate high-T_c superconductors. The experimental evidence of circulating currents was reviewed in Sec. 2.2.2, and now we will summarize the theoretical background of the model.

4.5.1 Circulating-current models for cuprates

Years before the first experimental indications of a time-reversal-symmetry breaking order parameter in the pseudogap phase [20], Varma postulated the existence of magnetic order in underdoped cuprates due to currents circulating in the CuO_2 layers [9]. In contrast to many other candidates for such hidden order, this model explicitly includes the oxygen sites of the CuO_2 layers as well as the Cu sites [18, 142]. This allows for at least two possible sets of intra-unit-cell current-loop patterns that preserve translational invariance in the ordered phase.

The first explicit proposal that one of these sets of current patterns was associated with a quantum phase transition around optimal doping was given in Ref. [9]. Here, the associated quantum critical region at higher temperatures was connected to the marginal-Fermi-liquid phenomenology, with an important new element being the implication of local quantum criticality. These calculations were later extended to explain the pseudogap phase in Ref. [143]. In Ref. [144], the experimental results [20] on breaking of time-reversal symmetry were analysed and found to be consistent with a different set of $q = 0$ current patterns, and this form of circulating-current order was later found to be energetically favoured in a more detailed calculation [18]. Reference [18] also put forward a generalized Ashkin-Teller model as a possible effective theory of circulating-current degrees of freedom. It was later shown through microscopic calculations that this is the correct effective theory in the classical limit [121], and Monte Carlo simulations have shown that the specific-heat signature of the phase transition in this theory indeed is very weak [145], in agreement with experiments. We mention also that the momentum-independent MFL fluctuation spectrum was recently shown to be capable of supporting d-wave superconductivity with high values of T_c [146], adding to the attraction of a circulating-current theory of the strange metal phase.

4.5.2 Local quantum criticality in a dissipative 2D XY model?

In Ref. [1], the Ashkin-Teller model introduced in Ref. [18] for circulating-current degrees of freedom was generalized in the following manner. First, it was written in the phase representation of Eq. (3.17), where the discreteness of the phase variable θ was represented by a fourfold anisotropy term $\propto h_4$ as in Eq. (3.21). This pseudospin representation of the four distinct current patterns is illustrated in Fig. 4.5. Second, this classical XY model is turned quantum by adding 1) a standard quantum-rotor kinetic term (4.22) as for a self-capacitive Josephson junction array and 2) Ohmic bond dissipation on the Caldeira-Leggett form (4.8). Third, the Ashkin-Teller coupling K_4 and the anisotropy field h_4 are argued to be irrelevant to the critical behaviour and are subsequently set to zero. The resulting (2+1)D XY model is apparently defined by exactly the same action as the resistively shunted Josephson junction array of Sec. 4.4.4. A more detailed treatment of this model was later published in Ref. [147].

The major result reported in Refs. [1, 147] is that this model exhibits local quantum criticality and moreover reproduces the fluctuation spectrum of a marginal Fermi

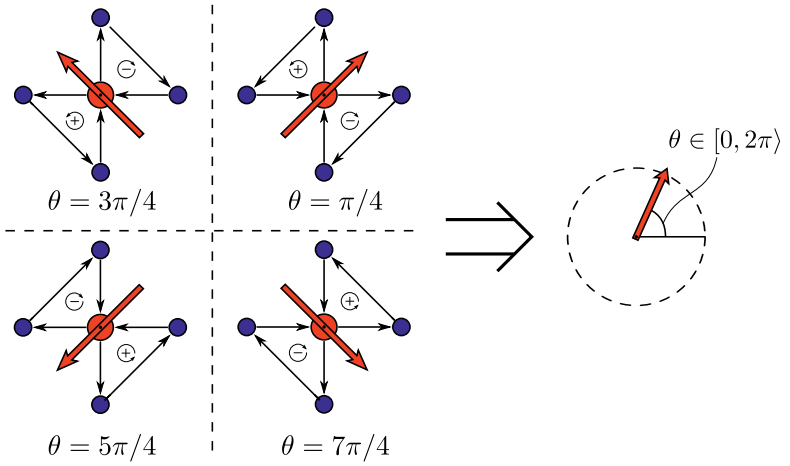

Figure 4.5: Pseudospin and phase representation of circulating-current degrees of freedom: A Z_4 pseudospin is associated to the circulating-current pattern within each unit cell, and each of the four possible orientations of this pseudospin corresponds to four distinct values of the phase variable θ. Assuming that the Z_4 anisotropy is irrelevant, the pseudospins can be described by $U(1)$ phase variables.

liquid. To be more precise, Refs. [1, 147] consider the correlation function

$$g(\mathbf{r}-\mathbf{r}',\tau-\tau') = \langle \mathrm{e}^{\mathrm{i}\theta_{\mathbf{r},\tau}} \mathrm{e}^{-\mathrm{i}\theta_{\mathbf{r}',\tau'}} \rangle, \tag{4.25}$$

corresponding to a real part $\langle \mathbf{s}_{\mathbf{r},\tau} \cdot \mathbf{s}_{\mathbf{r}',\tau'} \rangle$ as in Eq. (3.6), at the critical point. The result is that this correlation function should be a delta function in space, or in other words purely local, corresponding to a spatial correlation length $\xi = 0$. In imaginary time, on the other hand, the correlation function was found to be a power law. This spatiotemporal correlation function implies a fluctuation spectrum Im $\chi(\mathbf{q},\omega,T)$ that is momentum independent and linear in frequency for $\omega \ll T$.[6] This is the same result as the postulate [11] in Eq. (2.1), and would imply that the phenomenological MFL fluctuation spectrum had been derived from a more microscopic theory.

The physical picture underlying the result of Refs. [1, 147] is that this XY model harbours a new class of topological defects dubbed "warps", in addition to the usual spatial vortices of the classical 2D XY model. A real-space lattice representation of these warp defects was later given in Ref. [148]. This description appears to presume a compact phase field θ, which is conventionally also the premise when dealing with vortices as topological defects. Although the phase field of the analogous Josephson junction model is usually interpreted as noncompact, one may possibly argue in favour of using compact variables when θ originates with the physical orientation of a circulating-current pseudospin instead of the phase of a quantum wave function.

The above account leaves us with three fundamental questions that we seek to answer in this thesis: 1) The correlation function and resulting momentum-independent

[6] To be specific, Im $\chi(\mathbf{q},\omega,T) \propto \tanh(\omega/2T)$ below a high-frequency cutoff [1].

fluctuation spectrum indicates a dynamical critical exponent $z \to \infty$. Can bond dissipation give rise to such extreme local behaviour, when naive scaling of the model instead predicts that $z = 1$? 2) It does not seem to be obvious whether one should treat the degrees of freedom of this model as compact or noncompact variables, but does the nature of the criticality depend on this choice? 3) Is the fourfold anisotropy of the original pseudospin degrees of freedom in fact irrelevant at the critical point, or does it matter whether one uses discrete or continuous variables? We will return to these questions in Ch. 6.

4.5.3 Other possible realizations of local quantum criticality

Since much of this thesis work deals with the possible realization or otherwise of local quantum criticality in a specific model, it seems pertinent to list other possible realization of local quantum criticality in more or less related models.

One noteworthy theory that is often referred to as local quantum criticality is the theory of Si et al. of quantum criticality in heavy-fermion compounds [149, 150]. In this scenario, an antiferromagnetic QCP co-occurs with criticality of local magnetic moments, so that the critical point cannot be described by critical fluctuations of the AF order parameter alone. This theory can also be related to a spin-boson-like model with $s = 0^+$ [151]. Another well-known theory in the context of random transverse-field Ising models is that of an infinite-disorder fixed point [152], which corresponds to activated dynamical critical scaling with $\ln \omega \sim q^{\psi}$. Here the locality can be explained by disorder being perfectly correlated in the imaginary-time direction.

Variants of local quantum criticality have also been claimed for a number of dissipative models. Reference [153] studied a JJA model where the dissipative quantity is the phases and not the phase difference, and predicted a z that varies with dissipation strength and diverges for a certain value of α. A later study of a related noncompact site-dissipative model found $z \to \infty$ at the transition from a "floating" normal phase to the superconducting phase [154]. (Such a "floating" phase could itself also be regarded as being local [138, 139].) Finally, we mention that theories with local, MFL-like properties have recently also been found using gauge/gravity duality [155].

5 Monte Carlo methods

The principal set of tools we have used to investigate the models described in the preceding chapters is Monte Carlo simulations. From the point of view of equilibrium statistical mechanics, this is a set of numerical methods that are designed, simply put, to compute the partition function $\mathcal{Z}$ in a way that is statistically exact and essentially unbiased. We have used two variants of the Monte Carlo method: In Sec. 5.2 we describe so-called parallel tempering methods, and in Sec. 5.3 we describe Wolff's cluster algorithm and some of its generalizations. Before this, we will in Sec. 5.1 discuss briefly the basic ideas behind Monte Carlo and illustrate these with the immensely popular Metropolis algorithm, which also forms the foundation of our implementation of parallel tempering. The remaining sections of this chapter are devoted to explaining other components of the toolbox that is necessary to make sense of the data generated by the simulations. For details on the fundamentals of Monte Carlo simulations, we refer to textbooks [156, 74] and some recommended lecture notes [105, 157].

5.1 The basics of Monte Carlo simulations

In our Monte Carlo simulations, the goal is to calculate how various observables of a spin system in thermal equilibrium evolve as one varies a number of coupling parameters. In the macroscopic equilibrium state corresponding to a set of such coupling values, each microscopic spin configuration $\mathbf{s}$ will occur with a probability determined by the Boltzmann distribution

$$p[\mathbf{s}] = \frac{1}{\mathcal{Z}} \mathrm{e}^{-S[\mathbf{s}]}, \tag{5.1}$$

where the partition function $\mathcal{Z}$ and the action S were defined in Sec. 3.1. The thermal average of an arbitrary observable $A[\mathbf{s}]$ takes the form of a sum

$$\langle A \rangle = \sum_{\{\mathbf{s}\}} p[\mathbf{s}] A[\mathbf{s}] \tag{5.2}$$

over the set $\{\mathbf{s}\}$ of all possible configurations. Here, the Boltzmann factor $p[\mathbf{s}]$ appears as a weight factor determining the relative contribution of each configuration to the average. The total number of configurations $|\{\mathbf{s}\}|$ will be denoted by N_{config}.

A natural first step, given the ultimate goal of calculating $\langle A \rangle$ numerically, is to include only an appropriate fraction of the terms in the sum (5.2). For naive, random sampling of the configuration space, one has the estimator

$$\bar{A} = \frac{N_{\text{config}}}{N} \sum_{\{\mathbf{s}\}_N} p[\mathbf{s}] A[\mathbf{s}], \tag{5.3}$$

where the set $\{\mathbf{s}\}_N \subseteq \{\mathbf{s}\}$ contains N elements chosen at random from the set of all configurations. Since $\lim_{N \to N_{\text{config}}} \bar{A} = \langle A \rangle$, it is – in principle – straightforward to make this approximation as good as one desires. In practice, however, the number N_{config} becomes ridiculously large even for rather small system sizes. One then ends up spending most of the time on unimportant configurations that barely contribute to the thermal average but that inflate the variance of the estimator. The solution is *importance sampling*, where the sampled configurations are no longer the uniformly distributed set $\{\mathbf{s}\}_N$, but instead a set $\{\mathbf{s}\}'_N$ selected according to some conveniently chosen distribution. Choosing the Boltzmann distribution $p[\mathbf{s}]$ naturally ensures that the configurations sampled are precisely the configurations that dominate the thermal average for a given equilibrium state. If one can generate such sets $\{\mathbf{s}\}'_N$, the weight factor in Eq. (5.3) will cancel, and the estimator reduces to the simple average

$$\bar{A} = \frac{1}{N} \sum_{\{\mathbf{s}\}'_N} A[\mathbf{s}]. \tag{5.4}$$

The next challenge is how to sample configurations from the Boltzmann distribution. The way one does this is to generate each new configuration one samples from the previously selected configuration. The crude idea is that if configuration $\mathbf{s}$ is selected from the equilibrium distribution, one may find rules to turn this configuration into a new configuration $\mathbf{s}'$ in a random fashion. The rules should be such that $\mathbf{s}'$ does not differ more from $\mathbf{s}$ than that it could have been sampled from the same distribution. In this way, the simulation performs a random walk in the region of configuration space that is consistent with the equilibrium state.

More formally, choosing each new configuration solely based on the present configuration generates a *Markov chain* of configurations. When using Markov chains in Monte Carlo sampling, one conventionally requires two conditions on the rules for transitioning from one step in the chain to the next: *ergodicity* and *detailed balance*. The simulation is ergodic if – starting at an arbitrary configuration – any other configuration can be reached by a Markov chain with a finite number of steps. In other words, the simulation must be able to sample the entire configuration space. The detailed balance condition, on the other hand, can be shown to ensure that a Markov chain sampling equilibrium configurations will remain in equilibrium [74]. Mathematically, this is formulated as a conservation equation of probability,

$$p[\mathbf{s}] P(\mathbf{s} \to \mathbf{s}') = p[\mathbf{s}'] P(\mathbf{s}' \to \mathbf{s}), \tag{5.5}$$

where $p[\mathbf{s}]$ is the equilibrium (Boltzmann) probability distribution and $P(\mathbf{s} \to \mathbf{s}')$ is the probability for transitioning from configuration $\mathbf{s}$ to configuration $\mathbf{s}'$.

However, what kinds of configurations that are typical for the equilibrium distribution is in general not known at the outset of a simulation. Luckily, it can also be shown [74] that detailed balance (in conjunction with ergodicity) also ensures that a Markov chain on average always will approach equilibrium as it steps forward, irrespective of where it starts in the configuration space. This initial approach to the probability distribution one is interested in sampling is called *equilibration*, and it is important to make sure that one does not add to the thermal average contributions from configurations visited before the correct distribution is reached.

5.1.1 The Metropolis algorithm

In its simplest incarnation, the *Metropolis algorithm* describes a way to advance the Markov chain from the configuration $\mathbf{s}$ by proposing to change a single degree of freedom (spin) at a time. To be concrete, one proposes to *flip* the spin $\mathbf{s}_i$ at site i to a new value $\mathbf{s}'_i$.[1] One then accepts the resulting overall spin configuration $\mathbf{s}'$ with probability

$$P(\mathbf{s} \to \mathbf{s}') = \min\{1, \mathrm{e}^{-\Delta S}\}, \tag{5.6}$$

where $\Delta S = S[\mathbf{s}'] - S[\mathbf{s}]$ is the change in the action corresponding to the proposed change of the spin. This means that the new configuration $\mathbf{s}'$ will always be accepted by this prescription if is "energetically" favourable ($S[\mathbf{s}'] < S[\mathbf{s}]$). If it is not, one generates a uniformly distributed random number $u \in [0, 1]$ and accepts $\mathbf{s}'$ if $\ln u < -\Delta S$. Inserting Eq. (5.6) in Eq. (5.5), it is easy to show that detailed balance is satisfied. If the proposed update is rejected, the new configuration is simply set to be identical to the old one.

In practice, our update procedure steps through the lattice in a sequential way, proposing a randomly chosen new state of the spin at each site. In this sense, the step from one configuration to the next is a *local* update of the configuration. When one has tried to change all spins on the lattice, one has performed one *Monte Carlo sweep*. After each sweep, one may choose to sample the observable one is interested in and add the sample value to the estimate (5.4), before repeating the procedure for the next sweep.

5.1.2 Statistical errors and autocorrelation

One major problem with the Markov chain importance sampling scheme that was glossed over in Sec. 5.1 is that the observable samples of these configurations are in general not statistically independent. This is particularly apparent for local updates, where each new configuration may differ very little from the previous. If we for the moment assume that all the sampled configurations are randomly selected from the appropriate distribution, as was done for the estimator $\bar{A}$ in Eq. (5.3), we have the

[1] In this chapter, we will find it more convenient to label the sites of the space-time lattice by indices such as i than by spatial (and temporal) coordinates.

error estimate

$$\Delta\bar{A} = \sqrt{\frac{1}{N(N-1)}\sum_{i=1}^{N}\left(A_i - \bar{A}\right)^2} = \frac{\bar{\sigma}_A}{\sqrt{N}}. \tag{5.7}$$

Here, $\bar{\sigma}_A$ denotes the estimate of the standard deviation of the distribution of the observable A.

If we now take into account that there are correlations between the various samples A_i, it can be shown that the error estimate is modified, and

$$\Delta\bar{A} = \sqrt{\frac{1+2\tau_A}{N(N-1)}\sum_{i=1}^{N}\left(A_i - \bar{A}\right)^2} \approx \frac{\bar{\sigma}_A}{\sqrt{N/(2\tau_A)}}. \tag{5.8}$$

In other words, it is as if the number of samples has been reduced by a factor of $2\tau_A$ from Eq. (5.7), and this reflects that the data series $\{A_i\}$ effectively only contains $N/(2\tau_A)$ uncorrelated samples. The quantity τ_A is the (integrated) *autocorrelation time*, formally defined from $\tau_A = \int_0^\infty C_A(t)\,\mathrm{d}t$, where

$$C_A(t) = \frac{\langle A(t)A(0)\rangle - \langle A\rangle^2}{\langle A^2\rangle - \langle A\rangle^2} \approx \mathrm{e}^{-t/\tau_A} \tag{5.9}$$

is the autocorrelation function for observable A. The Monte Carlo time variable t – and therefore also τ_A – is in units of Monte Carlo sweeps.[2] How we actually calculate the error estimates in practice will be treated in Sec. 5.5.

The autocorrelation time τ_A is another example of the "temporal length scale" diverging at criticality that was first defined in Table 3.1. For the Metropolis algorithm, this can be understood by considering the number of Monte Carlo sweeps that are necessary to generate a substantially different (uncorrelated) configuration when the system consists of large correlated regions. This means that for a (classical) system of linear size L, the autocorrelation time diverges as $\tau_A \propto L^{z_{\mathrm{MC}}}$ at the critical point, with z_{MC} being a dynamical critical exponent associated with Monte Carlo time. This phenomenon is called *critical slowing down* and may be highly detrimental to studying critical phenomena by Monte Carlo simulations. The algorithms described in the following sections have in part been designed to alleviate this problem by introducing *global* updates.

5.2 Parallel tempering

An alternative way to understand critical slowing down is to consider the projection of the Markov chain in the high-dimensional configuration space onto the one-dimensional energy (action) space, as the transition probabilities are purely determined by the action. Although the random walk in configuration space is Markovian, the projected random walk in energy space is not [158]. Combined with broad energy

[2] The assumptions in this paragraph are that the autocorrelation time is appreciable, $\tau_A \gg 1$, that one considers long Monte Carlo time scales $t > \tau_A$, and that one is in equilibrium.

histograms (which are the projections of the probability distributions onto energy space), this makes the Metropolis updates inefficient in exploring the space of possible energy values at criticality.

The parallel tempering (also called replica exchange Monte Carlo) method is based on the idea of extending the ensemble from the canonical one [as characterized by the Boltzmann distribution (5.1) for a given coupling K] to the product of canonical ensembles at different coupling values $\{K\}$ [159, 160]. In other words, instead of simulating one system at a certain coupling value at a time, one simulates multiple replicas of the same system simultaneously, but at different coupling values. If one allows the replica at a certain coupling value to be swapped for another replica at another coupling, one extends the random walk to also traverse coupling space, which in effect may speed up the random walk in energy space. The idea is then that a replica at the critical coupling may be swapped to a subcritical coupling where the autocorrelation time is much lower. By the time it is swapped back to criticality again, the observables will no longer be correlated with observables sampled the last time the replica visited criticality.[3] In a way, it is as if the autocorrelation time is spread evenly among the available coupling values.[4]

To define precisely how the method works, consider varying only one coupling K, with the conjugate energy term being E. An action including also other coupling constants may then for the present purpose be written as $S[\mathbf{s}] = KE[\mathbf{s}] + \tilde{S}[\mathbf{s}]$. For a number of Monte Carlo sweeps, one applies the Metropolis algorithm to each replica separately at their respective coupling values, before proposing a swap between two of the replicas. The probability of swapping the spin configuration $\mathbf{s}$ at coupling K for the configuration $\mathbf{s}'$ generated at coupling K' is given by

$$P(\mathbf{s}; K \to \mathbf{s}'; K') = \min\{1, \mathrm{e}^{-(K-K')(E[\mathbf{s}']-E[\mathbf{s}])}\}. \tag{5.10}$$

In the extended ensemble of replicas at all the different coupling values, it is easy to show that this update satisfies detailed balance. The swap condition of Eq. (5.10) guarantees that each new configuration that coupling K receives from coupling K' occurs with a probability consistent with the Boltzmann distribution for coupling K. In other words, the parallel tempering swaps do not bring the replicas out of equilibrium. However, this also means that there has to be a substantial overlap between the energy histograms for the couplings K and K' if the swap is to be likely to take place. Therefore, one usually only allows for swaps between neighbouring coupling values in the series of available values $K^{(1)} < K^{(2)} < \ldots < K^{(M)}$.

[3] There are two equivalent ways to view this swap update: From the perspective of a given replica, which will then perform a random walk in coupling space, or from the perspective of a given coupling value, for which the random walk in configuration space will include particularly large jumps corresponding to the global updates of replica swaps. Since we are interested in the configurations contributing to the thermal average for each coupling, we will mostly take the second point of view.

[4] We present parallel tempering as a technique to reduce autocorrelations, but we should also point out that the original motivation for the method was to speed up equilibration and avoid the problem of metastable states in systems with "rough" free energy landscapes [157].

5.2.1 Distribution of coupling values

To get a suitable acceptance rate of swaps and thereby an efficient random walk in coupling space, some care must be taken in choosing the distribution of available coupling values. The naive uniform distribution will result in a pronounced dip around a phase transition, since energy histograms at different coupling values will be widely separated in energy space when energy changes rapidly as a function of coupling. Furthermore, a guiding principle is to always allocate resources where they are most needed [157], which in many cases is precisely around the phase transition. The natural goal is therefore to raise the density of coupling values in this region to increase the acceptance rate. To achieve this goal, we have employed an iterative procedure due to Hukushima et al. [161] that distributes coupling values so as to produce an acceptance rate independent of coupling. This method is based on the iterative mapping $K^{(i)} \to [K^{(i)} + R(\{K\})]$, where

$$R(\{K\}) = \frac{1}{\Delta \bar{E}} \left(K^{(i-1)} \bar{E}^{(i-1)} - K^{(i+1)} \bar{E}^{(i+1)} - \bar{E}^{(i)} \Delta K \right), \tag{5.11}$$

with $\Delta K = K^{(i-1)} - K^{(i+1)}$ and $\Delta \bar{E} = \bar{E}^{(i-1)} - \bar{E}^{(i+1)}$. The energy $\bar{E}^{(i)}$ is the thermal average estimate for the coupling $K = K^{(i)}$, and approximate values of these mean energies have to be found before each iteration.[5]

5.3 Cluster algorithms

Another widely used approach to global updates in Monte Carlo simulations is to use a cluster algorithm. Instead of flipping spins one by one, these algorithms identify clusters of spins that can be flipped simultaneously in such a way that detailed balance is still fulfilled. The original cluster algorithm is due to Swendsen and Wang [164], but we have used variants of the algorithm developed by Wolff [165].

5.3.1 The Wolff algorithm

The steps of the Wolff algorithm for a spin model with arbitrary-dimensional order parameter space can be described as follows [165]. First, one chooses a random lattice site i and a random unit vector $\hat{\mathbf{e}}$ in order parameter space. The spin $\mathbf{s}_i$ now constitutes the cluster, and it will be chosen as the first *current spin*. Second, one considers the set of spins $\{\mathbf{s}_j\}$ that interact with the current spin. For each of

[5] Finally, we mention briefly other approaches for optimizing the way the parallel tempering simulation is set up. Reference [162] argued that the optimal solution is to have an acceptance rate that is not constant, but rather somewhat peaked around phase transitions. This speeds up the random walk of the replicas across this bottleneck region in coupling space, and an elaborate method to achieve this was presented. A different approach was taken in Ref. [163], where the acceptance rate of swaps is kept constant and one instead adjusts the number of Monte Carlo sweeps between each replica swap after the autocorrelation time. For a discussion of these and other possible approaches, see Ref. [157].

them, one asks what would be change in the action ΔS if one had flipped it by the prescription

$$\mathbf{s}_j \to \mathbf{s}_j{}' \equiv \mathbf{s}_j - 2(\mathbf{s}_j \cdot \hat{\mathbf{e}})\hat{\mathbf{e}}. \tag{5.12}$$

For Ising spins σ_j, this is the usual spin-flip $\sigma_j \to -\sigma_j$. For a number of spin components $n > 1$, the operation corresponds to flipping the component of $\mathbf{s}_j$ that is parallel to the projection vector $\hat{\mathbf{e}}$. Third, one adds the spin $\mathbf{s}_j$ to the cluster with a probability

$$P_{\text{add}}(\mathbf{s}_j \to \mathbf{s}_j{}') = \max\{0, 1 - \mathrm{e}^{-\Delta S_{i,j}(\mathbf{s}_j \to \mathbf{s}_j{}')}\} \equiv \max\{0, p_{i,j}\}, \tag{5.13}$$

where the action contribution $S_{i,j}$ only includes the bond i–j. After this one chooses a new spin $\mathbf{s}_i$ from the cluster as the next current spin, considers each of the spins this spin is interacting with, and so on. When there are no more spins to consider for inclusion in the cluster, one finally flips all the spins in the cluster according to Eq. (5.12). The process is then repeated by going back to the first step to begin growing a new cluster.

We will assume that the term in the action corresponding to the interactions between the spin at site i and the spin at site j can be written as $-K_{i,j}\ \mathbf{s}_i \cdot \mathbf{s}_j$, as a generalization of the action (3.19) to an arbitrary model with ferromagnetic two-spin interactions. Then, the action difference becomes $\Delta S_{i,j}(\mathbf{s}_j \to \mathbf{s}_j{}') = 2K_{i,j}\tilde{\sigma}_i\tilde{\sigma}_j$, where we have introduced $\tilde{\sigma}_i = \mathbf{s}_i \cdot \hat{\mathbf{e}}$ as the projection of the spin $\mathbf{s}_i$ onto the vector $\hat{\mathbf{e}}$. Inserting this expression in Eq. (5.13), we see that $p_{i,j} = 0$ for the case that the projections $\tilde{\sigma}_i$ and $\tilde{\sigma}_j$ are oppositely directed. For the case that the projection of the spins onto $\hat{\mathbf{e}}$ have the same sign, the probability of including $\mathbf{s}_j$ in the cluster can be written as

$$p_{i,j} = 1 - \mathrm{e}^{-2K_{i,j}\tilde{\sigma}_i\tilde{\sigma}_j}. \tag{5.14}$$

At the critical point, the spin direction fluctuates on all length scales, and the Wolff algorithm has an easy time growing and flipping clusters of a variety of sizes. Subsequent spin configurations are therefore likely to differ *also when viewed at large length scales*, and critical slowing down is suppressed. In fact, the Monte Carlo dynamical critical exponent for a 2D Ising model is reduced to $z_{\text{MC}} \gtrsim 0$ (from $z_{\text{MC}} \approx 2$ for the Metropolis algorithm) [156], although this number increases somewhat when going to higher dimensions or, equivalently, to models with long-range interactions.

5.3.2 The Luijten-Blöte algorithm for long-range interactions

For a d-dimensional classical model with only short-range interactions, the time of a single Monte Carlo sweep with the Metropolis algorithm and the mean time used to generate of a single cluster with the Wolff algorithm both scale with system size as L^d. Introducing long-range interactions, so that each spin interacts with every other spin, the scaling of computation time with system size increases to L^{2d}. Even though the Wolff algorithm may still be effective in subduing critical slowing down, it is nevertheless very time-consuming to have to consider every other spin for inclusion in the cluster for each spin that is already included. This problem is overcome by using the generalized Wolff algorithm developed by Luijten and Blöte [166].

Let us start at a current spin $\mathbf{s}_i$ already added to the cluster and which will define the origin, $i = 0$. We will restrict ourselves to interactions of strength $K_{0,k}$ between this spin and spins located $k > 0$ lattice sites away along a single lattice direction. This could be either because the model we consider only has one dimension, or, in the case that $d > 1$, it could be because the interactions are long-ranged only along one of the dimensions. We are primarily interested in the latter case, where dissipation induces long-range interactions in the imaginary-time direction while short-range interactions are found in the remaining (spatial) directions. Using the Wolff algorithm, one could then consider spin $k = 1$, $k = 2$, ... for inclusion in the cluster, with

$$p_{0,k} = 1 - \mathrm{e}^{-2K_{0,k}} \tag{5.15}$$

being the probability of provisionally adding it. Note that in Eq. (5.15) we have not yet considered the relative direction of the two spins, which is why we indicated that spin k can only be added *provisionally* at this point. We will return to the condition for actually adding it shortly. Now, instead of asking for each of the spins $k = 1, 2, \ldots$ whether one should add it to the cluster, the probability of which decreases sharply as k increases, one could instead simply ask: At which distance lies the first spin to be provisionally added? The answer to this can be found by first calculating the probability that the first spin will be added at a distance k,

$$\tilde{P}(k) = \prod_{l=1}^{k-1}(1 - p_{0,l})p_{0,k}. \tag{5.16}$$

Next, one finds the cumulative probability distribution for the first spin to be added to be at a distance k away or closer,

$$C(k) = \sum_{l=1}^{k} \tilde{P}(k). \tag{5.17}$$

Then one can draw a uniformly chosen random number $u \in [0, 1]$, and the distance to the first spin will be chosen as the lowest value of k for which $u < C(k)$ is satisfied. To decide whether this spin should in fact be added to the cluster, we recall that the probability (5.15) for provisionally adding it assumed that the spin at k was pointing exactly the same direction as the current spin at 0. Therefore, one takes the relative spin direction into account by adding the provisionally added spin at k to the cluster with a probability

$$P_{\mathrm{add}}(\mathbf{s}_j \to \mathbf{s}_j{}') = \frac{\max\left\{0, 1 - \mathrm{e}^{-2K_{0,k}\tilde{\sigma}_0\tilde{\sigma}_k}\right\}}{1 - \mathrm{e}^{-2K_{0,k}}}, \tag{5.18}$$

with $\tilde{\sigma}_i$ being the spin projections defined in Sec. 5.3.1.

The next step is to rename $k \to j$ and again ask: At which new distance $k > j$ lies the next spin to be provisionally added to the cluster? One could then calculate a new cumulative probability distribution $C_j(k)$ in the same way as done above for $C_{j=0}(k) \equiv C(k)$, but where the product and sum in Eqs. (5.16) and (5.17), respectively, start at $l = j + 1$ instead of $l = 1$. Doing this for every new spin j will be very time-consuming. Therefore, we instead tabulate the values $C(k)$ prior

to the simulation and use for each new j that the appropriately shifted cumulative distribution can be calculated through [88]

$$C_j(k) = \frac{C(k) - C(j)}{1 - C(j)}. \tag{5.19}$$

Drawing again a random number $u \in [0, 1]$, we find the next distance k from the condition $u < C_j(k)$.

5.3.3 Cluster algorithms for competing interactions

It is straightforward to apply the Wolff algorithm to antiferromagnetic interactions, in which case only spins that are oppositely directed to the current spin will be added to the cluster. This can also be generalized to the case of *competing* interactions, where a spin may be coupled ferromagnetically to some spins and antiferromagnetically to other. What may happen now is that clusters are built that contain spins pointing in all directions, since any given spin can be added both through ferromagnetic and antiferromagnetic interactions. As a result, each cluster flip flips almost every spins on the lattice, the new configuration essentially becomes a rotated version if the old configuration, and the autocorrelation time explodes.

This problem has been known since the early days of the cluster algorithms [167], and solutions only seem to be available in special cases [168].[6] In the case of bond dissipation as discussed in Sec. 4.3.1 and 4.4.2, the Caldeira-Leggett term in the action gives rise to both ferromagnetic and antiferromagnetic interactions of the site variables. The problem is here accentuated by the long-ranged nature of these competing interactions, and the Luijten-Blöte algorithm is all but useless. We therefore resort to parallel tempering techniques when simulating bond dissipation.[7]

5.4 Finite-size analysis

There are a number of finite-size effects that are crucial to keep in mind in order to interpret Monte Carlo results – invariably obtained for systems of finite size – in a meaningful way. Deep in the disordered or ordered phases, most observables behave qualitatively as they would for an infinite system. What one observes close to a phase transition, on the other hand, may appear as a complete mess for the untrained eye due to the conspiracy of a number of finite-size effects: a) Divergences are rounded to bumps, b) discontinuous jumps are smeared, c) where a quantity should drop to zero one gets finite-valued tails, d) quasi-long-range-ordered systems seem remarkably

[6] A similar effect can also be detrimental when including an external magnetic field in cluster Monte Carlo simulation by the dummy spin technique [164], and when generalizing this technique to q-fold symmetry-breaking fields as for the model Eq. (3.21).

[7] A possible Metropolis-based alternative to treat long-range interactions would be a method that stochastically dilutes the long-range bonds during the simulation [169]. One could also use approximate approaches such as studying a power-law diluted version of the same model. Although the details would then differ from the original model, the universality class might be conserved.

long-range ordered, e) the system may seem more or less critical in an extended region around the phase transition (also when first order), and f) the apparent position of the transition point may be shifted either way. Such effects are natural when one recalls that true phase transitions only take place in the thermodynamic limit.

Alternatively, most effects can be traced back to the behaviour of the correlation length at criticality: Whereas ξ of an infinite system would grow to infinity as $t \to 0$, the actual ξ of the finite system will eventually "hit the edges" and scale with the system size instead of diverging, $\xi \propto L$. However, instead of treating the resulting deviations from the thermodynamic limit as errors [98], one may instead utilize the systematic dependence on L of various quantities through *finite-size analysis*. These ideas are the heuristic explanation of the finite-size scaling expression derived in Sec. 3.7.3, and are used to extract exponents in the papers.

5.4.1 The Binder cumulant

One central quantity in the analysis of our Monte Carlo simulations is the Binder cumulant, and we will therefore give a more detailed description of its usage. We will refer to the normalized fourth moment of the magnetization,

$$Q = \frac{\langle m^4 \rangle}{\langle m^2 \rangle^2}, \tag{5.20}$$

as the *Binder ratio*. This is a measure of the fluctuations in the system that is illustrated as a function of coupling in Fig. 5.1 and that has the following convenient properties. First, its scaling dimension is zero, and the value of the Binder ratio therefore does not scale with the system size at a critical point as $L \to \infty$. This allows us to identify the critical point K_c as the value of K where $Q(K)$ for different and large system sizes L cross. Second, for a continuous phase transitions, $Q(K)$ decreases monotonously from a well-defined limiting value in the disordered phase to another well-defined value in the ordered phase as K increases and the order parameter fluctuations decrease. For $K > K_c$, the order parameter fluctuations around the (finite) average $\langle |m| \rangle$ vanish in the thermodynamic limit, resulting in $Q = 1$. For $K < K_c$ and $L \to \infty$, the order parameter fluctuations around $\langle |m| \rangle = 0$ are Gaussian, which results in a higher value $Q = Q_{\max}$. Using Wick's theorem for a general n-component order parameter $\mathbf{m}$ with $m^2 = \sum_{i=1}^{n} m_i^2$, one can show that $\langle m^4 \rangle = (n^2 + 2n)\langle m_i^2 \rangle^2$. Using also that $\langle m^2 \rangle = n\langle m_i^2 \rangle$ and inserting these results in Eq. (5.20), we get the limiting low-K value

$$Q_{\max} = \frac{n+2}{n}. \tag{5.21}$$

Because of these properties, it is also conventional to consider the *Binder cumulant*

$$g = 1 - \frac{Q}{Q_{\max}}. \tag{5.22}$$

This quantity behaves as an order parameter in the sense that it increases from $g = 0$ for $K \ll K_c$ to a finite value $g = (Q_{\max} - 1)/Q_{\max}$ for $K \gg K_c$. We will

only consider one- and two-component order parameter fields, for which we have $Q_{\max}(n=1)=3$ and $Q_{\max}(n=2)=2$.

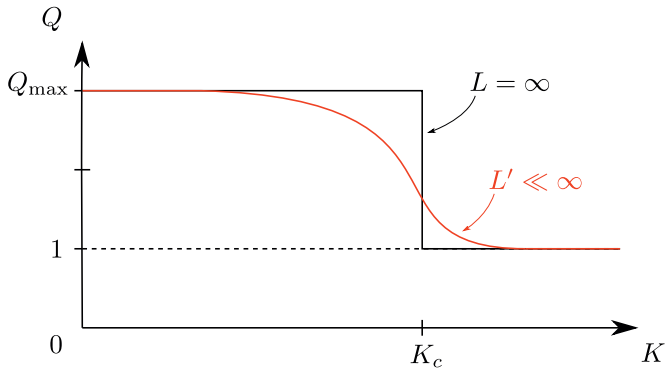

Figure 5.1: Sketch of the evolution of the Binder ratio Q as a function of a coupling parameter K varied across a continuous phase transition. Curves for different system sizes L and L' cross close to the critical coupling K_c, and the curve tends to a step function in the thermodynamic limit $L \to \infty$.

This nice, monotonous evolution from one limiting value to another as one varies K breaks down if the phase transition is first order. In that case, the ordered and the disordered phase will coexist at the transition point, implying a bimodal distribution of the order parameter $|m|$. This results in $Q > Q_{\max}$, or, equivalently, $g < 0$ [105]. As this feature of the distribution function sharpens for increasing system size, the Binder cumulant will diverge to $g \to -\infty$ at the transition point, making it a sensitive probe of first-order phase transitions.

Including corrections to scaling, the FSS expression (3.54) for the Binder ratio close to criticality takes the form[8]

$$Q(t,L) = (1 + cL^{-\omega})\mathcal{Q}(tL^{1/\nu}) \approx (1 + cL^{-\omega})(q_0 + q_1 tL^{1/\nu}), \tag{5.23}$$

where $q_0 = \mathcal{Q}(x=0)$ and $q_1 = \mathcal{Q}'(x)|_{x=0}$. Assuming a set of different system sizes, we can use this to find a more accurate estimate for the critical coupling. Letting the equation $Q(t,L) = Q(t,L')$ define the crossing point between two adjacent system sizes L and $L' < L$, Eq. (5.23) leads to the following FSS expression for the coupling values at the crossing points:

$$K_{\text{cross}}(L,L') = K_c + \frac{cq_0}{q_1}\left[\frac{(L'/L)^{-\omega}-1}{(L'/L)^{1/\nu}-1}\right] L^{-(\omega+1/\nu)}. \tag{5.24}$$

If we choose the set of system sizes such that L'/L is constant, this simplifies to

$$K_{\text{cross}}(L,L') = K_c + \tilde{c}L^{-\omega'}, \tag{5.25}$$

[8] To simplify notation, we have assumed that we have a classical system or that an additional finite-size scaling argument L_τ/L^z of $\mathcal{Q}$ has been fixed. We explain how this can be done in Sec. 5.4.3.

where $\omega' = \omega + 1/\nu$ and the constant prefactors have been lumped together in $\tilde{c}$. This expression illustrates the relative precision of the Binder crossing method of estimating K_c. Methods based on fitting observables evaluated at one system size at a time generically give corrections $\propto L^{-1/\nu}$, which vanishes more slowly for increasing system size than $L^{-\omega'}$. This is traced back to the fact that corrections $\propto L^{-1/\nu}$ cancel in Eq. (5.24), and the finite-size effects in estimating K_c are due to corrections to scaling $\propto c$.

5.4.2 Finding the correlation length exponent ν

Just as the crossing of Binder cumulant curves reveals the critical point, one can also find the correlation length exponent ν from the divergence of the slope these curves as $L \to \infty$. Differentiating the Binder ratio (5.23) at $K = K_c$ and neglecting corrections to scaling, we get[9]

$$\frac{\partial Q}{\partial K} = q_1 L^{1/\nu}. \tag{5.26}$$

The exponent ν can then be found from a linear fit in logarithmic coordinates in the usual manner:

$$\log \left.\frac{\partial Q}{\partial K}\right|_{K=K_c} = C + \frac{1}{\nu}\log L. \tag{5.27}$$

Here, $C = \log q_1$ is an unimportant constant.

A slightly more sophisticated method is based, not on the Binder ratio itself, but on the FSS expression of the magnetization moments that define it [170],

$$\langle |m|^k \rangle = L^{-k\beta/\nu}\mathcal{M}_k(tL^{1/\nu}). \tag{5.28}$$

The L-dependent factors cancel in the moment ratio $\langle m^4\rangle/\langle m^2\rangle^2$, but differentiating each of the moments separately, we get

$$\frac{\left(\partial\langle m^2\rangle/\partial K\right)^2}{\partial\langle m^4\rangle/\partial K} = \frac{\left[\mathcal{M}_2'(x)|_{x=0}\right]^2}{\mathcal{M}_4'(x)|_{x=0}} L^{1/\nu}. \tag{5.29}$$

This again allows us to find ν from a linear fit,

$$2\log\frac{\partial\langle m^2\rangle}{\partial K} - \log\frac{\partial\langle m^4\rangle}{\partial K} = \tilde{C} + \frac{1}{\nu}\log L. \tag{5.30}$$

To improve precision, the derivatives are calculated by their thermal averages

$$\frac{\partial\langle m^k\rangle}{\partial K} = \frac{\partial}{\partial K}\left[\frac{1}{\mathcal{Z}}\sum_{\{\mathbf{s}\}} m^k \mathrm{e}^{-S[\mathbf{s}]}\right] = \langle E\rangle\langle m^k\rangle - \langle Em^k\rangle, \tag{5.31}$$

with E being the energy term conjugate to K in the action, $S = KE + \ldots$.

[9] As in the previous section, we again assume a classical system.

5.4.3 Finding the dynamical critical exponent z

The scaling procedure described above assumes that one works with a scaling function $\mathcal{Q}$ with only one argument, an assumption that clearly breaks down for quantum critical systems. Rewriting (3.53), the scaling form of the Binder ratio now is

$$Q = \mathcal{Q}(tL^{1/\nu}, L_\tau/L^z), \tag{5.32}$$

so one has to determine z to fix the second argument before being able to employ the usual scaling procedure for the first argument.

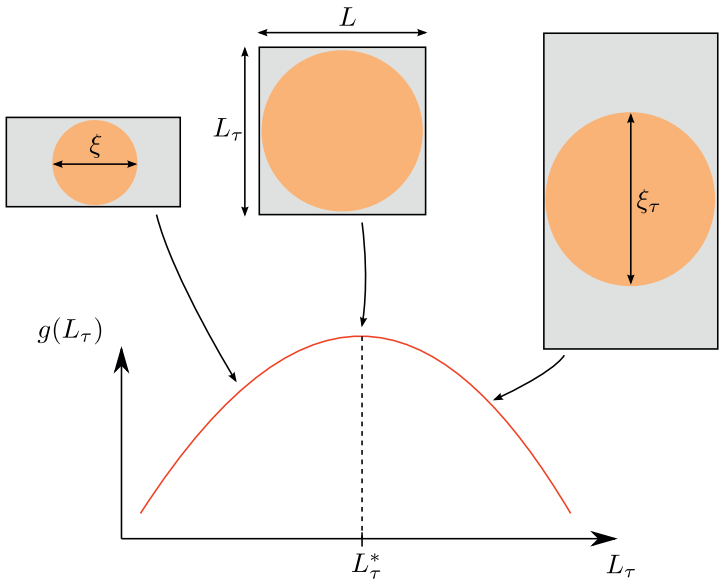

Figure 5.2: Schematic explanation of the behaviour of the Binder cumulant g at criticality as a function of temporal size L_τ for a fixed spatial size L. Assuming 1+1 dimensions, the correlation volume $\propto \xi \times \xi_\tau$ will be congruent with the system volume $L \times L^\tau$ at the optimal temporal extent $L_\tau = L_\tau^*$. (For isotropic interactions, as assumed in the figure, $L_\tau^* = L$.) Moving L_τ away from its optimal value, one of the correlation lengths will hit the edges of the system before the other, separating the system in uncorrelated segments. This increases overall fluctuations and decreases g.

A method based on the scaling (5.32) to determine both z and the critical point K_c self-consistently was first presented in Refs. [171, 172]. The underlying idea is that the Binder ratio measures the effect of fluctuations, and the fluctuations will increase when the aspect ratio given by L_τ/L^z deviates from the *optimal* aspect ratio given by the anisotropy of the diverging correlation volume $\propto \xi^d \times \xi_\tau$. It is easier to explain this by referring to Fig. 5.2, where we for simplicity consider a (1+1)D system. If the temporal extent L_τ is chosen much too small, the temporal correlation length ξ_τ will hit the edges of the system long before the spatial correlation length ξ as $K \to K_c$. In other words, there will still be relatively large fluctuations along the x direction at the pseudocritical point, and the system appears quasi-one-dimensional. If, on the other hand, L_τ is chosen much too large, one will also have an effectively one-dimensional system, this time with relatively large fluctuations in the τ direction.

In consequence, the fluctuations will be at a minimum and the Binder cumulant will have a maximum for a certain characteristic value $L_\tau = L_\tau^*$ for each value of L. Here, the system will appear as isotropic as it can possibly be, the anisotropy of the correlations lengths taken into account. Similarly as for the temporal correlation length ξ_τ, this characteristic temporal length L_τ^* will scale as $L_\tau^* \propto L^z$ for large L.

In practice, what one must do to find K_c and z is to map out curves as shown in Fig. 5.2 by simulating multiple values of L_τ for multiple values of L and K. An illustration of our implementation of the self-consistent procedure of Refs. [171, 172] is given in Fig. 2 of paper I, and here we also explain some of the details. A somewhat more sophisticated implementation is presented in paper II, where we also interpolate other observables to $L_\tau = L_\tau^*$ to be able to determine the other critical exponents in a consistent manner.

5.5 Error analysis

Say one wants to estimate the error $\Delta\bar{A}$ of a thermal average estimate $\bar{A}$ due to the finite number of samples N. This one can easily do using Eq. (5.8) by first estimating the variance and autocorrelation time of the sampled data set $\{A_i\}$. Complications arise, however, if one also wants the uncertainty of complicated non-linear functions f of a number of observables A, B, ... that may or may not be statistically independent. This is the case, for instance, for moment ratios of observables such as the Binder ratio introduced in Sec. 5.4.1. Also the results of curve fitting and interpolation procedures can be viewed as such complicated functions. The complications are not eased by considering that the full chain of post-processing and finite-size analysis consists of a number of such calculations and procedures, and at each step, uncertainties have to be estimated and propagated to the next step. Viewing the simulation as a numerical experiment, the solution to this problem is simple, but very time-consuming: One just repeats the experiment a large number M times and calculates error bars directly from the dispersion of the results. A smarter approach is found by turning to resampling ideas such as the *jackknife* and *the bootstrap* [173].

5.5.1 Bootstrap

One example of a complicated non-linear function is the characteristic temporal length L_τ^* defined in Sec. 5.4.3 as the maximum position the Binder cumulant g as a function of L_τ: It can be viewed as a function of the coefficients of the polynomial fit to $g(L_\tau)$, which in turn are functions of the magnetization data series for each of the simulated values of L_τ. Even when the uncertainties Δg can be regarded as known, and therefore in principle also the covariance matrix of the coefficients, these covariances make this an inconvenient way to obtain an estimate for ΔL_τ^*. A more elegant way may be to use a bootstrap procedure.

The idea of the bootstrap is to emulate repetitions of the numerical experiment by *resampling* the results obtained from the original simulation and basing the error estimate on the dispersion of the resampled results. To be concrete, we will consider

the example above, where we assume we have found the thermal average estimate $\bar{g}$ and estimated its uncertainty $\Delta\bar{g}$ for the Binder cumulant evaluated at a number of different L_τ. We then generate a set of M resampled average estimates $\{\tilde{g}_j\}$ chosen randomly from a Gaussian distribution with mean $\bar{g}$ and variance $(\Delta\bar{g})^2$. Hopefully, this resampled data set then represents the typical set of mean values $\bar{g}_j$ one would have obtained if one had repeated the original simulation (for this L_τ) M times. This resampling is done for each value of L_τ. For each $j = 1, 2, \ldots, M$, one then performs the polynomial fit on this set of $\tilde{g}_j$ at different L_τ to obtain an estimate for L_τ^*. Finally, the uncertainty of L_τ^* is estimated from the dispersion of these M resampled L_τ^* values.

More generally, we consider an arbitrary function f of estimates of the variables $A, B, \ldots$. Resampled variable estimates $\{\tilde{A}_j, \tilde{B}_j, \ldots\}$ for $j = 1, 2, \ldots, M$ are generated from the estimates $\bar{A} \pm \Delta\bar{A}$, $\bar{B} \pm \Delta\bar{B}$, ... We can then estimate the uncertainty of the quantity f as the standard deviation of the M results for f evaluated for the resampled variables:

$$\Delta f(\bar{A}, \bar{B}, \ldots) = \sqrt{\frac{1}{M-1} \sum_{j=1}^{M} \left[f(\tilde{A}_j, \tilde{B}_j, \ldots) - \tilde{f} \right]^2}. \tag{5.33}$$

The bootstrap average $\tilde{f}$ above is defined by

$$\tilde{f} = \frac{1}{M} \sum_{j=1}^{M} f(\tilde{A}_j, \tilde{B}_j, \ldots). \tag{5.34}$$

Variants of this technique can be implemented at all steps in the analysis, thus propagating the uncertainty to the end result.

5.5.2 Jackknife

Our point of departure when introducing the jackknife method will be that we want to estimate $\Delta\bar{A}$ from the original set of samples $\{A_i \mid i \in S\}$ from the Monte Carlo data series without the hassle of having to calculate the autocorrelation time. A clever way to circumvent autocorrelations is to divide the set S in M bins S_m $(m = 1, 2, \ldots, M)$ of equal size. One then calculates the average

$$\bar{A}_m = \frac{M}{N} \sum_{i \in S_m} A_i \tag{5.35}$$

of the observable for each of the bins. If the number of samples in each bin greatly exceeds the autocorrelation time, $N/M \gg \tau_A$, the estimates $\bar{A}_m$ for the different bins can be regarded as independent variables. This allows one to estimate the error in $\bar{A}$ from the distribution of the binned variables as

$$\Delta\bar{A} = \sqrt{\frac{1}{M(M-1)} \sum_{m=1}^{M} \left(\bar{A}_m - \bar{A} \right)^2}. \tag{5.36}$$

One problem with this somewhat naive method is that it is prone to instabilities if a relatively small number of independent samples in each bin make the individual estimates $\bar{A}_m$ noisy and unreliable. In the customary jackknife method, one therefore calculates M jackknife estimates $\bar{A}_{(m)}$ based on the samples in *all but* the mth bin,

$$\bar{A}_{(m)} = \frac{1}{M-1} \sum_{m' \neq m} \bar{A}_{m'}. \tag{5.37}$$

Based on this resampled set of averages $\{\bar{A}_{(m)}\}$, one can again estimate an uncertainty for $\bar{A}$. The only difference from Eq. (5.36) is that one must take into account that the jackknife estimates $\bar{A}_{(m)}$ for the mean are manifestly *interdependent* variables, being based on mostly the same data set, and this reduces the resulting standard deviations by a factor of $M-1$. The jackknife estimate for the error therefore becomes

$$\Delta\bar{A} = \sqrt{\frac{M-1}{M} \sum_{m=1}^{M} \left(\bar{A}_{(m)} - \bar{A}\right)^2}. \tag{5.38}$$

Analogously with Eq. (5.33) for the bootstrap method, one can also use the jackknife method to estimate the uncertainty of an arbitrary function $f(A, B, \ldots)$. A simple generalization of Eq. (5.38) gives the jackknife error estimate

$$\Delta f(\bar{A}, \bar{B}, \ldots) = \sqrt{\frac{M-1}{M} \sum_{m=1}^{M} \left[f(\bar{A}_{(m)}, \bar{B}_{(m)}, \ldots) - \bar{f}\right]^2}, \tag{5.39}$$

where we have introduced the jackknife average

$$\bar{f} = \frac{1}{M} \sum_{m=1}^{M} f(\bar{A}_{(m)}, \bar{B}_{(m)}, \ldots). \tag{5.40}$$

The beauty of the jackknife approach is that it makes it very easy to propagate the errors; one just feeds jackknife estimates $\{\bar{A}_{(m)}, \bar{B}_{(m)}, \ldots\}$ from the M jackknife bins into the analysis pipeline as if they were thermal averages obtained in M independent simulations. At the end of the pipeline one gathers the M values for the result and estimates the standard deviation, the only difference being the factor $M-1$ to account for the fact that these values are not, after all, obtained from independent simulations.

5.5.3 Reweighting

We conclude this section by a brief note on the concept of reweighting. When running Monte Carlo simulations, one samples observables for only a discrete set of coupling values. *Multiple histogram reweighting* [174] makes it possible to utilize the information available from all these coupling values to estimate the observables evaluated at any given other coupling value. An important condition for this estimate to be reliable is that there is a degree of overlap between the energy histograms of

the coupling values in question.[10] For details on the method, see Refs. [174, 156]. All Monte Carlo studies included in this thesis have profited greatly from the use of a multiple-histogram reweighting software package developed by Kari Rummukainen. This program also calculates jackknife estimates of the reweighted thermal averages.

[10]Incidentally, the requirement of relatively closely spaced coupling values also ensures that the acceptance rate of swaps is high when using parallel tempering. In fact, if focusing exclusively on the vicinity of a critical point, the acceptance rate may even become higher than what is typically [160, 157] recommended. The drawback is that one then cannot utilize the effect of shorter autocorrelation times away from criticality. Furthermore, data series for different couplings are no longer independent in the case of parallel tempering, and such cross-correlations reduce the amount of additional information possible to exploit by the reweighting procedure. There seems to be little knowledge about how to attain an optimal compromise for the coupling interval when performing reweighted parallel tempering simulations [175].

6 Summary of results and discussion

In this final chapter, we turn to the specific statistical mechanical models investigated in this thesis and the numerical results of our investigation. The aim of the chapter is to give a unified presentation of precisely how the models are defined and how they compare with respect to phase structure and dynamical critical scaling. Although we focus on the dissipative models considered in papers I to V, we will also summarize and comment on the results of papers VI and VII related to iron-based superconductors in Sec. 6.2.

6.1 Quantum phase transitions in spatially extended dissipative systems

In Sec. 6.1.1, we formulate the dissipative models we have studied and also try to state the motivation for studying them. The results for the phase diagrams are summarized and compared in 6.1.2, after which we do the same for the dynamical critical scaling (the value of z) in Sec. 6.1.3. We discuss the prospects for local quantum criticality in Sec. 6.1.4 and make some comments on the use of noncompact variables in Sec. 6.1.5.

6.1.1 Models

In an attempt to unify all the dissipative models that are formulated separately in papers I to V, we can express them as (d+1)-dimensional ($d > 0$) generalized clock models on the common form

$$\begin{aligned} S = &- K \sum_{\langle \mathbf{r},\mathbf{r}' \rangle} \sum_{\tau=1}^{L_\tau} \cos(\theta_{\mathbf{r},\tau} - \theta_{\mathbf{r}',\tau}) + \frac{K_\tau}{2} \sum_{\mathbf{r}} \sum_{\tau=1}^{L_\tau} \left(\frac{\partial \theta_{\mathbf{r}}}{\partial \tau} \right)^2 \\ &+ \frac{\alpha}{2} \sum_{\langle \mathbf{r},\mathbf{r}' \rangle} \sum_{\tau \neq \tau'}^{L_\tau} \left(\frac{\pi}{L_\tau} \right)^{1+s} \frac{[\varphi(\tau) - \varphi(\tau')]^2}{\sin^{1+s}(\frac{\pi}{L_\tau}|\tau - \tau'|)}, \end{aligned} \tag{6.1}$$

where the values allowed for the phase variables $\theta_{\mathbf{r},\tau}$ are for now left undetermined. We will call the first term the spatial term, the second term the kinetic term, and the third term is the dissipation term. The sites are the vertices of a square lattice

when $d+1=2$ and a cubic lattice when $d+1=3$, and $\mathbf{r}$ and τ are as before the spatial and temporal coordinates, respectively. The sum over $\langle \mathbf{r}, \mathbf{r}' \rangle$ is over all spatial bonds for the spatial term, but in the dissipation term, its interpretation depends on whether the as yet unspecified dissipative variables φ (with spatial indices suppressed) are bond or site variables. Similarly, the interpretation of the imaginary-time differentiation in the kinetic term depends on whether the phases $\theta_{\mathbf{r},\tau}$ will be compact or noncompact. It is also implicit that periodic boundary conditions are used in all directions, and that the width of the Trotter slices is fixed, $\Delta\tau = 1$. The different realizations of Eq. (6.1) are summarized in Table 6.1 and explained below.

In paper I and II, we study models with site dissipation. In paper I the motivation is to confirm that the value of the dynamical critical exponent is largely independent of spatial dimensionality for Ising symmetry and Ohmic dissipation, $s = 1$. In paper II, we investigate how the dynamical critical exponent (as well as the exponents η, ν, β and γ) depends on s for the case of super-Ohmic dissipation, $s > 1$, for $d = 1$ and both Ising-like and $U(1)$ symmetry. For site dissipation, the dissipative variable is taken to be the spin variables themselves, $\varphi(\tau) = \mathbf{s}_{\mathbf{r},\tau}$. The nominator of the dissipation term then becomes $[\varphi(\tau) - \varphi(\tau')]^2 = 2 - 2\,\mathbf{s}_{\mathbf{r},\tau} \cdot \mathbf{s}_{\mathbf{r},\tau'} = 2\left[1 - \cos(\theta_{\mathbf{r},\tau} - \theta_{\mathbf{r},\tau'})\right]$.[1] As this is a 2π-periodic function of the phases $\theta_{\mathbf{r},\tau}$, they can be taken to be compact variables, and we use[2] [Eq. (4.18)]

$$\frac{1}{2}\left(\frac{\partial \theta_{\mathbf{r}}}{\partial \tau}\right)^2 = -\cos(\theta_{\mathbf{r},\tau+1} - \theta_{\mathbf{r},\tau}) \qquad \text{(compact)}. \tag{6.2}$$

Table 6.1: Overview of the dissipative models studied in this thesis work. In the third column, the symmetries Z_q and $U(1)$ should not be taken literally in the noncompact case, where they are just labels indicating the number of states within each primary interval. In the fourth column, "site" refers to dissipation of spin variables and "bond" refers to dissipation of spin differences in the Z_2 case and phase differences otherwise.

Paper	Dimensionality	Degrees of freedom	Dissipation
I	(2+1)D	Compact Z_2	Ohmic site
I	(1+1)D	Compact Z_2	Ohmic bond
II	(1+1)D	Compact Z_4	Super-Ohmic site
II	(1+1)D	Compact $U(1)$	Super-Ohmic site
III	(1+1)D	Compact Z_4	Ohmic bond
III	(1+1)D	Noncompact Z_4	Ohmic bond
IV	(2+1)D	Compact $U(1)$	Ohmic bond
V	(2+1)D	Noncompact $U(1)$	Ohmic bond

Paper I is also a first study on the general effect of bond dissipation, which we for the Ising variables model by $\varphi(\tau) = \mathbf{s}_{\mathbf{r},\tau} - \mathbf{s}_{\mathbf{r}',\tau} \equiv \Delta s_{\mathbf{r},\mathbf{r}',\tau}$, $\mathbf{r}$ and $\mathbf{r}'$ being nearest neighbours. For all bond-dissipative models, we consider Ohmic dissipation, $s = 1$. As for the case of site dissipation of spin variables, the dissipation term can be

[1] In the Ising case, Z_2, we can write $\cos(\theta_{\mathbf{r},\tau} - \theta_{\mathbf{r},\tau'}) = \sigma_{\mathbf{r},\tau}\sigma_{\mathbf{r},\tau'}$ as in Sec. 3.3.1.

[2] Recall that $\cos(\theta_{\mathbf{r},\tau+1} - \theta_{\mathbf{r},\tau}) = 1 - \frac{1}{2}\left(\theta_{\mathbf{r},\tau+1} - \theta_{\mathbf{r},\tau}\right)^2 + \ldots$.

written in terms of dot products of spins or cosines of phases, and the model is again compact.

The first noncompact model we consider is found in paper III, which is intended as an investigation of the general effects of abandoning the compactness of the phase variables. This question is relevant in the context of resistively shunted Josephson junctions, as discussed in Sec. 4.4.3, but has nevertheless received little attention. The study was also motivated by the somewhat ambiguous definition of the phase field in the theory of circulating currents in the cuprates described in Sec. 4.5. Starting with a Z_4 model in (1+1) dimensions and adding bond dissipation in terms of the *phase* variables, and not the spin variables as above, we have $\varphi(\tau) = \theta_{\mathbf{r},\tau} - \theta_{\mathbf{r}',\tau} \equiv \Delta\theta_{\mathbf{r},\mathbf{r}',\tau}$. The dissipation term is no longer periodic in the phases $\theta_{\mathbf{r},\tau}$, and we use for the kinetic term that [Eq. (4.24)]

$$\frac{1}{2}\left(\frac{\partial\theta_{\mathbf{r}}}{\partial\tau}\right)^2 = \frac{1}{2}\left(\theta_{\mathbf{r},\tau+1} - \theta_{\mathbf{r},\tau}\right)^2 \qquad \text{(noncompact)}. \tag{6.3}$$

The aim of this paper is to investigate how the behaviour of this model differs from a similar model where one insists that $\theta_{\mathbf{r},\tau}$ should be regarded as compact phase variables. In this case, one should take into account that the phase differences $\Delta\theta_{\mathbf{r},\mathbf{r}',\tau}$ are only defined modulo 2π, and we therefore *compactify* the phase differences in the dissipation term. This is done in the same manner as when one calculates the vorticity of a compact phase field, as illustrated in Fig. 3.3. We thereby get new dissipative variables $\varphi(\tau) = \widetilde{\Delta\theta}_{\mathbf{r},\mathbf{r}',\tau} \in [-\pi,\pi\rangle$ that are periodic functions of $\theta_{\mathbf{r},\tau}$. Since the dissipation term is now manifestly compact, we can use the kinetic term (6.2).

In paper IV, the compact version of the model in paper III is extended to 2+1 space-time dimensions and continuous symmetry of the phase field. Our model is therefore a representation of the very same dissipative 2D XY model for circulating currents as that presented in Sec. 4.5, assuming that the order parameter field is to be interpreted as a compact $U(1)$-symmetric phase field. The aim is to investigate the dynamical critical exponent and the correlation functions of this model to see if it exhibits local quantum criticality.

Finally, in paper V we study the noncompact version of the model presented above. That is, we add bond dissipation with $\varphi(\tau) = \Delta\theta_{\mathbf{r},\mathbf{r}',\tau}$ to a (2+1)D XY model and use the kinetic term of Eq. (6.3). This is the model of a two-dimensional array of resistively shunted Josephson junctions with self-capacitance only, but can also be regarded as the circulating-current model if the phase variables are to be interpreted as noncompact. Our goal is again to look for local quantum criticality, as well as to investigate the structure of the zero-temperature phase diagram in light of the disparate predictions mentioned in Sec. 4.4.4.

6.1.2 Phase diagrams

We will first give an overview of the phase diagrams of the models presented above. There are essentially three different kinds of phase diagrams, as illustrated in Fig. 6.1.

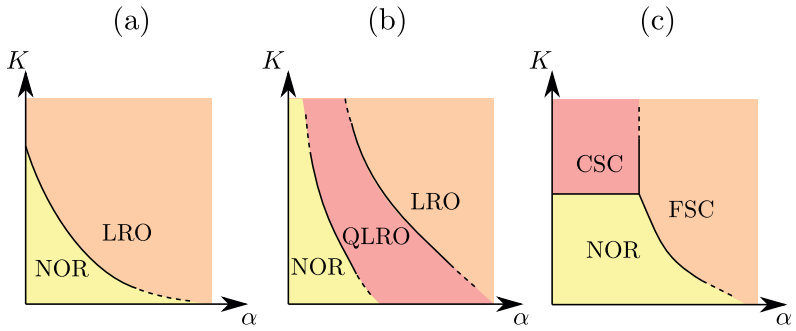

Figure 6.1: Schematic overview of the phase diagram topology for the dissipative models considered in this thesis work, in the space of spatial coupling K and dissipation strength α. NOR refers to a completely disordered phase (a normal phase in the context of superconducting systems), QLRO refers to a phase with quasi-long-range order, and LRO refers to a phase with long-range order. Diagram (a) is valid for all compact models, diagram (b) is the phase diagram of the noncompact (1+1)D Z_4 model of paper III, and diagram (c) is for the noncompact (2+1)D $U(1)$ model of paper V. For the latter, CSC stands for "critical superconducting" and FSC stands for "fully bond-ordered superconducting".

The compact models universally have two phases as shown in diagram (a): One disordered phase and one phase with uniform long-range order. The critical line separating the phases can be continuously connected to the critical point of the corresponding non-dissipative model at $\alpha = 0$, given that this model has a transition to long-range order for a finite K. The limit $K \to 0$ corresponds to independent (0+1)-dimensional systems with long-range interactions in the case of site dissipation, and whether or not these have a phase transition for a finite value of α depends on the symmetry and the decay exponent s. The case of bond dissipation is more complicated, and is discussed in some detail in paper I. For finite K, the phase transition is driven by proliferation of domain walls, point vortices or vortex loops, depending on symmetry and dimensionality.

For the noncompact (1+1)D Z_4 model, we get phase diagram (b) in Fig. 6.1. Remarkably, this diagram contains an intermediate critical phase with an emergent $U(1)$ symmetry and quasi-long-range order, similarly as for the two-dimensional Z_q models discussed in Sec. 3.4. This is surprising because classical Z_q models exhibit an intermediate phase only for $q \geq 5$, whereas in the quantum model we considered, $q = 4$. We conjecture that this is explained by the additional degrees of freedom associated with noncompactness of the phases that are not present in the classical (Ising-like) Z_4 model. The transition from the LRO to the QLRO phase is driven by proliferation of domain walls as before, whereas the transition from QLRO to disorder probably can be associated with the proliferation of instanton-like defects in the imaginary-time history of the bond variables $\Delta\theta$. We emphasize that the critical lines for $\alpha > 0$ cannot be continuously connected to those of the corresponding nondissipative model in the noncompact case, since a finite α is necessary to render the phases noncompact in the first place.

The third phase diagram (c) in Fig. 6.1 is obtained for the noncompact (2+1)D model of an array of resistively shunted Josephson junctions. The most ordered phase here is denoted FSC (fully bond-ordered superconducting), which has long-range order in space but not in time. Apparently, the imaginary-time interaction is not capable of ordering this direction in the complete absence of a spin gap, although the bond dissipation ensures temporal order in the sense of localization of phase differences $\Delta\theta$. The transition from the FSC phase to CSC phase is driven by proliferation of temporal bond instantons as the dissipation strength is lowered. This results in a phase with temporal disorder but spatial quasi-long-range order, hence the label "critical superconducting" (CSC). The transition from the CSC phase to the completely disordered NOR phase is driven by proliferation of vortex-like point defects on each Trotter slice.[3] The direct transition FSC–NOR is harder to characterize, but is probably driven by a combined proliferation of vortex-like and instanton-like defects.

For both phase diagram (a) and phase diagram (b) in Fig. 6.1, one can define paths in parameter space along which the system goes from the most ordered phase to the least ordered phase through a two-step phase transition. These phase diagrams also bear some resemblance to that shown in Fig. 3.1 for 2D $Z_{q\geq 5}$ models, and one can construct a unified picture where the steps of these two-step transitions can be associated with the proliferation of one topological defect each. For the classical clock models, these defects are vortices and domain walls, and the intermediate phase is a result of domain walls proliferating at a higher coupling than vortices [82, 176]. The situation for the noncompact Z_4 model considered in paper III is that domain walls proliferate before bond instantons, and in the noncompact $U(1)$ model studied in paper V, bond instantons proliferate first, followed by point vortices.[4]

6.1.3 Dynamical critical scaling

Our expectations regarding the value of the dynamical critical exponent z is largely based on the naive scaling estimates presented in Sec. 4.3.1. According to these arguments, Ohmic site-dissipative models should have $z \approx 2$ irrespective of symmetry and dimensionality, and bond-dissipative models should invariably have $z \approx 1$. This is confirmed by our numerical results for all models considered in papers I, III, IV and moreover seems to be valid for all points along the critical lines ($\alpha > 0$, $K > 0$) of phase diagrams (a) and (b) in Fig. 6.1. It is worth pointing out that for the noncompact Z_4 model, $z \approx 1$ within the entire intermediate critical phase itself, as well as along both transition lines.[5]

[3] How one defines vortex-like defects in a noncompact phase field is explained in Sec. 6.1.5 and – in more detail – in paper V.

[4] In all cases, the two-step transition takes the system from LRO to disorder via QLRO, but for the model in paper V, LRO and QLRO curiously enough only refers to the spatial ordering. We therefore stress that the picture appears to be more complicated for the noncompact $U(1)$ model. Furthermore, only for the classical $Z_{q\geq 5}$ models and the noncompact Z_4 model can the intermediate phase be associated with an emergent $U(1)$ symmetry.

[5] In a critical phase, z should strictly speaking be defined from the spatiotemporal correlation functions (3.45) and (3.46), as both ξ and ξ_τ are already infinite.

For non-Ohmic site-dissipative models, one observes significant deviations from naive scaling for $s > 1$, and the numerical results of paper II corroborate the corrected scaling ansatz $z = \max\{(2-\eta)/s, 1\}$ presented in Sec. 4.3.2 for both discrete and continuous symmetries. For our (1+1)-dimensional model, the anomalous dimension approaches the value $\eta = 0.25$ as the effective dimensionality $d_{\text{eff}} = 1 + z$ approaches 2, which illustrate the limitations of the naive scaling estimate far away from the mean-field limit $d_{\text{eff}} = 4$. As a related result, the dissipation term is rendered irrelevant for values $s > 1.75$ for $d = 1$, whereas naive scaling predicts that dissipation is relevant all the way up to $s = 2$. We expect that naive scaling will be a much better approximation for $d = 2$ (for all s) owing to much smaller values of η.[6]

Extra care was taken to substantiate the result $z = 1$ for the compact (2+1)D $U(1)$ model with bond dissipation because of the suggestion that such a model should exhibit local quantum criticality. We ruled out a number of possible explanations of why we were unable to observe a diverging z (if present), such as finite-size crossovers of the extracted exponent, weak activated dynamical scaling, incomplete equilibration, or that the result for z (obtained from analysing the Binder cumulant) should somehow not represent the anisotropy of the correlation function. Adding a strong fourfold anisotropy field, as required for the original circulating-current degrees of freedom, seemed to turn the continuous phase transition first order. Although this is somewhat surprising, it is not unreasonable that a hard Z_4 constraint generically alters the universality class (as long as the model is not in the mean-field regime) or even the order of the phase transition.

The only challenge posed to the simple naive-scaling picture of dynamical critical scaling comes from the noncompact (2+1)D $U(1)$ model of paper V. In this case, noncompact phases and continuous symmetry somehow conspire to prevent temporal ordering of the phases. The assumption of a transition to a uniformly ordered (either LRO or QLRO) state ($q \to 0$ *and* $\omega \to 0$) is rendered invalid, and the (uniform) magnetization m is not a useful order parameter. In a sense, this is consistent with a dynamical critical exponent $z \to 0$, which is in fact the result we obtain if we apply the usual Binder cumulant analysis to the transitions NOR–CSC and NOR–FSC. This is reasonable at least for the former, since CSC–NOR is a phase transition driven by purely spatial topological defects. The transition FSC–CSC, on the other hand, is predominantly temporal, yet it may not be correct to characterize it as a local transition since the spatial correlation length is already infinite in the CSC phase. The spatiotemporal anisotropy of the transition FSC–NOR has proved even harder to characterize due to the concomitant proliferation of both spatial and temporal defects, but we have seen no evident signs of locality.

6.1.4 Local quantum criticality

Although we have not observed local quantum criticality in any of the models we have investigated, we nevertheless wish to discuss the distinctions between the various scenarios hiding behind the simplistic label "$z = \infty$". If we formally define the

[6] In fact, we chose $d = 1$ in paper II because the relatively large η_{SR} of the underlying (1+1)D short-range-interacting model makes the deviations from naive scaling easier to discern.

dynamical critical exponent through $\xi_\tau \sim \xi^z$ and restrict ourselves to a single local critical point for which all critical fluctuations are described by the corresponding order parameter, there are principally two possibilities: 1) The spatial correlation length ξ diverges as a power law and the temporal correlation length ξ_τ diverges exponentially. 2) The spatial correlation length does not diverge at criticality, but the temporal correlation length diverges either algebraically or exponentially. The second class of local critical points may further be divided in two subclasses: a) The spatial correlations decay exponentially at the critical point, possibly with a relatively large but finite correlation length. b) The spatial correlations are truly local, as described by the limit $\xi \to 0$ for exponential decay or by some other realization of a delta function.[7] Scenario (1) corresponds to activated dynamical scaling, and scenario (2b) includes the variant of local quantum criticality originally predicted in Ref. [1].

Another question is how the spatial correlation length develops as one moves away from the critical point. For case (1), this is given by the form of the algebraic divergence, and for case (2a), the correlation length presumably evolves as some analytic function across the phase transition. The case (2b) is less clear. Unless the disordered phase is some form of local phase, one generally has a finite correlation length $\xi > 0$ for $K < K_c$. Furthermore, one might perhaps expect that some spatial correlations around $K = K_c$ are necessary if the system is to develop uniform long-range order for $K > K_c$ and not some form of columnar order where (0+1)-dimensional subsystems order independently. If the phase at $K > K_c$ on the other hand is a (uniform) QLRO phase, ξ would have to jump discontinuously from a small or vanishing value at $K = K_c$ to infinity for $K > K_c$ both for scenario (2a) and (2b).

We will end this relatively speculative chapter with a different possible realization of local quantum criticality. As in scenario (2) above, we assume that ξ_τ diverges at some $K = K_{c,1}$ whereas ξ does not. If ξ_τ remains infinite and ξ remains non-infinite also for $K > K_{c,1}$, this region would be a *local critical phase*. Such a phase would in principle be possible both for case (2a) and (2b), although the phase can be truly local only for the latter. If also ξ diverges at some $K_{c,2} > K_{c,1}$, one would have a two-step phase transition of a similar kind as those discussed in Sec. 6.1.2. This form of local quantum criticality was also discussed in paper V, but was not observed in our simulations.

6.1.5 Compactness and noncompactness

One potentially confusing issue is the use of an order parameter m given by Eq. (3.2), with

$$|m|^2 = \frac{1}{(L^d L_\tau)^2} \left[\left(\sum_{\mathbf{r},\tau} \cos\theta_{\mathbf{r},\tau} \right)^2 + \left(\sum_{\mathbf{r},\tau} \sin\theta_{\mathbf{r},\tau} \right)^2 \right], \tag{6.4}$$

[7] We can also envisage two other – possibly even more pathological – forms of dynamical critical scaling: 2c) The spatial correlation length diverges logarithmically (which in the case of algebraic temporal divergence would be yet another form of activated dynamical scaling, $\ln \xi_\tau \sim \xi^\psi$). 3) Both spatial and temporal divergences are exponential, $\xi \sim \exp(b/t^{\nu'})$ and $\xi_\tau \sim \exp(b_\tau/t^{\nu'_\tau})$, but with different exponents $\nu'_\tau > \nu'$.

also for noncompact phases $\theta_{\mathbf{r},\tau}$. Being periodic, this function projects the distribution of the phases on the extended interval $\langle -\infty, \infty \rangle$ onto the primary interval $[0, 2\pi\rangle$. As in paper V, we will denote this projection by $\tilde{\theta}_{\mathbf{r},\tau} \in [0, 2\pi\rangle$. When the value of m signifies order, this therefore means order of $\tilde{\theta}_{\mathbf{r},\tau}$, and one has no information about the distribution of phase values $\theta_{\mathbf{r},\tau}$ on the extended interval. Similarly, when we refer to vortex-like defects for noncompact models, these are vortices in $\tilde{\theta}_{\mathbf{r},\tau}$, as the noncompact phase field $\theta_{\mathbf{r},\tau}$ cannot support actual vortices. That the order parameter m does not provide a complete picture is particularly evident in the FSC phase of paper V. Here one has temporal order – in the sense of localization of the imaginary-time paths of $\Delta\theta$ – that m is simply not able to see.

One reason why we are only interested in the ordering of the phase modulo 2π is that the correlation function (4.25) is a 2π-periodic function. This compact correlation function is the defining quantity of local quantum criticality in Ref. [1], and therefore we use the corresponding compact order parameter. This choice of the order parameter also justifies the use of the labels Z_4 and $U(1)$ when referring to the order parameter symmetry. Although these terms do not describe the allowed states of the order parameter field $\theta_{\mathbf{r},\tau}$ in a strict, group-theoretical sense, they do describe the symmetry that is broken by the primary-interval projection $\tilde{\theta}_{\mathbf{r},\tau}$ in a phase that is ordered with respect to m.

6.2 The pairing state of iron-based superconductors

The questions we asked in paper VI and VII were: What are the signatures of an $s_{\pm}$-wave state in a minimal two-band model of iron-based superconductors, and how are these influenced by the coupling between the two bands? We studied conductance spectra and the Josephson effect both for clean and dirty $s_{\pm}$-wave superconductors. In particular, we wanted to investigate whether 0–π transitions could take place in such systems, as they are known to do in other exotic Josephson junctions.

In our case, competition between the two Andreev bound states for the two sign-shifted gaps provided a very transparent mechanism behind a 0–π transition. Hybridization of the two ABSs due to interband coupling did not change this simple result. In this way, signatures of the $s_{\pm}$-wave state in the Josephson effect is independent of interband coupling, whereas finite interband coupling turned out to be essential to reveal signatures of an $s_{\pm}$-wave state through conductance spectroscopy. This makes the Josephson effect a more promising probe of the pairing state, and the most realistic experiment would probably be one where one looks for 0–π transitions by tuning the temperature instead of intrinsic parameters of the junction. Unfortunately, clear-cut signatures of thermal 0–π shifts were predicted only in the diffusive limit, and has to date not been detected experimentally.

As explained in Sec. 2.4, the bulk of the experimental evidence now points to the $s_{\pm}$-wave state as the most likely pairing state. Nevertheless, most experiments mentioned in Sec. 2.4 can be regarded as *indirectly* phase-sensitive probes, and an experiment able to measure the phase of the superconducting order parameter directly for iron-based superconductors is still highly desirable. However, it has

been realized over the last couple of years that the gap function of these materials is less universal than initially hoped, with gap anisotropy and possible appearance of accidental nodes depending on doping and other details [61]. It is therefore important to point out that unambiguous determination of the pairing state for a single iron-based superconductor may not be as decisive as it was for the cuprates.

6.3 Concluding remarks

Summarizing the part of this thesis dealing with dissipative quantum phase transitions, we initially asked two interrelated questions: 1) What can one in general say about the dependence of the dynamical critical exponent z on the key attributes (dimensionality, symmetry, bath exponent) of a dissipative model? 2) Can one find local quantum criticality ($z \to \infty$) in models with Ohmic bond dissipation? The answer to the first question seems to be that the naive scaling estimate for z is remarkably robust. This also means that the answer to the second question is "no", with a few reservations mentioned in preceding sections. For instance, whether the variables are defined as compact or noncompact does not in general alter the dynamical critical scaling, but complications arise when one cannot find a single order parameter that gives a complete description of the phase transition. Noncompactness may also have a major impact on the phase diagram and on which topological defects that are possible. For these reasons, models with noncompact phases do not permit straightforward characterization of their phase transitions.

Having the theory of circulating currents in cuprate superconductors in mind, we have also been able to answer some of the questions posed in Sec. 4.5.2. Assuming that these currents can be described by a compact phase field, we have shown that it matters for the nature of the quantum phase transition whether this order parameter field has discrete or continuous symmetry, but in neither case is the transition local. The essentially spatiotemporally isotropic correlation function of this model does not give rise to the momentum-independent fluctuation spectrum posited by marginal-Fermi-liquid theory. At least for compact variables, the bond-dissipative (2+1)D XY model is not able to describe the putative quantum critical point of cuprate high-temperature superconductors.

Bibliography

[1] V. Aji and C. M. Varma, Phys. Rev. Lett. **99**, 067003 (2007).

[2] M. R. Norman, Science **332**, 196 (2011).

[3] K. Fossheim and A. Sudbø, *Superconductivity: Physics and Applications* (John Wiley & Sons, Ltd, Chichester, 2004).

[4] A. J. Leggett, Nature Phys. **2**, 134 (2006).

[5] J. Paglione and R. L. Greene, Nature Phys. **6**, 645 (2010).

[6] G. R. Stewart, Rev. Mod. Phys. **83**, 1589 (2011).

[7] J. Tallon and J. Loram, Physica C **349**, 53 (2001).

[8] N. E. Hussey, J. Phys.: Condens. Matter **20**, 123201 (2008).

[9] C. M. Varma, Phys. Rev. B **55**, 14554 (1997).

[10] S. Kivelson and H. Yao, Nature Mater. **7**, 927 (2008).

[11] C. M. Varma, P. B. Littlewood, S. Schmitt-Rink, E. Abrahams, and A. E. Ruckenstein, Phys. Rev. Lett. **63**, 1996 (1989).

[12] H. Alloul, T. Ohno, and P. Mendels, Phys. Rev. Lett. **63**, 1700 (1989).

[13] H. Alloul, F. Rullier-Albenque, B. Vignolle, D. Colson, and A. Forget, EPL **91**, 37005 (2010).

[14] J. Zaanen, A modern, but way too short history of the theory of superconductivity at a high temperature, in *100 years of superconductivity*, edited by H. Rogalla and P. H. Kes, Taylor & Francis, London, 2011, (e-print arXiv:1012.5461).

[15] J. Meng et al., Nature (London) **462**, 335 (2009).

[16] H.-B. Yang et al., Phys. Rev. Lett. **107**, 047003 (2011).

[17] S. E. Sebastian, G. G. Lonzarich, and N. Harrison, (2011), arXiv:1112.1373 (unpublished).

[18] C. M. Varma, Phys. Rev. B **73**, 155113 (2006).

[19] P. Bourges and Y. Sidis, C. R. Physique **12**, 461 (2011).

[20] A. Kaminski et al., Nature (London) **416**, 610 (2002).

[21] S. V. Borisenko et al., Phys. Rev. Lett. **92**, 207001 (2004).

[22] V. Arpiainen, A. Bansil, and M. Lindroos, Phys. Rev. Lett. **103**, 067005 (2009).

[23] H. A. Mook, Y. Sidis, B. Fauqué, V. Balédent, and P. Bourges, Phys. Rev. B **78**, 020506(R) (2008).

[24] Y. Li et al., Nature (London) **455**, 372 (2008).

[25] V. Balédent et al., Phys. Rev. Lett. **105**, 027004 (2010).

[26] Y. Li et al., Nature (London) **468**, 283 (2010).

[27] Y. Li et al., Nature Phys. **8**, 404 (2012).

[28] J. Xia et al., Phys. Rev. Lett. **100**, 127002 (2008).

[29] R.-H. He et al., Science **331**, 1579 (2011).

[30] B. Leridon, P. Monod, D. Colson, and A. Forget, EPL **87**, 17011 (2009).

[31] G. J. MacDougall et al., Phys. Rev. Lett. **101**, 017001 (2008).

[32] J. E. Sonier et al., Phys. Rev. Lett. **103**, 167002 (2009).

[33] W. Huang, V. Pacradouni, M. P. Kennett, S. Komiya, and J. E. Sonier, Phys. Rev. B **85**, 104527 (2012).

[34] S. Strässle, J. Roos, M. Mali, H. Keller, and T. Ohno, Phys. Rev. Lett. **101**, 237001 (2008).

[35] S. Strässle, B. Graneli, M. Mali, J. Roos, and H. Keller, Phys. Rev. Lett. **106**, 097003 (2011).

[36] C. Weber, A. Läuchli, F. Mila, and T. Giamarchi, Phys. Rev. Lett. **102**, 017005 (2009).

[37] M. Greiter and R. Thomale, Phys. Rev. Lett. **99**, 027005 (2007).

[38] S. Nishimoto, E. Jeckelmann, and D. J. Scalapino, Phys. Rev. B **79**, 205115 (2009).

[39] C. Xu and S. Sachdev, Nature Phys. **4**, 898 (2008).

[40] E. Abrahams and Q. Si, J. Phys.: Condens. Matter **23**, 223201 (2011).

[41] J. E. Hoffman, Rep. Prog. Phys. **74**, 124513 (2011).

[42] P. Richard, T. Sato, K. Nakayama, T. Takahashi, and H. Ding, Rep. Prog. Phys. **74**, 124512 (2011).

[43] D. N. Basov and A. V. Chubukov, Nature Phys. **7**, 272 (2011).

[44] D. Daghero, M. Tortello, G. A. Ummarino, and R. S. Gonnelli, Rep. Prog. Phys. **74**, 124509 (2011).

[45] A. A. Golubov and I. I. Mazin, Physica C **243**, 153 (1995).

[46] I. I. Mazin, D. J. Singh, M. D. Johannes, and M. H. Du, Phys. Rev. Lett. **101**, 057003 (2008).

[47] I. I. Mazin, Nature (London) **464**, 183 (2010).

[48] D. J. Scalapino, Physica C **470**, S1 (2010).

[49] M. Tinkham, *Introduction to Superconductivity* (Krieger Publishing Company, Malabar, FL, 1975).

[50] A. A. Golubov, M. Y. Kupriyanov, and E. Il'ichev, Rev. Mod. Phys. **76**, 411 (2004).

[51] M. Greiter, Ann. Phys. (Leipzig) **319**, 217 (2005).

[52] A. I. Buzdin, Rev. Mod. Phys. **77**, 935 (2005).

[53] V. V. Ryazanov et al., Phys. Rev. Lett. **86**, 2427 (2001).

[54] H. Miyazaki, Y. Takahide, A. Kanda, and Y. Ootuka, Phys. Rev. Lett. **89**, 197001 (2002).

[55] D. B. Haviland, K. Andersson, and P. Ågren, J. Low Temp. Phys. **118**, 733 (2000).

[56] Y. Takahide, R. Yagi, A. Kanda, Y. Ootuka, and S.-i. Kobayashi, Phys. Rev. Lett. **85**, 1974 (2000).

[57] A. J. Rimberg et al., Phys. Rev. Lett. **78**, 2632 (1997).

[58] J. S. Penttilä, U. Parts, P. J. Hakonen, M. A. Paalanen, and E. B. Sonin, Phys. Rev. Lett. **82**, 1004 (1999).

[59] T. Löfwander, V. Shumeiko, and G. Wendin, Supercond. Sci. Technol. **14**, R53 (2001).

[60] I. Mazin and J. Schmalian, Physica C **469**, 614 (2009).

[61] P. J. Hirschfeld, M. M. Korshunov, and I. I. Mazin, Rep. Prog. Phys. **74**, 124508 (2011).

[62] Y. Tanaka and S. Kashiwaya, Phys. Rev. Lett. **74**, 3451 (1995).

[63] X. Zhang et al., Phys. Rev. Lett. **102**, 147002 (2009).

[64] C. T. Chen, C. C. Tsuei, M. B. Ketchen, Z. A. Ren, and Z. X. Zhao, Nature Phys. **6**, 260 (2010).

[65] A. Christianson et al., Nature (London) **456**, 930 (2008).

[66] T. Hanaguri, S. Niitaka, K. Kuroki, and H. Takagi, Science **328**, 474 (2010).

[67] D. J. Van Harlingen, Rev. Mod. Phys. **67**, 515 (1995).

[68] P. Seidel, Supercond. Sci. Technol. **24**, 043001 (2011).

[69] K. D. Usadel, Phys. Rev. Lett. **25**, 507 (1970).

[70] G. E. Blonder, M. Tinkham, and T. M. Klapwijk, Phys. Rev. B **25**, 4515 (1982).

[71] C. W. J. Beenakker, Phys. Rev. Lett. **67**, 3836 (1991).

[72] N. Goldenfeld, *Lectures on Phase Transitions and the Renormalization Group* (Perseus Books, Reading, MA, 1992).

[73] J. Cardy, *Scaling and Renormalization in Statistical Physics* (Cambridge University Press, New York, 1996).

[74] J. Binney, N. J. Dowrick, A. Fisher, and M. Newman, *The Theory of Critical Phenomena* (Oxford University Press, New York, 1992).

[75] A. Pelissetto and E. Vicari, Phys. Rep. **368**, 549 (2002).

[76] R. J. Baxter, *Exactly Solved Models in Statistical Mechanics* (Academic, London, 1982).

[77] N. D. Mermin and H. Wagner, Phys. Rev. Lett. **17**, 1133 (1966).

[78] J. M. Kosterlitz and D. J. Thouless, J. Phys. C **6**, 1181 (1973).

[79] M. Hasenbusch, J. Phys. A: Math. Gen. **38**, 5869 (2005).

[80] S. Elitzur, R. B. Pearson, and J. Shigemitsu, Phys. Rev. D **19**, 3698 (1979).

[81] C. M. Lapilli, P. Pfeifer, and C. Wexler, Phys. Rev. Lett. **96**, 140603 (2006).

[82] G. Ortiz, E. Cobanera, and Z. Nussinov, Nucl. Phys. B **854**, 780 (2012).

[83] O. Borisenko et al., Phys. Rev. E **85**, 021114 (2012).

[84] J. Hove and A. Sudbø, Phys. Rev. E **68**, 046107 (2003).

[85] J. V. José, L. P. Kadanoff, S. Kirkpatrick, and D. R. Nelson, Phys. Rev. B **16**, 1217 (1977).

[86] M. Caselle and M. Hasenbusch, J. Phys. A **31**, 4603 (1998).

[87] J. Lou, A. W. Sandvik, and L. Balents, Phys. Rev. Lett. **99**, 207203 (2007).

[88] E. Luijten and H. W. J. Blöte, Phys. Rev. B **56**, 8945 (1997).

[89] M. E. Fisher, S.-k. Ma, and B. G. Nickel, Phys. Rev. Lett. **29**, 917 (1972).

[90] E. Luijten and H. W. J. Blöte, Phys. Rev. Lett. **76**, 1557 (1996).

[91] J. Sak, Phys. Rev. B **8**, 281 (1973).

[92] E. Luijten and H. W. J. Blöte, Phys. Rev. Lett. **89**, 025703 (2002).

[93] D. J. Thouless, Phys. Rev. **187**, 732 (1969).

[94] J. Bhattacharjee, S. Chakravarty, J. L. Richardson, and D. J. Scalapino, Phys. Rev. B **24**, 3862 (1981).

[95] E. Luijten and H. Meßingfeld, Phys. Rev. Lett. **86**, 5305 (2001).

[96] S. L. Sondhi, S. M. Girvin, J. P. Carini, and D. Shahar, Rev. Mod. Phys. **69**, 315 (1997).

[97] M. Vojta, Rep. Prog. Phys. **66**, 2069 (2003).

[98] T. Vojta, Rev. Comput. Chem. **26**, 167 (2008).

[99] M. Suzuki, Prog. Theor. Phys. **56**, 1454 (1976).

[100] A. Altland and B. Simons, *Condensed Matter Field Theory* (Cambridge University Press, Cambridge, 2010).

[101] M. Wallin, E. S. Sørensen, S. M. Girvin, and A. P. Young, Phys. Rev. B **49**, 12115 (1994).

[102] J. A. Hertz, Phys. Rev. B **14**, 1165 (1976).

[103] K. S. D. Beach, L. Wang, and A. W. Sandvik, (2005), arXiv:cond-mat/0505194v1 (unpublished).

[104] P. Coleman, C. Pépin, Q. Si, and R. Ramazashvili, J. Phys.: Condens. Matter **13**, R723 (2001).

[105] A. W. Sandvik, AIP Conf. Proc. **1297**, 135 (2010).

[106] H. Weber and P. Minnhagen, Phys. Rev. B **37**, 5986 (1988).

[107] P. W. Anderson, G. Yuval, and D. R. Hamann, Phys. Rev. B **1**, 4464 (1970).

[108] A. O. Caldeira and A. J. Leggett, Phys. Rev. Lett. **46**, 211 (1981).

[109] A. O. Caldeira and A. J. Leggett, Ann. Phys. (NY) **149**, 374 (1983).

[110] A. J. Leggett et al., Rev. Mod. Phys. **59**, 1 (1987).

[111] P. Werner, *Dissipative quantum phase transitions*, PhD thesis, ETH Zürich, 2005.

[112] G.-L. Ingold, Path integrals and their application to dissipative quantum systems, in *Coherent Evolution in Noisy Environments*, edited by A. Buchleitner and K. Hornberger, volume 611 of *Lecture Notes in Physics*, pp. 1–53, Springer Berlin / Heidelberg, 2002.

[113] K. Le Hur, Quantum Phase Transitions in Spin-Boson Systems: Dissipation and Light Phenomena, in *Understanding Quantum Phase Transitions*, edited by L. D. Carr, Taylor & Francis, Boca Raton, FL, 2010, (e-print arXiv:0909.4822).

[114] S. Chakravarty, Phys. Rev. Lett. **49**, 681 (1982).

[115] M. Vojta, N.-H. Tong, and R. Bulla, Phys. Rev. Lett. **94**, 070604 (2005).

[116] M. Vojta, N.-H. Tong, and R. Bulla, Phys. Rev. Lett. **102**, 249904(E) (2009).

[117] S. Kirchner, J. Low Temp. Phys. **161**, 282 (2010).

[118] S. Pankov, S. Florens, A. Georges, G. Kotliar, and S. Sachdev, Phys. Rev. B **69**, 054426 (2004).

[119] P. Werner, K. Völker, M. Troyer, and S. Chakravarty, Phys. Rev. Lett. **94**, 047201 (2005).

[120] P. Werner, M. Troyer, and S. Sachdev, J. Phys. Soc. Jpn. **74S**, 67 (2005).

[121] K. Børkje and A. Sudbø, Phys. Rev. B **77**, 092404 (2008).

[122] A. J. Bray and M. A. Moore, Phys. Rev. Lett. **49**, 1545 (1982).

[123] A. Schmid, Phys. Rev. Lett. **51**, 1506 (1983).

[124] M. P. A. Fisher and W. Zwerger, Phys. Rev. B **32**, 6190 (1985).

[125] K. K. Likharev and A. B. Zorin, J. Low Temp. Phys. **59**, 347 (1985).

[126] G. Schön and A. D. Zaikin, Phys. Rep. **198**, 237 (1990).

[127] C. P. Herrero and A. D. Zaikin, Phys. Rev. B **65**, 104516 (2002).

[128] N. Kimura and T. Kato, Phys. Rev. B **69**, 012504 (2004).

[129] P. Werner and M. Troyer, Phys. Rev. Lett. **95**, 060201 (2005).

[130] G. Refael, E. Demler, Y. Oreg, and D. S. Fisher, Phys. Rev. B **68**, 214515 (2003).

[131] W. Zwerger, Phys. Rev. B **35**, 4737 (1987).

[132] S. Chakravarty, G.-L. Ingold, S. Kivelson, and A. Luther, Phys. Rev. Lett. **56**, 2303 (1986).

[133] S. Chakravarty, G.-L. Ingold, S. Kivelson, and G. Zimanyi, Phys. Rev. B **37**, 3283 (1988).

[134] S. V. Panyukov and A. D. Zaikin, J. Low Temp. Phys. **75**, 361 (1989).

[135] P. A. Bobbert, R. Fazio, G. Schön, and A. D. Zaikin, Phys. Rev. B **45**, 2294 (1992).

[136] P. Goswami and S. Chakravarty, Phys. Rev. B **73**, 094516 (2006).

[137] G. Refael, E. Demler, Y. Oreg, and D. S. Fisher, Phys. Rev. B **75**, 014522 (2007).

[138] S. Tewari, J. Toner, and S. Chakravarty, Phys. Rev. B **72**, 060505(R) (2005).

[139] S. Tewari, J. Toner, and S. Chakravarty, Phys. Rev. B **73**, 064503 (2006).

[140] L. Capriotti, A. Cuccoli, A. Fubini, V. Tognetti, and R. Vaia, Phys. Rev. Lett. **91**, 247004 (2003).

[141] L. Capriotti, A. Cuccoli, A. Fubini, V. Tognetti, and R. Vaia, Phys. Rev. Lett. **94**, 157001 (2005).

[142] C. M. Varma, Phys. Rev. Lett. **75**, 898 (1995).

[143] C. M. Varma, Phys. Rev. Lett. **83**, 3538 (1999).

[144] M. E. Simon and C. M. Varma, Phys. Rev. Lett. **89**, 247003 (2002).

[145] M. S. Grønsleth et al., Phys. Rev. B **79**, 094506 (2009).

[146] V. Aji, A. Shekhter, and C. M. Varma, Phys. Rev. B **81**, 064515 (2010).

[147] V. Aji and C. M. Varma, Phys. Rev. B **79**, 184501 (2009).

[148] V. Aji and C. M. Varma, Phys. Rev. B **82**, 174501 (2010).

[149] Q. Si, S. Rabello, K. Ingersent, and J. L. Smith, Nature (London) **413**, 804 (2001).

[150] Q. Si, Quantum Criticality and the Kondo Lattice, in *Understanding Quantum Phase Transitions*, edited by L. D. Carr, Taylor & Francis, Boca Raton, FL, 2010, (e-print arXiv:1012.5440).

[151] M. T. Glossop and K. Ingersent, Phys. Rev. Lett. **95**, 067202 (2005).

[152] D. S. Fisher, Phys. Rev. Lett. **69**, 534 (1992).

[153] K.-H. Wagenblast, A. van Otterlo, G. Schön, and G. T. Zimányi, Phys. Rev. Lett. **78**, 1779 (1997).

[154] S. Tewari and J. Toner, Europhys. Lett. **74**, 341 (2006).

[155] T. Faulkner, N. Iqbal, H. Liu, J. McGreevy, and D. Vegh, Science **329**, 1043 (2010).

[156] D. P. Landau and K. Binder, *A Guide to Monte Carlo Simulations in Statistical Physics* (Cambridge University Press, New York, 2005).

[157] H. G. Katzgraber, (2011), arXiv:0905.1629 (unpublished).

[158] B. Bauer, E. Gull, S. Trebst, M. Troyer, and D. A. Huse, J. Stat. Mech. (**2010**) P01020.

[159] K. Hukushima and K. Nemoto, J. Phys. Soc. Jpn. **65**, 1604 (1996).

[160] D. J. Earl and M. W. Deem, Phys. Chem. Chem. Phys. **7**, 3910 (2005).

[161] K. Hukushima, Phys. Rev. E **60**, 3606 (1999).

[162] H. G. Katzgraber, S. Trebst, D. A. Huse, and M. Troyer, J. Stat. Mech. (**2006**) P03018.

[163] E. Bittner, A. Nußbaumer, and W. Janke, Phys. Rev. Lett. **101**, 130603 (2008).

[164] R. H. Swendsen and J.-S. Wang, Phys. Rev. Lett. **58**, 86 (1987).

[165] U. Wolff, Phys. Rev. Lett. **62**, 361 (1989).

[166] E. Luijten and H. W. K. Blöte, Int. J. Mod. Phys. C **6**, 359 (1995).

[167] D. Kandel, R. Ben-Av, and E. Domany, Phys. Rev. Lett. **65**, 941 (1990).

[168] M. Troyer, private communication, 2010.

[169] M. Sasaki and F. Matsubara, J. Phys. Soc. Jpn. **77**, 024004 (2008).

[170] A. M. Ferrenberg and D. P. Landau, Phys. Rev. B **44**, 5081 (1991).

[171] H. Rieger and A. P. Young, Phys. Rev. Lett. **72**, 4141 (1994).

[172] M. Guo, R. N. Bhatt, and D. A. Huse, Phys. Rev. Lett. **72**, 4137 (1994).

[173] B. Efron, *The Jackknife, the Bootstrap and Other Resampling Plans* (Society for Industrial and Applied Mathematics, Philadelphia, 1982).

[174] A. M. Ferrenberg and R. H. Swendsen, Phys. Rev. Lett. **63**, 1195 (1989).

[175] S. Trebst, private communication, 2010.

[176] R. Savit, Rev. Mod. Phys. **52**, 453 (1980).

Paper I

Monte Carlo simulations of dissipative quantum Ising models

Physical Review B **81**, 104302 (2010)

PHYSICAL REVIEW B **81**, 104302 (2010)

Monte Carlo simulations of dissipative quantum Ising models

Iver Bakken Sperstad, Einar B. Stiansen, and Asle Sudbø
Department of Physics, Norwegian University of Science and Technology, N-7491 Trondheim, Norway
(Received 8 February 2010; published 16 March 2010)

The dynamical critical exponent z is a fundamental quantity in characterizing quantum criticality, and it is well-known that the presence of dissipation in a quantum model has significant impact on the value of z. Studying quantum Ising spin models using Monte Carlo methods, we estimate the dynamical critical exponent z and the correlation length exponent ν for different forms of dissipation. For a two-dimensional quantum Ising model with Ohmic site dissipation, we find $z \approx 2$ as for the corresponding one-dimensional case, whereas for a one-dimensional quantum Ising model with Ohmic bond dissipation, we obtain the estimate $z \approx 1$.

DOI: 10.1103/PhysRevB.81.104302 PACS number(s): 75.10.Hk, 64.60.De, 05.50.+q

I. INTRODUCTION

Conventionally, quantum criticality can be described by a quantum-to-classical mapping,[1] whereby a d-dimensional quantum model is represented by a $(d+1)$-dimensional classical model in which the extra dimension corresponds to imaginary time, τ. It is well-known since the work of Hertz[2] that this temporal dimension and the spatial dimensions do not necessarily appear on an equal footing. In the presence of dissipative terms in the action, for instance, long-range interactions are introduced in the imaginary time direction,[3,4] making the model behave as if it were $(d+z)$-dimensional rather than $(d+1)$-dimensional. The dynamical critical exponent z can be regarded as a measure of the anisotropy between the temporal dimension and the spatial dimensions, as defined by the scaling of the temporal correlation length, $\xi_\tau \sim \xi^z$. Here, $\xi \sim |K-K_c|^{-\nu}$ is the spatial correlation length upon approaching a quantum critical point $K=K_c$, with K being some arbitrary (nonthermal) coupling constant. Knowing the value of z is therefore of fundamental importance in the study of quantum phase transitions, especially since this critical exponent determines the appearance of the quantum critical regime at finite temperatures above the quantum critical point.[5,6] Such quantum critical points with an accompanying quantum critical region have been suggested to be responsible, for instance, for the anomalous behavior of the normal phase of high-T_c cuprate superconductors.[7,8]

To illustrate the effect of dissipation on the dynamical critical exponent, consider first a generic ϕ^4-type nondissipative quantum field theory. The bare inverse propagator can be obtained from the quadratic part of the action as $\mathbf{q}^2+\omega^2$, meaning that one has isotropic scaling between the spatial dimensions and the temporal dimension, i.e., $z=1$. Adding local Ohmic dissipation by coupling each spin to a bath of harmonic oscillators,[3] the inverse propagator is modified to $\mathbf{q}^2+\omega^2+|\omega|$. Assuming a phase transition to an ordered state and taking the limit $\mathbf{q}\to\mathbf{0}$, $\omega\to 0$, the dissipative term $|\omega|$ will always dominate over the dynamic term ω^2, and so, by using $\omega \sim q^z$, we may naively make the prediction $z=2$. Note that according to this argument, the dynamical critical exponent for a given action is independent of the spatial dimensionality of the system. We will refer to these scaling arguments as naive scaling, and postpone any discussion of caveats and other possible scaling choices to Sec. IV.

If one replaces this Ohmic site dissipation with dissipation that also couples in space and not just in time, this situation may change significantly. A common form of dissipation in the context of arrays of resistively shunted Josephson junctions and related models, is the Ohmic dissipation of gradients, i.e., of the bond variable that is the difference of the quantum phase between the superconducting elements.[9] In Fourier space, this bond dissipation corresponds to an inverse propagator $\mathbf{q}^2+\omega^2+\mathbf{q}^2|\omega|$. (See, however, Sec. IV.) Once again letting $\mathbf{q}\to\mathbf{0}$, $\omega\to 0$, we can from naive scaling expect the dissipation to be weaker than in the onsite case since in this limit $\mathbf{q}^2|\omega| \ll \mathbf{q}^2$ for any positive z. A possible value is therefore $z=1$, for which the spatial term balances the dynamic term and dissipation can be considered perturbatively irrelevant in renormalization group sense.

Simple arguments of the kind given above have been the approach most commonly used whenever a dynamical critical exponent is to be determined. In recent years there has however been progress toward calculating the corrections to these lowest-order estimates for z both by field-theoretical renormalization group methods[10–12] and by Monte Carlo methods.[12–15] In addition, there has also been considerable recent interest in dissipative systems exhibiting more exotic forms of quantum criticality where the critical exponents are varying continuously.[16–18]

The most notable advance from our point of view is, however, the work by Werner *et al.*[13] justifying numerically the naive scaling estimate for the Ising spin chain with site dissipation by extensive Monte Carlo simulations. More precisely, it was found that the dynamical critical exponent was universal and satisfied $z=2-\eta$, with an anomalous scaling dimension $\eta \approx 0.015$. Apart from Ref. 13, almost no Monte Carlo simulations have been performed on extended quantum dissipative models. (See, however, Refs. 15 and 19 for reviews of Monte Carlo simulation for dissipative systems and quantum phase transitions.) The present work can therefore be regarded as a natural extension of the work done by Werner *et al.*, but more importantly as a first step toward more complex dissipative quantum models with bond dissipation. For instance, the dissipative XY model with bond dissipation is very interesting both as a model of granular superconductors or other systems which may be modeled as Josephson junction arrays.[9] In particular, such a dissipative XY model[20] and related Ashkin-Teller models[21,22] have been proposed to describe quantum critical fluctuations of loop-current order in cuprate superconductors.

Finding a value of z is also of considerable interest for purely classical models that include strongly anisotropic interactions. The reason is simply that performing a finite-size analysis to find the critical coupling or critical exponents requires a choice of system sizes that reflects an anisotropy in the scaling of the correlation lengths. In other words, one ideally needs to know the relative correlation length exponent $\nu_\tau/\nu = z$ *a priori* for the finite-size analysis to be correct.

In this work, we seek to employ Monte Carlo simulations of Ising models to answer the following questions: (1) can we confirm numerically that the dynamical critical exponent is indeed independent of dimensionality? (Neglecting the assumed small η) (2) how will the dynamical critical exponent for Ising variables change if one replaces the site dissipation with dissipation that also acts in space? The first question will be addressed in Sec. II, where we study the two-dimensional (2D) quantum Ising model with site dissipation. In Sec. III, we turn to the second question by studying a one-dimensional (1D) quantum Ising chain with bond dissipation in a similar manner. The results will be related to the naive scaling arguments for z, after which we conclude in Sec. V.

II. 2D QUANTUM ISING MODEL WITH SITE DISSIPATION

We first consider a quantum Ising spin model in two spatial dimensions coupled to a bath of harmonic oscillators,[3] i.e., a higher-dimensional version of the model considered in Ref. 13. In Fourier space, the quadratic part of the action for this model can be written as

$$S = \sum_{\mathbf{q}} \sum_{\omega} \left(\tilde{K}\mathbf{q}^2 + \tilde{K}_\tau \omega^2 + \frac{\alpha}{2}|\omega| \right) \sigma_{\mathbf{q},\omega}\sigma_{-\mathbf{q},-\omega}, \tag{1}$$

where σ is the Ising field. The discretized real space representation on a $L \times L \times L_\tau$-lattice then reads

$$\begin{aligned} S = &- K \sum_{x=1}^{L} \sum_{y=1}^{L} \sum_{\tau=1}^{L_\tau} [\sigma_{x,y,\tau}\sigma_{x+1,y,\tau} + \sigma_{x,y,\tau}\sigma_{x,y+1,\tau}] \\ &- K_\tau \sum_{x=1}^{L} \sum_{y=1}^{L} \sum_{\tau=1}^{L_\tau} \sigma_{x,y,\tau}\sigma_{x,y,\tau+1} \\ &+ \frac{\alpha}{4} \sum_{x=1}^{L} \sum_{y=1}^{L} \sum_{\tau \neq \tau'}^{L_\tau} \left(\frac{\pi}{L_\tau} \right)^2 \frac{(\sigma_{x,y,\tau} - \sigma_{x,y,\tau'})^2}{\sin^2(\pi/L_\tau|\tau - \tau'|)}. \end{aligned} \tag{2}$$

We have assumed a spatially isotropic system, so that $K_x = K_y = K$. Periodic boundary conditions are implicit in the imaginary time direction and are also applied for the spatial directions. Note that our representation is equivalent to that of Ref. 13, although superficially appearing slightly different.

We could, as Werner *et al.*, take a quantum Ising model in a transverse magnetic field as a starting point, and the field would then give rise to the quantum dynamics of the spins as represented by the second line in the action in Eq. (2). However, in this work we are not interested in the effect of a transverse field per se, and will therefore treat the dynamic term as a phenomenological term of unspecified origin. (See, however, Sec. IV). In the following, we will fix the value of the dynamic coupling of the Ising field to $K_\tau = -1/2 \ln(\tanh 1) \approx 0.1362$ and vary the spatial coupling K. For the $(1+1)$-dimensional model,[13] this choice ensures that $K_c = 1$ for $\alpha = 0$, whereas in the $d = 2$ case it is chosen primarily for computational convenience, and to allow for direct comparison with the $d = 1$ case. For the Monte Carlo simulations, we have used an extension of the Wolff cluster algorithm[23] by Luijten and Blöte,[24] which very effectively treats the long-range interaction in the imaginary time direction. We have mainly used an implementation of the Mersenne Twister[25] random number generator (RNG), but also confirmed that other RNGs yielded consistent result. We also make use of Ferrenberg-Swendsen[26] reweighting techniques which enable us to vary K continuously after the simulations have been performed.

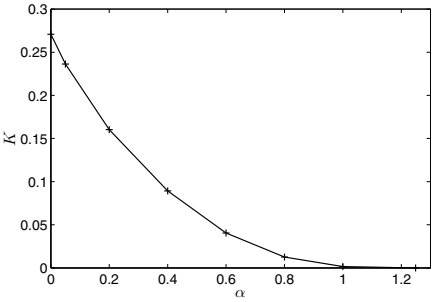

FIG. 1. Phase diagram for the 2D quantum Ising model with site dissipation for $K_\tau = -1/2 \ln(\tanh 1)$. The ordered phase is found for large values of spatial coupling K and dissipation strength α.

We will first present the phase diagram for this model in the α-K plane, as shown in Fig. 1. The phase diagram for the $(2+1)$-dimensional model is very similar to that for its $(1+1)$-dimensional counterpart, with a disorder-order phase transition for increasing dissipation and/or spatial coupling. Along the α-axis, a temporally ordered state is reached at $\alpha = \alpha_c$ through a purely dissipative phase transition when $K = 0$, in which case the model is simply a collection of decoupled $(0+1)$-dimensional dissipative two-level systems. The long-range interaction in the temporal chains decays as $1/|\tau_i - \tau_j|^2$, accordingly, the phase transition is of a kind closely related to the Kosterlitz-Thouless transition,[27] in which the ordered phase consists of tightly bound kinks and antikinks.

With the same temporal coupling values as for the $d = 1$ case, we can with relative ease determine the critical dissipation strength α_c for the independent subsystems, see the result stated in Ref. 13.

We have chosen a somewhat more quantitative approach to determine the dynamical critical exponent z than the one given in the presentation of Werner *et al.*, so we will use the exposition of our results to detail the method. This method is essentially the same as the one applied by the authors of Refs. 28 and 29 for spin glasses in a transverse field, but as it is rather scantily described in the literature, we include it here for completeness.

The basis of our approach is as follows. For systems with isotropic scaling, a well-known method to determine the

value of the critical coupling is to calculate the Binder ratio

$$Q = \frac{\langle m^4 \rangle}{\langle m^2 \rangle^2}, \tag{3}$$

and use this to plot the Binder cumulant $g \equiv 1 - Q/3$ as a function of coupling for several (e.g., cubic, in the $(2+1)$-dimensional case) system sizes. The Binder cumulant at the critical coupling is independent of system size (to leading order in L), and the crossing point of $g(K)$ for two different system sizes thus defines the (pseudo)critical point.

However, this finite-size scaling approach breaks down when the system size scales anisotropically. In this case, the scaling at criticality is given as a function with two independent scaling variables instead of just one,

$$Q(L, L_\tau) = \mathcal{G}\left(\frac{L}{\xi}, \frac{L_\tau}{\xi_\tau}\right), \tag{4}$$

and anisotropic systems according to $L_\tau \propto L^z$ are the appropriate choice instead of cubic systems. Hence, given the value of z, one should also observe data collapse as a function of L_τ / L^z for the Binder cumulant curves at the critical point.

In order to find z self-consistently, we consider first the Binder cumulant as a function of L_τ for given α, K and L. For very small L_τ, the system appears effectively two-dimensional, and consequently the increased influence of fluctuations makes this system more disordered than the corresponding three-dimensional system. In the opposite limit of $L_\tau \to \infty$ the system appears effectively one-dimensional, and with $L_\tau \gg \xi_\tau$ the system is again disordered. As g is a measure of the degree of order in the system, $g \to 0$ in both the above limits, and accordingly g must have a maximum for some finite value $L_\tau = L_\tau^*$. One way of interpreting L_τ^* is as the temporal size for which the system appears as isotropic as it possibly can be (or optimally three-dimensional), the anisotropic interactions taken into account.

The details of our procedure are as follows. First, we sample the Binder ratio as a function of coupling K for a large number of system sizes. For each value of L, we choose at least 14 values of L_τ close to the presumed peak position L_τ^* for the extent of the imaginary time dimension. The procedure for estimating z then follows in three steps. For each K, curves of the Binder cumulant g for all L are plotted as a function of L_τ, corresponding to the plot shown in panel (a) of Fig. 2. Second, a fourth order polynomial fit is made to these curves, localizing the points (L_τ^*, g^*) defining the peaks of the functions $g(L_\tau)$ with good precision. The obtained values for the peak Binder cumulants for each L are then plotted as a function of K, as shown in panel (b) of Fig. 2. A value for the critical coupling K_c can be found by estimating the value K to which the crossing point for two subsequent values of L converges for $1/L \to 0$. The third step for finding the dynamical critical exponent is a simple finite-size scaling analysis of the peak positions L_τ^* of the curves $g(L_\tau)$ as shown in panel (c) of Fig. 2, assuming the relation $L_\tau^* = aL^z$, with a being a nonuniversal prefactor. Finally, one may

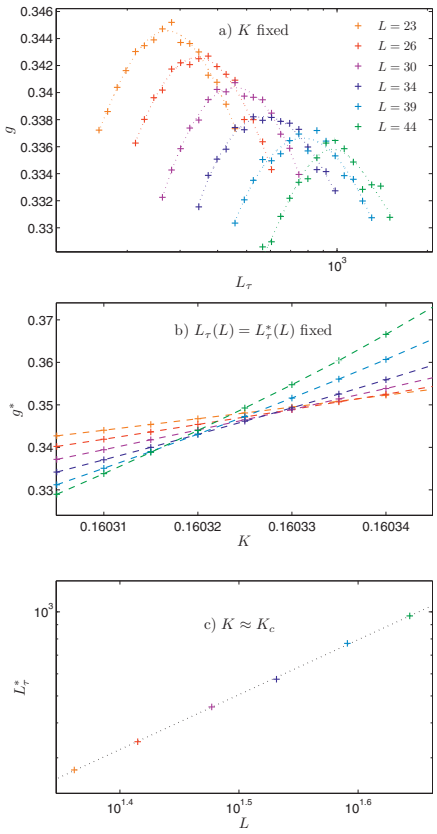

FIG. 2. (Color online) Illustration of the procedure for estimating the dynamical critical exponent z, as described in the text, here for the 2D quantum Ising model with site dissipation and $\alpha = 0.2$. (a) The Binder cumulant g as a function of temporal system size L_τ for a number of spatial system sizes L at $K = 0.160312$. (b) The peak value Binder cumulant g^* as a function of coupling K. (c) Finite-size analysis of the peak position of L_τ^* as a function of spatial system size L at criticality, $K_c = 0.160312(2)$, which yields the estimate $z = 1.97(3)$. The straight line represents a least-squares fit to the data points.

check the self-consistency of the obtained values for K_c and z by plotting the putative data collapse of the Binder cumulant as a function of L_τ / L^z, cf. Eq. (4).

Before moving on, we comment on the two interrelated (subleading) finite-size effects in the crossing point of Fig. 2: the crossing point between two subsequent Binder curves moves toward lower coupling for increasing system size, and accordingly the Binder cumulant at the crossing point decreases for increasing L. Consequently, the value of $g^*(K = K_c)$ will never be independent of system size L for finite systems. However, in our experience, this vertical deviation from collapse of the Binder curves—which is particularly evident when focusing on the peak of the Binder curves as in our analysis—does not itself affect the finite-size

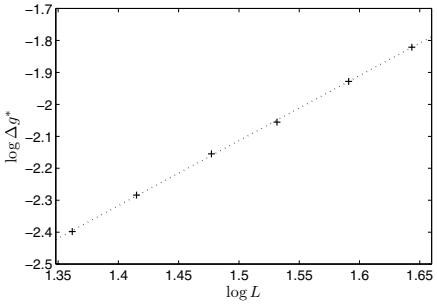

FIG. 3. Finite-size analysis for obtaining $1/\nu$ for the 2D quantum Ising model. Here we have evaluated the slope of the Binder cumulant g^* around $K=0.160312$ for $\alpha=0.2$, which yields $\nu=0.49(1)$. The straight line represents a least-squares fit to the data points.

estimate for z. More important is a possible horizontal deviation. Likewise, a slow convergence of the crossing points to K_c complicates the determination of the critical coupling for finite systems. The resulting uncertainty in z is dominated by this uncertainty in K_c, at least for the $d=2$ case.

It might be possible to obtain better precision for the critical coupling by using the finite-size analysis technique presented in Ref. 30 for the crossing points, but in the present case with an additional (and unknown) finite-size effect in z, this more rigorous approach seems by no means straightforward. To ensure that finite-size effects are negligible, we have checked the dependence of z on the lowest value of L included in the fitting procedure. In the analysis illustrated in Fig. 2, we have only retained system sizes such that the value of z seems to have converged. For the case $\alpha=0.2$ considered above, the resulting estimate is $z=1.97(3)$. No significant variation in the dynamical critical exponent is observed for stronger dissipation, and we conclude that we have $z\approx 2$ along the critical line. However, we have not been able to determine conclusively whether or not one has exactly anomalous scaling dimension $\eta=0$ in the relation $z=2-\eta$, which might be expected[10] since the value $d+z$ lies at the upper critical dimension for this phase transition for $d=2$.

We also give an estimate of the correlation length exponent ν using the peak values $g^*(K)$ of the Binder cumulant. The leading order scaling properties of the Binder ratio can be stated as[31] $Q(K,L)=\tilde{\mathcal{G}}([K-K_c]L^{1/\nu})$, and assuming negligible finite-size effects in the obtained dimensions $L_\tau^*(L)$, one finds the finite-size relation

$$\log\frac{\mathrm{d}g^*}{\mathrm{d}K} = C + \frac{1}{\nu}\log L, \tag{5}$$

The slope $\mathrm{d}g^*/\mathrm{d}K$ is estimated by the finite difference Δg^* over a small coupling interval around K_c, and C is an unimportant constant. The resulting finite-size analysis for $\alpha=0.2$ is illustrated in Fig. 3, and we find $\nu=0.49(1)$. This is very close to the expected (mean-field) value $\nu=1/2$ (Ref. 10), which is reasonable given that $z\approx 2$.

We finally note that, whereas increasing α does not lead to a significant change of z, it certainly does increase the prefactor a of the scaling relation $L_\tau \sim L^z$ and thereby the peak position L_τ^*. This reflects the increased anisotropy of the interactions, and can be seen also for $\alpha=0$ when K and K_τ are allowed to vary freely. At criticality one has $a=1$ for $K_\tau=K$, with increasing a for increasing anisotropy K_τ/K. In fact, for the analytically solvable 2D Ising model there even exists an exact mapping between system size anisotropy (i.e., a) and interaction anisotropy (i.e., K_τ/K).[32]

III. QUANTUM ISING CHAIN WITH BOND DISSIPATION

In this section, we will consider a $(1+1)$-dimensional quantum Ising model where the dissipative quantities of interest are bond variables involving Ising spins, rather than individual Ising spins themselves. The specific form of this dissipation kernel has been proposed as a candidate for describing the origin of the anomalous normal state properties of the cuprate high-T_c superconductors,[20] but in that case involving two sets of Ising spin on each lattice point. Such a model, unlike the one we will consider, may be mapped onto a four-state clock model, and may be approximated by an XY model with a fourfold symmetry breaking field, which in the classical case in two spatial dimensions is perturbatively irrelevant near criticality on the disordered side. Due to the degrees of freedom in our model being Ising spins with a spin gap, the present model should therefore not be regarded as directly comparable to a dissipative XY model that the authors of Ref. 20 consider. It should rather be regarded as a simple, but spatially extended model system, illustrating how bond dissipation can affect a quantum phase transition, which is certainly an important question on its own right.

In Fourier space, the action is given by

$$S = \sum_{\mathbf{q}}\sum_{\omega}\left(\tilde{K}\mathbf{q}^2 + \tilde{K}_\tau\omega^2 + \frac{\alpha}{2}|\omega|\mathbf{q}^2\right)\sigma_{\mathbf{q},\omega}\sigma_{-\mathbf{q},-\omega}. \tag{6}$$

The real space representation of this system is given by the action

$$S = -K\sum_{x=1}^{L}\sum_{\tau=1}^{L_\tau}\sigma_{x,\tau}\sigma_{x+1,\tau} + K_\tau\sum_{x=1}^{L}\sum_{\tau}^{L_\tau}\sigma_{x,\tau}\sigma_{x,\tau+1} + \frac{\alpha}{2}\sum_{x=1}^{L}\sum_{\tau\neq\tau'}^{L_\tau}\left(\frac{\pi}{L_\tau}\right)\frac{(\Delta\sigma_{x,\tau}-\Delta\sigma_{x,\tau'})^2}{\sin^2(\pi/L_\tau|\tau-\tau'|)}, \tag{7}$$

cf. the site dissipation case in Eq. (2). Here, $\Delta\sigma_{x,\tau}\equiv\sigma_{x+1,\tau}-\sigma_{x,\tau}$.

The interpretation of this representation remains mostly the same as in the previous section. The only difference is that the coupling to the heat bath is given in terms of the Ising field gradients rather than the Ising fields themselves. In the limit $\mathbf{q}\to\mathbf{0}$, $\omega\to 0$, we may anticipate from the Fourier representation of the action that the last term becomes irrelevant, which implies the value $z=1$ for the dynamical critical exponent. It is also evident from Eq. (7) that the bond dissipation is less effective than site dissipation in reducing quantum fluctuations. While site dissipation tends to align all

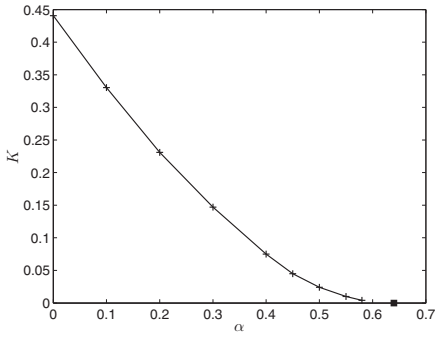

FIG. 4. Phase diagram of the quantum Ising chain with bond dissipation for $K_\tau=\ln(1+\sqrt{2})/2$. The ordered phase is found for large values of spatial coupling K and dissipation strength α. The filled square on the α axis represents an upper bracket for critical coupling α_c when the spatial coupling is tuned to zero, see the text.

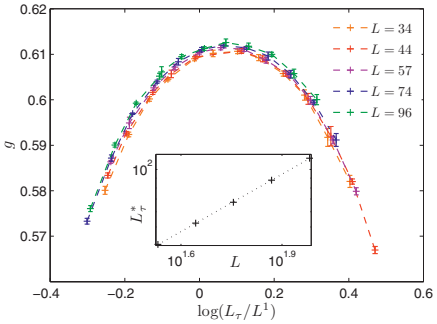

FIG. 5. (Color online) Data collapse of the Binder cumulant for $z=1$ at $K_c=0.3306$ for the 1D quantum Ising chain with bond dissipation and $\alpha=0.1$. The error bars are obtained from a jackknife analysis in the reweighting procedure. *Inset:* finite-size analysis resulting in dynamical critical exponent $z=1.007(15)$. The straight line represents a least-squares fit to the data points.

spins in the temporal direction, the bond dissipation tends to align the *difference* of nearest-neighbor spins along the Trotter slices. At least in the presence of a finite coupling $K\neq 0$, this is a less effective way of reducing temporal fluctuations of individual spins than onsite dissipation.

When expanding the dissipative term, it becomes clear that it contributes to both ferromagnetic and antiferromagnetic long-range interaction. This renders the system intractable to the Luijten-Blöte variant cluster algorithm used in the previous section. This algorithm builds up clusters with sizes comparable to the entire system and flips these as a whole, resulting in extreme correlations.[33] No cluster algorithm that effectively handles competing interactions has come to the authors' attention.

In the Monte Carlo simulations, we have therefore used a parallel tempering[34,35] algorithm which adequately handles the critical slowing down in the critical regime. A number of independent systems perform random walks in the space of coupling values, and this enables the systems to effectively explore a rugged energy landscape like the one generated by the dissipation term in Eq. (7).

The coupling values are distributed according to the iteration procedure introduced by Hukushima,[36] which renders the accept ratio of the attempted exchange of two adjacent coupling values independent of the coupling value. Consequently, the systems are allowed to wander relatively freely through the space of coupling values, although even more sophisticated distribution algorithms are available in that respect.[35]

The parameter K_τ is fixed at $\ln(1+\sqrt{2})/2\approx 0.4407$, the critical coupling K_c is thus the same as for the isotropic 2D Ising model when the dissipation strength is tuned to zero. Anticipating $z=1$, this choice also ensures that the simulations will be performed for convenient values of L and L_τ. The further steps necessary to find information about the critical properties are the same as discussed in Sec. II. The phase diagram of the system in the α-K plane is shown in Fig. 4.

For this model, the critical exponents are extracted for the two dissipation strengths $\alpha=0.1$ and 0.2. In Fig. 5, we show the results for the dynamical critical exponent for $\alpha=0.1$ as illustrated by the collapse of the Binder cumulant curves discussed in Sec. II for the value $z=1$. The results confirm the proposed value of z based in naive scaling arguments, and it appears that the bond dissipation term is indeed irrelevant.

The value of the dynamical critical exponent is very sensitive to finite-size effects and therefore challenging to obtain with the algorithm we have used given the limitations this entails. Increasing the dissipation strength makes these challenges more apparent, so to illustrate the dependence of z on system size we plot in Fig. 6 z as a function of system size for a fixed $K=K_c$ for $\alpha=0.2$. Note that three adjacent L values have been used to calculate every value for z, $\langle L\rangle$ denoting the average of these. The evolution of z is clearly seen to approach $z\approx 1$ in the thermodynamic limit. Even larger dissipation strengths tend to require much larger system sizes not practically feasible with the current algorithm. Results for such dissipation strengths are therefore not included here.

We have also attempted to extract the correlation length exponent ν for both dissipation strengths. When discarding

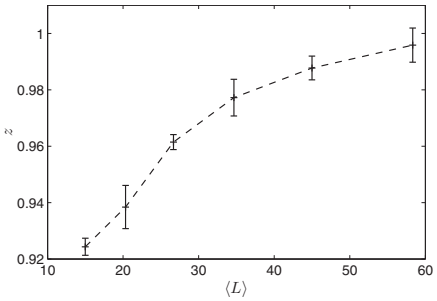

FIG. 6. The evolution of z as a function of system size for the 1D quantum Ising chain with bond dissipation with $\alpha=0.2$. Every point is calculated for the same coupling value $K_c=0.231$ from three adjacent system sizes, and the error bars are obtained from the least-squares fit in the finite-size analysis.

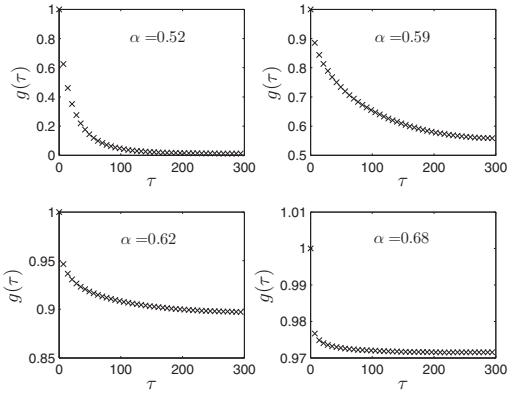

FIG. 7. The temporal spin-spin correlation function $g(\tau)=\langle\sigma_{x,\tau}\sigma_{x,0}\rangle$ for the 1D quantum Ising chain with bond dissipation at $K=0$ with $L=20$ and $L_\tau=600$. The decay of the correlation function is illustrated for four different dissipation strengths as the system goes from the disordered phase ($\alpha=0.52$) to the ordered phase ($\alpha=0.68$).

the smallest system sizes where finite-size effects are expected to be important, the values are found to be $\nu=1.00(2)$ for $\alpha=0.1$ and $\nu=1.005(8)$ for $\alpha=0.2$. This corresponds well with the exact value $\nu=1$ expected for the universality class of a 2D Ising model.

Sufficiently strong dissipation brings the critical coupling K_c toward zero, and, as indicated on the α-axis of the phase diagram in Fig. 4, the model undergoes a purely dissipative phase transition at some critical dissipation strength α_c. The ground state at $K=0$ consists of columns in the direction of imaginary time of ordered Ising spins. However, the direction of ordering is in general not uniform, as can be seen from Eq. (7), since a column can be flipped as a whole with no cost of energy. This nonuniform order prohibits the use of Binder cumulant curves to determine the critical coupling, so the exact value of α_c is difficult to deduct from the simulations. These obstacles make an estimate of the dynamical critical exponent unfeasible by our methods. Furthermore, since this phase transition is not of Kosterlitz-Thouless nature, any variety of the method of Ref. 27 also seem to be inapplicable to this model.

To corroborate that, there is in fact a phase transition to an ordered state for increasing α also at $K=0$, we present in Fig. 7 results for the temporal spin-spin-correlation $g(\tau)=\langle\sigma_{x,\tau}\sigma_{x,0}\rangle$. It is clear that this correlation function decays exponentially to zero for low dissipation strengths, while in the opposite limit of strong dissipation the correlation function quickly decays to some finite value. The character of the correlation function as α is tuned through the intermediate region is better illustrated in Fig. 8, where we have extracted the temporal correlation length ξ_τ. The diverging correlation length signifies a critical region with algebraic decay of the correlation function. The spatial correlation length ξ, on the other hand, we have found to be vanishing also in the critical region, and the behavior of the system depends only very weakly on its spatial extent L. From a crude finite-size analysis based on Fig. 8, we obtain the value $\alpha_c \leq 0.64$ as a best estimate for a upper bracket of the critical coupling, as we indicated in the phase diagram in Fig. 4.

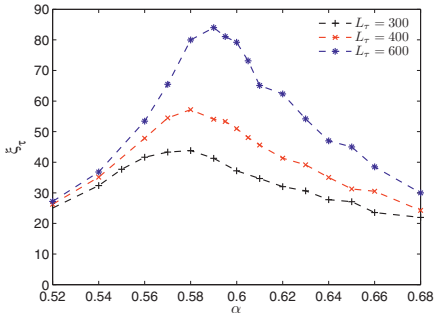

FIG. 8. (Color online) The temporal correlation length ξ_τ as a function of dissipation strength α for the 1D quantum Ising chain with bond dissipation at $K=0$. Because of the extremely anisotropic scaling in this limit, and to be sure to avoid any spatial finite-size effects, we have chosen to fix $L=20$.

IV. DISCUSSION

We will begin the discussion of our results by taking a closer look at the scaling arguments presented in Sec. I for finding the dynamical critical exponent. As indicated here, one important caveat of such arguments is that they only tell what exponent is naively expected to the lowest order approximation, and in general field-theoretical methods (see, e.g., Ref. 10) are needed to ascertain how higher order corrections modify this estimate. Furthermore, with several terms in the quadratic part of the action, it is not always obvious which terms should be required to balance at the critical point, or for which phase transitions this is valid.

For site dissipation, one obtains $z=2$ by balancing the spatial term and the dissipative term, since the dynamic term will be subdominant to the dissipative term for all positive z. For the bond dissipation case, a similar argument excludes the possibility $z=2$ for which the dissipative term would balance the dynamic term, since they both would be subdominant to the spatial term for all $z>1$. It is therefore interesting to ask if the possibility $z=0$, or alternatively $z \ll 1$, can be considered. In the limit that z is strictly zero, a dissipative term on the form $|\omega|$ would balance the dynamic term whereas a dissipative term on the form $\mathbf{q}^2|\omega|$ would balance the spatial term, but in the latter case both would be subdominant to the dynamic term. One interpretation is that $z=0$ in both cases would imply unrestrained quantum fluctuations resulting in spatial correlations being infinitely stronger than temporal correlations, so that each Trotter slice is essentially independent. In this interpretation, a strictly vanishing dynamical critical exponent may however be considered unphysical since we are assuming a transition to uniform order for the entire $(d+1)$-dimensional system by taking the limit $\mathbf{q}\to\mathbf{0}$, $\omega\to 0$.

Likewise, tuning $K_\tau \to 0$ may be considered unphysical since one removes the origin of the quantum nature of the

system. For this reason one cannot say that there will exist a quantum phase transition with $z=0$ for the bond dissipation model even if the ω^2 term had been removed from the action. The origin of the ω^2 term in a physical quantum model can be a transverse magnetic field in the Ising case or a Josephson charging energy in the XY case, and the interpretation of the prefactor K_τ is in general the inertia of the degrees of freedom. Even though we have chosen to operate with a nonspecific parameter K_τ, we therefore do not regard taking $K_\tau=0$ admissible in our simulations.

The opposite limit of $z=\infty$ may similarly be interpreted as spatially local criticality with correlations in the imaginary time direction independent of (the vanishing) correlations in the spatial directions, see, e.g., Refs. 16, 17, and 20. This is trivially the case in the limit $K=0$ for site dissipation with $\alpha>\alpha_c$, although one may argue that z is undefined in that case as the system is strictly decoupled in the spatial directions. The same argument cannot be applied to bond dissipation. For that model, the system does not experience dimensional reduction as $K\to 0$, but is still dependent (although very weakly) on the spatial extent of the $(d+1)$-dimensional system. We should however note that the approach taken here for determining the dynamical critical exponent is not applicable when z is either strictly zero or infinite, and also for a constant value $z\gg 1$ it would be very difficult to determine the dynamical critical exponent for practically attainable lattice sizes. If, on the other hand, one has $z\to\infty$ in the sense of activated dynamical scaling, the method is in principle feasible.[19]

Before continuing the discussion of the bond dissipation, we comment further on the relation between the real space representation of $\mathbf{q}^2|\omega|$ and the form of the bond dissipation used in Eq. (7). When Fourier transforming $\mathbf{q}^2|\omega|\sigma_{\mathbf{q},\omega}\sigma_{-\mathbf{q},-\omega}$ from Eq. (6) and discretizing the resulting differential operators, we arrive at

$$S_{\mathbf{q}^2|\omega|} \propto -\left(\frac{\pi}{L_\tau}\right)^2 \frac{\Delta\sigma_{x,\tau}\cdot\Delta\sigma_{x,\tau'}}{\sin^2(\pi/L_\tau|\tau-\tau'|)}. \tag{8}$$

Now, writing out the last term of Eq. (7) and comparing with Eq. (8) shows that the Fourier space representation of the bond dissipation can be written as

$$S_{\text{bond}} = (\mathbf{q}^2|\omega| + C'\mathbf{q}^2)\sigma_{\mathbf{q},\omega}\sigma_{-\mathbf{q},-\omega}. \tag{9}$$

Here, C' depends weakly on dimensions for finite systems. In other words, the bond dissipation is of the same form as $\mathbf{q}^2|\omega|$ dissipation, but with renormalized spatial nearest-neighbor coupling, which however does not alter the critical exponents of the model. This extra term originates with the counterterm introduced to cancel out the renormalization of the bare potential that arises due to the coupling with a heat bath.[3] For the Ising model, this renormalization is responsible for stabilizing ferromagnetic order at $K>0$.

We will now turn to the analysis of simulations on finite lattices, in particular with respect to the scaling relation $L_\tau = aL^z$ and the system anisotropy expressed by it. To interpret our results, it is useful to consider the dependence of both z and a on the dissipation strength α, and the variation in these quantities can be understood as follows. If the dissipation term is relevant and thus determining the universality class, we may assume that the value of z will be given by the form of this term even for infinitesimal $\alpha>0$ in the thermodynamic limit. In this case, increasing the dissipation strength α further will therefore not change z, but the prefactor a will have to change to reflect the increased interaction anisotropy. Correspondingly, when the dissipation term is an irrelevant perturbation, the dynamical critical exponent will remain $z=1$ in the thermodynamic limit. Upon increasing α, the dissipation will never grow strong enough to alter the universality class, but the nonuniversal prefactor a will in general change also in this case, and whether it increases or decreases is determined by how the dissipation changes the overall interaction anisotropy.

Regarding the evolution of a upon increasing α for the bond dissipation case, there are now two effects that must be considered separately. One implicit effect is that increasing α decreases $K=K_c$ at criticality, thereby increasing the anisotropy ratio K_τ/K, which results in a much larger a for large values of α. The other effect is that arising explicitly from the dissipation term and its contribution to the effective coupling strength in the imaginary time direction. Whereas a site dissipation term obviously increases the anisotropy when increasing the dissipation strength while keeping the other coupling values fixed, such an enhancement of a does not appear for bond dissipation. This can be seen—as we have checked—by evaluating a for increasing α for isotropic short-range coupling, i.e., $K_\tau=K$. One possible interpretation of this result is that although bond dissipation does not change universality, it favors $z<1$ behavior, which can also be recognized from Fig. 6. In other words, the dissipation term contributes to making the temporal dimension less ordered than the spatial dimension, in strong contrast to the case of site dissipation. This would in part explain why one needs much longer simulations and larger systems to obtain reliable results for strong bond dissipation.

Given that the exceedingly strong finite-size effects thwart a precise determination of z for higher values of α, one should in general also consider the possibility of continuously varying critical exponents. However, we have shown that $z\approx 1$ for $\alpha=0.1$ and presented solid arguments favoring that this is the case also for $\alpha=0.2$, as it is obviously also in the limit $\alpha=0$. Therefore, if the exponents are in fact continuously varying, they begin to vary only for dissipation strengths above $\alpha>0.2$, and would furthermore have to be varying very slowly.

V. CONCLUSION

This work represents a further step toward simulations of physically interesting extended quantum systems with dissipation. Using Monte Carlo methods, we have studied a model similar to that by Werner *et al.*,[13] but with higher spatial dimensionality, as well as a model with one spatial dimension but with bond dissipation instead of site dissipation. We have found that the $(2+1)$-dimensional model with site dissipation has a dynamical critical exponent very close to the corresponding $d=1$ model, i.e., $z\approx 2$. Bond

dissipation, on the other hand, is fundamentally different, and our results strongly suggest that this form of dissipation is irrelevant to the universality class, i.e., $z \approx 1$ and nonvarying. We therefore believe that the same dynamical critical exponent also applies to $(2+1)$-dimensional models with bond dissipation for the same degrees of freedom, although we have not been able to reach sufficiently large systems to show this convincingly by numerical means. In both cases, the numerical estimates for the dynamical critical exponent is consistent with those found by naive scaling arguments on the quadratic part of the action.

ACKNOWLEDGMENTS

We thank Steinar Kragset for his contribution during the early phases of this project. We also acknowledge discussions with Egil V. Herland, Mats Wallin, and Chandra M. Varma.

[1] M. Suzuki, Prog. Theor. Phys. **56**, 1454 (1976).
[2] J. A. Hertz, Phys. Rev. B **14**, 1165 (1976).
[3] A. O. Caldeira and A. J. Leggett, Ann. Phys. **149**, 374 (1983).
[4] S. Chakravarty, Phys. Rev. Lett. **49**, 681 (1982).
[5] S. L. Sondhi, S. M. Girvin, J. P. Carini, and D. Shahar, Rev. Mod. Phys. **69**, 315 (1997).
[6] M. Vojta, Rep. Prog. Phys. **66**, 2069 (2003).
[7] D. M. Broun, Nat. Phys. **4**, 170 (2008).
[8] C. M. Varma, P. B. Littlewood, S. Schmitt-Rink, E. Abrahams, and A. E. Ruckenstein, Phys. Rev. Lett. **63**, 1996 (1989).
[9] S. Chakravarty, G.-L. Ingold, S. Kivelson, and A. Luther, Phys. Rev. Lett. **56**, 2303 (1986).
[10] S. Pankov, S. Florens, A. Georges, G. Kotliar, and S. Sachdev, Phys. Rev. B **69**, 054426 (2004).
[11] S. Sachdev, P. Werner, and M. Troyer, Phys. Rev. Lett. **92**, 237003 (2004).
[12] P. Werner, M. Troyer, and S. Sachdev, J. Phys. Soc. Jpn. Suppl. **74**, 67 (2005).
[13] P. Werner, K. Völker, M. Troyer, and S. Chakravarty, Phys. Rev. Lett. **94**, 047201 (2005).
[14] L. F. Cugliandolo, G. S. Lozano, and H. Lozza, Phys. Rev. B **71**, 224421 (2005).
[15] P. Werner and M. Troyer, Prog. Theor. Phys. Suppl. **160**, 395 (2005).
[16] S. Tewari, J. Toner, and S. Chakravarty, Phys. Rev. B **72**, 060505(R) (2005).
[17] S. Tewari and J. Toner, EPL **74**, 341 (2006).
[18] P. Goswami and S. Chakravarty, Phys. Rev. B **73**, 094516 (2006).
[19] T. Vojta, Rev. Comput. Chem. **26**, 167 (2008).
[20] V. Aji and C. M. Varma, Phys. Rev. B **79**, 184501 (2009).
[21] V. Aji and C. M. Varma, Phys. Rev. Lett. **99**, 067003 (2007).
[22] K. Børkje and A. Sudbø, Phys. Rev. B **77**, 092404 (2008).
[23] U. Wolff, Phys. Rev. Lett. **62**, 361 (1989).
[24] E. Luijten and H. Blöte, Int. J. Mod. Phys. C **6**, 359 (1995).
[25] M. Matsumoto and T. Nishimura, ACM Trans. Model. Comput. Simul. **8**, 3 (1998).
[26] A. M. Ferrenberg and R. H. Swendsen, Phys. Rev. Lett. **63**, 1195 (1989).
[27] E. Luijten and H. Meßingfeld, Phys. Rev. Lett. **86**, 5305 (2001).
[28] M. Guo, R. N. Bhatt, and D. A. Huse, Phys. Rev. Lett. **72**, 4137 (1994).
[29] H. Rieger and A. P. Young, Phys. Rev. Lett. **72**, 4141 (1994).
[30] L. Wang, K. S. D. Beach, and A. W. Sandvik, Phys. Rev. B **73**, 014431 (2006).
[31] A. M. Ferrenberg and D. P. Landau, Phys. Rev. B **44**, 5081 (1991).
[32] G. Kamieniarz and H. W. J. Blöte, J. Phys. A **26**, 201 (1993).
[33] D. Kandel, R. Ben-Av, and E. Domany, Phys. Rev. Lett. **65**, 941 (1990).
[34] K. Hukushima and K. Nemoto, J. Phys. Soc. Jpn. **65**, 1604 (1996).
[35] H. Katzgraber, Modern Computation Science, Oldenburg, Germany, 16-28 August 2009 (unpublished).
[36] K. Hukushima, Phys. Rev. E **60**, 3606 (1999).

Paper II

Quantum criticality in spin chains with non-Ohmic dissipation

Physical Review B **85**, 214302 (2012)

Quantum criticality in spin chains with non-Ohmic dissipation

Iver Bakken Sperstad, Einar B. Stiansen, and Asle Sudbø
Department of Physics, Norwegian University of Science and Technology, N-7491 Trondheim, Norway
(Received 28 March 2012; revised manuscript received 8 May 2012; published 6 June 2012)

We investigate the critical behavior of a spin chain coupled to bosonic baths characterized by a spectral density proportional to ω^s, with $s > 1$. Varying s changes the effective dimension $d_{\text{eff}} = d + z$ of the system, where z is the dynamical critical exponent and the number of spatial dimensions d is set to one. We consider two extreme cases of clock models, namely Ising-like and U(1)-symmetric ones, and find the critical exponents using Monte Carlo methods. The dynamical critical exponent and the anomalous scaling dimension η are independent of the order parameter symmetry for all values of s. The dynamical critical exponent varies continuously from $z \approx 2$ for $s = 1$ to $z = 1$ for $s = 2$, and the anomalous scaling dimension evolves correspondingly from $\eta \gtrsim 0$ to $\eta = 1/4$. The latter exponent values are readily understood from the effective dimensionality of the system, being $d_{\text{eff}} \approx 3$ for $s = 1$, while for $s = 2$ the anomalous dimension takes the well-known exact value for the two-dimensional Ising and XY models, since then $d_{\text{eff}} = 2$. However, a noteworthy feature is that z approaches unity and η approaches $1/4$ for values of $s < 2$, while naive scaling would predict the dissipation to become irrelevant for $s = 2$. Instead, we find that $z = 1, \eta = 1/4$ for $s \approx 1.75$ for both Ising-like and U(1) order parameter symmetry. These results lead us to conjecture that for all site-dissipative Z_q chains, these two exponents are related by the scaling relation $z = \max\{(2 - \eta)/s, 1\}$. We also connect our results to quantum criticality in nondissipative spin chains with long-range spatial interactions.

DOI: 10.1103/PhysRevB.85.214302 PACS number(s): 05.30.Rt, 05.70.Jk, 75.10.Pq, 75.40.Mg

I. INTRODUCTION

The spin-boson model[1,2] (SBM) represents one of the most well-established frameworks for describing the effect of dissipation on a quantum system. In its simplest incarnation, it describes a two-level system coupled to an infinite number of harmonic oscillators with low-frequency spectral density $J(\omega) \propto \omega^s$, with ohmic damping ($s = 1$) being the most commonly studied case. Generalizations of this model include extensions to finite (spatial) dimensions $d > 0$[3,4] and models where the Z_2 (Ising) spin symmetry has been replaced by a higher symmetry.[5,6] Extended versions of such systems may also find applications in the study of quantum critical points in quantum magnets and strongly correlated systems,[6–9] and hence they are of considerable interest in contemporary condensed-matter physics.

Another generalization is to consider non-Ohmic spectral densities ($s \neq 1$), which may be relevant in the description of several different physical phenomena.[10–17] From a more fundamental physics point of view, the sub-Ohmic ($s < 1$) SBM and related models have been studied intensively in recent years[18–20] following claims that the so-called quantum-to-classical mapping may be violated in even the simplest variant of SBM for $s < 1/2$.[21] Its super-Ohmic counterpart $s > 1$ has, on the other hand, received relatively little attention. This may be due to the fact that the $(0 + 1)$-dimensional $[(0 + 1)\text{D}]$ SBM exhibits a (quantum) phase transition only for values of $s \leqslant 1$. For $d \geqslant 1$, however, the possibility of a phase transition arises for all s.

The SBM is generally described, via the quantum-to-classical mapping, by a classical $(d + 1)$D spin model with long-range interactions that decay as $1/\tau^{1+s}$ in imaginary time τ. Long-range interactions are interesting, as they allow one to increase the effective dimensionality continuously by tuning s to lower values. In classical spin glasses, for instance, low-dimensional models with long-range interactions have been studied to infer properties of higher-dimensional realizations of the same systems with purely short-range interactions.[22–24] In quantum models, the effective dimensionality is expressed by $d_{\text{eff}} = d + z$, with z being the dynamical critical exponent defined from the divergence of the correlation time $\xi_\tau \sim \xi^z$, where ξ is the spatial correlation length. At a second-order phase transition, we have in standard notation $\xi \sim |K - K_c|^{-\nu}$ as the coupling parameter K approaches its critical value K_c. The presence of dissipation in general causes z to deviate from the value $z = 1$, with a naive scaling estimate $z_0 = 2/s$.[25] Although this result is exact in mean-field theory ($d_{\text{eff}} \geqslant 4$), deviations may appear when decreasing d_{eff}. For the Ohmic case, it is known[26] that z obeys the scaling law $z = z_0 - \eta$, where η in general denotes the anomalous scaling dimension at the transition point to a disordered state. Below $d_{\text{eff}} = 4$ one has $\eta > 0$, and previous work[3] on $s = 1$ for $d = 1$ found $\eta \approx 0.015$ and $z \approx 1.985$.

One issue we address in this paper is how the exponents z and η evolve as one varies the dissipation parameter $s > 1$. For the Ohmic case considered previously, the deviations from naive scaling (i.e., from $z = z_0$) are barely significant due to the small value of η when $d_{\text{eff}} \approx 3$. This deviation should become more noticeable as the effective dimensionality decreases, although one cannot expect the relation $z = z_0 - \eta$, valid for $s = 1$, to hold also for larger s. In the limit $d + z \to 2$, the anomalous dimension might be expected to approach the relatively large value $\eta = 1/4$, which it takes for both the two-dimensional (2D) Ising and 2D XY model. A related issue is the value of s beyond which the dissipation term is irrelevant in the renormalization group sense, giving $z = 1$. Naive scaling indicates that $z = 1$ for $s \geqslant 2$, but as z is likely to decrease faster than $z_0 = 2/s$ as s increases, dissipation might turn irrelevant for a value of s smaller than 2.

Another issue which we address is how the critical exponents, in particular z and η, depend on the symmetry of the order parameter. In the limit $s = 1$, there is no significant difference between the values of η (and thereby z) for

discrete and continuous order parameter fields,[3,5] but it is not inconceivable that such a difference becomes noticeable for lower effective dimensions, that is, as s is increased.

In order to answer these questions and to study a class of dissipative models for which relatively little is known precisely, we present results from Monte Carlo simulations on both XY and Ising-like spin chains with non-Ohmic dissipation. In both cases, we consider super-Ohmic dissipation, which for the XY case allows us to interpolate between the universality class describing the three-dimensional (3D) XY model and the very different Berezinskii-Kosterlitz-Thouless (BKT) criticality of the 2D XY model. The models are presented in the next section, where we also describe the finite-size scaling procedure used to find the critical exponents. The dependence of these exponents on s are presented and discussed in Sec. III, before we give a summary of our findings in Sec. IV.

II. MODEL AND FINITE-SIZE SCALING METHODS

The starting point of the models we consider may be taken as a general $(1+1)$D ϕ^4-type quantum field theory of an $O(N)$ order parameter field ϕ. Including dissipation, the Fourier transform of its inverse bare propagator is of the form $q^2+\omega^2+|\omega|^s$, where the damping term $\propto|\omega|^s$ arises from the coupling of the field to baths of harmonic oscillators[27] with a low-frequency power-law spectral density characterized by the exponent s.

Parameterizing the order parameter field of such a $N=2$ quantum rotor model by an angle variable θ, we may formulate the discretized action as

$$\begin{aligned} S = &-K\sum_{x=1}^{L}\sum_{\tau=1}^{L_\tau}\cos(\theta_{x,\tau}-\theta_{x+1,\tau}) \\ &-K_\tau\sum_{x=1}^{L}\sum_{\tau=1}^{L_\tau}\cos(\theta_{x,\tau}-\theta_{x,\tau+1}) \\ &-\frac{\alpha}{2}\sum_{x=1}^{L}\sum_{\tau\neq\tau'}^{L_\tau}\left(\frac{\pi}{L_\tau}\right)^{1+s}\frac{\cos(\theta_{x,\tau}-\theta_{x,\tau'})}{\sin^{1+s}\left(\frac{\pi}{L_\tau}|\tau-\tau'|\right)} \end{aligned} \tag{1}$$

on a quadratic $L\times L_\tau$ lattice. Above, K is the spatial coupling constant to be varied, whereas the quantum coupling constant K_τ and the dissipation strength α are taken as fixed values during the simulations.

In order to study both continuous and discrete symmetry of the order parameter field, we consider two possible domains of the angle variables: U(1) symmetry is equivalent with $\theta\in[0,2\pi\rangle$, and for a discrete symmetry (Z_4), we choose to enforce the restriction $\theta\in\{0,\frac{\pi}{2},\pi,\frac{3\pi}{2}\}$. We refer to the former as the XY model and to the latter as the Z_4 model. Such a Z_4 model will be in the same universality class as a corresponding Z_2 (Ising) model, which is why we refer to this model as Ising-like. This equivalence is easily shown using the substitution $\cos\theta_{x,\tau}=(\sigma_{x,\tau}+\mu_{x,\tau})/2$ and $\sin\theta_{x,\tau}=(\sigma_{x,\tau}-\mu_{x,\tau})/2$ to rewrite the action as that of two Ising models in terms of decoupled Ising spins σ and μ. The order parameter for both symmetry variants is defined as $m=(LL_\tau)^{-1}\sum_{x,\tau}\exp(\mathrm{i}\theta_{x,\tau})$ in the standard manner.

When determining critical exponents of a quantum system using finite-size scaling (FSS), the system dimensions L, L_τ used have to be chosen such that they respect the system anisotropy reflected by the dynamical critical exponent, $L_\tau\propto L^z$. This is a problem when we do not know dynamical critical exponents *a priori*, and one usually has to first determine z by simulating several values of L_τ for each L, before running new simulations with L/L_τ^z fixed. We circumvent this problem by using the same data to determine z and to evaluate the FSS observables, by interpolating data for multiple L_τ values to $L_\tau=L_\tau^*(L)$. Here, L_τ^* is a characteristic temporal system size found for each spatial system size L, as explained below, and it is assumed that $L_\tau^*\propto L^z$. This has the advantage that one (along with z) can find all other critical exponents simultaneously, utilizing all (or most of) the data generated. Furthermore, we are also able to appropriately take the uncertainty in z into account when finding the uncertainty in the other exponents, by repeating the entire procedure for a number of jackknife bins based on the original data.

The procedure to find z is explained in more detail in, for example, Ref. 4, and is based on the Binder ratio

$$Q=\frac{\langle m^4\rangle}{\langle m^2\rangle^2}=\mathcal{Q}(|K-K_c|L^{1/\nu},L_\tau/L^z), \tag{2}$$

where brackets $\langle\cdots\rangle$ indicate ensemble averages and $\mathcal{Q}$ is a universal scaling function. The characteristic values $L_\tau^*(L)$ are found from the minima of Q as a function of L_τ for a given L, and the critical coupling K_c is found from the crossing points of these minima as a function of K. The correlation length exponent ν is determined through finite-size scaling of the related quantity

$$\frac{(\partial\langle m^2\rangle/\partial K)^2}{\partial\langle m^4\rangle/\partial K}\propto L^{1/\nu}, \tag{3}$$

where the derivatives are calculated by $\partial\langle m^n\rangle/\partial K=\langle E_x\rangle\langle m^n\rangle-\langle E_x m^n\rangle$, with $E_x=-\sum_{x,\tau}\cos(\theta_{x,\tau}-\theta_{x+1,\tau})$.

To extract critical exponents β and γ, we use the usual FSS forms for the magnetization

$$\langle|m|\rangle\propto L^{-\beta/\nu} \tag{4}$$

and the magnetic susceptibility

$$\chi=LL_\tau\langle m^2\rangle\propto L^{\gamma/\nu}, \tag{5}$$

respectively. The anomalous dimension η is then found from the scaling relation $\eta=2-\gamma/\nu$. We have also checked that the value of η obtained from the susceptibility data is in correspondence with that obtained (through $z+\eta$) from the critical two-point correlation function of the order parameter field, $G(L/2)\propto L^{2-d-z-\eta}$. All of the above observables are evaluated at $L_\tau=L_\tau^*$, and we are careful to only use system sizes L_τ relatively close to L_τ^* in the interpolation. Using a polynomial fit of as low order as 3 works very well in most cases, although more care must be taken when extracting ν.

The error estimates we report are jackknife estimates of statistical errors only, but include contributions from the uncertainty in L_τ^* and the critical coupling K_c. The value of K_c is in general extrapolated from the scaling form $K_c^*(L)=K_c+cL^{-\omega'}$ for the crossing points $K_c^*(L)$ of $Q(K,L_\tau=L_\tau^*)$ for adjacent system sizes L. For regions of s where the crossing

points coincide and the extrapolation procedure breaks down, we base the estimate of K_c on the largest values of L. When extracting critical exponents, we make sure to use system sizes large enough for the above mentioned FSS forms to be valid. Possible corrections to scaling are discussed below. We note in particular that we initially assume a second-order phase transition for all values of s we use, so critical exponents obtained in the case of a BKT transition should be regarded as effective exponents only. The special case of $s \approx 2$ for the XY model is therefore re-examined separately in Sec. III B. Corrections to the scaling form $L_\tau^* \propto L^z$ are discussed for a special case in Sec. III C.

The Monte Carlo simulations are performed using a Wolff cluster algorithm[28] for long-range interactions.[29] The results are obtained using an implementation of the MERSENNE TWISTER[30] random number generator, but other random number generators produce consistent results. Ferrenberg-Swendsen reweighting techniques[31] were applied to the data. For the simulations of the XY case, we use a model with Z_{32} symmetry to emulate the continuous U(1) symmetry.

III. RESULTS AND DISCUSSION

When extracting critical exponents for the model we consider in this paper, we anticipate that the only parameter in Eq. (1) relevant in determining the universality class is the interaction decay exponent s. (The values we present Monte Carlo results for are s =1, 1.25, 1.5, 1.625, 1.75, 1.875, and 2.) Nevertheless, we also find that the corrections to scaling are strongly affected by the strength of the dissipation term as quantified by α, for finite systems. In order to minimize finite-size effects and ensure a relatively fast onset of asymptotic values of the exponents, a specific value of α could in principle be tailored to each value of s.[32] Instead of adjusting α for each individual value of the decay exponent s, we have divided the span of s values into two regions where we have applied different sets of coupling constants. For $s > 1.625$, where we expect the dissipation term to be weakly relevant (in the sense of a small correction-to-scaling exponent) or even irrelevant, we set the coupling values according to $\alpha = 0.1$ and $K_\tau = -\ln(\tanh \frac{1}{2}) \approx 0.7719$. For $s \leqslant 1.5$ we find that it is more appropriate to choose a larger value of α while reducing K_τ in order to observe a rapid finite-size crossover to the asymptotic exponents. In this region we use $\alpha = 0.5$ and $K_\tau = 0.4$. For the intermediate value $s = 1.625$, we use $\alpha = 0.3$ and $K_\tau = 0.4$. We can easily confirm for the smallest values of s that the universality class does not depend on the value of α, but corrections to scaling makes this harder for larger s, as discussed in Sec. III C.

A. Results for the critical exponents

In Fig. 1 we present the dynamical critical exponent z as a function of s. A notable feature of the results is the similarity between the two order parameter symmetries. To the accuracy of our simulations, there is essentially no difference between the continuous U(1) symmetry and the discrete Z_4 symmetry. Also, the calculated z values do not conform to the scaling estimate $z_0 = 2/s$, but instead fall off faster for increasing s than expected from naive scaling.

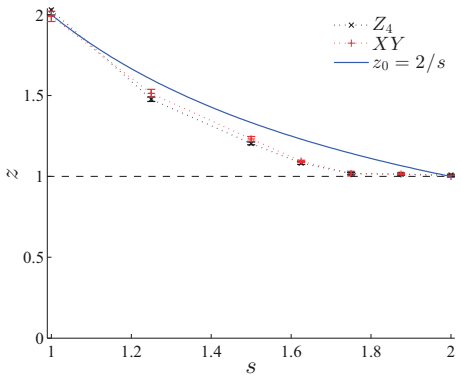

FIG. 1. (Color online) Dynamical critical exponent z as a function of s for the Z_4 and the XY model. The naive scaling estimate z_0 (the solid curve) does not coincide with the calculated z for values of s other than the integer-valued end points of our span of s values.

We present the evolution of η as a function of s in Fig. 2. Again, we find coinciding values for the two order parameter symmetries. For both Z_4 and U(1), η increases steadily with decreasing effective dimension of the system. Also shown in Fig. 2 is the quantity $\eta_0 = 2/s - z$, which quantifies the difference between the naive scaling estimate z_0 and the calculated z. For $s \leqslant 1.25$ the evolution of η_0 closely follows the calculated values of η, making the scaling relation $z = 2/s - \eta$ a fair approximation also for $s \gtrsim 1$. For larger values of s, however, this scaling relation has clearly broken down, as the values of z again approach the naive estimate as $s \to 2$. In this limit, η approaches the value $\eta = 1/4$, which is expected for both the 2D Ising model at the

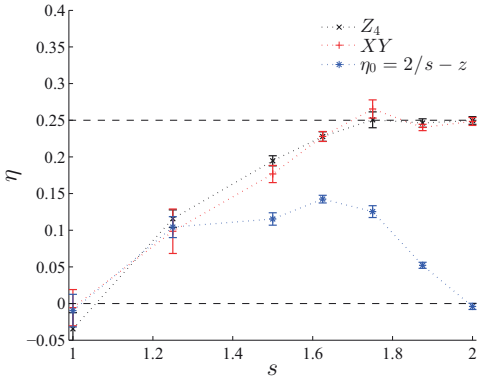

FIG. 2. (Color online) Anomalous scaling dimension η as a function of s for the Z_4 and the XY model. η_0 indicates the discrepancy between the naive scaling estimate $z_0 = 2/s$ and the actually calculated value of the dynamical critical exponent z (based on the mean for the Z_4 and XY model).

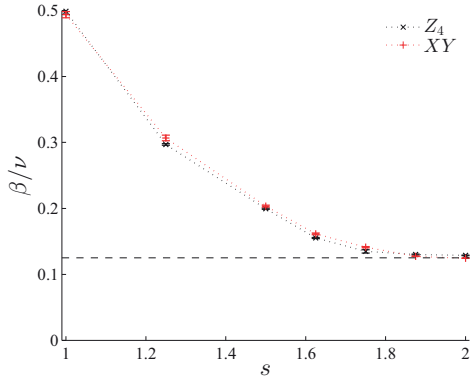

FIG. 3. (Color online) Critical exponent ratio β/ν as a function of s. This ratio appears to be independent of order parameter symmetry and is also well defined in the limit of large s. The dashed line represents $\beta/\nu = 1/8$.

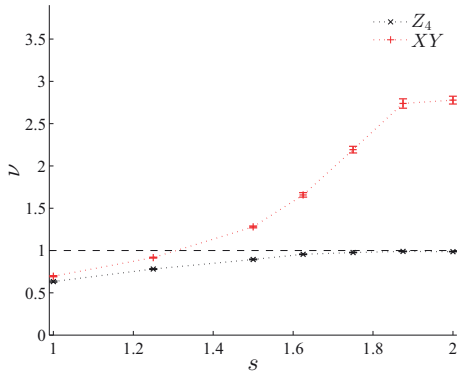

FIG. 4. (Color online) Correlation length exponent ν as a function of s. As the dissipation term becomes more short ranged with larger s, the exponent for the Z_4 model approaches the 2D Ising value $\nu = 1$. In the XY case, ν is expected to diverge in the limit $d_{\text{eff}} \to 2$. The results (obtained for finite L) presented for the largest values of s should therefore be regarded only as effective exponents.

critical point, as well as for the 2D XY model at the critical end point.

Next, we turn to the remaining critical exponents. Figure 3 shows the results for the ratio β/ν as obtained from the magnetization. We do not show the ratio γ/ν, although its behavior is easily inferred from Fig. 2 and the relation $\gamma/\nu = 2 - \eta$. Again, the FSS exponent seems to take essentially the same values for the XY model as for the Z_4 model. This is also the case for $s \to 2$, where we expect the dissipation to be irrelevant so that the effective dimensionality is reduced to $d_{\text{eff}} = 2$. For the XY model, the U(1) symmetry of the variables then cannot be spontaneously broken, and the strong-coupling phase of the model features only quasi-long-range order (QLRO). Nonetheless, the system develops a finite magnetization m as a finite-size effect, with a well-defined FSS exponent. The value $\beta/\nu \approx 0.125 = 1/8$ of this exponent when $s = 2$ (as well as the corresponding susceptibility ratio $\gamma/\nu \approx 7/4$) is also found for the classical 2D XY model and is, incidentally, the same as the corresponding ratio in the 2D Ising model. We discuss this issue in more detail in Sec. III E.

The correlation length exponent ν is shown in Fig. 4, while the critical exponent β is shown in Fig. 5. We do not show the results for the exponent γ here, but its behavior is qualitatively very similar to that of the exponent ν. In the Z_4 case, both exponents start out close to the 3D Ising limit for $s = 1$ and approach the 2D Ising limit indicated by the dashed line when $s \to 2$. Consider now the XY case. When $s = 1$, these exponents take on values close to those of the 3D XY model. However, the exponents β, ν, and γ are not well defined when $d_{\text{eff}} = d + z = 2$, as their values are formally infinite at a transition separating a disordered phase and a QLRO phase. This is the case when $s = 2$. Our FSS analysis for these exponents, which presupposes a second-order phase transition, is strictly speaking not applicable to the BKT transition. The resulting (effective) exponents β, ν, and γ appear to diverge as $L \to \infty$ close to $s = 2$. Note that although ξ is exponentially divergent at a BKT transition, we may still define z through the relation $\xi_\tau \propto \xi^z$.

Another observation in the U(1) case is that while the combination β/ν is monotonically decreasing with increasing s, β itself is exhibiting a nonmonotonic evolution as a function of s. The value of β is at first decreasing as the increasing value of s drives the system away from the 3D behavior, just as for the Z_4 case. However, as mentioned above, β is divergent in the 2D XY limit, and the reduction of β is therefore reversed at an intermediate value of s.

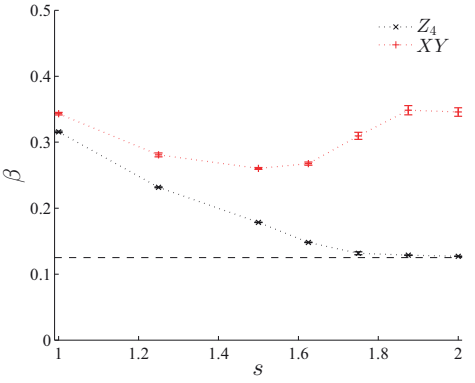

FIG. 5. (Color online) Critical exponent β as a function of s. For the Z_4 model, β evolves smoothly from the 3D Ising to the 2D Ising limit as s is increased from 1 to 2. The XY result, on the other hand, starts out near the 3D XY value for $s = 1$ and features a nonmonotic evolution of β with s, with a divergent β in the limit of large s; cf. Fig. 4.

B. Berezinskii-Kosterlitz-Thouless phase transition and the helicity modulus

The helicity modulus

$$\Upsilon = \frac{1}{LL_\tau}\left\langle \sum_{x=1}^{L}\sum_{\tau=1}^{L_\tau}\cos(\theta_{x,\tau}-\theta_{x+1,\tau})\right\rangle - \frac{K}{LL_\tau}\left\langle\left(\sum_{x=1}^{L}\sum_{\tau=1}^{L_\tau}\sin(\theta_{x,\tau}-\theta_{x+1,\tau})\right)^2\right\rangle, \quad (6)$$

is expected to scale as $\Upsilon \propto L^\kappa$ at a critical point where a U(1) symmetry is spontaneously broken, with $\kappa \equiv 2\beta/\nu - \eta$. For a 2D XY model, however, the exponent κ is exactly zero, reflecting the fact that at the BKT phase transition, the helicity modulus jumps to a finite value with logarithmic finite-size corrections. By direct comparison of the calculated values of Υ for $s = 2$ and the scaling form expected for a BKT transition,[33] unambiguous conclusions regarding the universality class of the phase transition at $s = 2$ could not be drawn. The presence of the presumably irrelevant dissipation term is still effective in driving the system away from BKT-type criticality at all but the very largest system sizes. In practice, the logarithmic scaling analysis[33] is usually best suited for small to moderate system sizes. Consequently, instead of scaling the helicity modulus directly, we resort to calculating κ via other observables and find that $2\beta/\nu - \eta = 0$ within statistical uncertainty for $s = 2$. Moreover, $2\beta/\nu - \eta$ is very close to zero for all $s \geqslant 1.75$. For even smaller values of s (where direct scaling of Υ is more reliable), we have confirmed that the scaling law $\kappa = 2\beta/\nu - \eta$ is valid also in the presence of dissipation. This scaling form is also equivalent to $\kappa = d_{\rm eff} - 2$. Thus, the helicity modulus vanishes continuously as $K \to K_c^+$, provided $d_{\rm eff} = d + z > 2$. The above equivalence assumes that hyperscaling is valid, and we have confirmed this validity for all values of s.

C. Boundary between long-range and short-range critical behavior

From Figs. 1 to 5, it is evident that all critical exponents are very close to their short-range values for $s \gtrsim 1.75$. The naive scaling estimate places the boundary at which the dissipation term becomes irrelevant at $s = 2$. For classical models with (isotropic) long-range interactions decaying with distance r as $1/r^{1+s}$, it has long been debated[34,35] whether the models feature the exponents of the corresponding short-range model already when s exceeds a value $s^* = 2 - \eta_{\rm SR}$. Here, $\eta_{\rm SR}$ denotes the anomalous dimension of the short-range model. Using large-scale Monte Carlo simulations, it has been shown[36] that for the long-range 2D Ising model, the anomalous dimension follows the conjectured exact[34] relation $\eta = 2 - s$ for $s < 1.75$, but that $\eta = 0.25 = \eta_{\rm SR}$ for $s > s^* = 1.75$. Although the long-range interaction of the dissipative quantum models we consider is highly anisotropic, in contrast to the isotropic classical long-ranged models, it is plausible that also in these models the threshold value of s beyond which dissipation is irrelevant is reduced from $s = 2$ to some lower value.

In order to establish this boundary more accurately also for the present case of anisotropic interactions, we have performed a more careful analysis of the case $s = 1.875$ for the Z_4 model. Including corrections to scaling, using the ansatz $L_\tau^* = aL^z(1 + bL^{-\omega})$, we find $z = 1.002(11)$. Hence, the decay exponent $s = 1.875$ may serve as an upper bound for the boundary value s^* necessary to render the dissipation term effectively short ranged. This, in turn, would render the system effectively Lorentz invariant with $z = 1$. To get the statistics required to include corrections to scaling in a stable manner, we included three different values of the dissipation strength α in a joint fit. This also provides an a posteriori justification of the choice of lower values of α for higher values of s.[37] Probably due to logarithmic corrections expected at the presumed boundary value $s^* = 1.75$,[36] we are not able to acquire the same level of accuracy for this value of s. Therefore we cannot rule out that the dissipation term is rendered effectively short ranged at some other value $s^* \in (1.75, 1.875)$. An exceedingly slow crossover to asymptotic critical exponents for values $s \approx s^*$ can conceivably be understood from the competition between the fixed point corresponding to short-range (Lorentz-invariant) criticality and the fixed point corresponding to long-range (dissipation-dominated) criticality.

We close this section with a remark on the evolution of the anomalous dimension. In the quantum dissipative model we have studied, the anomalous dimension increases for increasing s. This is a consequence of the effective dimensionality $d_{\rm eff} = d + z$ decreasing with increasing s. Lowering the dimensionality from the upper critical dimension, where $\eta = 0$, tends to increase η. This is quite different from the situation encountered in classical models with isotropic long-range interactions. Classical models with short-range interactions and an action of the form $S \sim q^2\phi_q\phi_{-q}$ (where ϕ_q is an appropriate order-parameter field) have propagators $G(q) \sim 1/|q|^{2-\eta}$. The corresponding long-range models with an action of the form $S \sim |q|^s\phi_q\phi_{-q}$ have propagators $G(q) \sim 1/|q|^s$, when $s < 2 - \eta_{\rm SR}$. One may now, as is customarily done in the literature on long-range classical isotropic models, define an effective anomalous scaling dimension for such systems by comparing with the corresponding expression for the short-range case, finding $\eta = 2 - s$, which decreases with increasing s. This relation is best viewed as a result of somewhat artificially imposing the standard scaling form of a propagator for short-range systems $(1/|q|^{2-\eta})$ on the form of the propagator for systems with long-range interactions, $1/|q|^s$.

D. Scaling relation between z and η

In Fig. 2, we demonstrated how the scaling relation $z = z_0 - \eta$ cannot be valid except close to the Ohmic limit $s = 1$ and that $\eta \approx 1/4$ for all $s \geqslant 1.75$. Moreover, from our numerics we think it is likely that $z(s) = 1$ for $s \geqslant 1.75$. A scaling relation between z and η which would fit well with these observations is

$$z = \max\left\{\frac{2-\eta}{s}, 1\right\}. \quad (7)$$

The scaling relation $z = (2 - \eta)/s$ has been suggested previously in Ref. 17 in the context of a damped nonlinear σ model.

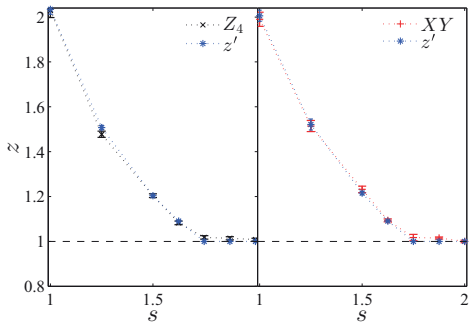

FIG. 6. (Color online) The dynamical critical exponent z as in Fig. 1, but compared with the scaling estimate $z' = (2-\eta)/s$. The values of η used in the scaling estimates are the same as reported in Fig. 2, with the left panel corresponding to the Z_4 model and the right panel to the XY model.

In Fig. 6, we show the same data for the dynamical exponent z as in Fig. 1 but compared with the ansatz (7) instead of the naive scaling estimate $z_0 = 2/s$. Although there are probably still some corrections to finite-size scaling, Eq. (7) seems to fit the data far better than the alternatives.

We next provide a heuristic argument for why the scaling relation (7) may be reasonable for $s < 2 - \eta_{\rm SR}$. Building on the arguments in Sec. III C for classical isotropic long-range-interacting systems, we take as a starting point that a dissipative quantum model with action of the form $S \sim (q^2 + |\omega|^s)\phi_{q,\omega}\phi_{-q,-\omega}$ can be viewed as an anisotropic long-range-interacting system. Introducing the suitably chosen frequency coordinate $\tilde{\omega}^s = q^2 + |\omega|^s$, the propagator takes the isotropic form $G(\tilde{\omega}) \sim 1/|\tilde{\omega}|^s$. Recall that in the quantum case, the anomalous scaling dimension η is defined from the *spatial* correlation function $G(x) \sim 1/x^{d+z-2+\eta} \equiv 1/x^{\theta_x}$. To find η, we Fourier transform the propagator to obtain the imaginary-time correlation function. In terms of the frequency coordinate $\tilde{\omega}$, the system effectively has $d'_{\rm eff} = 1 + d/z$ dimensions. Therefore, the correlation function decay exponent in terms of the isotropic space-time coordinate $\tilde{\tau} \equiv (\tau^2 + x^{2z})^{1/2}$ would be $\theta_{\tilde{\tau}} = (z+d)/z - s$. Comparing with the imaginary-time decay exponent $\theta_\tau = \theta_x/z = (d + z - 2 + \eta)/z$, we find $sz = 2 - \eta$, which is equivalent to Eq. (7).

Finally, we point out that our results for the scaling relation (7) for dissipative models should also have relevance for *nondissipative* quantum spin chains with long-range *spatial* interactions.[38,39] One arrives at exactly such a model by simply interchanging the x and τ coordinates of the action we have considered. The dynamical critical exponent of this model is given by $z' = 1/z = s/(2-\eta)$, with the quantity $\eta(s)$ evolving as shown in Fig. 2. This quantity will, however, not be identical to the anomalous scaling dimension of the model, η', which is given by the classical result $\eta' = 2 - s$. Hence, there exists no independent scaling relation between the dynamical critical exponent z' and the anomalous dimension η' for a nondissipative quantum spin chain with long-range interactions.

E. Dependence on symmetry

For $s = 1$, we have $z \approx 2$, $d_{\rm eff} \approx 3$, while for $s = 2$, we have $z = 1$, $d_{\rm eff} = 2$. For these two cases, it is known either analytically or numerically that the exponent η is very similar for the Ising and XY models.[40] There appears to be no particular deep reason for this. For instance, the well-known value $\eta = 1/4$ comes about for completely different reasons in the 2D Ising and 2D XY models, and their similarity thus appears to be accidental. Using the scaling relations $2\beta/\nu - \eta = d_{\rm eff} - 2$ [assuming Eq. (7)] and $\gamma/\nu = 2 - \eta$, it follows that the similarities in β/ν and γ/ν for the Ising and XY models are as coincidental as they are for η, both in 2D and 3D. It appears that these coincidences persist in all dimensions between 2 and 3. There is good reason to expect that the same also holds in the sub-Ohmic regime $s < 1$. Such values of s increase the effective dimensionality beyond 3, eventually driving all exponents to their universal mean-field values at the upper critical dimension.

We next comment on other values of q, and how our results apply to those cases. The Ising and XY models represent extreme cases of Z_q clock models, with $q = 2$, $q = \infty$, respectively. The partition function for the $q = 4$ case is simply the square of the case $q = 2$, and hence they give identical results. For larger $q > 4$, anisotropy is irrelevant,[41] and we thus expect the results of U(1) to emerge. We therefore conjecture that the results of this paper for z, η, β/ν, and γ/ν, are valid for all Z_q clock models. The only possible exception is the case $q = 3$, also equivalent to the three-state Potts model, where the anisotropy with respect to a U(1)-symmetric model is known to be relevant. Although we have not checked this, it may still be possible that Eq. (7) holds also for a dissipative Z_3 clock model, at least for $s > 1$.[42]

An alternative perspective on this, supporting the notion that the scaling relation $z = (2-\eta)/s$ is valid for all q, may be provided by the following qualitative argument. The variation of z with the parameter s determining the range of the dissipation expresses a variation in the effective space-time dimensionality of the system. This is determined by the interaction of the spins at a given site in the imaginary-time direction. Due to the long-range character of this interaction, each spin interacts with a large number of fluctuating copies of itself along a chain in the imaginary-time direction. Due to the summation over many spins at different Trotter slices, the discrete nature of the spins in a Z_q clock model is washed out, even in the case $q = 2$. Therefore, the manner in which the dissipation affects the effective dimensionality does not depend on whether the spins at each space-time lattice point take on discrete or continuous values.

IV. SUMMARY

We have performed Monte Carlo simulations on a generalized spin-boson model in one spatial dimension featuring non-Ohmic site dissipation and two variants of order parameter symmetry, namely Ising-like and U(1). By tuning the imaginary-time decay exponent of the dissipative interaction, $s \in [1,2]$, we are able to continuously vary the effective dimensionality of the system. Apparently, the order parameter symmetry has very little bearing on the evolution of the

effective dimensionality, $d_{\text{eff}} = d + z$, as a function of the decay parameter s. While naive scaling estimates a crossover from criticality dominated by the dissipation term to an irrelevant dissipation term at $s = 2$, we measure exponents in relatively good correspondence with the underlying, short-range interacting model at a somewhat lower value $s \approx 1.75$. Our results also suggest that for $1 \leqslant s \leqslant 2$, the exponents z and η to a good approximation obey the scaling relation $z = \max\{(2 - \eta)/s, 1\}$.

ACKNOWLEDGMENTS

A.S. was supported by the Norwegian Research Council under Grant No. 205591/V30 (FRINAT). I.B.S. and E.B.S. thank NTNU for financial support. The work was also supported through the Norwegian consortium for high-performance computing (NOTUR). Useful communications with E. V. Herland, D. A. Huse, F. S. Nogueira, and Z. Tešanović are acknowledged.

[1] A. J. Leggett, S. Chakravarty, A. T. Dorsey, M. P. A. Fisher, A. Garg, and W. Zwerger, Rev. Mod. Phys. **59**, 1 (1987).

[2] K. Le Hur, in *Understanding Quantum Phase Transitions*, edited by L. D. Carr (Taylor & Francis, Boca Raton, FL, 2010).

[3] P. Werner, K. Völker, M. Troyer, and S. Chakravarty, Phys. Rev. Lett. **94**, 047201 (2005).

[4] I. B. Sperstad, E. B. Stiansen, and A. Sudbø, Phys. Rev. B **81**, 104302 (2010).

[5] P. Werner, M. Troyer, and S. Sachdev, J. Phys. Soc. Jpn. **74S**, 67 (2005).

[6] M. Vojta, Phil. Mag. **86**, 1807 (2006).

[7] M. Vojta, Rep. Prog. Phys. **66**, 2069 (2003).

[8] Q. Si, in *Understanding Quantum Phase Transitions*, edited by L. D. Carr (Taylor & Francis, Boca Raton, FL, 2010).

[9] V. Aji and C. M. Varma, Phys. Rev. Lett. **99**, 067003 (2007).

[10] K.-H. Wagenblast, A. van Otterlo, G. Schön, and G. T. Zimányi, Phys. Rev. Lett. **78**, 1779 (1997).

[11] P. P. Orth, I. Stanic, and K. Le Hur, Phys. Rev. A **77**, 051601(R) (2008).

[12] T. Vojta, J. A. Hoyos, P. Mohan, and R. Narayanan, J. Phys.: Condens. Matter **23**, 094206 (2011).

[13] J. A. Hoyos, C. Kotabage, and T. Vojta, Phys. Rev. Lett. **99**, 230601 (2007).

[14] A. M. Lobos, A. Iucci, M. Müller, and T. Giamarchi, Phys. Rev. B **80**, 214515 (2009).

[15] R. M. Lutchyn, V. Galitski, G. Refael, and S. Das Sarma, Phys. Rev. Lett. **101**, 106402 (2008).

[16] M. T. Glossop and K. Ingersent, Phys. Rev. Lett. **95**, 067202 (2005).

[17] A. Gamba, M. Grilli, and C. Castellani, Nucl. Phys. B **556**, 463 (1999).

[18] A. Winter, H. Rieger, M. Vojta, and R. Bulla, Phys. Rev. Lett. **102**, 030601 (2009).

[19] S. Kirchner, Q. Si, and K. Ingersent, Phys. Rev. Lett. **102**, 166405 (2009).

[20] S. Kirchner, J. Low Temp. Phys. **161**, 282 (2010).

[21] M. Vojta, N.-H. Tong, and R. Bulla, Phys. Rev. Lett. **94**, 070604 (2005); See, however, M. Vojta, N.-H. Tong, and R. Bulla, *ibid.* **102**, 249904(E) (2009).

[22] G. Kotliar, P. W. Anderson, and D. L. Stein, Phys. Rev. B **27**, 602(R) (1983).

[23] H. G. Katzgraber, D. Larson, and A. P. Young, Phys. Rev. Lett. **102**, 177205 (2009).

[24] A. Sharma and A. P. Young, Phys. Rev. B **83**, 214405 (2011).

[25] J. A. Hertz, Phys. Rev. B **14**, 1165 (1976).

[26] S. Pankov, S. Florens, A. Georges, G. Kotliar, and S. Sachdev, Phys. Rev. B **69**, 054426 (2004).

[27] A. O. Caldeira and A. J. Leggett, Ann. Phys. (NY) **149**, 374 (1983).

[28] U. Wolff, Phys. Rev. Lett. **62**, 361 (1989).

[29] E. Luijten and H. Blöte, Int. J. Mod. Phys. C **6**, 359 (1995).

[30] M. Matsumoto and T. Nishimura, ACM Trans. Model. Comput. Simul. **8**, 3 (1998).

[31] A. M. Ferrenberg and R. H. Swendsen, Phys. Rev. Lett. **63**, 1195 (1989).

[32] M. Hasenbusch, K. Pinn, and S. Vinti, Phys. Rev. B **59**, 11471 (1999).

[33] H. Weber and P. Minnhagen, Phys. Rev. B **37**, 5986 (1988).

[34] M. E. Fisher, S.-k. Ma, and B. G. Nickel, Phys. Rev. Lett. **29**, 917 (1972).

[35] J. Sak, Phys. Rev. B **8**, 281 (1973).

[36] E. Luijten and H. W. J. Blöte, Phys. Rev. Lett. **89**, 025703 (2002).

[37] To be more specific, we carried out the joint fit for system sizes in the interval $L = 57$ to $L = 607$ for three data sets $\alpha = 0.05$, 0.1, 0.2, where only the exponents z and ω were constrained to be equal for all data sets. The value of the correction-to-scaling exponent was found to be $\omega = 0.42(25)$. The values of the correction amplitudes b were all negative within statistical uncertainty and decreasing with increasing α. This implies that α would have to be set to a vanishingly small value to reduce the corrections to scaling for $s = 1.875$, and also justifies using relatively low values of α for the largest values of s.

[38] A. Dutta and J. K. Bhattacharjee, Phys. Rev. B **64**, 184106 (2001).

[39] N. Laflorencie, I. Affleck, and M. Berciu, J. Stat. Mech.: Theory Exp. (2005) P12001.

[40] A. Pelissetto and E. Vicari, Phys. Rep. **368**, 549 (2002).

[41] S. Elitzur, R. B. Pearson, and J. Shigemitsu, Phys. Rev. D **19**, 3698 (1979).

[42] We expect that a three-state Potts model with effective dimensionality d_{eff} may have a first-order phase transition for $d_{\text{eff}} \geqslant 3$.

Paper III

Criticality of compact and noncompact quantum dissipative Z_4 models in (1+1) dimensions

Physical Review B **83**, 115134 (2011)

PHYSICAL REVIEW B **83**, 115134 (2011)

Criticality of compact and noncompact quantum dissipative Z_4 models in (1 + 1) dimensions

Einar B. Stiansen, Iver Bakken Sperstad, and Asle Sudbø
Department of Physics, Norwegian University of Science and Technology, N-7491 Trondheim, Norway
(Received 15 December 2010; revised manuscript received 4 February 2011; published 28 March 2011)

Using large-scale Monte Carlo computations, we study two versions of a $(1 + 1)$D Z_4-symmetric model with ohmic bond dissipation. In one of these versions, the variables are restricted to the interval $[0,2\pi\rangle$, while the domain is unrestricted in the other version. The compact model features a completely ordered phase with a broken Z_4 symmetry and a disordered phase, separated by a critical line. The noncompact model features three phases. In addition to the two phases exhibited by the compact model, there is also an intermediate phase with isotropic quasi-long-range order. We calculate the dynamical critical exponent z along the critical lines of both models to see if the compactness of the variable is relevant to the critical scaling between space and imaginary time. There appears to be no difference between the two models in that respect, and we find $z \approx 1$ for the single phase transition in the compact model as well as for both transitions in the noncompact model.

DOI: 10.1103/PhysRevB.83.115134 PACS number(s): 75.40.Mg, 64.60.De, 05.30.Rt

I. INTRODUCTION

The standard way of introducing dissipation in a quantum mechanical system is to couple some variable describing the system to the degrees of freedom of an external environment.[1] The environment is modeled as a bath of harmonic oscillators which couple linearly to the system variables. The oscillator degrees of freedom, appearing in the action to second order, may be integrated out to produce an effective theory for the composite system given in terms of the system variables.

The presence of a dissipative term introduces strongly retarded (nonlocal in time) self-interactions of the system variables. This long-range interaction in imaginary time may have serious consequences for the quantum critical behavior of the system. This effect can usually be described by a dynamical critical exponent z defined by the anisotropy of the divergence of the correlation lengths at criticality, $\xi_\tau \sim \xi^z$, where ξ and ξ_τ are the correlation lengths in space and imaginary time, respectively. An Ising spin chain with site dissipation was shown by extensive Monte Carlo simulations in Ref. 2 to have $z \approx 2$. The same model, augmented to two spatial dimensions, was investigated by the present authors in Ref. 3. The result $z = 1.97(3)$ suggests that the dynamical critical exponent is independent of the number of spatial dimensions, in agreement with naive scaling arguments which make no reference to dimensionality.[4] On the other hand, when coupling the reservoir to bond variables involving Ising spins the dissipation term was found to be irrelevant to the universality class, i.e., $z \approx 1$.[3] In general, dissipation suppresses certain types of quantum fluctuations, though the larger value of z for site dissipation signifies that bond dissipation is far less effective than site dissipation in reducing fluctuations.

Ohmic dissipation in terms of gradients or bonds is common in models describing shunted Josephson junctions or granular superconductor systems.[5,6] Here, the bonds represent the difference of the quantum phases between the superconducting grains. In this context it is well known that the coupling of the environment to the system may affect the natural domain of the system variables.[7] For Josephson junctions, this means that the domain of the phase variables reflects quantization of the charges on each superconducting grain. If the charges are quantized in units of Cooper pairs, $2e$, the domain of the quantum phase is 2π periodic. Ohmic shunting leads to an unbounded $-\infty < \theta < \infty$ domain,[7] reflecting a continuous transfer of charges across the junction. We will henceforth refer to the variable defined on a restricted 2π interval as *compact* and the extended variable as *noncompact*.

Moreover, dissipation in terms of bonds has also been proposed in an effective model describing the low-energy physics of fluctuating loop currents to describe anomalous normal state properties of high-T_c cuprates.[8,9] A quantum statistical mechanical model for such degrees of freedom has been derived from a microscopic three-band model of the cuprates.[10] The classical part of the derived action consists in its original form of two species of Ising variables within each unit cell, coupled by a four-spin Ashkin-Teller term. This model has been proven, through large-scale Monte Carlo simulations, to support a phase transition with a nondivergent nonanalyticity in the specific heat on top of an innocuous background.[11] The breaking of the Ising-like symmetry describes a suggested ordering of loop currents upon entering the pseudogap phase of the cuprates. Neglecting the Ashkin-Teller interaction term present in this theory, the classical model may be mapped onto a four-state clock model, with the basic variable being an angle parametrizing the four possible current loop orientations.[8,10,11]

The quantum version of this model includes a kinetic energy term describing the quantum dynamics of the angle variables. Adding dissipation of angle differences as in the Caldeira-Leggett approach for Josephson junctions, the model has been reported to exhibit local quantum criticality. Local quantum criticality in this context means that the model exhibits a fluctuation spectrum which only depends on frequency, but is independent of the wave vector.[8] This essentially implies a dynamical critical exponent $z \to \infty$. A point which quite possibly is of importance in this context, is that while the starting point in Ref. 8 is a model with two Ising-like variables, the actual dissipative quantum model discussed is one with global $U(1)$ symmetry.

While the physical picture of fluctuating configurations of current loops suggests an identification of the angles θ and

$\theta + 2\pi$, the presence of the clearly noncompact dissipation term makes this not entirely obvious. It is therefore the intent of this work to investigate if the restriction of the variable domain influences the dynamical critical exponent z, and thereby if it may have consequences for possible manifestations of local quantum criticality in similar models. Since it is still an open question exactly what the consequences are of how the variable domains are defined in dissipative quantum models, a numerical comparison of the compact and noncompact case is of general interest. We will therefore not restrict the interpretation of the model to Ising variables associated with loop currents, although the Z_4 symmetry reflecting this starting point will be maintained. Moreover, due to the long-ranged interactions in the imaginary-time direction, the Monte Carlo computations are extremely demanding. Since we are interested in a proof of principle of the importance of compactness versus noncompactness, we will in this paper limit ourselves to a $(1 + 1)$D model.

We will perform Monte Carlo simulations on two versions of a dissipative Z_4 model described in more detail in Sec. II, one with compact variables (i.e., a clock model) and one with noncompact variables. The simulation details are described in Sec. III, after which we present the results, first for the noncompact case in Sec. IV, then for the compact case in Sec. V.

Our main finding is that, although the critical scaling of space and imaginary time is equal for both cases, i.e., $z = 1$, there is a major difference in phase structure. Whereas the compact model displays a conventional order-disorder phase transition, the noncompact model develops an intermediate phase characterized by power-law decay in spin correlations (quasi-long-range order) and a $U(1)$ symmetric distribution of the complex order parameter. The appearance of this intermediate phase is related to the fact that the kinetic energy term must be treated differently for the compact and noncompact cases, as we discuss in detail in the Appendix.

It is well established that this kind of critical phase occurs in classical 2D Z_q clock models and XY models with Z_q anisotropy,[12–14] but only for larger values of q than we are considering. It is remarkable that the noncompact model presented in this paper exhibits a critical phase with emergent $U(1)$ symmetry, when the dissipationless starting point is a pure $Z_4 = Z_2 \times Z_2$ model (i.e., a double Ising model) with the angle variables restricted to four discrete values by a *hard* constraint. We will discuss this in more detail in Sec. VI, after which we summarize our results in Sec. VII.

II. THE MODEL

The starting point for our model is a chain of N_x quantum rotors, or equivalently planar spins, the alignment of which is described by a set of angle variables $\{\theta_x\}$. Although these variables could also be denoted as the phases of the quantum rotors, we will refer to them simply as angles. Requiring that the spins satisfy Z_4 symmetry, the angles can be parametrized as $\theta = 2\pi n/4$ with integer n, making our model similar to a four-state (or Z_4) clock model. Being quantum spins, their dynamics is described by their evolution in imaginary time τ, with N_τ denoting the number of Trotter slices used to discretize the imaginary time dimension. The variables $\{\theta_{x,\tau}\}$ are thus defined on the vertices of a $(1 + 1)$D quadratic lattice of size $N_x \times N_\tau$.

In order to investigate if the restriction on the angle variable is relevant to the dynamical critical exponent z or not, we will consider two variants of this model, with the complete action for both stated below for later reference. In the compact (C) case, we restrict the parametrization variable n to just four values, so that the angle θ is restricted to one primary interval, corresponding to the four primary states of the four-state clock model. In the noncompact (NC) case we have no such restriction, and n can take any integer values. The general form of the action is

$$S^{\mathrm{C,NC}} = S_\tau^{\mathrm{C,NC}} + S_x + S_{\mathrm{diss}}, \tag{1}$$

where the kinetic energy for the compact and the noncompact case, respectively, is given by

$$S_\tau^{\mathrm{C}} = -K_\tau \sum_{x=1}^{N_x} \sum_{\tau=1}^{N_\tau} \cos(\theta_{x,\tau+1} - \theta_{x,\tau}), \tag{2}$$

$$S_\tau^{\mathrm{NC}} = \frac{K_\tau}{2} \sum_{x=1}^{N_x} \sum_{\tau=1}^{N_\tau} (\theta_{x,\tau+1} - \theta_{x,\tau})^2. \tag{3}$$

The spatial interaction defines a periodic potential

$$S_x = -K \sum_{x=1}^{N_x} \sum_{\tau=1}^{N_\tau} \cos(\theta_{x+1,\tau} - \theta_{x,\tau}), \tag{4}$$

and the dissipation term is defined according to

$$S_{\mathrm{diss}} = \frac{\alpha}{2} \sum_{x=1}^{N_x} \sum_{\tau \neq \tau'}^{N_\tau} \left(\frac{\pi}{N_\tau}\right)^2 \frac{(\Delta\theta_{x,\tau} - \Delta\theta_{x,\tau'})^2}{\sin^2\left(\frac{\pi}{N_\tau}|\tau - \tau'|\right)}. \tag{5}$$

The bond variable or angle difference is written as $\Delta\theta_{x,\tau} = \theta_{x+1,\tau} - \theta_{x,\tau}$.

Note that the only apparent difference between the compact and the noncompact model is the form of the kinetic energy term. When the angles are compact the short-range temporal interaction is given by a cosine term, in contrast to noncompact angles for which a quadratic form of the kinetic term must be used. The reason for this difference can be traced to the fact that, whereas canonical conjugate variables of compact angles are discrete due to the 2π periodicity of the quantum wave functions, no such restriction applies when the angles are noncompact. From a qualitative point of view the two separate forms of the temporal interaction term is expected. Considering the imaginary time history of a single variable, it is clear that a cosine interaction in imaginary time will render the ground state of the noncompact model massively degenerate. A Trotter slice may be shifted by 2π relative to the neighboring Trotter slices without any penalty in the action. However, a quadratic interaction term in the imaginary time direction lifts this degeneracy and tends to localize the angle variables.

There is nothing new about the derivation of these different kinetic terms, but as the difference is crucial to the phase structure of our models and is also rarely discussed in the literature, we include the derivation in the Appendix. In addition, in order to simulate the compact model we also need

an appropriate reinterpretation of the dissipation term. We find it natural to postpone this to Sec. V.

The action is on a form identical to the model in Sec. III in Ref. 3 apart from the nature of the variables and the resultant treatment of the dissipation term. However, we still expect the scaling arguments presented in Ref. 3 to be valid since no reference to the actual type of variable is used. The action in Fourier space may be written

$$S \sim (\mathbf{q}^2 + \omega^2 + |\omega|\mathbf{q}^2)\theta_q \theta_{-q}, \tag{6}$$

neglecting any prefactors. Taking the limit $\mathbf{q} \to 0$, $\omega \to 0$ we anticipate that the term $\sim|\omega|\mathbf{q}^2$ describing the dissipation is subdominant for all positive z. Accordingly, we expect at least naively that $z = 1$ for both compact and noncompact variables. This will be investigated in detail in our simulations, and we make no assumption of the veracity of naive scaling applied to this problem.

III. DETAILS OF THE MONTE CARLO COMPUTATIONS

When expanding the dissipative term, it becomes clear that it contributes both to ferromagnetic and antiferromagnetic long range interactions. This renders the system intractable to the Luijten-Blöte[15] extension of the Wolff cluster algorithm[16] which has been used with great success in systems with noncompeting interactions. Also, for the case of noncompact variables there does not exist a straightforward way of defining (pseudo)spin projections, a necessary point for the Wolff embedding technique.[16] Considerable progress has been made in constructing new effective algorithms for long range interacting systems with extended variables.[17–19] However, these algorithms are presently restricted to $(0 + 1)$D systems, and do not seem to generalize easily to $N_x > 1$.[18] Furthermore, the basic degrees of freedom in these algorithms are the phase *differences* between two superconducting grains in an array of Josephson junctions. Our aim is to investigate the ordering of the phases themselves. Hence, the existing nonlocal algorithms may not be utilized. In the Monte Carlo simulations, we have therefore used a parallel tempering algorithm[20,21] in which several systems (typically 16 or 32) are simulated simultaneously at different coupling strengths.

A Monte Carlo sweep corresponds to proposing a local update by the Metropolis-Hastings algorithm for every grid point in the system in a sequential way. For the case of noncompact variables the proposed new angles are generated by randomly choosing to increase or decrease the value, then propagating the value by randomly choosing the increment on the interval $\{\frac{\pi}{2}, \pi, \frac{3\pi}{2}, 2\pi\}$. In the case of compact variables, a new angle value in the primary interval is randomly chosen. After a fixed number of Monte Carlo sweeps (typically $3 - 10$) a parallel tempering move is made. In this move, a swap of configurations between two neighboring coupling values is proposed, and the swap is accepted with probability Ξ_{PT} given by

$$\Xi_{PT} = \begin{cases} 1 & \text{if } \Delta < 0, \\ \mathrm{e}^{-\Delta} & \text{if } \Delta \geqslant 0. \end{cases} \tag{7}$$

Here, $\Delta = \kappa'(\bar{S}[X;\kappa'] - \bar{S}[X';\kappa']) - \kappa(\bar{S}[X;\kappa] - \bar{S}[X';\kappa])$, where κ is the coupling value varied, representing in our case K or α, and X represents the angle configuration. $\bar{S}$ indicates the term of the action proportional with the coupling parameter κ.

All Monte Carlo simulations were initiated with a random configuration. Depending on system sizes various numbers of sweeps were performed for each coupling value. For the phase transition separating the disordered state from the critical phase in the noncompact model $5 - 10 \times 10^6$ sweeps were made. Also, $1 - 5 \times 10^5$ sweeps at each coupling value were discarded for equilibration. For the compact model and the second transition of the noncompact model as much as 30×10^6 sweeps where performed and typically 5×10^5 sweeps discarded.

The Mersenne-Twister[22] random number generator was used in all simulations and the random number generator on each CPU was independently seeded. It was confirmed that other random number generators yielded consistent results. We also make use of the Ferrenberg-Swendsen reweighting technique,[23] which enables us to continuously vary the coupling parameter after the simulations have been performed.

IV. RESULTS: NONCOMPACT MODEL

In this section we consider the noncompact version of the dissipative Z_4 model. Using Eqs. (3), (4), and (5) we have the following action:

$$S^{\mathrm{NC}} = S_\tau^{\mathrm{NC}} + S_x + S_{\mathrm{diss}}. \tag{8}$$

In contrast to the compact model, the angle variables are in this case not restricted to the primary interval. The variables are straightforwardly generalized to take the values $\theta = 2\pi n/4$, where $n = 0, \pm 1, \pm 2, \ldots$. We seek to fix K and K_τ and investigate how the system behaves under the influence of increasing dissipation strength controlled by the dimensionless parameter α.

The kinetic coupling strength has been fixed to $K_\tau = 0.4$ for computational reasons, as this ensures that the simulations will be performed at convenient values of N_x and N_τ. We have performed simulations at four different spatial coupling constants $K = 0.4$, 0.5, 0.6, and 0.75. These choices are also made for computational convenience, as the limit of vanishing dissipation as well as the limit $K \to 0$ are both very computationally demanding. For all coupling values there is a disordered phase at low values of the dissipation strength. In this phase the noncompact angles exhibit wild fluctuations and consequently $\langle \mathrm{e}^{\mathrm{i}\theta_{x,\tau}} \rangle = 0$. However, we also have $\langle \mathrm{e}^{\mathrm{i}\Delta\theta_{x,\tau}} \rangle \neq 0$ in this phase, a trivial consequence of the cosine potential acting as an external field on the bond variables. The bond variables occasionally drift from one minimum of the extended cosine potential to another. As the dissipation strength is increased, fluctuations in these variables are suppressed, and the system features two consecutive phase transitions separated by a critical phase. This intermediate phase is characterized by power-law decay of spatiotemporal

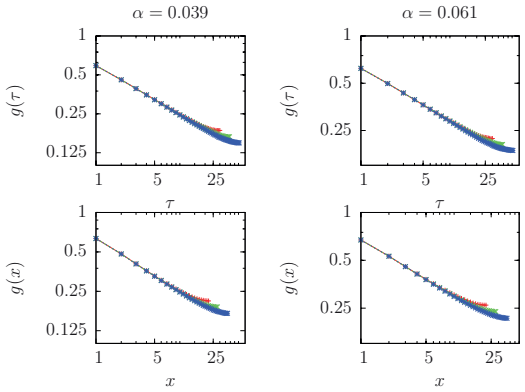

FIG. 1. (Color online) Correlation functions, Eq. (9), at two values of the dissipation strength α within the critical phase for spatial coupling $K = 0.75$. System sizes are $N_x = 44,57,74$, with optimal choices of N_τ at $\alpha_c^{(1)}$, see text. Top row: Correlation functions for the temporal direction. Bottom row: Correlation functions for the spatial direction.

spin correlations on the form

$$g(\mu) = \langle e^{i(\theta_\mu - \theta_0)} \rangle, \quad \mu \in (x,\tau). \tag{9}$$

The correlation functions for both spatial and imaginary time direction are shown in Fig. 1 for two different dissipation strengths both within the the critical phase.

A very similar critical phase, as well as phase transitions associated with it, has recently enjoyed increased interest in various versions of classical clock models.[24–26] We will proceed under the assumption that a similar picture is valid in our case. Indeed, simulations performed on a classical 2D six-state clock give qualitatively very similar results for all observables considered below, which supports the supposition that these two phenomena are related.

Considering the complex order parameter of the system,

$$m = \frac{1}{N_x N_\tau} \sum_{x,\tau} e^{i\theta_{x,\tau}} = |m| e^{i\phi}, \tag{10}$$

the intermediate critical phase can be identified by observing the distribution of m in the complex plane.[26] In the disordered phase, the order parameter is a Gaussian peak centered at the origin. In the intermediate phase, quasi-long-range order develops in the complex order parameter, and so $|m|$ acquires a nonzero value as a finite-size effect. The order parameter is, however, free to rotate in the ϕ direction. This can be described as the vanishing of the excitation gap naively expected for discrete Z_q models, or equivalently as an emergent $U(1)$ symmetry.[27] This symmetry is broken at a larger value of the dissipation strength, when true long range order is established when the magnetization selects one of the four well-defined directions in the complex plane originating with the underlying Z_4 symmetry. Typical distributions of the complex order parameter in the three phases is shown in Fig. 2.

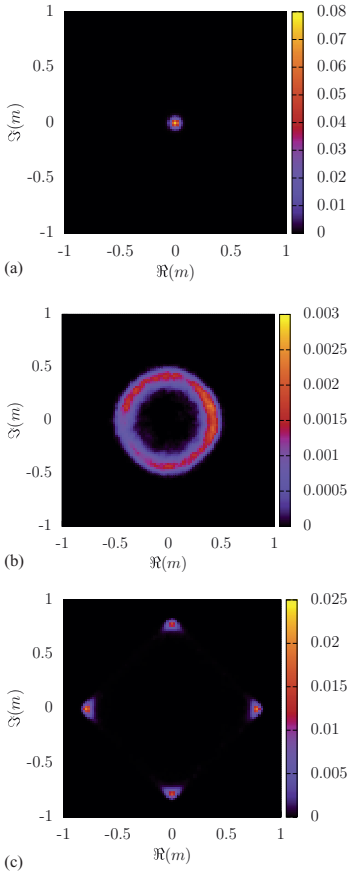

FIG. 2. (Color online) Evolution of the complex order parameter when dissipation strength α is increased for $K = 0.75$ and system size $N_x = 74$, $N_\tau = 103$ which corresponds to a near optimal aspect ratio at the phase transition at $\alpha \approx \alpha_c^{(1)}$. The color scale indicates relative density of the distribution. (a) Two dimensional Gaussian distribution of the order parameter in the complex plane corresponding to the disordered phase with $\alpha = 0.0 < \alpha_c^{(1)}$. (b) Intermediate critical phase exhibiting a finite-size-induced nonvanishing $|m|$ that rotates in the ϕ direction. The critical phase exists in a finite interval of dissipation strengths $\alpha_c^{(1)} < \alpha = 0.04 < \alpha_c^{(2)}$. The remaining anisotropy is attributed to insufficient sampling.[28] (c) The rotational symmetry of the intermediate critical phase is broken and long-range order is established as the order parameter relaxes into one of the four directions in the complex plane. The long-range ordered phase corresponds to the strong dissipation limit, $\alpha = 0.18 > \alpha_c^{(2)}$.

Although not presented here, we have also confirmed that the susceptibility of the order parameter diverges over a finite interval of dissipation strengths, also a clear evidence of a critical phase.

The phase transition between the disordered state and the intermediate critical phase at dissipation strength $\alpha = \alpha_c^{(1)}$ is

detected by the Binder cumulant $g = 1 - Q/3$, where

$$Q = \frac{\langle |m|^4 \rangle}{\langle |m|^2 \rangle^2}. \tag{11}$$

The brackets indicate ensemble averaging. The scaling at criticality of the Binder cumulant for anisotropic systems is given in terms of two independent scaling variables,[2]

$$g(N_x, N_\tau) = \mathcal{G}\left(\frac{N_x}{\xi}, \frac{N_\tau}{\xi^z}\right). \tag{12}$$

At a critical point the correlation length ξ diverges, and one should be able to observe data collapse of the Binder cumulant as a function of N_τ / N_x^z for the correct value of z. The value of $g(N_x, N_\tau)$ is independent of N_x at the critical coupling, this may be used to align the plots of g as a function of N_τ horizontally. The exponent z can then be found by optimal collapse of data onto a universal curve. The cumulant curves have a maximum at $N_\tau = N_\tau^*$. At this temporal size, the system appears as isotropic as it can be, the anisotropic interactions taken into account. See Ref. 3 for a thorough discussion of this finite-size analysis.

In the intermediate phase, the system is critical over a finite interval of dissipation strengths. According to the scaling Eq. (12), curves of the Binder cumulant for increasing system sizes will therefore merge in this interval for $N_x \to \infty$.[29] For systems of finite sizes as considered here, the curves will however intersect close to the transition instead, and we find $\alpha_c^{(1)}$ by inspecting the convergence of the crossing points. As discussed in Ref. 3, the functional form of this convergence is unknown in our case (cf. also Sec. VI and Ref. 29), and all we can do is to report our best estimate for the $N_x \to \infty$ transition point. The uncertainty estimated accordingly is not insignificant, but the effective critical exponent z is found to not be very sensitive to this error in α_c.

By further increasing the dissipation strength, the rotational symmetry of the global order parameter is broken at $\alpha = \alpha_c^{(2)}$. The Binder cumulant given by Eq. (11) will not pick up this transition because $|m|$ does not contain any information on the angular direction of the global magnetization. Therefore, we consider an alternative magnetization measure[26,27]

$$m_\phi = \langle \cos(4\phi) \rangle, \tag{13}$$

where ϕ is the global phase as indicated by Eq. (10). This anisotropy measure vanishes when ϕ is evenly distributed and tends toward unity when the excitation gap opens and ϕ gets localized. We show in Fig. 3 both order parameters for the system $N_x = 74$, $N_\tau = 103$ as a function of α. This N_τ corresponds to the nearest integer N_τ^* at $\alpha \approx \alpha_c^{(1)}$. Actually, the optimal N_τ decreases with increasing α, so the given system size does not represent an optimally chosen aspect ratio for other dissipation strengths. The rotational symmetry of the complex order parameter is clearly seen to be broken at a higher dissipation strength than the onset of the intermediate critical phase.

Because ϕ measures a global rotation of the order parameter, extremely long simulations is needed to explore the ϕ space with a local update algorithm. This limits the efficiency of constructing a Binder cumulant from m_ϕ and extracting $\alpha_c^{(2)}$ from a universal point because this would involve calculating

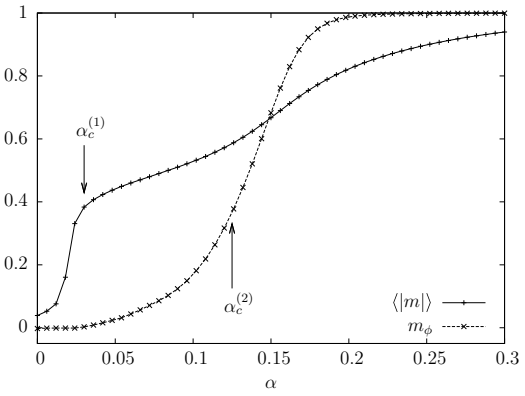

FIG. 3. The order parameter $\langle |m| \rangle$ and the anisotropy measure m_ϕ of the noncompact Z_4 model with $K = 0.75$ and system size $N_x = 74$, $N_\tau = 103 \approx N_\tau^*$. This size represents a near optimal aspect ratio at $\alpha \approx \alpha_c^{(1)}$. The two phase transitions are indicated by arrows, note that the intermediate critical phase $\alpha_c^{(1)} < \alpha < \alpha_c^{(2)}$ features a rotationally symmetric order parameter distribution.

moments of a already statistically compromised ensemble. To alleviate these difficulties, we instead make a scaling ansatz for the anisotropy measure itself,

$$m_\phi = \mathcal{M}_\phi\left(\frac{N_x}{\xi}, \frac{N_\tau}{\xi^z}\right), \tag{14}$$

based on the fact that the naive scaling dimension of this magnetization measure is zero. Near criticality, we expect m_ϕ to scale with system size in the same way as the Binder cumulant Eq. (12). Hence, we may calculate a dynamical critical exponent for this transition by exactly the same procedure as in Sec. V and Ref. 3. Again we expect a merging of m_ϕ curves as $\alpha \to \alpha_c^{(2)}$ from above in the limit of large N_x, but for the present system sizes we use the crossing points of m_ϕ curves to estimate $\alpha_c^{(2)}$. In Fig. 4, we plot the resulting phase diagram in the $\alpha - K$ plane. The intermediate phase is evidently very wide also when compared to the uncertainty assigned to the transition line, and we feel confident that it is a genuine phase and not merely an effect of the admittedly moderate finite system sizes we are restricted to.

We extract the dynamical critical exponent z along both of the critical lines $\alpha_c^{(1)}$ and $\alpha_c^{(2)}$ for all spatial coupling strengths. The data collapse of the Binder cumulant g at $K = 0.75$ and $\alpha = 0.030 \approx \alpha_c^{(1)}$ is shown in Fig. 5. Increasing the dissipation strength further brings the system to the second phase transition at $\alpha = 0.125 \approx \alpha_c^{(2)}$, the collapse of m_ϕ at this point is shown in Fig. 6.

In Table I, we present the numerical estimates of the dynamical critical exponent. The values of z are obtained using the scaling relation $N_\tau^* = a N_x^z$, with uncertainties based on a bootstrap analysis. These uncertainties also include the uncertainty in α_c. Within the accuracy of the simulations, the value of the critical exponent is $z = 1$ for all the coupling values at both phase transitions (although precise results are harder to obtain for the second). This is in accordance with the scaling argument presented in Sec. II.

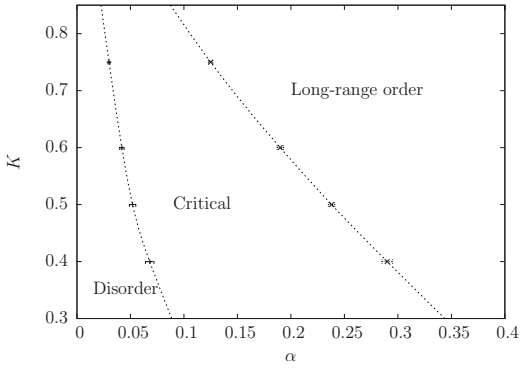

FIG. 4. Phase diagram for the noncompact model, Eq. (8) with $K_\tau = 0.4$. The dotted lines are guides to the eye. For fixed K the model features two consecutive phase transitions surrounding the intermediate critical phase (with quasi-long-range order). The simulation results (symbols along the dotted lines) are restricted to a region in coupling space amenable to simulations.

V. RESULTS: COMPACT MODEL

We now turn to the compact version of the dissipative Z_4 model,

$$S^{\mathrm{C}} = S_\tau^{\mathrm{C}} + S_x + S_{\mathrm{diss}}, \tag{15}$$

where the three terms are given by Eqs. (2), (4), and (5), respectively. Note that we now use a kinetic term S_τ^{C} having the same cosine-form as the spatial interaction term S_x. Regarding the use of the same dissipation term S_{diss} as in the noncompact case, one may argue that adding a Caldeira-Leggett term for the angle differences $\Delta\theta$ is a rather artificial way to model dissipation for a compact clock model in the first place, since its variance under 2π translations of θ implicitly

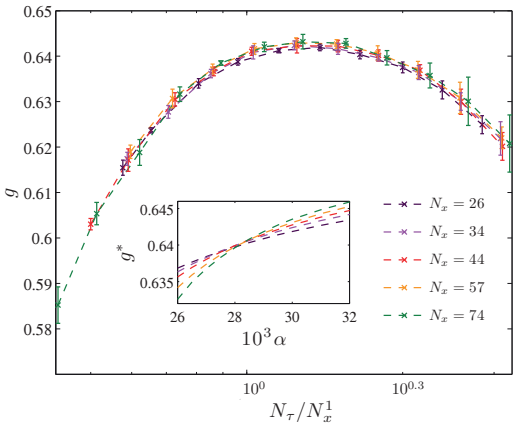

FIG. 5. (Color online) Data collapse of the Binder cumulant, $g = 1 - Q/3$, with Q given by Eq. (11), for the noncompact Z_4 model at $K = 0.75$ and $\alpha = 0.030 \approx \alpha_c^{(1)}$ with $z^{(1)} = 1$. Inset: Intersection of the Binder cumulant as a function of dissipation strength.

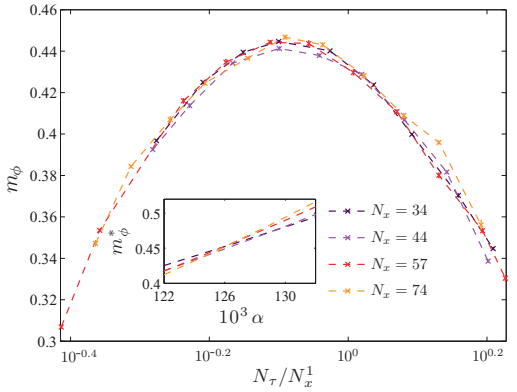

FIG. 6. (Color online) Data collapse of the anisotropy measure m_ϕ, Eq. (13), for the noncompact Z_4 model at $K = 0.75$ and $\alpha = 0.125 \approx \alpha_c^{(2)}$ with $z^{(2)} = 1$. The actual uncertainties are probably larger than indicated by the error bars for reasons discussed in the text. Inset: Intersection of the anisotropy measure as a function of dissipation strength.

assumes noncompact variables. However, adding exactly such a dissipation term is crucial for the demonstration of local quantum criticality in a similar Z_4 model[8] that is not obviously noncompact. Therefore, our motivation for the comparative study in the present section of a compactified version of the action (8) is to investigate whether an equivalent dissipation term for compact variables gives the model the same critical properties as reported for noncompact variables in the previous section, and thus whether the compactness of the variables as such is essential. Constructing an appropriate compactified version of the dissipative model does, however, require a reinterpretation of the variables in the Caldeira-Leggett term, so we will begin with a careful discussion of how we should treat this term in our simulations.

We first impose the following restriction on the interpretation of the compactified dissipation term: The term as a whole should be invariant under translations $\theta \to \theta + 2\pi$, since these two states are indistinguishable. As a corollary, any configurations that are physically indistinguishable when the angles are restricted to four values $\theta \in \{-\pi, -\pi/2, 0, \pi/2\}$ (or any equivalent parametrization) should give the same contribution to the dissipation term. Consequently, we cannot simply simulate the model with the dissipation term (5) as it stands, because the angle differences $\Delta\theta_{x,\tau}$ now only make physical sense modulo 2π. We therefore have to bring

TABLE I. Numerical estimates for critical coupling and critical exponents $z^{(1),(2)}$ for the two phase transitions $\alpha_c^{(1),(2)}$ of the noncompact model.

K	$\alpha_c^{(1)}$	$z^{(1)}$	$\alpha_c^{(2)}$	$z^{(2)}$
0.75	0.030(2)	0.99(1)	0.125(2)	1.01(2)
0.6	0.042(2)	0.99(2)	0.190(3)	0.96(3)
0.5	0.053(2)	1.02(2)	0.238(3)	0.97(3)
0.4	0.068(4)	0.97(3)	0.287(5)	0.99(4)

$\Delta\theta_{x,\tau}$ back to the primary interval $[-\pi,\pi\rangle$, as is well known for phase differences in superconducting systems without dissipation and other realizations of the (compact) XY model. Furthermore, we also choose to do the same for the difference between the two (compactified) $\Delta\theta_{x,\tau}$ terms in Eq. (5), as the alternative would result in different Boltzmann factors being associated with physically equivalent situations. Our procedure then is equivalent to requiring that the entire difference $\Delta\theta_{x,\tau} - \Delta\theta_{x,\tau'}$ should be restricted to the primary interval $[-\pi,\pi\rangle$, i.e., treating the dissipation term as a 2π-periodic function.

The details of the Monte Carlo simulations are described in Sec. III also for the compact model. The only difference that may be of any consequence is that we found it more convenient to vary the spatial coupling while fixing the dissipation strength in this case, but we have checked that the direction in coupling space taken by the simulations has no impact on the result.

The dissipationless ($\alpha = 0$) four-state clock model is completely isomorphic to the Ising model with interaction $K/2$. Thus, we may employ the criterion $\sinh(K_c)\sinh(K_\tau) = 1$ in order to calculate K_c for a fixed value of K_τ. The temporal coupling parameter is fixed at $K_\tau = -\ln(\tanh\frac{1}{2}) \approx 0.7719$ such that $K_c = 1$ when the dissipation is tuned to zero.

The most striking difference we found when compactifying the angles is that the intermediate phase with quasi-long-range order vanishes. This means that one has only a single disorder-order phase transition, as is the result one would usually expect for any model with Z_4 symmetry. We have verified that the Z_4 symmetry and the apparent $U(1)$ symmetry of the complex order parameter (in the disordered phase) are spontaneously broken simultaneously at a single critical point. This is found by observing that the inflection points of magnetization curves for m and m_ϕ coincide asymptotically, in contrast to the curves shown in Fig. 3 for the noncompact case.

The phase diagram for the compact Z_4 model with bond dissipation is shown in Fig. 7. It differs considerably from that

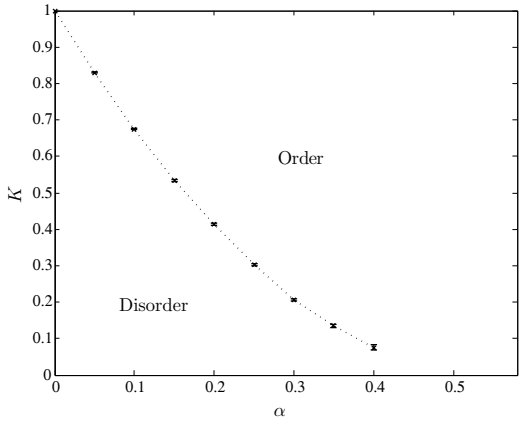

FIG. 7. Phase diagram for the compact model of Eq. (15) with $K_\tau = -\ln(\tanh\frac{1}{2})$, the dotted line indicating a critical line separating the disordered phase from a phase with long-range order. The line is not drawn beyond $\alpha = 0.4$ because of increasing uncertainties.

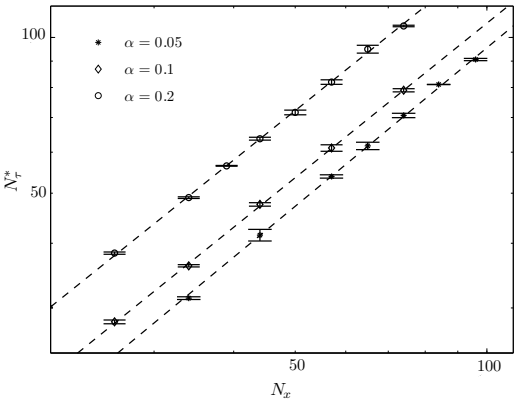

FIG. 8. Finite-size analysis of the maximum N_τ^* of the cumulant curves as a function of spatial system size N_x used to obtain the dynamical critical exponent z for the compact model. The dashed lines show the power-law fits, cf. Table II for the results.

of its noncompact counterpart, not only in the evident absence of any intermediate critical phase, but also in that the limit $\alpha \to 0$ is well behaved. Here, the model is reduced to two uncoupled 2D Ising models, for which exact results are known and simulations are straightforward. In the limit of $K \to 0$ the simulations are on the other hand very difficult for the same reasons as those investigated by us in a similar model in Ref. 3. Therefore, we have not strived to extend the phase diagram all the way down to the α axis in this work. Due to the qualitative difference in the kinetic terms for the compact and noncompact model, it is not possible to make quantitative comparison between the position of the phase transition line in Fig. 7 and the two phase transition lines in Fig. 4.

Turning next to the nature of the critical line in the phase diagram, we show in Fig. 8 and Table II results for the three points along the line for which we made the most effort to extract the dynamical critical exponent. These points are chosen so that the relative influence of the dissipation term should be qualitatively comparable with that for the points $(\alpha_c^{(1)},K)$ chosen for the first transition of the noncompact model. As for the noncompact model here and the Ising model with bond dissipation studied in Ref. 3, there is no significant variation in the dynamical critical exponent from the expected value $z = 1$, although the tendency to greater finite-size effects for increasing α remains for both the compact and the noncompact model.

TABLE II. Critical coupling K_c and dynamical critical exponent z for different values of the dissipation strength α for the compact model.

α	K_c	z
0.05	0.8303(4)	1.02(2)
0.1	0.6753(7)	0.99(2)
0.2	0.414(2)	0.99(2)

VI. DISCUSSION

The models discussed in this paper are in some sense generalizations of the Ising spin system with bond dissipation discussed in Ref. 3. For the compact Z_4 model the modifications come from the increase of the number of states from $q = 2$ to $q = 4$, while one for the noncompact model adds an additional extension of the configuration space. The phase diagram for the compact model is very much like that observed for the dissipative Ising model,[3] both featuring a single order-disorder phase transition line. The noncompact model on the other hand exhibits much richer physics in the sense that it presents, for fixed K and K_τ, two phase transitions surrounding an intermediate critical phase with power-law decaying spin correlations and emergent $U(1)$ symmetry. The most pressing question then pertains to the occurrence of this phase: Why is the discrete structure of the angle variables rendered irrelevant in a region of parameter space for our Z_4 model, when such behavior is previously known to occur only in Z_q models with $q > 4$? Even our compactified model differs from a pure $Z_4 = Z_2 \times Z_2$ clock model, since the dissipation term couples the two underlying Z_2 models in a nontrivial way. Such models can no longer be expected *a priori* to behave as an Ising model, and there is in principle no reason why they may not even present intermediate phases. The absence of such a phase in our compact model does however indicate that we must turn to the other obvious difference between our model and a Z_4 clock model, namely that the variables in our noncompact model are free to drift outside the primary interval. Somehow, this added degree of freedom is enough to close the excitation gap.

As observed in Fig. 4, the underlying Z_4 symmetry stemming from the discreteness of the variables is irrelevant in the intermediate phase. Consequently, the system displays an effective continuous symmetry. Since $z = 1$, the effective long-wavelength low-energy propagator is on a Gaussian form $1/(\omega^2 + q^2)$. In addition, the system is effectively two dimensional due to $z = 1$. In two dimensions, Gaussian fluctuations are sufficient to induce a critical phase given a continuous symmetry. This is analogous to the mechanism producing a critical phase in the classical 2D XY model with an $Z_{q>4}$ anisotropy[12] [soft constraint with underlying $U(1)$ symmetry], and also for classical $Z_{q>4}$ clock models[14] (hard constraint). The difference in our case is that the underlying symmetry is $Z_{q=4}$.

To comment further on the origin of the critical phase, it appears that the quadratic form of the kinetic energy in the problem is essential for observing it. This quadratic short-range interaction term in imaginary time facilitates Gaussian fluctuations. Were we to use a cosine-like form of this term for noncompact variables (as one does for compact variables), this intermediate phase would not be found. The kinetic energy term is bounded from below, but not from above. Upon entering the intermediate phase from the ordered side, this term tends to suppress strong θ fluctuations, much more so than a kinetic term which is bounded from below *and* above, such as a cosine-like term. Only at even lower values of the dissipation are the excitation energies of larger θ fluctuations so low that wild θ fluctuations are possible due to the boundedness of the spatial coupling. At this point, the system disorders completely. If the quadratic kinetic energy term is replaced by a cosine-like term, wild θ fluctuations are facilitated precisely at the critical point where the Z_4 symmetry becomes irrelevant, and the system disorders directly from the Z_4-ordered state. Hence, for a compact model there will only be one phase transition separating the Z_4-ordered state from the completely disordered phase.

We now comment on the critical scaling between space and imaginary time in the models we have studied. For the compact case one has the conventional case of a critical line along which the correlation length diverges as $\xi \sim |K - K_c|^{-\nu}$ in space and $\xi_\tau \sim |K - K_c|^{-z\nu}$ in imaginary time, with z appearing to remain equal to unity along the line. This picture is no longer valid in the noncompact case, as ξ and ξ_τ are formally infinite in the entire intermediate critical phase, and z cannot be defined from the anisotropy of their divergence in this region. Furthermore, supposing that the intermediate phase shares qualities with the corresponding phase in classical $Z_{q>4}$ models, the correlation lengths can be expected to diverge exponentially as this critical phase is approached from either side as for the Kosterlitz-Thouless (KT) transition, and not as a power law as for conventional critical points. However, as long as the correlation length *does* diverge, and this divergence is exponential both in space and imaginary time, the dynamical critical exponent is still well defined through $\xi_\tau \sim \xi^z$. Therefore, our finite size analysis is valid as $\alpha \to \alpha_c^{(1)-}$ and $\alpha \to \alpha_c^{(2)+}$ irrespective of whether these points turns out to possess KT criticality or not. At both phase transitions we have $z = 1$, signaling equally strong divergence of correlation lengths in space and imaginary time.

To infer from simulations on finite systems that the correlation length in fact diverges exponentially is exceedingly difficult,[29–31] and we have not attempted to determine the exact nature of the phase transitions, but leave this an open question. The phase transitions (one or both) may be in the KT universality class, or it may belong to a class of related topological phase transitions.[25] This identification of the exact universality class is controversial even for classical clock models.[24,32,33]

If we generalize the noncompact action in Sec. IV by redefining the phase space such that the variable can take on all real values, Eq. (8) may represent the action for a one-dimensional array of Josephson junctions.[5,6] Recent theoretical work[34,35] report that such systems may display local quantum criticality, in the sense that the spatial coupling renormalizes to zero at the quantum phase transition so that the behavior is essentially $(0 + 1)$ dimensional. This suggests that local quantum criticality need not be restricted to $(2 + 1)$D models such as the one presented in Ref. 8, but that similar unconventional criticality may be found in $(1 + 1)$D as well. Although it should be remembered that our $(1 + 1)$D model has discrete angle variables, our simulations do not show any traces of local critical behavior, in the sense that the scaling of Binder cumulants do not give $z \gg 1$.

Strictly speaking, the dynamical critical exponent is not well defined inside the intermediate phase, and the isotropic behavior is instead maintained by the decay exponents for the power-law spin correlation functions in space and time being equal. Nevertheless, for finite N_x one may still assume the

scaling relation $N_\tau^* = aN_x^z$ and use the ordinary procedure to extract the (effective) exponent z as long as the system is critical, which yields $z \approx 1$ in the entire intermediate phase. We may then inspect how the nonuniversal prefactor a changes as a reflection of the anisotropy of the interaction in time and space. In the noncompact model it is possible to investigate the development of a at constant K_τ/K and varying α without leaving the critical region. We find that a decreases for increasing α, indicating that the dissipation term contributes to making the temporal dimension less ordered than the spatial one. This is also in contrast with a tendency toward $(0+1)$D behavior when increasing the dissipation strength, as suggested in the models mentioned above.

VII. CONCLUSIONS

We have performed Monte Carlo simulations on two distinct Z_4-symmetric dissipative lattice models. In one model the phase variables are only defined on the interval $[0,2\pi\rangle$, while the other model has no restrictions on the variables. The different domains of the variables have implications for the short-range interaction term in imaginary time, which again leads to essential differences in the behavior of the two models. The compact model features only one phase transition in which the Z_4 symmetry is spontaneously broken. On the other hand, the noncompact model displays three phases, namely a disordered phase with exponentially decaying spin correlations, an intermediate critical phase with quasi-long-range order, and finally a long-range ordered phase.

Along the phase-transition line of the compact model, we find the dynamic critical exponent $z = 1$, independent of the dissipation strength. In the noncompact model, we find the value $z = 1$ for both phase transitions and the power-law decay exponents for space and imaginary time are equal in the entire phase exhibiting quasi-long-range order.

We have shown that the issue of compactness versus noncompactness of the fundamental variables of the Z_4 models have important ramifications for their long-distance, low-energy physics.

ACKNOWLEDGMENTS

The authors acknowledge useful discussions with Egil V. Herland, Mats Wallin, and Henrik Enoksen. A.S. was supported by the Norwegian Research Council under Grant No. 167498/V30 (STORFORSK). E.B.S. and I.B.S thank NTNU for financial support. The work was also supported through the Norwegian consortium for high-performance computing (NOTUR).

APPENDIX: QUANTUM-TO-CLASSICAL MAPPING FOR COMPACT AND NONCOMPACT VARIABLES

In this appendix we will outline the quantum-to-classical mapping for a quantum rotor model and show how the kinetic term in the resulting classical model depends on whether the variables are interpreted as compact or noncompact. We will first reproduce the derivation as given in Refs. 36 and 37, for the case of compact variables, after which we will generalize and reinterpret it for the noncompact case. Although there is nothing novel about this derivation, the form of the kinetic term often seems to be taken for granted in the literature, and a correct interpretation of the classical action in the noncompact case is crucial for our results. As a starting point we take the (dissipationless) Hamiltonian $H_0 = T + U$ for a spatially extended system of particles, each moving on a ring. The kinetic energy of the rotors is given by

$$T = -\frac{1}{2I}\sum_x \frac{\partial^2}{\partial\theta_x^2}, \tag{A1}$$

where I is some inertia parameter. The (periodic) potential energy is given by Josephson-like coupling of the rotors,

$$U = -K\sum_x \cos(\hat{\theta}_{x+1} - \hat{\theta}_x), \tag{A2}$$

with K being the coupling strength. Here we have used the angle representation where we for simplicity let θ be a continuous variable, and $\hat{\theta}$ is the corresponding operator. Characteristic of a rotor model is the invariance of the system upon translations of the angle $\theta \to \theta + 2\pi$. The eigenfunctions describing the system should therefore be 2π periodic, a requirement which immediately yields discretized angular momenta and energy levels.

The partition function of the rotor system may be given by

$$\mathcal{Z} = \mathrm{Tr}(\mathrm{e}^{-\beta(T+U)}). \tag{A3}$$

We let $k_B = 1$ such that β equals inverse temperature. The trace may be evaluated by introducing a path integral over M time slices between $\tau = 0$ and $\tau = \beta$, with the width of the time slices given by $\Delta\tau = \beta/M$. For every time step indexed by τ, we insert a complete set of states,

$$\mathcal{Z} \approx \lim_{M\to\infty}\int \mathcal{D}\theta \prod_{\tau=0}^{M-1}\langle\theta(\tau+1)|\mathrm{e}^{-\Delta\tau T}\mathrm{e}^{-\Delta\tau U}|\theta(\tau)\rangle. \tag{A4}$$

Here, $|\theta(\tau)\rangle$ is an angular eigenstate of all rotors with Trotter index τ. Since $|\theta(\tau)\rangle$ is an eigenstate of $\hat{\theta}$ we get

$$\mathrm{e}^{-\Delta\tau U}|\theta(\tau)\rangle = |\theta(\tau)\rangle\mathrm{e}^{K\cos(\theta_{x+1,\tau}-\theta_{x,\tau})}. \tag{A5}$$

A general matrix element describing the kinetic energy is given by

$$T_{x,\tau} = \langle\theta_x(\tau+1)|\mathrm{e}^{-\Delta\tau T}|\theta_x(\tau)\rangle. \tag{A6}$$

Next, for each τ we insert a complete set of eigenstates of the kinetic energy $|n_x(\tau)\rangle$. Because θ and n are conjugate variables, we have the identity $\langle n_x(\tau)|\theta_x(\tau)\rangle = \exp[-in_{x,\tau}\theta_{x,\tau}]$. Inserting this, we get the general form of the matrix element for the kinetic energy

$$T_{x,\tau} = \sum_{n_{x,\tau}} \mathrm{e}^{in_{x,\tau}\theta_{x,\tau+1}}\mathrm{e}^{-in_{x,\tau}\theta_{x,\tau}}\mathrm{e}^{-\frac{1}{2I}\Delta\tau n_{x,\tau}^2}. \tag{A7}$$

Using the Poisson summation formula, we may write the summation over integer-valued angular momenta in Eq. (A7)

as an integral over the continuous field $\tilde{n}$ at the cost of introducing another summation variable m:

$$\begin{aligned} T_{x,\tau} &= \sum_{m=-\infty}^{\infty} \int \mathrm{d}\tilde{n} \mathrm{e}^{\mathrm{i}\tilde{n}(\theta_{x,\tau+1}-\theta_{x,\tau})-\frac{1}{2I}\Delta\tau\tilde{n}^2} \mathrm{e}^{2\pi\mathrm{i}m\tilde{n}} \\ &= \sum_{m=-\infty}^{\infty} \mathcal{C}\mathrm{e}^{-\frac{I}{2\Delta\tau}(\theta_{x,\tau+1}-\theta_{x,\tau}-2\pi m)^2} \\ &\approx \mathcal{C}\mathrm{e}^{K_\tau \cos(\theta_{x,\tau+1}-\theta_{x,\tau})}, \end{aligned} \tag{A8}$$

where $K_\tau = \frac{I}{\Delta\tau}$, and $\mathcal{C} = \sqrt{\frac{2\pi I}{\Delta\tau}}$ is a constant prefactor which is henceforth dropped from the expressions. The last approximation of Eq. (A8) is the Villain approximation of the cosine function, which is known not to alter the universality class of the phase transition.

Reintroducing the matrix elements to the partition function and renaming $\Delta\tau K \to K$, we get

$$Z = \int \mathcal{D}\theta \mathrm{e}^{K_\tau \sum_\tau \sum_x \cos(\theta_{x,\tau+1}-\theta_{x,\tau})} \mathrm{e}^{K \sum_\tau \sum_x \cos(\theta_{x+1,\tau}-\theta_{x,\tau})}, \tag{A9}$$

i.e., an anisotropic XY model in $(1+1)$ dimensions. Note however, that we were able to cast the kinetic energy matrix element into the form of a sequence of Gaussians because the angular momentum eigenvalues where restricted to integer values. This is only the case when the canonical conjugate variable θ is restricted to a $[0,2\pi\rangle$ interval. In other words, the partition function given in Eq. (A9) reflects the interpretation of Eqs. (A1) and (A2) in terms of rotors.

Equations (A1) and (A2) may also describe particles moving in an extended potential, in which case the state of the system after a 2π translation is distinguishable from the state prior to the translation. Introducing dissipation to this system by coupling $\Delta\theta$ to a bosonic bath explicitly breaks the peri odicity of the quantum Hamiltonian, and consequently the variable θ should be treated as an extended variable from the outset. This necessitates a modification of the above procedure as the summation over the eigenstates in Eq. (A7) has to be replaced by an integral over a continuum of momentum states. Then, the kinetic energy matrix element instead becomes

$$\begin{aligned} T_{x,\tau} &= \int \mathrm{d}n_{x,\tau} \mathrm{e}^{\mathrm{i}n_{x,\tau}(\theta_{x,\tau+1}-\theta_{x,\tau})-\frac{1}{2I}\Delta\tau n_{x,\tau}^2} \\ &= \mathrm{e}^{-\frac{I}{2\Delta\tau}(\theta_{x,\tau+1}-\theta_{x,\tau})^2}, \end{aligned} \tag{A10}$$

where a constant factor has been ignored. Inserting this expression into the kinetic part of the partition function yields

$$\begin{aligned} \mathcal{Z}_\tau &= \lim_{M\to\infty} \int \mathcal{D}\theta \mathrm{e}^{-\frac{I}{2}\sum_{\tau=0}^{M-1}\Delta\tau(\frac{\theta_{x,\tau+1}-\theta_{x,\tau}}{\Delta\tau})^2} \\ &\equiv \int \mathcal{D}\theta \mathrm{e}^{-\frac{I}{2}\int_0^\beta \mathrm{d}\tau(\frac{\partial\theta_x}{\partial\tau})^2}. \end{aligned} \tag{A11}$$

The continuum expression for the action is the one conventionally stated in the literature both for compact and noncompact variables. However, it is always implicit that the imaginary time dimension is discrete by construction,[38] and for most numerical computations it has to be treated as such in any case. One then has to choose one of two alternative discretizations of the short-range interaction in the imaginary time direction, depending on the interpretation of the system and the compactness of the variables. As shown above, the cosine-like term of Eq. (2) is the natural discretization for compact variables, whereas the quadratic term used in Eq. (3) is associated naturally to noncompact variables.

[1] A. O. Caldeira and A. J. Leggett, Ann. Phys. (NY) **149**, 374 (1983).
[2] P. Werner, K. Völker, M. Troyer, and S. Chakravarty, Phys. Rev. Lett. **94**, 047201 (2005).
[3] I. B. Sperstad, E. B. Stiansen, and A. Sudbø, Phys. Rev. B **81**, 104302 (2010).
[4] J. A. Hertz, Phys. Rev. B **14**, 1165 (1976).
[5] S. Chakravarty, G.-L. Ingold, S. Kivelson, and A. Luther, Phys. Rev. Lett. **56**, 2303 (1986).
[6] S. Chakravarty, G.-L. Ingold, S. Kivelson, and G. Zimanyi, Phys. Rev. B **37**, 3283 (1988).
[7] G. Schön and A. D. Zaikin, Phys. Rep. **198**, 237 (1990).
[8] V. Aji and C. M. Varma, Phys. Rev. Lett. **99**, 067003 (2007).
[9] V. Aji and C. M. Varma, Phys. Rev. B **79**, 184501 (2009).
[10] K. Børkje and A. Sudbø, Phys. Rev. B **77**, 092404 (2008).
[11] M. S. Grønsleth, T. B. Nilssen, E. K. Dahl, E. B. Stiansen, C. M. Varma, and A. Sudbø, Phys. Rev. B **79**, 094506 (2009).
[12] J. V. José, L. P. Kadanoff, S. Kirkpatrick, and D. R. Nelson, Phys. Rev. B **16**, 1217 (1977).
[13] H. H. Roomany and H. W. Wyld, Phys. Rev. B **23**, 1357 (1981).
[14] S. Elitzur, R. B. Pearson, and J. Shigemitsu, Phys. Rev. D **19**, 3698 (1979).
[15] E. Luijten and H. Blöte, Int. J. Mod. Phys. C **6**, 359 (1995).
[16] U. Wolff, Phys. Rev. Lett. **62**, 361 (1989).
[17] P. Werner and M. Troyer, Phys. Rev. Lett. **95**, 060201 (2005).
[18] P. Werner, G. Refael, and M. Troyer, J. Stat. Mech.: Theory Exp. (2005) P12003.
[19] P. Werner and M. Troyer, Prog. Theor. Phys. Suppl. **160**, 395 (2005).
[20] K. Hukushima and K. Nemoto, J. Phys. Soc. Jpn. **65**, 1604 (1996).
[21] H. G. Katzgraber, Modern Computation Science, Oldenburg, Germany, 16-28 August 2009, (unpublished).
[22] M. Matsumoto and T. Nishimura, ACM Trans. Model. Comput. Simul. **8**, 3 (1998).
[23] A. M. Ferrenberg and R. H. Swendsen, Phys. Rev. Lett. **63**, 1195 (1989).
[24] C. M. Lapilli, P. Pfeifer, and C. Wexler, Phys. Rev. Lett. **96**, 140603 (2006).
[25] S. K. Baek and P. Minnhagen, Phys. Rev. E **82**, 031102 (2010).
[26] S. K. Baek, P. Minnhagen, and B. J. Kim, Phys. Rev. E **80**, 060101(R) (2009).
[27] J. Lou, A. W. Sandvik, and L. Balents, Phys. Rev. Lett. **99**, 207203 (2007).
[28] J. Hove and A. Sudbø, Phys. Rev. E **68**, 046107 (2003).
[29] D. Loison, J. Phys.: Condens. Matter **11**, L401 (1999).

[30]E. Luijten and H. Meßingfeld, Phys. Rev. Lett. **86**, 5305 (2001).
[31]M. Itakura, J. Phys. Soc. Jpn. **70**, 600 (2001).
[32]C.-O. Hwang, Phys. Rev. E **80**, 042103 (2009).
[33]S. K. Baek, P. Minnhagen, and B. J. Kim, Phys. Rev. E **81**, 063101 (2010).
[34]S. Tewari, J. Toner, and S. Chakravarty, Phys. Rev. B **72**, 060505(R) (2005).
[35]S. Tewari, J. Toner, and S. Chakravarty, Phys. Rev. B **73**, 064503 (2006).
[36]M. Wallin, E. S. Sørensen, S. M. Girvin, and A. P. Young, Phys. Rev. B **49**, 12115 (1994).
[37]S. L. Sondhi, S. M. Girvin, J. P. Carini, and D. Shahar, Rev. Mod. Phys. **69**, 315 (1997).
[38]J. W. Negele and H. Orland, *Quantum Many-Particle Systems* (Perseus Books, Reading, MA 1998).

Paper IV

Quantum criticality in a dissipative (2+1)-dimensional XY model of circulating currents in high-T_c cuprates

Physical Review B **84**, 180503(R) (2011)

RAPID COMMUNICATIONS

PHYSICAL REVIEW B **84**, 180503(R) (2011)

Quantum criticality in a dissipative (2+1)-dimensional XY model of circulating currents in high-T_c cuprates

Iver Bakken Sperstad, Einar B. Stiansen, and Asle Sudbø

Department of Physics, Norwegian University of Science and Technology, N-7491 Trondheim, Norway

(Received 20 September 2011; revised manuscript received 14 October 2011; published 8 November 2011)

We present large-scale Monte Carlo results for the dynamical critical exponent z and the spatio-temporal two-point correlation function of a (2+1)-dimensional quantum XY model with bond dissipation, proposed to describe a quantum critical point in high-T_c cuprates near optimal doping. The phase variables of the model, originating with a parametrization of circulating currents within the CuO_2 unit cells in cuprates, are compact, $\{\theta_{\mathbf{r},\tau}\} \in [-\pi,\pi\rangle$. The dynamical critical exponent is found to be $z \approx 1$, and the spatio-temporal correlation functions are explicitly demonstrated to be isotropic in space-imaginary time. The model thus has a fluctuation spectrum where momentum and frequency enter on equal footing, rather than having the essentially momentum-independent marginal Fermi-liquid-like fluctuation spectrum previously reported for the same model.

DOI: 10.1103/PhysRevB.84.180503 PACS number(s): 74.72.Kf, 74.20.Mn, 74.40.Kb, 71.10.Hf

Quantum critical points describe systems with diverging length scales at zero temperature, and have come into much focus in recent years as possible descriptions of anomalous phenomena in strongly correlated fermion systems and systems with competing orders.[1] One prime example of this is represented by the high-T_c superconducting cuprates, where various types of quantum critical phenomena have been proposed as essential for understanding the many unusual normal-state transport properties these systems exhibit. This has, over the past quarter of a century, represented one of the major challenges in condensed-matter physics.[2]

One successful phenomenological framework is to describe the the normal phase around optimal doping as a marginal Fermi liquid (MFL),[3] the weakest possible violation of having a nonzero quasiparticle residue at the Fermi surface. Among the merits of the MFL phenomenology is that it describes transport properties in this strange metallic phase in good accordance with experiments. This follows naturally from the essentially momentum-independent, linear-in-frequency, fluctuation spectrum of the MFL hypothesis.[3]

More recent works have pursued a more microscopic foundation of MFL. The underlying picture is that there exists a quantum critical point (QCP) residing at $T = 0$ beneath the superconducting dome.[4] The degrees of freedom associated with this QCP are circulating currents within the unit cells of the CuO_2 layers. The main idea is that the MFL phenomenology arises from the quantum critical fluctuations of these currents above the QCP at $T > T_c$. It has also been demonstrated how the same fluctuations may give rise to d-wave high-T_c superconductivity.[5] The ordering of such circulating currents upon lowering the temperature from the strange metal region into the pseudogap region is a candidate for a possible competing order in this part of the phase diagram.[6] Magnetic order conforming with such circulating currents has in fact been observed in several experiments.[7–11] It must be mentioned that others argue that such signatures may have a quite different origin,[12–15] and also numerical results disagree on the presence of such circulating currents,[16–18] but the model remains one of the central theories of the physics of high-T_c cuprates.[2,19]

A remarkable implication of a q-independent fluctuation spectrum, such as that posited in MFL theory, is that the associated QCP exhibits *local* quantum criticality (LQC). Defining the dynamical critical exponent z from the scaling of momentum and frequency at the quantum critical point, $\omega \sim q^z$, this means that, formally, $z = \infty$. It is a highly nontrivial question as to how such a remarkable property of a quantum critical point can arise in an extended system. Recently, it was argued[20,21] that precisely such local criticality is found in a (2+1)-dimensional quantum XY model with bond dissipation of the Caldeira-Leggett[22] form. The angle variables of this model were associated with circulating current degrees of freedom, as will be explained below.

The results of Ref. 20 would imply that the previously hypothesized MFL fluctuation spectrum has been derived from a microscopic theory applicable to cuprates. In a broader perspective, it is of considerable interest to investigate in detail if such unusual behavior can occur in model systems of condensed matter, as related variants of locality have also been considered in the context of gauge/gravity duality[23] and QCPs in disordered systems and heavy fermion compounds.[1]

From naive scaling arguments[24,25] applied to the dissipative model proposed in Ref. 20, one might expect that dissipation is irrelevant in the renormalization group sense. The result would then not be LQC, but instead conventional quantum criticality with isotropic scaling $z = 1$. Here, we report results from Monte Carlo simulations performed directly on the (2+1)-dimensional quantum XY model with bond dissipation and compact angle variables, considered in Ref. 20. Our results strongly indicate that in this model $z = 1$.

The dissipative (2+1)-dimensional [(2+1)D] XY action considered in Ref. 20 takes the form

$$\begin{aligned} S = &-K \sum_{\langle \mathbf{r},\mathbf{r}'\rangle} \sum_{\tau=1}^{L_\tau} \cos(\Delta\theta_{\mathbf{r},\mathbf{r}',\tau}) \\ &-K_\tau \sum_{\mathbf{r}} \sum_{\tau=1}^{L_\tau} \cos(\theta_{\mathbf{r},\tau+1} - \theta_{\mathbf{r},\tau}) \\ &+\frac{\alpha}{2} \sum_{\langle \mathbf{r},\mathbf{r}'\rangle} \sum_{\tau\neq\tau'}^{L_\tau} \left(\frac{\pi}{L_\tau}\right)^2 \frac{(\Delta\theta_{\mathbf{r},\mathbf{r}',\tau} - \Delta\theta_{\mathbf{r},\mathbf{r}',\tau'})^2}{\sin^2\left(\frac{\pi}{L_\tau}|\tau-\tau'|\right)} \end{aligned} \quad (1)$$

when put on a cubic $L \times L \times L_\tau$ lattice. The bond variables are given by $\Delta\theta_{\mathbf{r},\mathbf{r}',\tau} = \theta_{\mathbf{r},\tau} - \theta_{\mathbf{r}',\tau}$, where the sum over $\mathbf{r}$ and $\mathbf{r}'$

goes over nearest neighbors in the x-y plane. Periodic boundary conditions are implicit in the imaginary time direction, and are also applied in the spatial directions.

Such a model has previously been employed as an effective description of a resistively shunted Josephson junction array,[26] and it may also be viewed as a generic quantum rotor model with dissipative currents. A third possible interpretation in the context of high-T_c cuprates is as follows. Suppose the angles θ *a priori* can take only four possible values. These four values then represent the directions of a pseudospin associated with the four possible ordered circulating current patterns within each CuO_2 unit cell (see, e.g., Fig. 1 of Ref. 27). The first two terms represent the standard interaction energies in space-imaginary time of these circulating currents in neighboring unit cells, and have been derived from microscopics.[27] The last term is the term responsible for dissipating the ordered circulating currents.[20]

In Eq. (1), the angles are continuous variables. We will discuss a possible *a posteriori* justification for this later in this Rapid Communication by showing that an added fourfold anisotropy term is perturbatively irrelevant. Reference 20, moreover, appears to treat $\theta_{\mathbf{r},\tau}$ as compact variables, also in the presence of a dissipation term that apparently renders the action nonperiodic in the angle variables.[28] In order to investigate numerically the same model considered in Ref. 20, we therefore *compactify* the expression $\Delta\theta_{\mathbf{r},\mathbf{r}',\tau} - \Delta\theta_{\mathbf{r},\mathbf{r}',\tau'}$ so that it is defined modulo 2π. We will discuss alternative choices later.

The calculations of Ref. 20 were not restricted to any specific parameter regime, but predicted that every point on the $T = 0$ quantum critical surface in $\alpha - K - K_\tau$ (parameter) space (for $\alpha > 0$) should be a local QCP. Accordingly, we choose convenient coupling constants when searching for LQC in our simulations, and for the results presented here, the dissipation strength is fixed at $\alpha = 0.05$.

The phase diagram (not shown) is qualitatively very similar to those found for related compact (1+1)D models with bond dissipation.[25,29] It features a single critical surface that separates a disordered from a fully ordered phase, and which is continuously connected to the 3D XY critical line at $\alpha = 0$. For similar models in (1+1) dimensions, only the region of relatively moderate dissipation was accessible to simulations, as increasing α increases finite-size effects, resulting in apparent values $z < 1$ for the dynamical critical exponent. As expected, this problem is no less severe in (2+1) dimensions. Available system sizes are restricted by the absence of cluster algorithms to treat models with bond dissipation appropriately,[25] and we are therefore confined to local Metropolis updates.

To locate the phase transition, we vary the spatial coupling K and use the crossing point for different system sizes L of the Binder cumulant $g = 1 - \langle|m|^4\rangle/(2\langle|m|^2\rangle^2)$. Here, $m = \sum_{\mathbf{r},\tau} \exp[\mathrm{i}\theta_{\mathbf{r},\tau}]$ is the order parameter of the $U(1)$-symmetric degrees of freedom. Due to the anisotropy of the interactions, we have to calculate g for multiple values of L_τ for each spatial system size L, as described in more detail, e.g., in Ref. 25. The value $L_\tau = L_\tau^*$ where the function $g(L_\tau)$ reaches its maximum corresponds to the *optimal* temporal extent for which the system appears as isotropic as it can be, the anisotropic interactions taken into account.

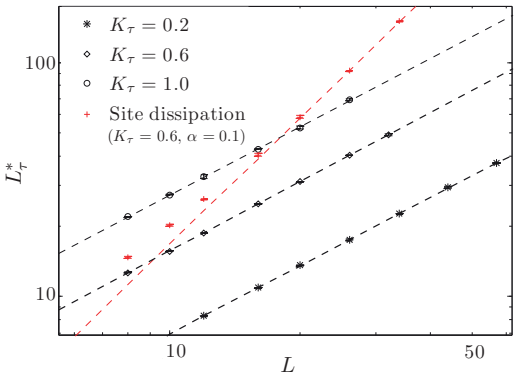

FIG. 1. (Color online) Finite-size analysis of the maximum L_τ^* of the Binder cumulant curves $g(L_\tau)$ as a function of spatial system size L. For the black data points, the dynamical critical exponents z as given in Table I are obtained from the slope of the fitting lines (dashed). The red (gray) points show similar results for site dissipation for comparison, where a fit of the three largest systems yields $z = 1.84(3)$.

For a conventional QCP, at which the correlation length ξ_τ in imaginary time scales with the correlation length ξ in space as $\xi_\tau \sim \xi^z$ with a finite z, we expect to observe the scaling relation $L_\tau^* \sim L^z$. This scaling procedure then allows one to extract the dynamical critical exponent z from Binder cumulant data. For a local QCP formally having $z = \infty$, we expect this scaling to break down. Our strategy to search for possible LQC in the model (1) is therefore to perform the above procedure *assuming* conventional criticality, and then look for indications that this hypothesis should be rejected.

The results of this finite-size analysis is shown in Fig. 1, with the values of the dynamical critical exponent z given in Table I. Here, we have chosen three different values of the quantum coupling K_τ in order to investigate both the limit of relatively weak quantum coupling and the opposite limit leading to relatively strong system anisotropy.

The results show that the effective dynamical critical exponent is $z \lesssim 1$ for all the parameter sets considered, and we expect that we could obtain $z \approx 1$ if we were able to reach higher values of L. (For a smaller value $\alpha = 0.02$, we obtained $z = 1$ within statistical uncertainty.) It is conceivable that signatures of LQC would be visible only for systems larger than the admittedly moderate system sizes accessible to present algorithms. However, were that the case, the true

TABLE I. Critical coupling K_c and dynamical critical exponent z for different values of the quantum coupling K_τ, but for the same dissipation strength $\alpha = 0.05$. Uncertainty estimates for z have been calculated by a bootstrap procedure, including the uncertainty in K_c.

K_τ	K_c	z
0.2	0.48068(5)	0.968(8)
0.6	0.28244(4)	0.985(8)
1.0	0.18008(5)	0.970(11)

$z \to \infty$ nature of the model would likely reveal itself as strongly increasing effective values of z as a finite-size effect for increasing L. For comparison, we have also carried out simulations with equivalent parameters of a (2+1)D XY model with *site* dissipation, for which $z = 2$ is expected.[25,30] The results are included in Fig. 1, and already for system sizes comparable to those for bond dissipation, we observe (finite-size) crossover behavior with $z \to 2$. For bond dissipation, we observe no tendency toward $z > 1$ for either of the parameter sets, and it is hard to imagine how crossover to $z \to \infty$ scaling should be much slower than crossover to $z = 2$ scaling.

For all results reported here, we have used parallel tempering[31] to reduce autocorrelation times, and to ensure that the simulations are well equilibrated. To emulate the continuous $U(1)$ symmetry, the simulations are made for Z_q clock models, with $q = 128$ for $K_\tau = 0.2, 1.0$, and $q = 32$ for $K_\tau = 0.6$. The nature of the criticality remains unchanged also when increasing to $q = 1024$. The results are obtained using an implementation of the Mersenne Twister[32] random number generator, but other random number generators produced consistent results.

Although we found no indication of LQC from the scaling of the Binder cumulant, we also considered the correlations of the order parameter field directly

$$C(\mathbf{r} - \mathbf{r}', \tau - \tau') = \langle e^{i\theta_{\mathbf{r},\tau}} e^{-i\theta_{\mathbf{r}',\tau'}} \rangle. \tag{2}$$

The correlation functions presented here are obtained for the parameter set $K_\tau = 0.6$, with $L_\tau = L_\tau^*$ and $K = K_c$ as obtained from the previous simulations, and therefore serve as a self-consistency check of the Binder scaling procedure. From Fig. 2, it is evident that the correlation function at the critical point decays isotropically in space-imaginary time. In other words, there are no signs of locality.

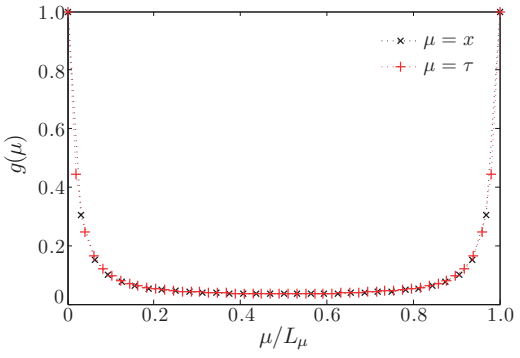

FIG. 2. (Color online) Correlation functions at the critical point $K_c = 0.282\,44$ for dissipation strength $\alpha = 0.05$ and quantum coupling $K_\tau = 0.6$. The system size $L = 32$, $L_\tau = 49 \approx L_\tau^*$ corresponds to the rightmost data point of the midmost data series in Fig. 1. The correlation function is defined in the spatial direction as $g(x) = g(|\mathbf{r} - \mathbf{r}'|) = C(\mathbf{r} - \mathbf{r}', 0)$ and in the temporal direction as $g(\tau) = C(\mathbf{0}, \tau)$, with C defined in Eq. (2). Also, $L_x \equiv L$. Error bars are smaller than the linewidth, and the dotted lines are guides to the eye.

Furthermore, we have verified that the same conclusion may be drawn for the other values of K_τ considered, and also for larger system sizes with aspect ratios found from extrapolation based on the power law shown in Fig. 1. As an additional test, we compared the correlation functions shown here with those obtained by setting $\alpha = 0$ in Eq. (1). Letting $K_\tau > K$, values of L_τ and K_c were determined by the same procedure as for the dissipative model. There is no indication that adding dissipation changes the scaling of the temporal correlation length ξ_τ with respect to the spatial correlation length ξ.

Depending on how $\Delta\theta_{\mathbf{r},\mathbf{r}',\tau}$ is interpreted in the dissipation term, it may be argued either that the correct treatment is to compactify only the gradients $\Delta\theta_{\mathbf{r},\mathbf{r}',\tau}$, restricting them to the interval $[-\pi, \pi\rangle$, or to do so to the difference $\Delta\theta_{\mathbf{r},\mathbf{r}',\tau} - \Delta\theta_{\mathbf{r},\mathbf{r}',\tau'}$ as well. Although we have chosen the latter, as in Ref. 29, we also performed simulations with the former compactification scheme. The results are qualitatively similar, with the difference merely amounting to a renormalization of the dissipative coupling α. In other words, the absence of LQC in this model is not contingent on the choice of compactification scheme.

As explained in connection with Eq. (1), the underlying circulating current degrees of freedom are most naturally described by discrete, Z_4-symmetric variables. In Ref. 21, it was argued that a model with continuous $U(1)$ symmetry nonetheless would be a correct description. The result of LQC would then also apply to the four-state model of the original degrees of freedom since a fourfold anisotropy field, given by

$$S_4 = h_4 \sum_{\mathbf{r},\tau} \cos(4\theta_{\mathbf{r},\tau}), \tag{3}$$

would be irrelevant at the critical point of the action (1). We have investigated the effect of a fourfold anisotropy in our simulations by including the term (3) in the action. Using the approach of Ref. 33, we find the same result for the dissipative (2+1)D XY model as reported there for the classical 3D XY model, namely, that the h_4 term is perturbatively irrelevant.

The soft constraint represented by a (finite) anisotropy term is not obviously the same as the hard constraint constituted by the discrete Z_4 variables of the original model (the limit $h_4 = \infty$). We may only speculate whether a putative LQC fixed point for a $U(1)$ theory might survive in the limit $h_4 \to \infty$, but note that our simulations showed no signs of locality neither when enforcing a soft nor a strong Z_4 constraint on the variables.[34]

Finally, we briefly consider variants of LQC other than that of Ref. 21, which predicts a strictly infinite z for $\xi_\tau \sim \xi^z$ so that ξ is strictly vanishing at criticality. Another conceivable sense in which $z \to \infty$ is by activated dynamical scaling,[35] i.e., scaling on the form $\ln \xi_\tau \sim \xi^\psi$. In this case, as we expect also in the first case, locality would manifest itself in our simulations as a strongly increasing value of $z > 1$ as the thermodynamical limit was approached. This is not observed in our results. We have also verified explicitly, by an appropriate modification of the scaling,[35] that our results are not consistent with activated dynamical scaling.

In conclusion, we find no signs of local quantum criticality in the compact (2+1)D XY model with bond dissipation, but instead conventional quantum criticality with indications of

isotropic scaling of imaginary time and space. This implies that the fluctuation spectrum of the model is a function of the combination $\sqrt{q^2+\omega^2}$, rather than being dependent only on the frequency ω, but not on the momentum q (which would be a hallmark of local quantum criticality). Our results therefore differ in a fundamental way from those obtained from the same model in Ref. 20.

The authors acknowledge useful discussions with Egil V. Herland, Chandra M. Varma, and Vivek Aji. A.S. was supported by the Norwegian Research Council under Grant No. 205591/V30 (FRINAT). E.B.S. and I.B.S thank NTNU for financial support. The work was also supported through the Norwegian consortium for high-performance computing (NOTUR).

[1] H. v. Löhneysen, A. Rosch, M. Vojta, and P. Wölfle, Rev. Mod. Phys. **79**, 1015 (2007).

[2] J. Zaanen, in *100 Years of Superconductivity*, edited by H. Rogalla and P. H. Kes (Taylor & Francis, London, 2011) (in press) (e-print arXiv:1012.5461).

[3] C. M. Varma, P. B. Littlewood, S. Schmitt-Rink, E. Abrahams, and A. E. Ruckenstein, Phys. Rev. Lett. **63**, 1996 (1989).

[4] C. M. Varma, Phys. Rev. B **55**, 14554 (1997).

[5] V. Aji, A. Shekhter, and C. M. Varma, Phys. Rev. B **81**, 064515 (2010).

[6] C. M. Varma, Phys. Rev. B **73**, 155113 (2006).

[7] B. Fauqué, Y. Sidis, V. Hinkov, S. Pailhès, C. T. Lin, X. Chaud, and P. Bourges, Phys. Rev. Lett. **96**, 197001 (2006).

[8] A. Kaminski, S. Rosenkranz, H. M. Fretwell, J. C. Campuzano, H. R. Z. Li, W. G. Cullen, H. You, C. G. Olson, C. M. Varma, and H. Höchst, Nature (London) **416**, 610 (2002).

[9] Y. Li, V. Balédent, G. Yu, N. Barišić, K. Hradil, R. A. Mole, Y. Sidis, P. Steffens, X. Zhao, P. Bourges, and M. Greven, Nature (London) **468**, 283 (2010).

[10] Y. Li, V. Balédent, N. Barišić, Y. Cho, B. Fauqué, Y. Sidis, G. Yu, X. Zhao, P. Bourges, and M. Greven, Nature (London) **455**, 372 (2008).

[11] V. Balédent, B. Fauqué, Y. Sidis, N. B. Christensen, S. Pailhès, K. Conder, E. Pomjakushina, J. Mesot, and P. Bourges, Phys. Rev. Lett. **105**, 027004 (2010).

[12] J. E. Sonier, V. Pacradouni, S. A. Sabok-Sayr, W. N. Hardy, D. A. Bonn, R. Liang, and H. A. Mook, Phys. Rev. Lett. **103**, 167002 (2009).

[13] S. Strässle, B. Graneli, M. Mali, J. Roos, and H. Keller, Phys. Rev. Lett. **106**, 097003 (2011).

[14] S. V. Borisenko, A. A. Kordyuk, A. Koitzsch, T. K. Kim, K. A. Nenkov, M. Knupfer, J. Fink, C. Grazioli, S. Turchini, and H. Berger, Phys. Rev. Lett. **92**, 207001 (2004).

[15] G. J. MacDougall, A. A. Aczel, J. P. Carlo, T. Ito, J. Rodriguez, P. L. Russo, Y. J. Uemura, S. Wakimoto, and G. M. Luke, Phys. Rev. Lett. **101**, 017001 (2008).

[16] M. Greiter and R. Thomale, Phys. Rev. Lett. **99**, 027005 (2007).

[17] S. Nishimoto, E. Jeckelmann, and D. J. Scalapino, Phys. Rev. B **79**, 205115 (2009).

[18] C. Weber, A. Läuchli, F. Mila, and T. Giamarchi, Phys. Rev. Lett. **102**, 017005 (2009).

[19] M. Vojta, Adv. Phys. **58**, 699 (2009).

[20] V. Aji and C. M. Varma, Phys. Rev. Lett. **99**, 067003 (2007).

[21] V. Aji and C. M. Varma, Phys. Rev. B **79**, 184501 (2009).

[22] A. O. Caldeira and A. J. Leggett, Ann. Phys. (NY) **149**, 374 (1983).

[23] T. Faulkner, N. Iqbal, H. Liu, J. McGreevy, and D. Vegh, Science **329**, 1043 (2010).

[24] J. A. Hertz, Phys. Rev. B **14**, 1165 (1976).

[25] I. B. Sperstad, E. B. Stiansen, and A. Sudbø, Phys. Rev. B **81**, 104302 (2010).

[26] S. Chakravarty, G.-L. Ingold, S. Kivelson, and A. Luther, Phys. Rev. Lett. **56**, 2303 (1986).

[27] K. Børkje and A. Sudbø, Phys. Rev. B **77**, 092404 (2008).

[28] G. Schön and A. D. Zaikin, Phys. Rep. **198**, 237 (1990).

[29] E. B. Stiansen, I. B. Sperstad, and A. Sudbø, Phys. Rev. B **83**, 115134 (2011).

[30] P. Werner, M. Troyer, and S. Sachdev, J. Phys. Soc. Jpn. Suppl. **74**, 67 (2005).

[31] K. Hukushima and K. Nemoto, J. Phys. Soc. Jpn. **65**, 1604 (1996).

[32] M. Matsumoto and T. Nishimura, ACM Trans. Model. Comput. Simul. **8**, 3 (1998).

[33] M. Caselle and M. Hasenbusch, J. Phys. A **31**, 4603 (1998).

[34] Here, we focused on the *perturbative* relevance of h_4. A substantial $h_4 > 1$ does seem to change the nature of the phase transition. The observation of diverging Binder cumulants $g \to -\infty$ points to a first-order phase transition both for the strongly anisotropic XY case and for the Z_4 case.

[35] T. Vojta, Rev. Comput. Chem. **26**, 167 (2008).

Paper V

Three distinct types of quantum phase transitions in a (2+1)-dimensional array of dissipative Josephson junctions

Physical Review B **85**, 224531 (2012)

PHYSICAL REVIEW B **85**, 224531 (2012)

Three distinct types of quantum phase transitions in a $(2+1)$-dimensional array of dissipative Josephson junctions

Einar B. Stiansen, Iver Bakken Sperstad, and Asle Sudbø
Department of Physics, Norwegian University of Science and Technology, N-7491 Trondheim, Norway
(Received 22 December 2011; revised manuscript received 11 April 2012; published 25 June 2012)

We have performed large-scale Monte Carlo simulations on a model describing a $(2+1)$-dimensional array of dissipative Josephson junctions. We find three distinct stable quantum phases of the system. The most ordered state features long-range spatial ordering in the phase θ of the superconducting order parameter, but temporal ordering only in spatial gradients $\Delta\theta$, not in θ. Significantly, the most ordered state therefore does not have three-dimensional (3D) XY ordering. Rather, it features two-dimensional (2D) spin waves coexisting with temporally disordered phases θ. There is also an intermediate phase featuring quasi-long-range spatial order in θ coexisting with a gas of instantons in $\Delta\theta$. We briefly discuss possible experimental signatures of such a state, which may be viewed as a local metal and a global superconductor. The most disordered state has phase disorder in all spatio-temporal directions, and may be characterized as a gas of proliferated vortices coexisting with a gas of $\Delta\theta$ instantons. The phase transitions between these phases are discussed. The transition from the most ordered state to the intermediate state is driven by proliferation of instantons in $\Delta\theta$. The transition from the intermediate state to the most disordered state is driven by the proliferation of spatial point vortices in the background of a proliferated $\Delta\theta$-instanton gas, and constitutes a Berezinskii-Kosterlitz-Thouless phase transition. The model also features a direct phase transition from the most ordered state to the most disordered state, and this transition is neither in the 2D XY nor in the 3D XY universality class. It comes about via a simultaneous proliferation of point vortices in two spatial dimensions and $\Delta\theta$ instantons, with a complicated interplay between them. The results are compared to, and differ in a fundamental way from, the results that are found in dissipative quantum rotor systems. The difference originates with the difference in the values that the fundamental degrees of freedom can take in the latter systems compared to dissipative Josephson junction arrays.

DOI: 10.1103/PhysRevB.85.224531 PACS number(s): 74.81.Fa, 05.30.Rt, 74.40.Kb, 74.50.+r

I. INTRODUCTION

In general, dissipation suppresses quantum fluctuations and may support states of spontaneously broken symmetry. A remarkable consequence of this is the dissipation-driven quantum phase transition in a single resistively shunted Josephson junction in which the phase difference is localized in a minimum of the periodic Josephson potential.[1] In the parameter space of Josephson coupling and dissipation strength, this corresponds physically to a phase diagram with one metallic phase and one superconducting phase. While the behavior of a single dissipative Josephson junction is theoretically well understood, the picture is less complete for spatially extended systems. Other than the fully disordered phase and the fully ordered phase expected from the single-junction system, the phase diagram of arrays of dissipative Josephson junctions is conjectured to host additional phases in both one[2–7] and two[2,8,9] dimensions. These new, exotic phases can broadly be characterized by having various combinations of global and/or local phase fluctuations or order.

Most of the analytical works on similar models have been based on mean-field analyses or perturbative renormalization group arguments. Since these approaches are valid in a limited region of the parameter space, in particular regions far away from phase transitions, a nonperturbative approach is of importance. Previous numerical work on models of dissipative Josephson junctions has mostly focused on lower-dimensional systems. The first Monte Carlo simulation of a single dissipative Josephson junction was presented in Ref. 10, where a fluctuation measure of the imaginary-time path of the phase difference was introduced to characterize the localization transition. Improved and extended results for the same model were later reported in Ref. 11. For one spatial dimension, Ref. 12 reported four physically distinct phases for a dissipative Josephson junction chain. This simulation was performed on a dual model and not directly on the phase degrees of freedom. A model for a $(2+1)$-dimensional [$(2+1)$D] dissipative Josephson junction array (JJA) has been treated numerically by Ref. 13. In essence, their results support the simplest scenario for a zero-temperature phase diagram,[14,15] with one phase with and another without spatio-temporal order. This is also what was found in a large-scale Monte Carlo simulation on the dissipative $(2+1)$D XY quantum rotor model.[16]

Finally, our investigations are also motivated by a rather different physical system which can be described by a closely related model. In Ref. 17, a quantum XY model with bond dissipation in two spatial dimensions was used to describe quantum critical fluctuations in cuprate high-T_c superconductors. The principal result of analytical work on this model is that the dissipation-driven quantum critical point is local, in the sense that the fluctuation spectrum is frequency dependent but momentum independent.[17] Although the physical system we have in mind primarily is that of a Josephson junction array, we return to a discussion of the possibilities of local quantum criticality later in the paper.[18]

The purpose of this paper is to numerically investigate the phase diagram of a specific model of a $(2+1)$-dimensional dissipative Josephson junction array. We pay special attention to the manifest anisotropy that exists between the spatial and temporal dimensions. To be specific, the fluctuations of the quantum paths of the phase gradients will be explicitly

characterized in terms of roughening transitions, allowing us to consider the (temporal) localization transition separately from the onset of (spatial) phase coherence. In particular, we will identify a partially superconducting phase with spatial, but no temporal phase coherence. This corresponds to a dissipative JJA which may sustain a nonzero Josephson current, but where one nonetheless has voltage fluctuations over each junction. We investigate two phase transitions where the spatio-temporal aspects are well separated and can be characterized in terms of either a spatial vortex-antivortex unbinding, or proliferation of instantonlike defects. We also discuss a direct quantum phase transition from an ordered state to a disordered state involving simultaneous disordering in space and imaginary time. This corresponds to a quantum phase transition on a dissipative JJA where one transitions from a state sustaining a Josephson current and allowing no voltage fluctuations to a normal state, but via an unusual quantum phase transition that is neither in the two-dimensional (2D) XY nor three-dimensional (3D) XY universality class.

A. Model

An array of Josephson junctions consists of superconducting islands arranged in a regular network. Separating the islands are tunnel junctions in which Cooper pairs are able to tunnel from one superconducting grain to the neighboring grain. The fundamental degrees of freedom are the phases of the superconducting order parameters residing on the grains. A classical two-dimensional JJA is described by the 2D XY model,

$$H = -K \sum_{\langle \mathbf{x},\mathbf{x}' \rangle} \cos(\theta_{\mathbf{x}} - \theta_{\mathbf{x}'}), \tag{1}$$

where the summation goes over nearest neighboring sites on a square lattice. $\theta_{\mathbf{x}}$ is the phase of the complex order parameter of the superconducting grain at position $\mathbf{x}$. Although the $U(1)$ symmetry of the phase variables cannot be spontaneously broken in two dimensions at any nonzero temperature (implicit in the classical description), the system nevertheless undergoes a Berezinskii-Kosterlitz-Thouless (BKT) transition in which it develops quasi-long-range order (QLRO) with power-law-decaying correlation functions in the low-temperature regime. The low-temperature phase corresponds to a dipole phase where the vortices and antivortices of the phase field are bound in pairs. At the transition the vortices proliferate and destroy the QLRO. For a given phase configuration, a single vortex is identified on a plaquette by a nontrivial line integral of the phase difference around the plaquette, taking the compactness of the phase field into account.

The quantum generalized version of the model includes two additional terms describing quantum fluctuations in imaginary time τ. The action reads[3,12,13,15,17,19,20]

$$S = \frac{1}{2E_C} \sum_{\mathbf{x}} \int_0^\beta d\tau \left(\frac{\partial \theta_{\mathbf{x},\tau}}{\partial \tau} \right)^2 - K \sum_{\langle \mathbf{x},\mathbf{x}' \rangle} \int_0^\beta d\tau \cos(\Delta\theta_{\mathbf{x},\mathbf{x}',\tau}) + \frac{\alpha}{2} \sum_{\langle \mathbf{x},\mathbf{x}' \rangle} \int_0^\beta \int_0^\beta d\tau d\tau' \left(\frac{\pi}{\beta} \right)^2 \frac{(\Delta\theta_{\mathbf{x},\mathbf{x}',\tau} - \Delta\theta_{\mathbf{x},\mathbf{x}',\tau'})^2}{\sin^2\left(\frac{\pi}{\beta}|\tau - \tau'|\right)}, \tag{2}$$

where we have defined the lattice gradient $\Delta\theta_{\mathbf{x},\mathbf{x}',\tau} = \theta_{\mathbf{x},\tau} - \theta_{\mathbf{x}',\tau}$. The first term describes the self-capacitance of a single island; the second term is the familiar Josephson interaction, coupling each superconducting island to the nearest neighbors by a periodic potential. The last term describes the Ohmic dissipation as modeled by a bath of harmonic oscillators coupling to the bond variables.[21]

A subtle consequence of the presence of this Ohmic shunt mechanism is that the phase variables become noncompact,[22] as the dissipation term in Eq. (2) breaks the 2π periodicity of the Josephson potential. Thus, the phases are no longer defined with compact support $\theta \in [-\pi,\pi\rangle$, as they would be in the nondissipative case or in a $(2+1)$D dissipative quantum rotor model. Instead, we have $\theta \in \langle -\infty,\infty\rangle$. *The impact of this decompactification on the problem is enormous*. It reflects that a sudden increase along imaginary time in the phase difference (e.g., $\Delta\theta_{\mathbf{x},\mathbf{x}',\tau} \to \Delta\theta_{\mathbf{x},\mathbf{x}',\tau} + 2\pi$) would produce a voltage imbalance over the barrier. A dissipative, measurable current would then flow through the shunting resistors until the imbalance is relaxed. Hence, the variables cannot be defined modulo 2π, since $\Delta\theta_{\mathbf{x},\mathbf{x}',\tau}$ and $\Delta\theta_{\mathbf{x},\mathbf{x}',\tau} + 2\pi$ represent distinguishable states. The noncompactness of the variables implies that we may no longer identify vortices in the same manner as described above, as a line integral around a plaquette always yields zero for a noncompact phase field. In Appendix A, we introduce a reformulation of the phase variables in terms of a compact part and an additional field describing the tunneling between wells in the extended Josephson potential. This enables us to identify vortices in the compact part of the phase. The phase transitions involving spatial ordering may therefore still be described by vortex proliferation even though the variables are of a noncompact nature.

As a description of a dissipative JJA, there are a few simplifications built into the action (2). We have only considered the effect of self-capacitance and neglected mutual capacitive coupling with neighboring grains. Also, the dissipation term only accounts for one source of dissipation, namely the flow of normal electrons through the shunting resistors. Additional dissipative effects like quasiparticle tunneling[22] and Cooper pair relaxation[4,23] have been neglected.

In order to study the behavior of a two-dimensional array of Josephson junctions at zero temperature under the influence of Ohmic dissipation, we perform large-scale Monte Carlo simulations on a discretized version of Eq. (2),

$$S = \frac{K_\tau}{2} \sum_{\mathbf{x}}^{N} \sum_{\tau}^{N_\tau} (\theta_{\mathbf{x},\tau+1} - \theta_{\mathbf{x},\tau})^2 - K \sum_{\langle \mathbf{x},\mathbf{x}' \rangle} \sum_{\tau}^{N_\tau} \cos(\Delta\theta_{\mathbf{x},\mathbf{x}',\tau}) + \frac{\alpha}{2} \sum_{\langle \mathbf{x},\mathbf{x}' \rangle} \sum_{\tau \neq \tau'}^{N_\tau} \left(\frac{\pi}{N_\tau} \right)^2 \frac{(\Delta\theta_{\mathbf{x},\mathbf{x}',\tau} - \Delta\theta_{\mathbf{x},\mathbf{x}',\tau'})^2}{\sin^2\left(\frac{\pi}{N_\tau}|\tau - \tau'|\right)}. \tag{3}$$

Here, $K_\tau = 1/E_C \Delta\tau$ and the spatial coupling has been renamed $K\Delta\tau \to K$. Our goal is to investigate the behavior of the system in the K-α-space, K_τ therefore defines the energy scale and will be kept at suitable values in the simulations.

The phase variables are defined on the vertices of a three-dimensional cubic grid. The spatial linear extent of the grid is given by N, and the number of Trotter slices used to discretize the temporal direction is given by N_τ. Thus, $\Delta\tau = \beta/N_\tau$, and the size of the space-time lattice is $N \times N \times N_\tau$. Periodic boundary conditions in imaginary time are implicit from the path integral construction, and are also applied in the spatial directions in the standard manner. The noncompactness of the variables also dictates the form of the kinetic term. Because θ is an extended variable, its derivative must be expressed by discretized differentiation. We refer to the appendix of Ref. 24 for details.

B. Outline and overview of main results

For outlining the road map to this paper, the phase diagram of the system is helpful. This is illustrated schematically in Fig. 1. *In all regions of the phase diagram, the phases θ are disordered in the imaginary-time direction.*

In Sec. II, we introduce the various observables used to identify the phases and phase transitions of the model defined in Eq. (3). In Sec. III, the details of the Monte Carlo simulations are presented in a concise form.

In Sec. IV, we take a large value of the Josephson coupling K and investigate the behavior of the system as it crosses from the CSC phase to the FSC phase in Fig. 1 upon increasing α. There is a phase transition at a critical dissipation strength, $\alpha_c^{(2)}$, above which the system is fully bond-ordered superconducting (FSC). For $\alpha < \alpha_c^{(2)}$ the system features unbounded temporal fluctuations, while at the same time featuring spatial phase coherence. Due to algebraically decaying spatial correlations in this regime, we will refer to the phase as critical superconducting (CSC). In other words, the phase configurations of the system rotate more or less as a "rigid body" in time, thus at the same time giving rise to a finite superfluid density (helicity modulus) as well as voltage fluctuations across the junctions. A detection of the CSC phase thus requires simultaneous measurements of the superfluid density of the system, as well as ac measurements of voltages across junctions.

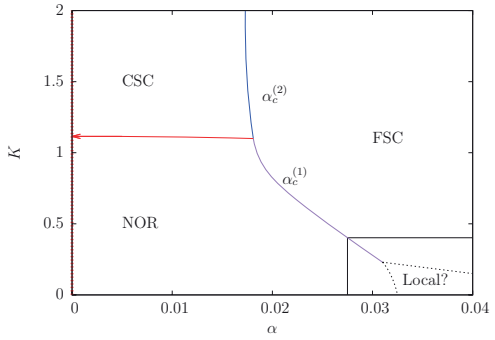

FIG. 1. (Color online) A schematic phase diagram of the system defined by Eq. (3), based on the Monte Carlo calculations presented below. Here, we have used the value $K_\tau = 0.002$, corresponding to the parameters in Sec. IV. NOR refers to the normal phase, where vortices are proliferated and the bonds $\Delta\theta$ are disordered in the τ direction. CSC refers to the critical superconducting state, where the θ variables feature power-law correlations in space, while $\Delta\theta$ remains disordered. FSC refers to the fully bond-ordered superconducting state, which features an additional ordering compared to the CSC phase, namely $\Delta\theta$ ordering in the imaginary-time direction. A hypothetical fourth, local phase has *not* been observed in our simulations, as indicated by the box in the lower right corner. See text in Sec. I B for more details.

In Sec. V, we consider the transition between the NOR phase and the CSC phase, and this is found to be a purely spatial phase transition of the BKT type.

In Sec. VI, we investigate the response of the system to increasing dissipation at low and intermediate Josephson couplings, as it crosses from the NOR phase to the FSC phase in Fig. 1. This is the most difficult case to analyze, as the system transitions from a spatio-temporally disordered phase directly to the spatio-temporally ordered state FSC upon crossing the critical line $\alpha_c^{(1)}$.

In Sec. VII, the topological defects driving the various phase transitions as well as how such a model may exhibit local quantum criticality (LQC), are discussed. This may be briefly summarized as follows.

On the line separating CSC from NOR, and on the line separating CSC from FSC, the spatial and temporal aspects of the phase transitions can be considered separately. The CSC-NOR transition is driven by point vortices and is in the 2D XY universality class. The FSC-CSC transition is driven by instantons in $\Delta\theta$ and may be characterized as a roughening transition in the space of $\Delta\theta$. On the critical line $\alpha_c^{(1)}$, there is a complicated interplay between temporal and spatial fluctuations. This critical line is neither in the 2D XY nor in the 3D XY universality class.

An additional fourth phase could conceivably have been present in the phase diagram, featuring temporal order and unbound vortices. The most likely position in the phase diagram for such a hypothetical phase would be at weak Josephson coupling and strong dissipation strength. This is shown by the dotted lines within the box in the lower right corner of Fig. 1. The local transition line would involve ordering of temporal fluctuations without onset of spatial phase coherence, and as such would describe a local quantum critical point. Our simulations, however, show no sign of such behavior in the parameter range we have considered.

The limit $\alpha = 0$ is in principle ill defined in this model since a finite dissipation is essential for the decompactification of the variables. This is indicated by drawing the $\alpha = 0$ axis as a red dotted line in Fig. 1. Thus, the value $\alpha = 0$ is also a singular endpoint of the horizontal (red) line in the phase diagram, and this is indicated by terminating this line in an arrow.

In Appendix A, we provide some more details and discussion on the fundamental implications of the noncompactness of the phase field. In Appendix B, we take a closer look at the NOR phase and investigate the description of Refs. 25, 19 of such a normal phase as a so-called floating phase.

II. OBSERVABLES

In order to describe the various phases and transitions introduced in the previous section, several quantities will be

calculated. To monitor the degree of (spatial) superconducting order, we calculate the spatial helicity modulus, or phase stiffness. This quantity measures the increase in the free energy when applying an infinitesimal twist across the system, $\theta_{\mathbf{x}} \to \theta_{\mathbf{x}} - \boldsymbol{\delta} \cdot \mathbf{x}$. It probes the degree of phase coherence in the system and thus its ability to sustain a supercurrent. The only term in the action that contributes to the helicity modulus is the Josephson interaction term. Hence, the helicity modulus Υ_x is given by

$$\Upsilon_x = \frac{1}{N^2 N_\tau}\left\langle \sum_{\langle \mathbf{x},\mathbf{x}'\rangle}\sum_{\tau}^{N_\tau} \cos(\Delta\theta_{\mathbf{x},\mathbf{x}',\tau})\right\rangle - \frac{K}{N^2 N_\tau}\left\langle \left(\sum_{\langle \mathbf{x},\mathbf{x}'\rangle}\sum_{\tau}^{N_\tau} \sin(\Delta\theta_{\mathbf{x},\mathbf{x}',\tau})\right)^2\right\rangle. \quad (4)$$

Here, the brackets indicate ensemble averaging. In the context of the classical 2D XY model, $\Upsilon_x = 0$ defines the disordered state where vortices are proliferated. In the same manner, $\Upsilon_x \neq 0$ signals the finite rigidity of the quasiordered state.

The same XY models used to describe superconducting systems also describe magnetic systems of planar spins, and the superconducting phase θ can formally be associated with the direction of the XY spins. Conventionally, the order of a superconducting system is therefore often described by a magnetization order parameter,

$$m = \frac{1}{N^2 N_\tau}\sum_{\mathbf{x},\tau} e^{i\theta_{\mathbf{x},\tau}}, \quad (5)$$

which probes the uniformity of the spin direction across the entire $(2+1)$-dimensional volume of the system.

It should be noted that these two order parameters are periodic and consequently insensitive to tunneling events where the phase difference on a single junction jumps to a neighboring potential well, $\Delta\theta \to \Delta\theta + 2\pi$. Consequently, Υ_x and m do not probe the dissipation-induced localization *per se*. In order to quantify this, we calculate the mean square displacement (MSD) of the bond variable $\Delta\theta$ along imaginary time,

$$W^2_{\Delta\theta}(N_\tau) = \frac{1}{N_\tau}\left\langle \sum_{\tau}^{N_\tau} (\Delta\theta_\tau - \overline{\Delta\theta})^2\right\rangle. \quad (6)$$

Here, we have defined $\overline{\Delta\theta} = 1/N_\tau \sum_\tau \Delta\theta_\tau$. The MSD is often used in the context of stochastically growing interfaces or diffusion processes, and it is natural to adopt some concepts from these areas for our problem. For instance, the degree to which the imaginary-time history of $\Delta\theta$ may be regarded as "rough" can be quantified by the scaling characteristics of the MSD with the length N_τ of the "interface." Normally, one finds

$$W^2_{\Delta\theta} \propto N_\tau^{2H}, \quad (7)$$

if the imaginary-time history of $\Delta\theta$ describes self-affine configurations. $H = 1/2$ corresponds to a Markovian random walk, and such linear scaling of the MSD is also referred to as normal diffusion. A deviation from linear growth of $W^2_{\Delta\theta}$ as a function of N_τ is the hallmark of *anomalous diffusion*.[26] In particular, $H < 1/2$ is referred to as subdiffusive behavior. A smooth interface is characterized by the MSD being independent of the system length.

To describe the phases and phase transitions, we will also investigate correlations of the order parameter field considered in Eq. (5). We define the spatial and temporal correlation function by

$$G_\theta(\mu; q) = \langle e^{iq(\theta_\mu - \theta_0)}\rangle, \quad (8)$$

where $\mu \in \{\mathbf{x}, \tau\}$. The extra factor q in the exponent is introduced for later reference in Appendix B, but will be set to the conventional value $q = 1$ otherwise. In Appendix B we will also consider bond correlations, defined here for convenience as

$$G_{\Delta\theta}(\mu; q) = \langle e^{iq(\Delta\theta_\mu - \Delta\theta_0)}\rangle. \quad (9)$$

For completeness we also present the susceptibility of the action,

$$\chi_S = \frac{1}{N^2 N_\tau}\langle (S - \langle S\rangle)^2\rangle, \quad (10)$$

as an additional means of locating the expected dissipation-induced phase transitions. This is the quantum mechanical equivalent of the classical heat capacity and is expected to present a nonanalyticity at a critical point.

III. DETAILS OF THE MONTE CARLO CALCULATIONS

Considerable progress has been made in constructing new, effective, nonlocal algorithms for long-range-interacting systems with extended variables.[11,27,28] However, these algorithms are presently restricted to $(0+1)$D systems, and do not seem to generalize easily to $N > 1$.[27] In the Monte Carlo simulations, we have therefore combined local updates with a parallel tempering algorithm[29,30] in which several systems are simulated simultaneously at different coupling strengths.

A Monte Carlo sweep corresponds to proposing a local update by the Metropolis-Hastings algorithm sequentially for every grid point in the system. The proposed new phases are generated by first randomly choosing to increase or decrease the value, then propagating the value by a random increment of size $2\pi n/32$, where $n \in \{1, 32\}$. In other words, the continuous symmetry of the variables is emulated by 32 discrete states per 2π interval. We have confirmed that adding additional states will not change the results.

After a fixed number of Monte Carlo sweeps a parallel tempering move is made. In this move, a swap of configurations between two neighboring coupling values is proposed, and the swap is accepted with probability Ξ_{PT} given by

$$\Xi_{\mathrm{PT}} = \begin{cases} 1 & \text{if } \Delta < 0, \\ e^{-\Delta} & \text{if } \Delta \geqslant 0. \end{cases} \quad (11)$$

Here, $\Delta = \kappa'(\bar{S}[X;\kappa'] - \bar{S}[X';\kappa']) - \kappa(\bar{S}[X;\kappa] - \bar{S}[X';\kappa])$, where κ is the coupling value varied, representing in our case α or K, and X represents the phase configuration. $\bar{S}$ indicates the part of the action conjugate to the coupling parameter κ. Both the Metropolis updates and the parallel tempering swaps are ergodic and respect detailed balance.

All Monte Carlo simulations were initiated with a random configuration. Depending on system size, various numbers of sweeps were performed for each coupling value. Error bars are provided for all observables except correlation functions, but are usually smaller than the data points. Measurements on

which we perform scaling have, broadly speaking, a relative error well below 1%. The MERSENNE TWISTER[31] random number generator was used in all simulations and the random number generator on each CPU was independently seeded. It was confirmed that other random number generators yielded consistent results. In some simulations we also made use of the Ferrenberg-Swendsen reweighting technique,[32] which enables us to continuously vary the coupling parameter after the simulations have been performed.

In order to identify sharply defined nonanalyticities and observe converged scaling of $W^2_{\Delta\theta}$ at the dissipation-induced phase transitions, relatively large values of N_τ are needed. This limits the range of spatial sizes accessible in simulations with a single-site update algorithm. In the sections where we focus on the temporal scaling, we have fixed the spatial size at $N = 20$ and varied the temporal size in the range $N_\tau = 50$ to $N_\tau = 350$. In Sec. V we find that in the CSC phase the temporal size of the system is irrelevant in determining the spatial properties of the system. Consequently, the temporal size is fixed at $N_\tau = 20$ and the spatial size is varied in the range $N = 10$ to $N = 100$. To investigate the spatial correlations in θ across the NOR-FSC phase transition, we have also performed simulations on a $N_\tau = 30$ system with $N = 50$ and $N = 100$.

IV. THE CSC-FSC TRANSITION $\alpha_c^{(2)}$

In this section, we consider the behavior of the system under the influence of strong Josephson coupling K [i.e., for a value of K where the corresponding classical system would be topologically ordered even in the absence of dissipation (above the horizontal line in the phase diagram of Fig. 1)]. The coupling parameter will be fixed at $K = 1.5$ in this section, while the dissipation strength α is varied. We will use a quantum coupling $K_\tau = 0.002$. The main focus is on scaling of observables describing temporal fluctuations. Hence, the spatial system size is fixed at $N = 20$.

We start by presenting typical configurations of the bond variable $\Delta\theta$ as a function of τ. At strong coupling, the bond variables are located predominantly in the vicinity of the potential minima located at $2\pi n$, where n is an integer. Due to the noncompact nature of the variables, $\Delta\theta$ are free to tunnel between neighboring minima at weak dissipation. When considering the single-junction problem, this sudden tunneling of the bond variable from one Trotter slice to the next, $\Delta\theta_{\tau+1} - \Delta\theta_\tau \approx 2\pi n_{\rm I}$, is often referred to as instanton or anti-instanton configurations, depending on the sign of the integer-valued "instanton charge," $n_{\rm I}$. Note that the noncompactness allows for tunneling of $\Delta\theta$ also between minima of the potential located further away than nearest neighbor. This corresponds to instanton charges with values larger than unity. The tunneling behavior is easily identified in the topmost curve in Fig. 2, where frequent instantons and anti-instantons are apparent. In this temporally disordered state, the quantum paths of $\Delta\theta$ appear to be well described in terms of a gas of proliferated instantons. Beyond a threshold value of α, we observe a localization of $\Delta\theta$ in one of the minima of the Josephson potential. The imaginary-time history of a bond variable corresponding to this phase forms an essentially smooth surface and is given in the lower curve in Fig. 2. However, even though the phase gradients are localized, closely bound pairs of instantons and anti-instantons may still be present.

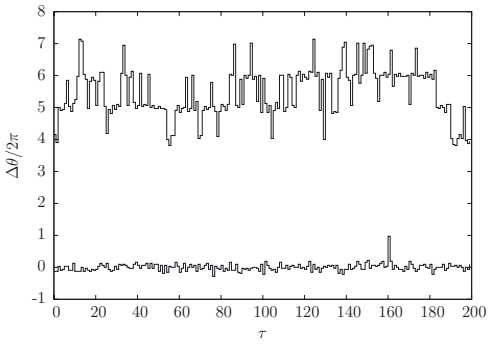

FIG. 2. The bond variable $\Delta\theta$ as a function of imaginary time τ for two different values of dissipation strength, $\alpha = 0.0102$ and $\alpha = 0.0281$, in the strong Josephson coupling regime. In the topmost curve, the bond variable clearly spends most of the time in the vicinity of the potential minima, although tunneling events between minima are frequent. The lowermost curve corresponds to the fully bond-ordered superconducting state where $\Delta\theta$ is localized and $W^2_{\Delta\theta}$ does not scale with N_τ. Note that in the CSC phase (topmost curve) the quantum paths of $\Delta\theta$ are well described in terms of instantons where the fluctuations in imaginary time are mostly given by integer multiples of 2π, in contrast to the situation for the corresponding quantum paths of $\Delta\theta$ in the NOR phase; see Fig. 8.

In Fig. 3, we show the mean square displacement as a function of dissipation strength. The temporal bond fluctuations are clearly suppressed for increasing values of α. The different curves represent different values of N_τ. Two regions of different scaling behavior of $W^2_{\Delta\theta}$ as a function of N_τ can immediately be discerned. For weak dissipation, $W^2_{\Delta\theta}$ increases with N_τ, while $W^2_{\Delta\theta}$ is independent of the temporal size at strong dissipation. Separating the two regions is a

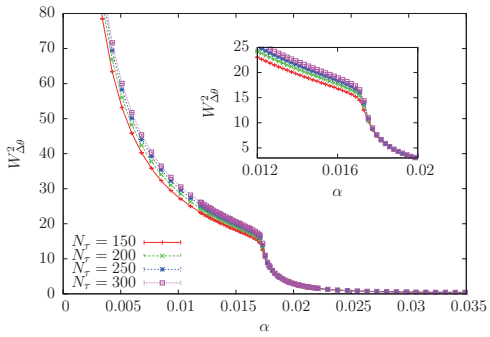

FIG. 3. (Color online) $W^2_{\Delta\theta}$, Eq. (6), as a function of dissipation strength for a system with $K_\tau = 0.002$, $K = 1.5$, $N = 20$, and various values of N_τ. Note the kink in the curves at $\alpha = \alpha_c^{(2)}$ and the saturation of $W^2_{\Delta\theta}$ at a finite value for $\alpha > \alpha_c^{(2)}$. Error bars are smaller than the data points. (Inset) A blow-up of the region around $\alpha_c^{(2)}$.

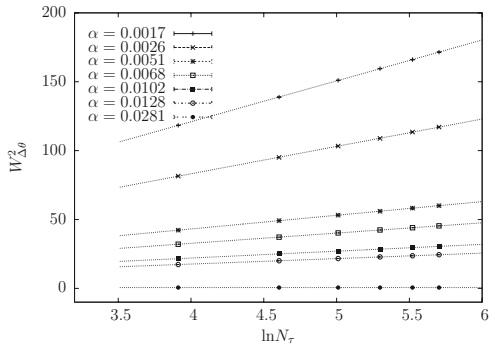

FIG. 4. $W^2_{\Delta\theta}$ as a function of $\ln N_\tau$ for various values of the dissipation strength α ranging from the weak-dissipation limit to the ordered state at the top and bottom, respectively. The dotted lines indicate the logarithmic growth of $W^2_{\Delta\theta}$. Error bars are much smaller than the data points.

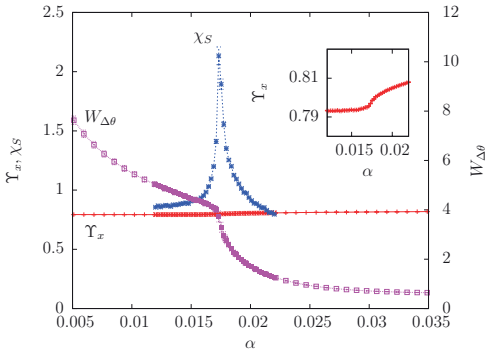

FIG. 5. (Color online) The spatial helicity modulus Υ_x, Eq. (4), action susceptibility χ_S, Eq. (10), and mean fluctuation $W_{\Delta\theta}$, Eq. (6), as a function of dissipation strength α for a system in the strong Josephson-coupling regime with $K_\tau = 0.002$, $K = 1.5$, $N = 20$, and $N_\tau = 250$. (Inset) A blow-up of the helicity modulus around the $\alpha_c^{(2)}$ transition. For $\alpha > \alpha_c^{(2)}$, the dissipation renormalizes the spatial coupling strength so that a kink in Υ_x is visible at the localization transition. However, this renormalization is miniscule. Proliferation of instantons across the line $\alpha_c^{(2)}$ in Fig. 1 does not trigger a proliferation of vortices.

precipitous drop in $W^2_{\Delta\theta}$ at a value of α that we will identify as the localization transition point $\alpha_c^{(2)}$.

Further information on the delocalized phase (CSC) can be found from investigating the dependence of $W^2_{\Delta\theta}$ on the temporal system size N_τ. Here, the MSD scales with N_τ according to

$$W^2_{\Delta\theta} = a(\alpha) \ln N_\tau, \tag{12}$$

where $a(\alpha)$ is a continuously varying proportionality constant. In Fig. 4 we have plotted $W^2_{\Delta\theta}$ as a function of $\ln N_\tau$ for various dissipation strengths. All but the lowest curve represent dissipation strengths well below $\alpha_c^{(2)}$. A clear logarithmic dependence is seen for all values of dissipation strength in the CSC phase. The lowest curve with zero slope corresponds to $\alpha > \alpha_c^{(2)}$, where temporal fluctuations are effectively quenched and $W^2_{\Delta\theta}$ does not scale with N_τ. In this way the increase of temporal fluctuations in $\Delta\theta_\tau$ as α is lowered may also be interpreted as a roughening transition at which the profile described by $\Delta\theta$ changes from smooth to rough. However, it should be noted that the logarithmic scaling presented in Fig. 4 does not conform to the scaling ansatz (7) for a self-affine interface. Instead, $\Delta\theta$ is anomalously diffusive in the sense that $H = 0$. This is sometimes referred to as *superslow diffusion*.[33] In comparison, Ref. 10 found that for the corresponding normal phase of a single resistively shunted Josephson junction, the MSD follows the power law (7) with the exponent decreasing continuously with dissipation strength (from $H = 1/2$ for $\alpha \gtrsim 0$ to $H \approx 0$ for $\alpha = \alpha_c$).

As we show in Fig. 5, $W_{\Delta\theta}$ as well as the action susceptibility χ_S and the helicity modulus Υ_x all feature nonanalytic behavior at the critical value $\alpha_c^{(2)}$. Figure 5 therefore supports the notion that the transition at $\alpha_c^{(2)}$ is indeed a genuine dissipation-induced quantum phase transition. Since we have shown that the system for $\alpha > \alpha_c^{(2)}$ has both spatial phase coherence and temporal localization of $\Delta\theta$, we can identify this region as a fully bond-ordered superconducting (FSC) phase. However, $\Upsilon_x > 0$ even for $\alpha < \alpha_c^{(2)}$, indicating that also the weak-dissipation CSC phase features spatial phase coherence. The kink in the helicity modulus shown in the inset in Fig. 5 may be attributed to the (slightly) reduced spatial rigidity as the bond variables delocalize in imaginary time when leaving the FSC phase. An important conclusion to be drawn from this is that in the regime of strong Josephson coupling, proliferation of instantons does not trigger a proliferation of vortices at $\alpha_c^{(2)}$ in Fig. 1.

A possible physical interpretation of the behavior at strong Josephson coupling and weak dissipation is a phase where there are fluctuations of voltage (and thus also of normal currents through the shunts) even though a finite superfluid density allows the system as a whole to sustain an unimpeded supercurrent. For reasons that will be apparent in the next section, we have chosen to refer to this state as a critical superconducting (CSC) phase. Similar conclusions have been made earlier for $(1+1)$D systems (e.g., in Refs. 4, 7, and 12), where the authors claimed to have found an additional superconducting state characterized by spatial coherence but large local fluctuations. An experimental signature of the FSC-CSC phase transition would be to measure an abrupt increase in voltage fluctuations across each junction while the system maintains a Josephson current across the system as the dissipation strength is reduced. The phase CSC therefore represents a locally metallic (on each junction) and globally superconducting (throughout the system) state.

V. THE NOR-CSC TRANSITION

We next consider the phase transition separating the CSC phase from the fully disordered state NOR. First, we note that the region at weak dissipation and low Josephson coupling in the phase diagram of Fig. 1 is spatially phase incoherent, $\Upsilon_x = 0$. This is therefore identified as the normal, metallic phase (NOR) of the dissipative JJA. To verify that the CSC state identified in the previous section by its finite spatial coherence

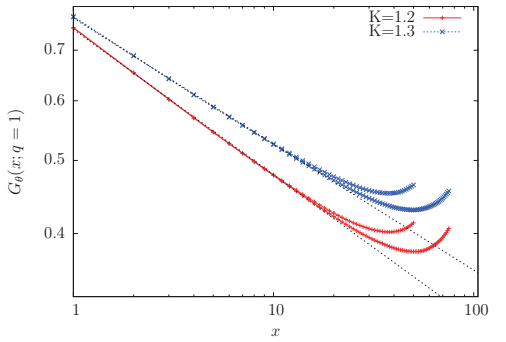

FIG. 6. (Color online) The spatial correlation functions $G_\theta(x;q=1)$, Eq. (8), calculated for $\alpha = 0.005$, $K_\tau = 0.002$, $N_\tau = 20$, and for two values of the Josephson coupling and two values of the spatial extent N. Both coupling values correspond to the CSC phase. The dotted lines show the power-law fit of the correlation functions.

is a distinct phase, we next show that it is separated from the NOR phase by a genuine phase transition and not just a crossover caused by the limited spatial extent of the systems.

In Fig. 6, we show algebraically decaying correlation functions in the spatial direction in the CSC phase, indicating QLRO within each Trotter slice. In combination with the observation of vanishing order in the temporal direction (as measured by $W^2_{\Delta\theta}$), this motivates an interpretation of the CSC phase as a dimensionally reduced critical phase in which the Trotter slices are decoupled from each other. We verified that varying N_τ had no impact on the results for any of the observables probing spatial behavior. Thus, the extent of the systems is fixed at $N_\tau = 20$ in the following.

We anticipate the phase transition separating the NOR phase from the CSC phase to be in the BKT universality class. At the transition point, the helicity modulus is expected to scale according to the finite-size scaling function[34]

$$\Upsilon_x(N) = \Upsilon_x(\infty)\left(1 + \frac{1}{2\ln N + C}\right), \qquad (13)$$

where $\Upsilon_x(\infty)$ is the value of the helicity modulus as $N \to \infty$ and C is an undetermined constant. The critical value K_c may be extracted by varying K until an optimal fit is achieved. In addition, at a BKT transition, the value of $\Upsilon_x(\infty)$ obtained at optimal fit should satisfy the universal relation $\Upsilon_x(\infty)K_c = 2/\pi$.

By treating both parameters as variables in the fitting procedure, no *a priori* assumption on the value of the jump is made. This value may consequently be used as an additional check on the validity of the conjecture of identifying the transition as a BKT transition.

In Fig. 7 we present Υ_x for various spatial system sizes and the corresponding fit with Eq. (13). Figure 7(a) shows results for the dissipationless limit, $\alpha = 0$,[35] while Fig. 7(b) gives the corresponding results for $\alpha = 0.005$. At both dissipation strengths we observe optimal fit at $K \approx 1.12$. The insets presented in both figures show $\Upsilon_x(\infty)K$, which should be compared to the broken line indicating the expected $2/\pi$ universal jump of a BKT transition. These results demonstrate

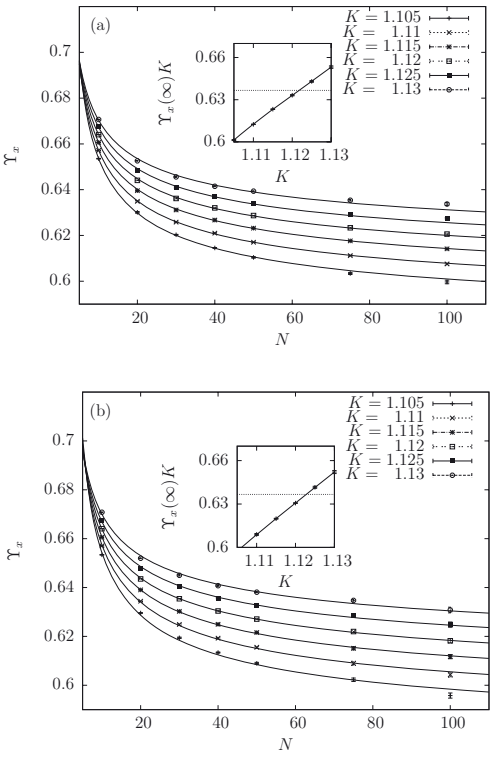

FIG. 7. Comparison of calculated values of the spatial helicity modulus Υ_x with the scaling function (13) for two different dissipation strengths. For both values of α, a good fit is observed at $K \approx 1.12$. (a) The spatial helicity modulus Υ_x as a function of spatial system sizes N for $\alpha = 0.0$, $K_\tau = 0.002$, and various Josephson coupling values. (b) Spatial helicity modulus Υ_x as a function of spatial system sizes N for $\alpha = 0.005$, $K_\tau = 0.002$, and various Josephson coupling values. (Inset) The universal jump of the helicity modulus is expected to be $2/\pi$ for a BKT transition. This value is indicated by a broken line in the insets. The universal jump as calculated from the fitting procedure is shown to be in good correspondence with the BKT scenario.

that the NOR-CSC transition is a BKT transition. The temporal interaction terms are evidently completely incapable of establishing temporal order at this transition. In particular, when comparing Figs. 7(a) and 7(b) corresponding to no dissipation and weak dissipation, respectively, no significant difference is visible. Even though the dissipation term has a major impact on the temporal fluctuations,[36] the spatial helicity modulus appears completely unaffected by the presence of dissipation in the CSC phase.

The classification of the NOR-CSC transition is important in two respects. First, the finite-size analysis shows that the existence of a finite helicity modulus in the CSC phase is not a mere finite-size effect. Secondly, the analysis places the transition in the BKT universality class. This would not have

been possible if there were a divergent correlation length in the temporal direction. Such an effect would have been likely to show up as a breakdown of the scaling procedure. In this way the analysis gives an indirect verification that the transition is of a purely spatial nature, and that the CSC phase is temporally disordered and spatially quasiordered.

VI. THE NOR-FSC TRANSITION $\alpha_c^{(1)}$

The transition line $\alpha_c^{(1)}$ is the only transition line in the phase diagram that exhibits a simultaneous temporal and spatial order-disorder transition. Hence, it involves an interplay between instantons (or instantonlike objects) and vortices, but in a complicated way that is not easy to disentangle.

In this section, the Josephson coupling strength will be fixed at an intermediate value of $K = 0.4$, for which a classical counterpart of our model would be well inside the disordered phase ($\Upsilon_x = 0$). The quantum coupling is set to $K_\tau = 0.1$. Note that this differs from the value of K_τ used to compute the phase diagram in Fig. 1.

Figure 8 shows typical configurations of the bond variable $\Delta\theta$ as a function of τ for two dissipation strengths corresponding to regimes where the model behaves quantitatively different. The topmost curve corresponds to weak dissipation, with anomalous diffusive behavior of the value of $\Delta\theta$. The lowest curve represents the regime of strong dissipation, where the imaginary-time history of $\Delta\theta$ is qualitatively less rough and where we can therefore show below that the bond variable is localized.

We see from Fig. 9 that the amplitude of the temporal bond fluctuations are rapidly decreasing with increasing α. At a critical value of the dissipation strength $\alpha = \alpha_c^{(1)}$, the MSD features a steep drop marking the localization transition where the tunneling of $\Delta\theta$ is suppressed sufficiently to give the bond variables a well-defined value in imaginary time.[37] We are once

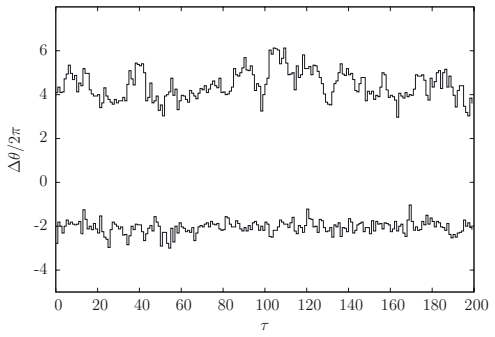

FIG. 8. The bond variable $\Delta\theta$ as a function of imaginary time τ for two different values of the dissipation strength, $\alpha = 0.011$ and $\alpha = 0.021$, in the weak and intermediate Josephson coupling regime. These values correspond to the normal phase and the ordered phase, respectively. The quantum paths of $\Delta\theta$ in the normal phase (relatively low values of K) exhibit fairly slow variations in time, and are not necessarily well described in terms of instantons. Note the contrast to the quantum paths in the topmost curve above and the topmost curve in Fig. 2.

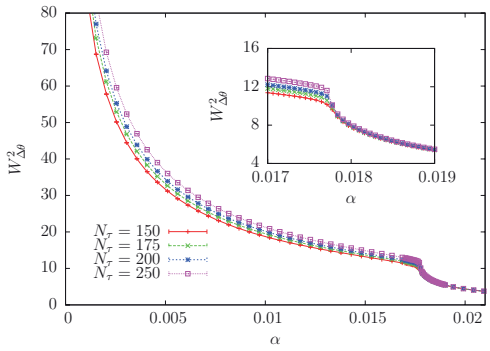

FIG. 9. (Color online) $W^2_{\Delta\theta}$, Eq. (6), as a function of dissipation strength α for a system with $K_\tau = 0.1$, $K = 0.4$, $N = 20$, and various values of N_τ. Note the kink in the curves at $\alpha = \alpha_c^{(1)}$ and the saturation of $W^2_{\Delta\theta}(N_\tau)$ at a finite value for $\alpha > \alpha_c^{(1)}$. Error bars are smaller than the data points. (Inset) Blow-up of the region around $\alpha_c^{(1)}$.

again able to distinguish between two separate states based on the scaling properties of the MSD. In Fig. 10, we present a plot of the MSD as a function of $\ln N_\tau$ for several values of α. The lowermost curve in the figure again represents the FSC phase, $\alpha > \alpha_c^{(1)}$, where the MSD is independent of N_τ. All other curves represent dissipation strengths below the localization transition, and for these a clear logarithmic scaling is observed. In this way, there are distinct delocalized and localized regimes for the bond variable also at weak Josephson coupling, and the temporal fluctuations in each of them behave in exactly the same way as for strong Josephson coupling.[38]

To confirm that the temporal transition at $\alpha = \alpha_c^{(1)}$ also marks the onset of spatial ordering, we show in Fig. 11 the helicity modulus Υ_x. Note the abrupt manner in which the phase stiffness attains a finite value at $\alpha = \alpha_c^{(1)}$. Even though the spatial extent of the system is relatively small, there is no weak-dissipation tail which would have been visible for too

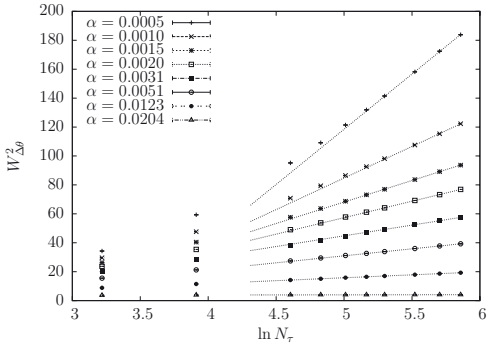

FIG. 10. $W^2_{\Delta\theta}$, Eq. (6), as a function of $\ln N_\tau$ for various values of α ranging from the weak-dissipation limit to the ordered state at the top and bottom, respectively. The logarithmic behavior found at large N_τ is indicated by dotted lines. Error bars are much smaller than the data points.

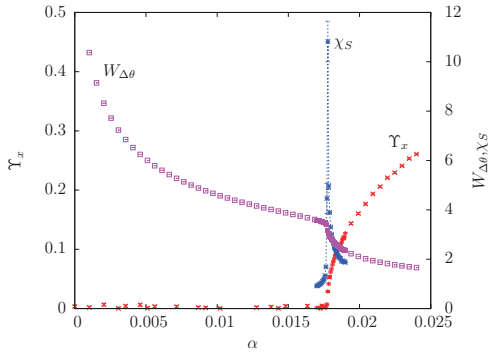

FIG. 11. (Color online) Spatial helicity modulus Υ_x, Eq. (4), action susceptibility χ_S, Eq. (10), and mean fluctuation $W_{\Delta\theta}$, Eq. (6), as a function of dissipation strengths for a system with $K_\tau = 0.1$, $K = 0.4$, $N = 20$, and $N_\tau = 250$. Note that Υ_x vanishes continuously at $\alpha_c^{(1)}$ (no jump).

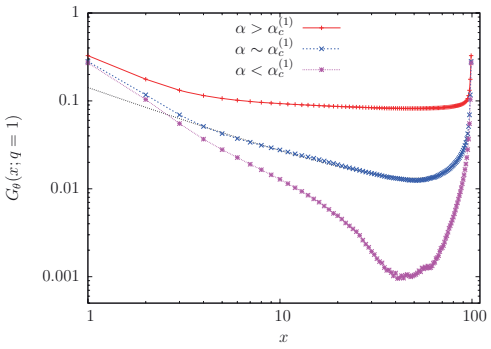

FIG. 12. (Color online) Double-logarithmic plot of the spatial correlation functions $G_\theta(x; q = 1)$ at values of α corresponding to above, close to, and below the NOR-FSC phase transition. The relevant coupling values are $K = 0.4$ and $K_\tau = 0.1$, and the system size is given by $N = 100$ and $N_\tau = 30$. At $\alpha \sim \alpha_c^{(1)}$ the correlation function appears to be linear at long distances, indicating scale-invariant spatial fluctuations. The dotted line indicates this linear behavior. Thus, $\xi \to \infty$, or at the very least $\xi > N/2$.

small system sizes. In the same figure we also show the root mean square displacement, $W_{\Delta\theta}$, and the action susceptibility, χ_S. It is clear that all observables feature a nonanalyticity at the same point. We can therefore conclude that the transition NOR-FSC is a quantum phase transition involving simultaneous onset of spatial and temporal order.

In Fig. 11, we note that the nonanalyticity in Υ_x on the line $\alpha_c^{(1)}$ is brought out very sharply at the system sizes we consider in this case, namely $20 \times 20 \times 250$. Assuming hyperscaling and two diverging length scales ξ (spatial) and ξ_τ (temporal), we may write

$$\Upsilon_x \sim \xi^{2-d-z} \sim \xi^{2-d}\xi_\tau^{-1} \sim N_\tau^{-1}. \tag{14}$$

Here we have introduced the dynamical critical exponent z defined by $\xi_\tau \sim \xi^z$. The sharpness can thus be explained by the large system size and diverging length scale in the τ direction. Very little finite-size effects may then be expected due to the limited spatial extent of the system, since $d = 2$ and the spatial correlation length drops out of the scaling.

Ordinarily, it would have been natural to attempt a scaling analysis of this phase transition based on the Binder ratio,

$$Q = \frac{\langle |m|^4 \rangle}{\langle |m|^2 \rangle^2}, \tag{15}$$

in order to extract the dynamical critical exponent of the system z. Here m is the magnetization order parameter of the superconducting phases defined in Eq. (5). An ordinary quantum critical point is characterized by diverging lengths in space and time, ξ and ξ_τ, respectively. The Binder ratio is then expected to scale according to

$$Q = Q\left(\frac{N}{\xi}, \frac{N_\tau}{\xi_\tau}\right). \tag{16}$$

The correlation lengths entering here are correlation lengths of the phase-correlation function, measuring θ correlations in the spatial and τ directions. Thus, it should be possible to collapse the Binder ratio curves, at criticality, as a function of N_τ/N^z for the correct value of z.

We have attempted such an analysis in this case, and failed. In our computations, we have been able to identify a diverging length scale ξ based on the above scaling approach, but not a diverging length scale ξ_τ. The reason is that in our model, the coupling in spatial directions is effective in ordering the phases θ, while the coupling in the τ direction is only effective in ordering bond variables $\Delta\theta$, while the θ variables never order in the τ direction. One may therefore define a diverging length ξ entering Eq. (16), but not a diverging length ξ_τ. A diverging length scale in the τ direction may very well exist for the bond variables $\Delta\theta$, but not for the phase variables θ.

The onset of long-range order in the θ variables in the spatial directions may be described by the spatial correlation function $G_\theta(x; q = 1)$, Eq. (8). In Fig. 12 we present spatial correlations corresponding to dissipation strengths slightly below the NOR-FSC transition ($\alpha < \alpha_c^{(1)}$), close to the transition ($\alpha \approx \alpha_c^{(1)}$), and slightly above the transition ($\alpha > \alpha_c^{(1)}$). The spatial correlation length appears to behave as expected for a second-order phase transition into a phase with long-range (spatial) order, implying that the NOR-FSC transition is associated with a diverging length scale in the spatial directions.

VII. DISCUSSION

Since the work of Hertz,[39] quantum critical points are commonly characterized by their dynamical critical exponent z. Underlying Hertz' scaling theory is Landau's notion that all relevant fluctuations of a system may be ascribed to fluctuations of an order parameter.[40] This is evident when considering that the exponent z is defined from a divergence of a length scale of the order parameter correlation function. Such a characterization may therefore be insufficient when the critical point cannot be well described by one single order parameter, a problem which has been pointed out in different cases in recent theoretical works.[41,42]

The model studied in this paper may be related to a problem of this kind in the sense that we are unable to find one single order parameter adequately describing the spatial, temporal, and spatio-temporal phase transitions separating the NOR, FSC, and CSC phases in Fig. 1. To substantiate this, we show in Appendix A that the noncompact θ variables may instead be formulated by a combination of a compact phase field $\tilde{\theta} \in [-\pi,\pi\rangle$ and an additional integer-valued field k containing information on what 2π interval the original variable belongs to. Using the reformulation of the θ variables described in Appendix A, it is clear that the magnetization order parameter m only probes the order of the compactified part of the phase, $\tilde{\theta}$, but is completely oblivious to the state of the integer-valued field k. Since the state of this field describes whether or not the phase differences $\Delta\theta$ are localized, m is fundamentally incapable of describing the localization transition concurring with the onset of coherence of $\tilde{\theta}$. As a result, we are unable to define a dynamical critical exponent z.

The phase transition from CSC to FSC is primarily temporal in the sense that it only involves condensation of instantons from a state where the spatial topological defects are already tightly bound. However, this localization of $\Delta\theta$ also contributes to spatial ordering by coupling the Trotter slices along imaginary time, thereby reducing spatial fluctuations sufficiently to render the system behavior 3D. Accordingly, CSC-FSC is also of a mixed character, as the transition separates a phase with spatial QLRO (CSC) from a phase where spatial long-range order is established (FSC).

The phase transition from NOR to CSC is of a purely spatial nature. As one increases the Josephson coupling for weak dissipation, this transition involves only the binding of the (spatial) vortex degrees of freedom while the (temporal) instantons remain proliferated. This conclusion is supported by the signatures of a BKT-type transition found in Sec. V. In this way, the system behaves as a stack of decoupled two-dimensional layers in the CSC phase, each exhibiting critical fluctuations in the $\tilde{\theta}$ field.

The phase transition from FSC to NOR is much more complicated than the ones from FSC to CSC and from CSC to NOR, and appears to be of a type not previously considered in connection with superconductor-metal phase transitions. Since one cannot characterize the anisotropy of the phase transitions quantitatively in terms of an exponent z, we resort to more qualitative considerations of the spatial and temporal degrees of freedom. In the case of intermediate coupling, one has a concomitant binding of vortices and localization of $\Delta\theta$ upon entering the FSC phase from the NOR phase. This corresponds to the ordering of the degrees of freedom relevant to space ($\tilde{\theta}$) and time (k), respectively. Due to this simultaneity, we characterize the NOR-FSC phase transition as a mixed spatio-temporal phase transition. It is an interplay between two distinct types of topological defects (point vortices and temporal fluctuations in $\Delta\theta$) that determines the character of the phase transition. This phase transition is therefore neither of the BKT type, nor in the 3D XY universality class. The former is characterized by proliferation of pointlike vortices in two dimensions, while the latter is characterized by the proliferation of $(2+1)$-dimensional vortex loops.[43–45] Dissipation, and the associated decompactification of the θ variables, leads to a disordering of the θ variables in the imaginary-time direction in all regions of the phase diagram. Decompactification essentially chops up the vortex loops into spatial point vortices and instantonlike objects in $\Delta\theta$, thereby destroying the Lorentz-invariant physics of vortex-loop proliferation at the quantum phase transition.

In order to exhaust all combinations of spatial and temporal order/disorder, one could also imagine a fourth phase exhibiting temporal order without accompanying spatial phase coherence. This would correspond to $W^2_{\Delta\theta} = \text{const.}$ and $\Upsilon_x = 0$ (i.e., a phase with localized bond variables and proliferated vortices). The most probable location of such a phase would be at weak spatial coupling and large dissipation strength, corresponding to the lower right corner of Fig. 1. This scenario opens the possibility of a purely temporal ordering coinciding with exponentially decaying spatial correlations upon entering this hypothetical phase from the NOR phase. Due to this locality, such a transition could be a possible realization of a local quantum critical point ("$z = \infty$") in a spatially extended system. In order to emphasize that the existence of this local phase is only a possibility that we have not actually found in our computations, we have drawn a box of solid lines around the specific region in Fig. 1 and indicated possible realizations of the phase transitions by dotted lines. Although the existence of such a phase has been conjectured by analytical work[2,5,9] and there is numerical work supporting this view,[12] we find no signatures pointing to the existence of such a local phase in any of the parameter sets considered. Rather, our results strongly indicate that a spatial coupling is always rendered relevant by a large enough dissipation parameter α.[19] In this way, the localization of $\Delta\theta$ will always induce an onset of spatial phase coherence. This is equivalent to saying that instantonlike excitations will always proliferate prior to, or simultaneously with, the unbinding of vortices as the strength of dissipation α is reduced. Local quantum criticality (in the sense of having temporal critical fluctuations coinciding with spatial disorder) would follow from vortices proliferating prior to instantons as the disordered state (NOR) is approached from the fully bond-ordered superconducting state (FSC) by reducing α.

Finally, we compare the phase diagram found in this paper with the phase diagram calculated for a model similar to Eq. (3) using compact variables.[16] Figure 13 shows two schematic phase diagrams, and the following discussion pertains to their topology. The topmost diagram summarizes the results found in this paper, while the lowermost diagram is the phase diagram for the $(2+1)$D dissipative quantum rotor model. In the latter case, the diagram features one single phase transition line separating a completely ordered state from a disordered state. The phase transition separating them is driven by a proliferation of vortex loops. This transition line is isotropic in space time ($z = 1$) meaning that the entire line is in the 3DXY universality class. From the lowermost phase diagram it is clear that if we start in the limit of no dissipation, $\alpha = 0$, and increase α for $K > K_{3DXY}$, the dissipation term only contributes to further dampening the innocuous three-dimensional spin-wave excitations. This can only increase the superfluid density in the ordered phase. However, in the noncompact model the regime $K > K_{\text{BKT}}$, and weak dissipation, represents a phase involving both two-dimensional spatial spin waves and a proliferated instanton gas. Increasing α from this regime may therefore

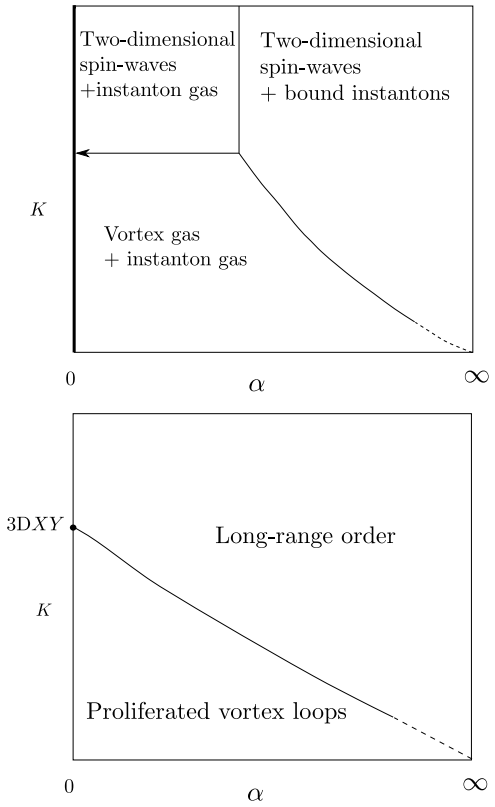

FIG. 13. Comparison of the phase diagrams of the noncompact (topmost) and compact (lowermost) models. (Topmost diagram) The phase diagram found in this work. All phases feature disordered θ variables in the imaginary-time direction. A notable feature is the phase CSC where bound vortex antivortex pairs coexist with disordered bond variables $\Delta\theta$ in the τ direction. This is a consequence of the θ variables being defined with noncompact support. This is only true for finite α as the quadratic form of the dissipation term is the origin of the decompactification. Consequently, the physics found at finite α cannot be analytically connected to the limit $\alpha = 0$. The description at $\alpha = 0$ would require compact phases and thereby a loss of the instanton degrees of freedom. For $\alpha = 0$ there is a phase transition at a critical value of K, but this phase transition is in the 3D XY universality class, as in the lowermost diagram. $\alpha = 0$ is therefore a singular endpoint of the horizontal line in the topmost diagram. (Lowermost diagram) The phase diagram found for a $(2+1)$D bond-dissipative quantum rotor model with compact variables. In this case the diagram features only a single transition line where the system undergoes a spatio-temporally isotropic ($z = 1$) phase transition in the 3D XY universality class. See Ref. 16 for details.

drive a phase transition because the dissipation term is effective in binding these temporal defects. Therefore, the feature of the phase diagram of the noncompact model that really sets it apart from the phase diagram of the dissipative 3D XY model (i.e., the compact case) is the existence of a phase at weak dissipation involving spatial ordering concomitant with temporal disorder. The resulting phase CSC has no counterpart in the dissipative 3D XY model, since in the latter model the phases θ are compact. Compact phases θ promote vortex loops as the critical fluctuations, while noncompact phases θ promote vortices and instantons as relevant fluctuations driving the phase transitions.

The phase CSC corresponds to a resistively shunted Josephson junction array which may sustain a finite Josephson current through the array, but nonetheless features finite voltage fluctuations across each junction of the junction array. This may be viewed locally (at a single junction) as a metallic state, but globally (throughout the system) as a superconductor. The most complicated aspect of the phase diagram of the noncompact model is the direct phase transition between the NOR phase and the FSC phase, which is considerably more difficult to characterize than the $z = 1$ order-disorder transition in the dissipative 3D XY model.

A $(2+1)$-dimensional model with bond dissipation has recently been considered as an effective theory of quantum criticality at optimal doping in high-T_c cuprates.[17] The claim of this work is that the phase correlators of the model at the critical point decay algebraically as $1/\tau$ while they are short ranged in space. Such a phase transition would be an example of local quantum criticality. Monte Carlo simulations on the $(2+1)$-dimensional quantum rotor model gives an order-disorder transition in the 3D XY universality class, which is quite different from local quantum criticality. From the results of the present paper, it appears to be important to specify whether the phase variables are compact or noncompact (cf. Fig. 13). The phase transitions separating the CSC phase from the FSC phase, or the CSC phase from the NOR phase, are not of the type described in Ref. 17. To verify whether or not the remaining phase transition separating the FSC phase from the NOR phase is an example of local quantum criticality one would ideally need a single order parameter measuring spatial and temporal correlations in phases, θ. Since we do not have this at our disposal, we have not been able to determine what sort of universality class the critical line separating FSC and NOR belongs to, apart form concluding that it is not in the 2D XY or 3D XY universality class. However, the spatial correlation functions presented in Fig. 12 suggest that the NOR-FSC transition line is not a line with local spatial phase correlations.

We end with an important remark on the temporal phase fluctuations we have focused on in this paper. The quantity $W^2_{\Delta\theta}$ in Eq. (6) measures temporal fluctuation in *phase gradients* $\Delta\theta$, defined on a *spatial* bond of the lattice. One could also study a corresponding measure of temporal fluctuations of the phases θ themselves. We have done this, and find the following. In all parts of the phase diagram in Fig. 1, the quantity

$$W^2_\theta(N_\tau) = \frac{1}{N_\tau}\left\langle \sum_\tau^{N_\tau} (\theta_\tau - \overline{\theta})^2 \right\rangle, \tag{17}$$

diverges with N_τ. This underlines that the instantons or instantonlike objects we have discussed in this paper are temporal fluctuations in phase gradients $\Delta\theta$, not instantons

in phases θ. On the other hand, the helicity modulus Eq. (4) measures long-range or quasi-long-range spatial ordering of phases θ, and we find such orderings in the FSC and CSC phases. Thus, the FSC phase does not exhibit 3D XY ordering. It features spatial ordering of θ and $\Delta\theta$, but temporal ordering only of $\Delta\theta$. This supports the statement made above, that the NOR-FSC transition is not in the 3D XY universality class. It is a new type of phase transition involving a complicated interplay between spatial point vortices and instantonlike excitations in $\Delta\theta$.

VIII. CONCLUSIONS

The model discussed in this paper describes a two-dimensional array of quantum dissipative Josephson junctions. By extensive Monte Carlo simulations we have shown that the model features three distinct phases (see Fig. 1) featuring different behaviors of spatio-temporal fluctuations. We have quantified these fluctuations by the mean square fluctuation $W^2_{\Delta\theta}$, Eq. (6), and the spatial helicity modulus Υ_x, Eq. (4).

The normal phase (NOR) is found at weak dissipation and weak Josephson coupling strength. In this phase, the spatial helicity modulus is zero, signaling a vanishing stiffness to infinitesimal phase twists on each Trotter slice. The phase differences of the individual junctions are highly fluctuating in imaginary time and the system therefore exhibits metallic behavior. Increasing the dissipation strength drives the system to a phase transition where the phase differences $\Delta\theta$ are localized into one of the minima of the Josephson potential. This localization of bond variables in imaginary time occurs simultaneously with an onset of rigidity towards phase twists across the spatially extended system. We identify this phase with a fully bond-ordered superconducting state (FSC).

At strong coupling and weak dissipation we identify an intriguing phase exhibiting finite phase stiffness and algebraically decaying spatial correlations. The imaginary-time direction remains disordered with wildly fluctuating bond differences. This dimensionally reduced phase is referred to as a critical superconducting (CSC) phase. The finite helicity modulus in this phase indicates that the system may sustain a dissipationless current going through the entire JJA. There are, however, voltage fluctuations present which in principle should make it experimentally distinguishable from a fully bond-ordered superconducting phase, and also distinct from the more standard 3D XY ordered fully superconducting state where even the phases θ are ordered in all directions.

We have found no signs of a phase which is temporally ordered (in the sense of having a bounded $W^2_{\Delta\theta}$) and proliferated vortices. Such a phase would naturally facilitate the observation of local quantum criticality in which a spatially disordered and temporally (quasi)ordered system disorders in the imaginary-time direction.

ACKNOWLEDGMENTS

The authors acknowledge useful discussions with E. V. Herland, A. Hansen, I. Simonsen, V. Aji, C. M. Varma, and J. Zaanen. A.S. was supported by the Norwegian Research Council under Grant No. 205591/V30 (FRINAT). E.B.S. and I.B.S thank NTNU for financial support. The work was also supported through the Norwegian consortium for high-performance computing (NOTUR). A.S. thanks the Aspen Center for Physics under NSF Grant No. 1066293, where part of this work was done, for hospitality.

APPENDIX A: REFORMULATING THE NONCOMPACT DEGREES OF FREEDOM

To gain further insight into the three phases reported in this work and the transitions between them, we consider the following decomposition of the phase degrees of freedom:

$$\theta_{\mathbf{x},\tau} \to \tilde{\theta}_{\mathbf{x},\tau} + 2\pi k_{\mathbf{x},\tau}. \tag{A1}$$

The noncompact starting point θ is thereby exchanged for a compact phase field, $\tilde{\theta} \in [-\pi,\pi\rangle$, plus an integer-valued field k, keeping track of the specific 2π interval the original variable belonged to. In the partition function, this reformulation amounts to

$$\begin{aligned} Z &= \int \mathcal{D}\theta e^{-S} = \int_{-\infty}^{\infty} \prod_{\mathbf{x},\tau} (d\theta_{\mathbf{x},\tau}) e^{-S} \\ &\to \sum_{\{k\}} \int \mathcal{D}\tilde{\theta} e^{-S} = \sum_{\{k\}} \int_{-\pi}^{\pi} \prod_{\mathbf{x},\tau} (d\tilde{\theta}_{\mathbf{x},\tau}) e^{-S}. \end{aligned} \tag{A2}$$

Note that k is defined on every point in space time and has nothing to do with the winding number found in some realizations of quantum rotor models with compact phases.

It should also be noted that the 2π-periodic spatial interaction is only sensitive to the $\tilde{\theta}$ field. Also, the compactness of $\tilde{\theta}$ enables the identification of vortices in this field in a similar way as discussed in connection with the classical 2D XY model, Eq. (1). The finite Υ_x observed in the CSC and FSC phases may thereby be attributed to phase coherence in $\tilde{\theta}$. In addition to the vortex degrees of freedom found in the classical version of the system, the noncompactness of the quantum version introduces an additional degree of freedom (k) associated with the tunneling of bond variables from one minimum of the extended Josephson potential to another.

In the NOR phase, we found $\Upsilon_x = 0$, which may be understood as a phase featuring proliferated vortices of the $\tilde{\theta}$ field, as well as proliferated instantons in $\Delta\theta$. Increasing the Josephson coupling (for small α) drives the system into the CSC phase with $\Upsilon_x \neq 0$, which corresponds to a binding of vortices into dipoles. Nonetheless, the bond variables remain anomalously diffusive, $W^2_{\Delta\theta} \propto \ln N_\tau$, in both the NOR and the CSC phase. At strong coupling, the bond variables tend to stay in the vicinity of the minima of the potential wells, $\Delta\theta \approx 2\pi\Delta k$. From the viewpoint of the reformulated variables, the delocalized bond variables in the CSC phase is an expression of an unbroken symmetry $\Delta k \to \Delta k + \Lambda$, where Λ is an integer. Moreover, the integer field k may be directly connected with the instanton charges in the strong-coupling limit by $\Delta k_{\tau+1} - \Delta k_\tau = n_{\mathrm{I}}$. The delocalization of $\Delta\theta$ manifests itself as proliferated instanton/anti-instanton configurations in this regime, and the CSC phase may therefore be described as an instanton gas. This is illustrated in the topmost curve of Fig. 2, illustrating the quantum paths of $\Delta\theta$ in the CSC phase of Fig. 1.

For weak Josephson coupling, the excitations in the imaginary-time path of $\Delta\theta$ are strictly speaking not well described by topological instanton defects. This is quite

evident from the topmost curve of Fig. 8, describing the quantum paths of $\Delta\theta$ in the NOR phase of Fig. 1. Nevertheless, as the quantum fluctuations still respect the same symmetry $\Delta k \to \Delta k + \Lambda$, we choose to refer to such excitations as instantons also in the NOR phase. In the FSC phase, on the other hand, localization of bond variables implies that the symmetry is broken for both weak and strong coupling. Starting at large K and large α, the picture is therefore as follows: In the FSC phase, both the defects associated with $\tilde{\theta}$ (vortices) and with k (instantons) are absent or tightly bound. Lowering α into the CSC phase, instantons are proliferated while the vortices remain bound. Lowering K from the CSC phase into the NOR phase, the vortices proliferate as well.

APPENDIX B: CORRELATION FUNCTIONS IN THE NOR PHASE

It has recently been proposed[19,25] that the metallic state of Josephson junction arrays might exhibit nontrivial behavior. Here, it was argued that the $(0+1)$-dimensional constituents of the array may slide past each other in what was denoted a "floating phase."[25] Similar dimensionally decoupled phases are also believed to be relevant to other physical systems such as layered superconductors[46] and stacks of two-dimensional arrays of membrane proteins.

These papers employed a renormalization group analysis to show that the spatial coupling between the superconducting islands is perturbatively irrelevant on the disordered side of the transition. They also calculated the correlation functions Eq. (8) and (9) in this regime and found that they had a form that indicated unconventional, purely local fluctuations. Monte Carlo studies[11] of a single resistively shunted Josephson junction also indicated that a similar form of correlation functions could be found in $(0+1)$D systems as well. The correlation functions employed in these analyses featured a noninteger parameter q that was introduced to probe fluctuations with another periodicity than the underlying Josephson potential. In the presence of a finite Josephson potential, expectation values such as $\langle \exp(i\Delta\theta_{\mathbf{x},\mathbf{x}',\tau})\rangle$ will generally not be equal to zero in any phase. This is, however, due to the corresponding symmetry being explicitly—and not spontaneously—broken, and has consequently nothing to do with a phase transition. The parameter q was therefore introduced to assure correlation functions decaying to zero in the disordered phase. Similar correlation functions have also been considered before in investigations of roughening transitions of crystal surfaces with quenched bulk disorder.[47] We will refer to them as *fractional correlation functions*.

Figure 14 shows both spatial and temporal correlation functions, Eq. (8), at a dissipation strength deep in the NOR phase where the Josephson potential is expected to be irrelevant[25] and we are far away from the phase transition at $\alpha = \alpha_c^{(1)}$. The correlation functions in the bottom row include a noninteger factor $q = 1/3$; the top row shows the correlation functions without $(q = 1)$ this noninteger factor. Comparing the correlation function of the temporal direction with the spatial direction for $q = 1/3$, it is clear that the spatial and temporal behaviors of the system *appear* completely decoupled.[48] As we discuss below, this local behavior of the fractional correlation functions is misleading.

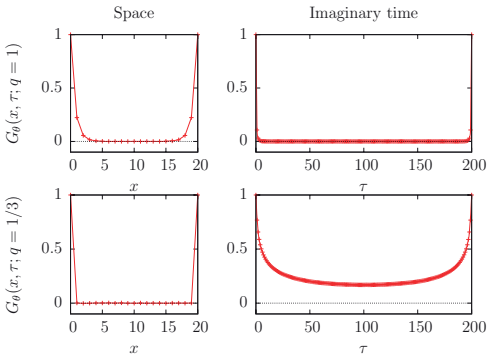

FIG. 14. (Color online) Correlation functions, Eq. (8), in both space (left column) and imaginary time (right column) in the normal phase. The relevant coupling parameters are $\alpha = 0.012$, $K = 0.4$, and $K_\tau = 0.1$. There is a pronounced difference between the correlations along the spatial and temporal directions for $q = 1/3$.

Appendix A introduced a reformulation of the phase variables that clarifies the difficulties concerning the construction of a globally defined order parameter describing our system. The reformulation of the phase variables also offers an alternative viewpoint on the fractional correlation functions. For example, imagine a 2D XY model, Eq. (1), being formulated with noncompact phase variables instead of the standard compact variables. In the partition function, the summation over k is trivial, yielding only a renormalization of the ground-state energy, because there is no coupling between different k sectors in the action. The remaining integration over $\tilde{\theta}$ is the partition function of the ordinary 2D XY model. When performing Monte Carlo simulations on the 2D XY model with a noncompact formulation of the phases, we find the usual QLRO phase at strong Josephson coupling, in which the correlation function $G_\theta(\mathbf{x}; q = 1)$ of Eq. (8) decays algebraically. However, consider probing the QLRO phase with a *fractional* correlation function, $q < 1$. This correlation function involves contributions from several k sectors, ultimately averaging the correlator to zero for all distances. The same result holds for the disordered phase, and so, although the QLRO phase is phase coherent and the disordered phase is not, the fractional correlation function essentially cannot tell them apart.

Applying exactly the same arguments as above to our CSC phase with spatial QLRO, one realizes that the spatial fractional correlation function will vanish also here. In analogy with the classical 2D XY model, we argue that this should not be regarded as a signature of completely spatial decoupling in neither the CSC phase nor the NOR phase. The apparent locality of the normal phase, and by extension the corresponding floating phase of Ref. 25, is consequently not a result of the dissipative interaction *per se*. Rather, a floating phase with such vanishing spatial fractional correlations follows as a direct result of the noncompactness of the phase variables, which in turn is caused by their coupling to a dissipative bath.

In the following we provide supplementary details regarding the fractional correlation functions. To be specific,

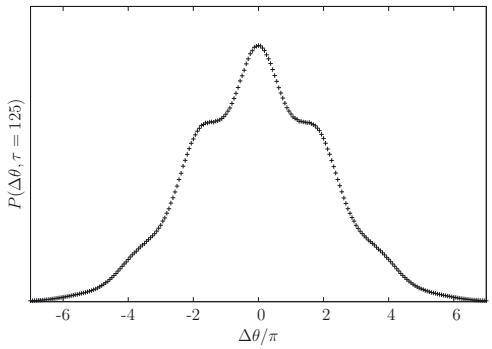

FIG. 15. The distribution of $\Delta\theta_\tau - \Delta\theta_0$, $P(\Delta\theta, \tau = 125)$, in arbitrary units for a system with $K_\tau = 0.1$, $K = 0.4$, and dissipation strength $\alpha = 0.011$. The distribution is extracted from the Monte Carlo simulations and is conjectured to follow Eq. (B1).

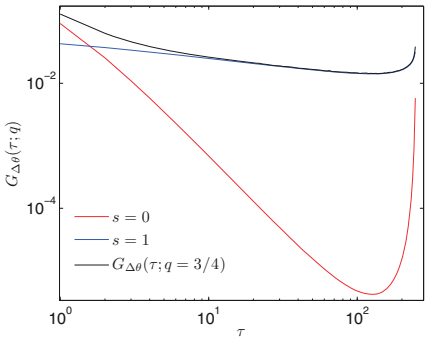

FIG. 16. (Color online) The unequal-time bond correlation function, $G_{\Delta\theta}(\tau; q = 3/4)$, for a system with $K = 0.4$, $K_\tau = 0.1$, $\alpha = 0.011$, $N = 20$, and $N_\tau = 250$. The black curve is the correlation function Eq. (9) sampled directly from the Monte Carlo simulations. The red (lowermost gray) and blue (uppermost gray) curve are the $s = 0$ and $s = 1$ terms of Eq. (B3), respectively, and are calculated as explained in the text.

we will investigate the fractional bond correlation functions $G_{\Delta\theta}(\tau; q)$ more carefully, and prove that a power-law tail is expected in the weak dissipation regime. We first consider the distribution function $P(\Delta\theta, \tau)$, as was also the starting point of Ref. 19. This function describes the diffusion of the phase difference $\Delta\theta_\tau$ with respect to its value at $\tau = 0$. The distribution broadens for increasing τ and is illustrated for a fixed imaginary-time distance in Fig. 15. We find that the distribution function can be very well fitted by the functional form,

$$P(\Delta\theta, \tau) = P_0 e^{-\frac{\Delta\theta^2}{2\sigma_G^2}} \sum_n e^{-\frac{(\Delta\theta - 2\pi n)^2}{2\sigma^2}}, \tag{B1}$$

where P_0 is a normalization constant. The distribution is made up of a sequence of sub-Gaussians with standard deviation σ centered around the minima of the Josephson potential. In addition, there is an overall Gaussian convolution characterized by a standard deviation σ_G. We find empirically that whereas σ is dependent on K, it is independent of the distance τ in imaginary time. The overall variance $\mathcal{G}(\tau)$ of the distribution, as defined by

$$\mathcal{G}(\tau) = \langle (\Delta\theta_\tau - \Delta\theta_0)^2 \rangle, \tag{B2}$$

grows logarithmically with τ. This variance can furthermore to a very good approximation be identified with the variance σ_G^2 of the convolution function.

The calculations in Ref. 19 were based on a strong-coupling limit for the distribution function, with an additional assumption that the spatial coupling will renormalize to zero regardless of its bare value. For large values of K, we have demonstrated that the system will eventually reach a superconducting state (i.e., the CSC phase or the FSC phase) for all $\alpha > 0$. It is also clear from Fig. 15 that there is an appreciable broadening of the sub-Gaussians ($\sigma > 0$) compared to the delta function distribution implicit in the strong-coupling limit ($\sigma \to 0$).

We next consider the implications of a finite σ on the correlation function $G_{\Delta\theta}(\tau; q)$. Assuming Eq. (B1), we calculate

$$\langle e^{iq(\Delta\theta_\tau - \Delta\theta_0)} \rangle = e^{-\frac{1}{2}\sigma^2 \kappa q^2} \sum_{s=-\infty}^{\infty} e^{-\frac{1}{2}\sigma_G^2 (q - s/\kappa)^2}, \tag{B3}$$

where $\kappa = \sigma_G^2/(\sigma_G^2 + \sigma^2)$. The sum over n has been traded for an integral at the cost of introducing an integer Poisson summation variable s. The n variable is subsequently integrated out. Comparing with Eq. (12) in Ref. 19, the broadening of the sub-Gaussians has introduced an overall prefactor and a multiplicative adjustment of the Poisson summation variable. The strong-coupling result is easily recovered in the limit $\sigma \to 0$. In the limit $\tau \to \infty$, the term with the slowest decay is dominant, hence the sum may be substituted by the term with the smallest $(q - s/\kappa)^2$. For a logarithmically diverging σ_G, we also have $\kappa \to 1$, meaning that Eq. (B3) is a scale-free power law in this limit.

In Fig. 16, we show a plot of $G_{\Delta\theta}(\tau; q = 3/4)$ and the two terms from Eq. (B3) corresponding to $s = 0$ and $s = 1$. We have set σ_G^2 equal to $\mathcal{G}(\tau)$ as measured from the Monte Carlo simulations in order to compare the analytical result Eq. (B3) with the fractional correlation function found numerically. σ is specified from fitting Eq. (B1) to data from Monte Carlo simulations. At short distances the $s = 0$ term is still contributing, but a clear crossover to the dominant $s = 1$ term is visible for larger values of τ. The excellent fit between the curves validates the functional form of the distribution (B1).

It is interesting to compare the behavior presented above with available numerical results for a single resistively shunted Josephson junction. Ref. 11 reports temporal fractional correlation functions in a $(0 + 1)$D system that are power law in much the same way as those in Ref. 19. They also report a logarithmically diverging MSD, but only at the phase boundary. This is in contrast to the results presented in Secs. VI and IV, where we find logarithmic growth as a generic feature of the weak-dissipation phases. Following Ref. 11, it is natural to consider the possibility that a logarithmically diverging MSD is the signature of critical behavior for models

describing Josephson junctions. A logarithmically diverging MSD follows from a logarithmically diverging $\mathcal{G}(\tau)$, and we have shown that the latter generates fractional bond correlators that are algebraically decaying in imaginary time. A possible scenario could be that the increased dimensionality of the problem has damped the fluctuations such that, in contrast to the single junction, the entire weak-dissipation regime features critical temporal correlations of the bond variables. However, we expect such a critical phase to produce divergent susceptibilities of the action. The simulations do not support this scenario and we find nonanalytic χ_S only at the points $\alpha = \alpha_c^{(1),(2)}$. Thus, a power-law form of the temporal fractional bond correlators can not necessarily be ascribed to critical behavior of the system.

[1] A. Schmid, Phys. Rev. Lett. **51**, 1506 (1983).
[2] W. Zwerger, EPL **9**, 421 (1989).
[3] R. Fazio and H. van der Zant, Phys. Rep. **355**, 235 (2001).
[4] G. Refael, E. Demler, Y. Oreg, and D. S. Fisher, Phys. Rev. B **75**, 014522 (2007).
[5] S. E. Korshunov, Zh. Eksp. Teor. Fiz. **95**, 1058 (1989).
[6] P. Goswami and S. Chakravarty, Phys. Rev. B **73**, 094516 (2006).
[7] P. A. Bobbert, R. Fazio, G. Schön, and G. T. Zimanyi, Phys. Rev. B **41**, 4009 (1990).
[8] S. Panyukov and A. Zaikin, Phys. Lett. A **124**, 325 (1987).
[9] S. V. Panyukov and A. D. Zaikin, J. Low Temp. Phys. **75**, 361 (1989).
[10] C. P. Herrero and A. D. Zaikin, Phys. Rev. B **65**, 104516 (2002).
[11] P. Werner and M. Troyer, Phys. Rev. Lett. **95**, 060201 (2005).
[12] P. A. Bobbert, R. Fazio, G. Schön, and A. D. Zaikin, Phys. Rev. B **45**, 2294 (1992).
[13] L. Capriotti, A. Cuccoli, A. Fubini, V. Tognetti, and R. Vaia, Phys. Rev. Lett. **94**, 157001 (2005).
[14] S. Chakravarty, G.-L. Ingold, S. Kivelson, and A. Luther, Phys. Rev. Lett. **56**, 2303 (1986).
[15] S. Chakravarty, G.-L. Ingold, S. Kivelson, and G. Zimanyi, Phys. Rev. B **37**, 3283 (1988).
[16] I. B. Sperstad, E. B. Stiansen, and A. Sudbø, Phys. Rev. B **84**, 180503(R) (2011).
[17] V. Aji and C. M. Varma, Phys. Rev. Lett. **99**, 067003 (2007).
[18] A dissipation kernel differing from the Caldeira-Leggett form has been calculated for coupling of a loop-current order parameter to gapless excitations at the Fermi level of high-T_c cuprates. Namely, it was shown in Ref. 49 that the mechanism leading to dissipation is scattering of the bosonic order parameter off gapless fermionic particle-hole excitations at the Fermi level. This produces Landau damping of the form ω/q, which is a manifestly nonlocal dissipation kernel. For an alternative formulation of the coupling of the bosonic order parameter to gapless fermions on the Fermi surface, see Ref. 50.
[19] S. Tewari, J. Toner, and S. Chakravarty, Phys. Rev. B **73**, 064503 (2006).
[20] V. Aji and C. M. Varma, Phys. Rev. B **82**, 174501 (2010).
[21] A. O. Caldeira and A. J. Leggett, Ann. Phys. (NY) **149**, 374 (1983).
[22] G. Schön and A. D. Zaikin, Phys. Rep. **198**, 237 (1990).
[23] G. Refael, E. Demler, Y. Oreg, and D. S. Fisher, Phys. Rev. B **68**, 214515 (2003).
[24] E. B. Stiansen, I. B. Sperstad, and A. Sudbø, Phys. Rev. B **83**, 115134 (2011).
[25] S. Tewari, J. Toner, and S. Chakravarty, Phys. Rev. B **72**, 060505(R) (2005).
[26] R. Metzler and J. Klafter, Phys. Rep. **339**, 1 (2000).
[27] P. Werner, G. Refael, and M. Troyer, J. Stat. Mech. (2005) P12003.
[28] P. Werner and M. Troyer, Prog. Theor. Phys. Suppl. **160**, 395 (2005).
[29] K. Hukushima and K. Nemoto, J. Phys. Soc. Jpn. **65**, 1604 (1996).
[30] H. G. Katzgraber, arXiv:0905.1629.
[31] M. Matsumoto and T. Nishimura, ACM Trans. Model. Comput. Simul. **8**, 3 (1998).
[32] A. M. Ferrenberg and R. H. Swendsen, Phys. Rev. Lett. **63**, 1195 (1989).
[33] A. V. Chechkin, R. Gorenflo, and I. M. Sokolov, Phys. Rev. E **66**, 046129 (2002).
[34] H. Weber and P. Minnhagen, Phys. Rev. B **37**, 5986 (1988).
[35] As mentioned in Sec. I B, the limit $\alpha = 0$ is not physical for the model Eq. (3) with noncompact phase variables. Nevertheless, the spatial behavior of the system changes continuously as one (artificially) reduces the parameter α to zero, so the value $\alpha = 0$ of Fig. 7(a) should simply be regarded as the limit of very weak dissipation.
[36] Although not explicitly shown, we observed diffusive ($H = 1/2$) scaling of $W^2_{\Delta\theta}$ for all values of K in the artificial limit $\alpha = 0$. The diffusive behavior of $W^2_{\Delta\theta}$ found at $\alpha = 0$, is replaced by logarithmic scaling for any finite value $0 < \alpha < \alpha_c^{(1),(2)}$.
[37] As a comment relevant to both this section and Sec IV, a fluctuation measure similar to $W^2_{\Delta\theta}$ was calculated in Ref. 10 for a single dissipative Josephson junction. It was suggested that this quantity exhibited a cusp at the localization transition, but later high-quality Monte Carlo simulations revealed a smoothly changing MSD around the critical dissipation strength.[11] Apparently, the α dependence of the MSD is not suitable for locating the critical point in $(0+1)$D. From the kink shown in the inset in Figs. 9 and 3, this is not the case for the spatially extended model considered here. A similar kink in a fluctuation measure may also have been present in previous results for a related $(2+1)$D RSJJA model,[13] but this curve was based on too few points for the feature to be convincingly resolved.
[38] It should be noted that there are stronger finite-size effects in $W^2_{\Delta\theta}$ in the NOR phase than in the CSC phase.
[39] J. A. Hertz, Phys. Rev. B **14**, 1165 (1976).
[40] D. Belitz, T. R. Kirkpatrick, and T. Vojta, Phys. Rev. B **65**, 165112 (2002).
[41] Q. Si, S. Rabello, K. Ingersent, and J. L. Smith, Nature (London) **413**, 804 (2001).
[42] D. Belitz, T. R. Kirkpatrick, and T. Vojta, Rev. Mod. Phys. **77**, 579 (2005).
[43] H. Kleinert, Gauge Fields in Condensed Matter (World Scientific, Singapore, 1989).
[44] A. K. Nguyen and A. Sudbø, Phys. Rev. B **60**, 15307 (1999).

[45] Z. Tešanović, Phys. Rev. B **59**, 6449 (1999).
[46] B. Horovitz, Phys. Rev. B **45**, 12632 (1992).
[47] J. Toner and D. P. DiVincenzo, Phys. Rev. B **41**, 632 (1990).
[48] Although not explicitly shown here, the fractional bond correlators behave qualitatively similar to the site correlators. With a noninteger q, $G_{\Delta\theta}(x;q)$ is zero for all spatial distances while $G_{\Delta\theta}(\tau;q)$ is slowly decaying in imaginary time.
[49] K. Børkje and A. Sudbø, Phys. Rev. B **77**, 092404 (2008).
[50] V. Aji, A. Shekhter, and C. M. Varma, Phys. Rev. B **81**, 064515 (2010).

Paper VI

0–π phase shifts in Josephson junctions as a signature for the $s_{\pm}$-wave pairing state

Physical Review B **80**, 020503(R) (2009)

RAPID COMMUNICATIONS

PHYSICAL REVIEW B **80**, 020503(R) (2009)

0-π phase shifts in Josephson junctions as a signature for the $s_{\pm}$-wave pairing state

Jacob Linder, Iver B. Sperstad, and Asle Sudbø
Department of Physics, Norwegian University of Science and Technology, N-7491 Trondheim, Norway
(Received 23 April 2009; published 2 July 2009)

We investigate Josephson junctions with superconducting ferropnictides, both in the diffusive and ballistic limit. We focus on the proposed $s_{\pm}$-wave state and find that the relative phase shift intrinsic to the $s_{\pm}$-wave state may provide 0-π oscillations in the Josephson current. This feature can be used to discriminate this pairing state from the conventional s-wave symmetry. The 0-π oscillations appear both as a function of the ratio of the interface resistances for each band and, more importantly, as a function of temperature, which greatly aids in their detection.

DOI: 10.1103/PhysRevB.80.020503 PACS number(s): 74.20.Rp, 74.50.+r, 74.70.Dd

The discovery of high-T_c superconductivity in the ferropnictides[1] has triggered an avalanche of investigations (see the reviews[2] and references therein) from a broad range of communities in condensed-matter physics. A crucial issue which remains unresolved is the nature of the superconducting order-parameter (OP) symmetry in ferropnictide superconductors. This topic is particularly intriguing since the ferropnictides feature a multiband Fermi surface where the Cooper pairs may reside.

In order to identify the symmetry of the superconducting OP, several recent experimental studies[3,4] utilized the method of point-contact spectroscopy in order to study the symmetry of the superconducting OP in the ferropnictides. The findings were, however, not easily reconcilable. Using an extended Blonder-Tinkham-Klapwijk (BTK) theory[5] to fit their data, some groups[3] found a zero-bias conductance peak, indicative of a nodal order parameter such as d-wave. However, other groups[4] interpreted their data in terms of one or more nodeless OPs, such as s-wave.

One of the leading candidates for the pairing symmetry is the so-called $s_{\pm}$-wave state proposed in Refs. 6 and 7. This pairing symmetry consists of two s-wave order parameters for the electronlike and holelike Fermi surfaces that differ in sign. Some progress has been made in mapping out the ramifications of the $s_{\pm}$-wave symmetry to quantum transport properties of the ferropnictides.[8–10] For instance, it has been predicted that subgap surface states should appear in the presence of interband scattering.[10] Unfortunately, such subgap surface states are not unique for the $s_{\pm}$-wave state and do not provide unambiguous evidence for this pairing symmetry.

To shed more light on the pairing symmetry in the ferropnictide superconductors, we present results for both the proximity effect and the Josephson current in hybrid structures involving normal-metal elements and superconducting ferropnictides. The motivation for this is that both of these phenomena are expected to produce valuable information about the pairing state in the superconductor. We take into account the intrinsic multiband nature of this material class and include results for the diffusive limit of transport, in contrast to previous theoretical works on these systems.

For Josephson junctions with conventional superconductors (s-wave), it is well known that the supercurrent decays in a monotonous fashion as a function of both temperature and interlayer width, when the material separating the superconductors is nonmagnetic. If the interlayer is ferromagnetic, the current oscillates and goes to zero at certain critical widths and temperatures. This phenomenon is known as 0-π oscillations[11] and serves as a signature of either ferromagnetic correlations or nodal OPs, such as d-wave, present in the Josephson junction.

In this Rapid Communication, we show that the aforementioned prerequisites for 0-π oscillations are rendered unnecessary in the presence of an $s_{\pm}$-wave pairing state. We find that 0-π oscillations may occur in a Josephson junction consisting of a conventional s-wave superconductor and a $s_{\pm}$-wave superconductor separated by a normal (nonmagnetic) interlayer and thus in the complete absence of any ferromagnetic elements or nodal superconducting OPs. This effect is explained in terms of the relative phase shift between the bands in the $s_{\pm}$-wave superconductor and constitutes a signature of the $s_{\pm}$-wave state, which can be probed in experiments. In fact, using such an observation in conjunction with other experiments that report a nodeless OP, ruling out d-wave pairing, would strongly support the realization of a $s_{\pm}$-wave state. Our results are qualitatively independent of the interband scattering strength and are induced solely by the $s_{\pm}$-wave symmetry. This renders our prediction more robust than recent proposals regarding subgap bound states as probes for the $s_{\pm}$-wave state, which rely heavily on substantial interband scattering.

We will employ the quasiclassical theory of superconductivity in form of the Usadel[12] equation and the accompanying Kupriyanov-Lukichev boundary conditions[13] modified for a multiband situation.[14] The quasiclassical approach is justified under the condition that the Fermi energy is much larger than the superconducting gap and the impurity scattering self-energy, which should be a safe assumption for the ferropnictides. The notation and conventions of Ref. 15 will be used in what follows. For equilibrium situations, it suffices to consider the retarded part of the matrix Green's function, $\hat{g}$, which is parametrized conveniently by the quantity θ_{σ}^{N}, $\sigma = \uparrow, \downarrow$. The Green's function satisfies $\hat{g}^2 = \hat{1}$ and consists of entries with $c_{\sigma}^{N} = \cosh(\theta_{\sigma}^{N})$ and $s_{\sigma}^{N} = \sinh(\theta_{\sigma}^{N})$ as measures of the proximity effect induced by the multiband superconductor. In this parametrization, the Usadel equation[12] is obtained as $D_N \partial_x^2 \theta_{\sigma}^{N} + 2i\varepsilon s_{\sigma}^{N} = 0$, where D_N is the diffusion coefficient in the normal metal and ε is the quasiparticle energy. In the superconducting region, we use the bulk Green's functions $\hat{g}_{\lambda}$ (Refs. 11 and 15) for each band as denoted by the

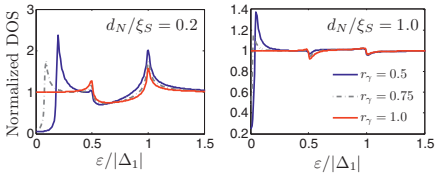

FIG. 1. (Color online) Plot of the DOS at $x=0$ (at the $N|I$ interface) for thin ($d_N/\xi_S=0.2$) and thick ($d_N/\xi_S=1.0$) normal-metal regions. We have set $r_\Delta=0.5$ and considered several values of r_γ.

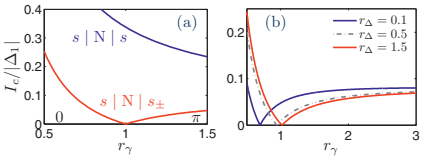

FIG. 2. (Color online) (a) Plot of the critical current for an s-wave$|N|s$-wave and s-wave$|N|s_\pm$-wave junction, using $r_\Delta=1.0$ and $|\Delta_s/\Delta_1|=1.0$. (b) Plot of the critical current in the s-wave$|N|s_\pm$-wave case, using $|\Delta_s/\Delta_1|=0.5$. In both (a) and (b), we have set $d_N/\xi_S=1.0$.

index $\lambda=(1,2)$, with belonging gaps $\Delta_\lambda=|\Delta_\lambda|e^{i\varphi_\lambda}$. The unique feature of the $s_\pm$-wave state is that the relative phase between the bands is π, i.e., $\varphi_1=\varphi$ and $\varphi_2=\varphi+\pi$, where φ is the superconducting phase associated with the broken $U(1)$ gauge symmetry.

The Usadel equation must be supplemented with boundary conditions at the interface of the superconducting region. Under the assumption of a low interface transparency, we may employ generalized Kupriyanov-Lukichev boundary conditions that for an $N|s_\pm$-wave interface at $x=d_N$ take the form $d_N\hat{g}_N\partial_x\hat{g}_N|_{x=d_N}=\Sigma_\lambda\frac{1}{\gamma_\lambda}[\hat{g}_N,\hat{g}_\lambda]|_{x=d_N}$ where d_N is the thickness of the normal-metal layer while $\gamma_\lambda=R_B^\lambda/R_N$. Here, R_N is the resistance of the normal-metal region, while R_B^λ is the effective barrier resistance for band λ. At $x=0$, we have $\partial_x\theta_\sigma^N=0$, corresponding to zero outgoing current at the insulating/vacuum interface.

Let us first briefly investigate the full proximity-effect regime in a $N|s_\pm$ junction by solving the Usadel equation numerically with its boundary conditions. The normalized density of states (DOS) reads as $N(\varepsilon)/N_0=\frac{1}{2}\Sigma_\sigma\mathrm{Re}\{c_\sigma^N\}$. There are three parameters that are free to vary in our theory. One is the thickness of the normal-metal layer d_N/ξ_S, where $\xi_S=\sqrt{D_N/|\Delta_1|}$. The two others are the ratio between the gaps and the ratio between the barrier parameters, defined respectively as $r_\Delta=|\Delta_2/\Delta_1|$ and $r_\gamma=\gamma_2/\gamma_1$. In Fig. 1, we contrast the thin junction case $d_N/\xi_S\ll 1$ with a thick junction $d_N/\xi_S=1$ for a representative choice of parameters. We fix $r_\Delta=0.5$ and plot the DOS in the N region at $x=0$ for several values of r_γ, with $\gamma_1=5$ corresponding to a low barrier transparency. There are in general three peaks in the energy-resolved DOS. Two of these peaks pertain to the bulk gaps of the $s_\pm$ superconductor, while the third demarcates the opening of a minigap in the spectrum. This is qualitatively the same as what would be expected for a multiband superconductor with a conventional s-wave symmetry, such as MgB_2.[14]

Therefore, the proximity effect and its impact on the DOS do not appear to provide a unique diagnostic tool in order to distinguish $s_\pm$-wave symmetry from ordinary s-wave symmetry. We thus turn our attention to the Josephson coupling for $s_\pm$-wave superconductors as a possible mean to reveal this symmetry. To this end, we will consider a s-wave$|N|s_\pm$-wave junction, where the s-wave gap is given by $\Delta_s=|\Delta_s|e^{i\varphi_s}$, and assume a weak proximity effect that allows us to linearize the Usadel equation and proceed analytically, facilitating the interpretation of the obtained results. Also, the linearized approach is expected to yield excellent results in the experimentally relevant low-transparency case. The supercurrent is given by $I_J\sim\int_{-\infty}^{\infty}d\varepsilon\,\mathrm{Tr}\{\hat{\rho}_3(\hat{g}\partial_x\hat{g})^K\}$, where $\hat{\rho}_3=\mathrm{diag}(1,1,-1,-1)$ and 'K' denotes the Keldysh component of the Green's function.[11] After solving the Usadel equation, one may insert $\hat{g}$ into the above equation for the supercurrent. We find the following expression for the normalized zero-temperature Josephson current:

$$I_J=I_0\sin\Delta\varphi,\quad I_0=\int_0^\infty d\varepsilon\,\mathrm{Re}\{\mathcal{RL}/[ikd\sin(kd)]\},\quad (1)$$

where $\mathcal{L}=\Sigma_\lambda\delta_\lambda^L\mathcal{F}_\lambda^L/\gamma_\lambda$ and $\mathcal{R}=\Sigma_\lambda\delta_\lambda^R\mathcal{F}_\lambda^R/\gamma_\lambda$. Here, $\Delta\varphi=\varphi-\varphi_s$ is defined as the phase difference between band $\lambda=1$ in the right superconductor and the left superconductor, $k=\sqrt{2i\varepsilon/D_N}$, while $\mathcal{F}_\lambda^{L,R}$ describe the anomalous Green's functions on the left/right side of the junction. These are proportional to the off-diagonal entries in the bulk Green's functions for the superconductors, which have the form $\mathcal{F}_\lambda^{L,R}\propto s_\lambda^{L,R}$. We defined $\delta_{\lambda=1}=1$ and $\delta_{\lambda=2}=-1$. Note that the above expressions are valid for both a s-wave and $s_\pm$-wave superconductor on either side of the diffusive normal metal, which is why we have included the band index also on the left side. In the s-wave case, we have $\mathcal{F}_\lambda=\delta_\lambda\sinh[\mathrm{arctanh}(|\Delta_s|/\varepsilon)]$, while in the $s_\pm$-wave case we have $\mathcal{F}_\lambda=\sinh[\mathrm{arctanh}(|\Delta_\lambda|/\varepsilon)]$.

We now solve Eq. (1) numerically to obtain the Josephson critical current, corresponding to $I_c=|I_0|$, which is the relevant quantity measured experimentally. In Fig. 2(a), we plot the critical current as a function of the ratio between the interface barriers for each band, r_γ, for both s-wave$|N|s$-wave and s-wave$|N|s_\pm$-wave junctions. In the former case, the current decays monotonously as is well known. However, the situation is very different when we replace, say, the right s-wave superconductor with an $s_\pm$-wave state. *The current now displays* 0-π oscillations, even in the complete absence of any ferromagnetic elements. This is very different from the conventional s-wave case, where a ferromagnetic element is required in order to induce the 0-π oscillations. Thus, experimental observation of such 0-π oscillations in a Josephson junction with ferropnictides would provide a strong indication of the presence of an $s_\pm$-wave state. In Fig. 2(b), we give results up to large r_γ for the s-wave$|N|s_\pm$-wave case. As seen, the current saturates after the 0-π oscillation since $r_\gamma\gg 1$ means that one of the band interface transparencies tends to zero and does not contribute to transport.

The appearance of the 0-π oscillations in the current may be understood as follows. The transport of charge in an s-wave$|N|s_{\pm}$-wave junction takes place both through inter- and intraband channels, as may be inferred directly by observing that the product $\mathcal{LR}$ in Eq. (1) produces precisely such terms. Due to the relative phase shift of π between the two bands in the $s_{\pm}$-wave state, these contributions to the critical current have opposite signs. For simplicity, consider the case where all gap magnitudes are equal in the Josephson junction, $|\Delta_\lambda|=|\Delta_s|$, which leads to equal anomalous Green's functions $\mathcal{F}$ on both sides of the junction. We then have $\mathcal{LR}=\mathcal{F}^2(1/\gamma_1^2-1/\gamma_2^2)$ in Eq. (1), which is clearly seen to change sign at $r_\gamma=1$. This does not occur in a conventional s-wave superconductor, where there is no relative phase shift. *The basic mechanism behind the* 0-π oscillations is thus that variations in the barrier parameters γ_λ for the bands will lead to either a dominant contribution between bands with no phase shift relative each other or bands with order parameters that differ in sign.

Let us also consider the ballistic limit to show that the mechanism for the 0-π oscillations persists in clean samples. The only other change in the physical system under consideration is that we replace the normal interlayer with a thin insulating barrier (I), which in the BTK approach introduces the dimensionless barrier strengths Z_λ. In this manner, we can parametrize the relative barrier resistance in an analogous manner as with r_γ in the diffusive case by introducing $r_Z=Z_2/Z_1$. We construct and solve the full 4×4 Bogoliubov–de Gennes equation for the two-band system, where we for generality also include coupling between the two bands parameterized by the interband coupling strength α. This yields in general four current-carrying Andreev bound states (ABSs) $E_\lambda^{\pm}(\Delta\varphi)$. The Josephson current for this s-wave$|I|s_{\pm}$-wave Josephson junction is then found in the ordinary way from[16] $I_J=2e\Sigma_{i=1}^4\frac{\partial E_i}{\partial\varphi}f(E_i)$, where E_i denotes the four ABS and $f(E)$ is the Fermi-Dirac distribution function.

To present an explicit illustration of the mechanism of 0-π oscillations in a $s_{\pm}$ system in the ballistic limit, we proceed analytically for the special case of $\alpha=0$. Here, we have for simplicity assumed that $|\Delta_\lambda|=|\Delta_s|\equiv|\Delta|$. This gives solutions for the ABS on the well known[16] form $E_1^{\pm}=\pm|\Delta|\sqrt{1-D_1\sin^2(\Delta\varphi/2)}$ and $E_2^{\pm}=\pm|\Delta|\sqrt{1-D_2\cos^2(\Delta\varphi/2)}$, with $D_\lambda=4/(4+Z_\lambda^2)$. At $T=0$, the above expression for the Josephson current yields in the tunneling limit $I_J=I_1\sin\varphi$, with $I_1=(D_1-D_2)I_0/4$ and $I_0=2e|\Delta|$. It is obvious that for $Z_2<Z_1$ one will have $I_1<0$, i.e., the system being in the π state, as explained for the diffusive case. As shown in Fig. 3, the crossover point above which the $\lambda=1$ contribution dominates instead is $r_Z=1$. Notice however that the current does not vanish entirely at the crossover point due to a second-harmonic component in the current-phase relation (as shown in the inset of Fig. 3), which dominates close to the transition point. This is demonstrated explicitly by taking the approximation to the next order in the limit $Z_2=Z_1$, which yields $I_J=I_2\sin(2\Delta\varphi)$, with $I_2=-I_0D_\lambda^2/16$. We note that this nonsinusoidality of the current-phase relation was absent in the diffusive case since the linearized Usadel equation corresponds to a first-order approximation in the interface resistance. We also emphasize

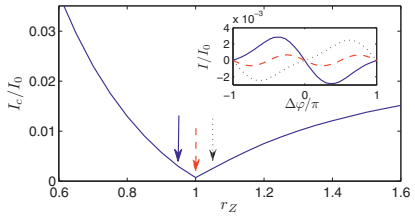

FIG. 3. (Color online) Critical current for a ballistic s-wave$|I|s_{\pm}$-wave Josephson junction as a function of the relative barrier strength r_Z. Interband coupling is neglected, and we have set $Z_1=6$, $T=0$, and $|\Delta_\lambda|=|\Delta_s|$. *Inset:* current-phase relation for selected values of r_Z, as indicated by the arrows in the main figure.

that in this treatment, interband coupling is not essential for the occurrence of the 0-π-transition. However, we have verified numerically that the results of Fig. 3 are qualitatively valid also for $\alpha>0$ so that the predicted experimental signature should be equally distinct for strong interband coupling.

From the analysis above, it is seen that the crucial ingredient for the observation of the 0-π oscillations is having different barrier parameters for each band λ, or alternatively different probabilities for Cooper-pair tunneling. As suggested in Ref. 9, these probabilities may be artificially altered by selecting materials with appropriate Fermi surfaces. Different Fermi-vector mismatches would then lead to different tunneling probabilities. In our case, the size of the Fermi surface of the diffusive normal-metal region could be modified by doping. Thus, whereas 0-π oscillations in S|F|S junctions can be seen as a function of the width d_F of the ferromagnetic layer,[17] necessitating the fabrication of several samples with different widths, the present scenario requires fabrication of several samples with the doping level in the normal metal varying in a systematic way. We note that it was also observed in Ref. 9, although in the context of a superconducting s-wave$|s_{\pm}$-wave$|s$-wave trilayer, that a π junction could be fabricated in a similar manner.

Although the above procedure is in principle feasible, it is very challenging to quantitatively relate the Fermi-vector mismatch directly to the parameter r_γ. However, we find that *the* 0-π oscillations also occur as a function of temperature in the diffusive limit, thus constituting an alternative, and simpler, approach to the recipe sketched above for altering r_γ. Assuming a Bardeen-Cooper-Schrieffer (BCS) temperature dependence for the gaps, with a critical temperature $T_{c,\lambda}=T_c$ for the $s_{\pm}$-wave superconductor and $T_{c,s}$ for the s-wave superconductor,[20] we plot the results in Fig. 4. As seen, 0-π oscillations appear as a function of temperature for a wide range of interface parameters r_γ. For large values of r_Δ, a normal monotonous decay of the critical current is seen. Although the exact relation between r_γ and r_Δ which renders possible the 0-π oscillations is difficult to extract analytically from Eq. (1), the basic mechanism is nevertheless the same as the one explained previously. From Fig. 4, we see that the absence of 0-π oscillations not necessarily rules out that $s_{\pm}$ state, whereas the presence of them rules out the s-wave state.

Finally, we point out that very strong impurity interband

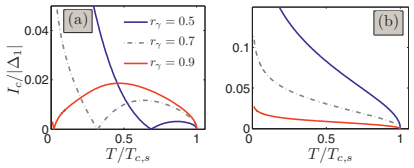

FIG. 4. (Color online) Plot of the critical current as a function of temperature for an s-wave$|N|s_\pm$-wave junction, using $d_N/\xi_S=1.0$ and $|\Delta_s/\Delta_1|=0.5$. In (a), we have $r_\Delta=0.3$ while in (b) $r_\Delta=1.3$.

scattering Γ would eventually suppress the critical temperature for the $s_\pm$ ground state.[18] The difference between the DOS on the hole and electron Fermi pockets would determine how fast the suppression rate increases with Γ as compared to, e.g., a d-wave scenario. For intraband scattering, however, the $s_\pm$ state is protected by Anderson's theorem. In our model, we have incorporated interband scattering only near the interface. A further extension of the model considered here could be to incorporate magnetic correlations in the $s_\pm$ state and also investigate strong interband scattering in the bulk of the superconductor to see how it affects the transport properties,[19] although we expect that they would remain qualitatively the same as reported here since the basic mechanism for the 0-π oscillations would remain intact.

In summary, we have investigated the Josephson coupling properties of junctions with $s_\pm$-wave superconductors. In contrast to previous literature, we have here included results for both the ballistic and diffusive regimes. The relative phase shift of the bands intrinsic for the $s_\pm$-wave state leads to 0-π oscillations in an s-wave$|N|s_\pm$-wave Josephson junction, even in the absence of any ferromagnetic elements. The mechanism behind these oscillations is a competition between the sign-dependent contribution of transport from different bands in the $s_\pm$-wave superconductor to the s-wave superconductor. The 0-π oscillations are seen as a function of temperature, thus vastly facilitating the experimental testing of our predictions compared to methods that involve changing the parameters of the model system. Our results may aid in identifying the possible existence of an $s_\pm$-wave pairing state in the superconducting ferropnictides.

T. Yokoyama and Y. Tanaka are thanked for very useful discussions. J.L. and A.S. were supported by the Research Council of Norway [Grants No. 158518/431 and No. 158547/431 (NANOMAT), and Grant No. 167498/V30 (STORFORSK)].

[1] Y. Kamihara, T. Watanabe, M. Hirano, and H. Hosono, J. Am. Chem. Soc. **130**, 3296 (2008).

[2] I. Mazin and J. Schmalian, arXiv:0901.4790 (unpublished); L. Boeri, O. Dolgov, and A. Golubov, arXiv:0902.0288 (unpublished); T. Chen, S. Huang, Z. Tesanovic, R. Liu, X. Chen, and C. Chien, arXiv:0902.4008 (unpublished).

[3] O. Millo, I. Asulin, O. Yuli, I. Felner, Z. A. Ren, X. L. Shen, G. C. Che, and Z. X. Zhao, Phys. Rev. B **78**, 092505 (2008); L. Shan, Y. Wang, X. Zhu, G. Mu, L. Fang, C. Ren, and H.-H. Wen, EPL **83**, 57004 (2008); K. Yates, L. Cohen, Z. Ren, J. Yang, W. Lu, X. Dong, and Z. Zhao, Supercond. Sci. Technol. **21**, 092003 (2008); P. Samuely, P. Szabo, Z. Pribulova, M. Tillman, S. Budko, and P. Canfield, *ibid.* **22**, 014003 (2009); P. Szabo, Z. Pribulova, G. Pristas, S. Budko, P. Canfield, and P. Samuely, Phys. Rev. B **79**, 012503 (2009); K. Yates, K. Morrison, J. Rodgers, G. Penny, Janwillemgbos, J. Paulattfield, and L. Cohen, New J. Phys. **11**, 025015 (2009).

[4] T. Y. Chen, Z. Tesanovic, R. H. Liu, X. H. Chen, and C. L. Chien, Nature (London) **453**, 1224 (2008); R. Gonnelli, D. Daghero, M. Tortello, G. Ummarino, V. Stepanov, J. Kim, and R. Kremer, Phys. Rev. B **79**, 184526 (2009); R. S. Gonnelli, D. Daghero, M. Tortello, G. A. Ummarino, V. A. Stepanov, R. K. Kremer, J. S. Kim, N. D. Zhigadlo, and J. Karpinski, Physica C **469**, 512 (2009).

[5] G. E. Blonder, M. Tinkham, and T. M. Klapwijk, Phys. Rev. B **25**, 4515 (1982); Y. Tanaka and S. Kashiwaya, Phys. Rev. Lett. **74**, 3451 (1995).

[6] I. I. Mazin, D. J. Singh, M. D. Johannes, and M. H. Du, Phys. Rev. Lett. **101**, 057003 (2008).

[7] K. Seo, B. A. Bernevig, and J. Hu, Phys. Rev. Lett. **101**, 206404 (2008).

[8] J. Linder and A. Sudbø, Phys. Rev. B **79**, 020501(R) (2009).

[9] W. Tsai, D. Yao, B. A. Bernevig, and J. Hu, arXiv:0812.0661 (unpublished).

[10] P. Ghaemi, F. Wang, and A. Vishwanath, Phys. Rev. Lett. **102**, 157002 (2009); A. Golubov, A. Brinkman, O. Dolgov, I. Mazin, and Y. Tanaka, arXiv:0812.5057 (unpublished); M. Araujo and P. Sacramento, Phys. Rev. B **79**, 174529 (2009); S. Onari and Y. Tanaka, *ibid.* **79**, 174526 (2009); D. Wang, Y. Wan, and Q. Wang, arXiv:0901.1419 (unpublished); Y. Nagai and N. Hayashi, Phys. Rev. B **79**, 224508 (2009).

[11] F. S. Bergeret, A. F. Volkov, and K. B. Efetov, Rev. Mod. Phys. **77**, 1321 (2005).

[12] K. Usadel, Phys. Rev. Lett. **25**, 507 (1970).

[13] M. Kupriyanov and V. F. Lukichev, Sov. Phys. JETP **67**, 1163 (1988).

[14] A. Brinkman, A. A. Golubov, and M. Y. Kupriyanov, Phys. Rev. B **69**, 214407 (2004).

[15] J. Linder, T. Yokoyama, and A. Sudbø, Phys. Rev. B **77**, 174514 (2008).

[16] H.-J. Kwon, K. Sengupta, and V. M. Yakovenko, Eur. Phys. J. B **37**, 349 (2003).

[17] T. Kontos, M. Aprili, J. Lesueur, F. Genet, B. Stephanidis, and R. Boursier, Phys. Rev. Lett. **89**, 137007 (2002).

[18] Y. Bang, H. Y. Choi, and H. Won, Phys. Rev. B **79**, 054529 (2009).

[19] V. Stanev, J. Kang, and Z. Tesanovic, Phys. Rev. B **78**, 184509 (2008).

[20] Note that at $T\neq 0$, an additional term $\tanh(\beta\varepsilon/2)$ appears in the integrand of Eq. (1), where $\beta=1/T$.

Paper VII

Quantum transport in ballistic $s_{\pm}$-wave superconductors with interband coupling: conductance spectra, Josephson current, and crossed Andreev reflection

Physical Review B **80**, 144507 (2009)

Quantum transport in ballistic $s_{\pm}$-wave superconductors with interband coupling: Conductance spectra, crossed Andreev reflection, and Josephson current

Iver Bakken Sperstad, Jacob Linder, and Asle Sudbø
Department of Physics, Norwegian University of Science and Technology, N-7491 Trondheim, Norway
(Received 7 August 2009; revised manuscript received 17 September 2009; published 6 October 2009)

We study quantum transport in ballistic $s_{\pm}$-wave superconductors where coupling between the two bands is included and apply our model to three possible probes for detecting the internal phase shift of such a pairing state: tunneling spectroscopy in a N$|s_{\pm}$-wave junction, crossed Andreev reflection in a two-lead N$|s_{\pm}$-wave$|$N system, and Josephson current in a s-wave$|$I$|s_{\pm}$-wave Josephson junction. Whereas the first two probes are insensitive to the superconducting phase in the absence of interband coupling, the Josephson effect is intrinsically phase dependent and is moreover shown to be relatively insensitive to the strength of the interband coupling. Focusing on the Josephson current, we find a 0-π transition as a function of the ratio of effective barrier transparency for the two bands, as well as a similar phase-shift effect as a function of temperature. An essential feature of this $s_{\pm}$-wave model is nonsinusoidality of the current-phase relation and we compute the dependence of the critical current on an external magnetic field, showing how this feature may be experimentally observable for this system. We also comment on the possible experimental detection of the phase-shift effects in $s_{\pm}$-wave superconductors.

DOI: 10.1103/PhysRevB.80.144507 PACS number(s): 74.20.Rp, 74.50.+r, 74.70.Dd

I. INTRODUCTION

During the last few years, multiband superconductivity has again been at the forefront of condensed-matter physics and particularly so after the discovery of high-temperature superconductivity in the family of intrinsically multiband iron-based materials.[1–3] As with all newly discovered superconductors with unconventional behavior, one principal question is to determine the pairing symmetry of the superconductor. In the pnictide superconductors much effort has been devoted to this central issue, so far without entirely conclusive answers. Nevertheless, the leading contender has for some time been $s_{\pm}$-wave pairing,[4] which in its simplest realization for the iron-based superconductors means that the holelike and electronlike Fermi surfaces both host s-wave superconductivity but with opposite sign of the order parameter. (In the past, similar sign-shifted order parameters have also been considered as a candidate pairing state e.g., of high-T_c cuprates.[5])

Distinguishing such a state from an isotropic s-wave pairing state is highly nontrivial since both s-wave and $s_{\pm}$-waves states have the same symmetry and do not have nodes in the order parameter on the Fermi surface. In order to establish conclusively the internal phase shift characterizing a possible $s_{\pm}$-wave state in the iron-based superconductors it is therefore crucial to devise phase-sensitive pairing probes. A large number of proposals for such experiments have been put forth in the literature recently. Theories for multiband tunneling spectroscopy have been developed[6–11] as well as calculations of the surface density of states for a $s_{\pm}$ superconductor.[12,13] In a related context, Andreev bound states (ABS) are often pointed out as possible pairing probes.[14–18] Another class of experiments suggested involves Josephson junctions, both single junctions,[19–23] trijunction loops,[24,25] and also various corner geometries employed for Josephson interferometry.[26,27] Yet another work considered possible signatures in the ac Josephson effect.[28] In addition, we should mention that the Josephson effect for multiband superconductors with sign-shifted order parameters has previously been discussed also in the context of MgB_2 (Ref. 29) and bilayer cuprates.[30]

Of the probes listed above, tunneling spectroscopy is probably the one that is experimentally most accessible (see Refs. 31 and 32 and references therein) and results here are routinely compared with the theory of Blonder, Tinkham and Klapwijk (BTK) for Andreev reflection.[33] Recently, one theoretical work[9] augmented the BTK approach to also incorporate interband scattering in the superconducting region, which was shown to result in interference effects and subgap bound states in the conductance spectra. However, as pointed out soon after,[10] the phenomenological approach employed in Ref. 9 may fail to capture the effect of interband coupling correctly. In this work, we will present an alternative approach of including interband scattering into the BTK framework.

Another probe which has not been considered in the literature so far is crossed Andreev reflection[34] (CAR). This is a process contributing to the nonlocal conductance in a two-lead normal-metal/superconductor junction[35] in which an electron impinging on the superconductor from one of the leads is converted to a hole in the other lead. This phenomenon has previously attracted attention as a possible probe both for ferromagnetic superconductors[36] and noncentrosymmetric superconductors.[37] However, crossed Andreev reflection has not yet, to the best of our knowledge, been considered in the context of the $s_{\pm}$-wave pairing state.

Yet another possible experimental signature, which was first proposed in the context of iron-based superconductors by the present authors in Ref. 38 is 0-π transitions.[39,40] To explain this phenomenon, we draw upon results from Josephson junctions with ferromagnetic elements. For such systems, e.g., a S|F|S junction, the critical current I_c switches sign for given thicknesses d_F of the ferromagnetic interlayer, resulting in nonmonotonous dependence of I_c on d_F. This

phenomenon is ascribed to the junction switching between being a (conventional) 0 junction with zero phase difference across the junction in the ground state and a π junction, which has phase difference π across the junction in the ground state. Furthermore, the critical thicknesses d_F of S|F|S systems are often temperature dependent, which allows for the observation of thermally induced 0-π transitions at $T=T_{0\pi}$ as well as transitions as a function of interlayer width.

The possibility of π junctions consisting of $s_\pm$-wave superconductors has been mentioned previously in some theoretical works[19,24,25,41] but in Ref. 38 we showed that 0-π transitions were possible in a diffusive s-wave|N|$s_\pm$-wave junction both as a function of temperature and as a function of the ratio of interface resistances for each band. The present work is motivated by the question of whether these effects persist in the ballistic limit and we perform a complementary, more comprehensive study of the Josephson effects for a simple model capturing the essential features of a $s_\pm$-wave superconductor with interband coupling. We find that the 0-π transition for varying ratio of interband resistance persists but that nonsinusoidality of the current-phase relation is significant for the present case. For varying temperature we find a somewhat weaker phase-shift effect, which we will relate to the more clear-cut 0-π transition reported for the diffusive case. These results for the temperature dependence of the Josephson current can be compared with the nonmonotonous Josephson current between a multigap and a single-gap superconductor previously obtained by Agterberg *et al.*[29]

The outline of this work is as follows. In Sec. II we present the theoretical framework that is employed to obtain our results. This framework will then be applied first to tunneling spectroscopy of a N|$s_\pm$-wave structure in Sec. III A, after which we will turn to the study of crossed Andreev reflection in a N|$s_\pm$-wave|N junction in Sec. III B. The Josephson junction, to which we will devote the largest share of attention, will be treated in Sec. III C. The three experimental setups are shown schematically in Fig. 1. Some aspects of our model and the possible physical realization of the effects found here are discussed in Sec. IV, and we conclude the present work in Sec. V.

II. THEORY

We consider the Bogoliubov-de Gennes (BdG) equations for a two-band superconductor with dispersions $\varepsilon_{\boldsymbol{k},\lambda}$ measured from the Fermi level E_F and gaps Δ_λ, $\lambda=\{1,2\}$, which read

$$\begin{pmatrix} \hat{H}_1 & \hat{0} \\ \hat{0} & \hat{H}_2 \end{pmatrix}\begin{pmatrix} \psi_1 \\ \psi_2 \end{pmatrix} = E\begin{pmatrix} \psi_1 \\ \psi_2 \end{pmatrix}, \quad \hat{H}_\lambda = \begin{pmatrix} \varepsilon_{\boldsymbol{k},\lambda} & \Delta_\lambda \\ \Delta_\lambda^* & -\varepsilon_{\boldsymbol{k},\lambda} \end{pmatrix}. \quad (1)$$

Above, we have used a fermion basis

$$\Psi_{\boldsymbol{k}} = [\eta_{1,\boldsymbol{k}}^\dagger, \eta_{1,-\boldsymbol{k}}, \eta_{2,\boldsymbol{k}}^\dagger, \eta_{2,-\boldsymbol{k}}], \quad (2)$$

where $\eta_{\lambda,\boldsymbol{k}}$ are fermion operators for band λ. Considering here positive excitation energies $E>0$, the solution for the wave functions ψ_λ is obtained as a generalized BCS expression,

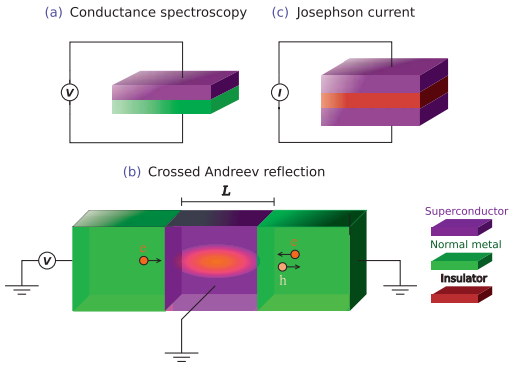

FIG. 1. (Color online) Schematic drawing of the systems under consideration in this work: (a) the model of N|$s_\pm$-wave junction for tunneling spectroscopy as studied in Sec. III A, (b) the model of the two-lead N|$s_\pm$-wave|N junction for the study of crossed Andreev reflection in Sec. III B, and (c) the model of the s-wave|I|$s_\pm$-wave Josephson junction considered in Sec. III C. For system (b), we have illustrated how an electron in the left-hand lead is converted to a hole in the right-hand lead by the formation (together with a electron from the right-hand lead) of a Cooper pair in the superconducting interlayer.

$$\psi_\lambda = \left\{ \begin{pmatrix} u_\lambda \\ v_\lambda e^{-i\phi_\lambda} \end{pmatrix}, \begin{pmatrix} v_\lambda e^{i\phi_\lambda} \\ u_\lambda \end{pmatrix} \right\}, \quad (3)$$

where the coherence functions are

$$u_\lambda^2 = 1 - v_\lambda^2 = \frac{1}{2}(1 + \sqrt{E^2 - |\Delta_\lambda|^2}/E) \quad (4)$$

while the phases ϕ_λ correspond to the broken U(1) gauge symmetry of the superconducting state. For the $s_\pm$ state, we have $\phi_1 - \phi_2 = \pi$. Note that in Eq. (1), no assumptions have been made about the pairing mechanism responsible for the presence of energy gaps Δ_λ in our model nor of the origin of a possible internal phase shift. Our motivation in this work is merely to investigate the experimental consequences of such a phase shift, when present.

In order to capture interference effects between the bands, it is important to consider carefully the boundary conditions in the presence of interband coupling. The above scenario corresponds however to a two-band superconductor with no explicit coupling between the bands. [Once again, since we make no assumptions on the pairing mechanism, the gaps of the two bands in Eq. (1) might be implicitly coupled through two-particle scattering processes, although whether or not this would be the case in a microscopic theory will have no consequences for the present model.] Hopping between the bands will be taken into account by adding a single-particle hopping term $H_{\rm hop}$ to the Hamiltonian,

$$H_{\rm hop} = \alpha \int d\boldsymbol{r}[\eta_1(\boldsymbol{r})\eta_2^\dagger(\boldsymbol{r}) + \eta_2(\boldsymbol{r})\eta_1^\dagger(\boldsymbol{r})], \quad (5)$$

where $\eta(\boldsymbol{r})$ are fermion field operators in real space while α

denotes the hopping parameter. Upon including the standard delta-function barrier potential V_0 at an interface, one may then write down the full BdG equations in the system. Let us, to be definite, consider an $\mathrm{N}|s_{\pm}$ junction, where the superconductor occupies the half space $x>0$. We then have $\hat{H}\Psi = E\Psi$, where

$$\hat{H} = \begin{pmatrix} \varepsilon_{k,1} + V_0\delta(x) & \Delta_1\Theta(x) & \alpha\delta(x) & 0 \\ \Delta_1^*\Theta(x) & -\varepsilon_{k,1} - V_0\delta(x) & 0 & -\alpha\delta(x) \\ \alpha\delta(x) & 0 & \varepsilon_{k,2} + V_0\delta(x) & \Delta_2\Theta(x) \\ 0 & -\alpha\delta(x) & \Delta_2^*\Theta(x) & -\varepsilon_{k,2} - V_0\delta(x) \end{pmatrix}. \tag{6}$$

It is seen that the two bands couple through the interface scattering as long as $\alpha \neq 0$, in a simple model which nevertheless should be able to capture the main qualitative effects.

Before turning to applications of this theory, we state the resulting boundary conditions for the $\mathrm{N}|s_{\pm}$ junction. For an incoming electron from band $\lambda' = 1$ on the N side ($x \leq 0$), we write the wave function as

$$\psi_N = [1,0,0,0](e^{ikx} + r_1 e^{-ikx}) + r_1^A[0,1,0,0]e^{ikx} + r_2[0,0,1,0]e^{-ikx} + r_2^A[0,0,0,1]e^{ikx}, \tag{7}$$

where $k = k_{\mathrm{F}}$. Here and in what follows, we assume that the Fermi level E_{F} is much larger than (Δ_λ, E), such that the wave vectors simply read $k_{\mathrm{F}} = \sqrt{2mE_{\mathrm{F}}}$. We also take E_{F} to be the same everywhere in the system since the effect of any Fermi wave-vector mismatch (FWVM) can be accounted for by adjusting the barrier transparency. Note that although the formalism used in Eq. (7) imposes the multiband basis also on the normal-metal wave function, this does not necessarily imply that the normal metal has two physically distinct bands.

For an incoming electron from band $\lambda' = 2$, the N-side wave function is simply obtained by letting $[1,0,0,0]e^{ikx}$ go to $[0,0,1,0]e^{ikx}$ in Eq. (7). Here, $\{r_\lambda, r_\lambda^A\}$ are the normal and Andreev reflection scattering coefficients for band λ. We let the wave function on the superconducting side ($x>0$) be unspecified for the moment. The general boundary conditions can then found from Eq. (6) as

$$\psi_N(x=0) = \psi_S(x=0),$$

$$(\partial_x\psi_S - \partial_x\psi_N)|_{x=0} = 2m[V_0\ \mathrm{diag}(\hat{1},\hat{1}) + \alpha\ \mathrm{offdiag}(\hat{1},\hat{1})]\psi_N, \tag{8}$$

where $\hat{1}$ is the 2×2 unit matrix and diag and offdiag denote diagonal and off-diagonal 4×4 block matrices in which these unit matrices are embedded. At this point we also introduce two dimensionless parameters characterizing the system, namely, the barrier strength $Z = 2mV_0/k$ and the interband coupling strength $\tilde{\alpha} = 2m\alpha/k$.

III. RESULTS

A. Conductance spectra

As a first application of our model, we calculate the conductance of a $\mathrm{N}|s_{\pm}$-wave junction and compare it to that of its s-wave counterpart. This was also done in Ref. 9 but in contrast to their approach, we construct our wave functions and boundary conditions from the full 4×4 BdG equations, as required for a multiband scenario. In this case, the wave function on the superconducting side reads

$$\psi_S = s_1[u_1, v_1 e^{-i\phi_1}, 0, 0]e^{ikx} + t_1[v_1 e^{i\phi_1}, u_1, 0, 0]e^{-ikx} + s_2[0,0,u_2,v_2 e^{-i\phi_2}]e^{ikx} + t_2[0,0,v_2 e^{i\phi_2}, u_2]e^{-ikx}, \tag{9}$$

with $\{s_\lambda, t_\lambda\}$ being the transmission coefficients for band λ. We will use the gauge $\phi_1 = 0$ and make explicit use of the internal phase shift by writing $e^{i(\phi_1-\phi_2)} \equiv \delta = \pm 1$ for the superconductor being a two-band s-wave superconductor or a $s_{\pm}$-wave superconductor, respectively. For the normal-metal side, we use ψ_N from Eq. (7). We can then solve Eqs. (8) for the given wave functions but as the resulting expressions for $\{r_\lambda, r_\lambda^A, s_\lambda, t_\lambda\}$ do not allow a simple interpretation in our case, we give the solution in Appendix A.

To illustrate the influence of the interband coupling on quantum transport, we have plotted in Fig. 2 the probabilities of the various reflection processes for an incoming electron from band $\lambda' = 1$ for the case of a transparent interface. For decoupled bands, all electrons are Andreev reflected into the same band (for subgap energies) and it is shown how this situation is altered for $\alpha > 0$ in a different manner for a $s_{\pm}$-wave superconductor and a two-band s-wave superconductor. The difference between the s-wave and $s_{\pm}$-wave cases is reduced for increasing Z relative to $\tilde{\alpha}$, and $|r_2|^2$ and $|r_2^A|^2$ are in general decreased by increasing Z and increased by increasing $\tilde{\alpha}$. Interband scattering also effectively acts to reduce the interface transparency, although less so for the $s_{\pm}$ state. Apart from these general relations, the dependence of the probabilities on the coupling $\tilde{\alpha}$ is by no means trivial and we do not attempt to give any further physical interpretation of this parameter.

The conductance for a two-band superconductor normalized to the normal-state conductance G_0 may, within the BTK formalism, be given as

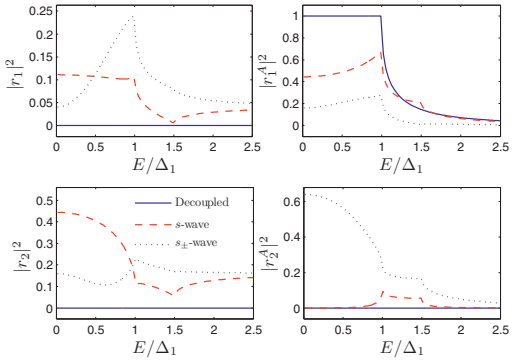

FIG. 2. (Color online) Comparison of the probabilities of the reflection processes in a N$|s_{\pm}$-wave junction and a two-band N$|s$-wave junction as described in the text. We have chosen zero barrier strength, $Z=0$, and gap ratio $r_{\Delta}=1.5$. We have used a value $\tilde{\alpha}=1$ for the interband coupling (for the s-wave and $s_{\pm}$-wave cases) while for the decoupled case we have $\tilde{\alpha}=0$.

$$G/G_0 = \frac{1}{2F}\sum_{\lambda'} G_{\lambda'}, \tag{10}$$

with $G'_{\lambda}=1+|r_1^A|^2+|r_2^A|^2-|r_1|^2-|r_2|^2$ for incoming electron in band λ' (see Appendix A) and $F=1-|r_1|^2$ where the coefficient is evaluated for $|\Delta_1|=|\Delta_2|=0$.

In panel (a) of Fig. 3 we have plotted representative results for the conductance spectra for different values of the interband coupling. We have chosen the ratio between the gaps somewhat arbitrarily as $r_{\Delta}=|\Delta_2|/\Delta_1=1.5$ and have included the limiting case of $\tilde{\alpha}=0$, which here simply corresponds to the well-known BTK result with a double gap structure. Furthermore, for values $\tilde{\alpha}>Z$ when Z is small, the interband coupling enforces the formation of subgap peaks close to the gap edge which are damped and shifted to lower energies for decreasing $\tilde{\alpha}$. This feature becomes more prominent when $r_{\Delta}\to 1$ (not shown), which makes it observable also for larger Z, although also then in a restricted region of parameter space. As shown in panel (b) of Fig. 3, no features of this kind appear in the corresponding model without an internal phase shift in the superconductor. In the conductance spectra of our model, we do not find the very strong low-energy conductance peaks reported in Ref. 9, but rather features more reminiscent of those of Ref. 10, which may be reasonable since their approach was also based on the full BdG equations.

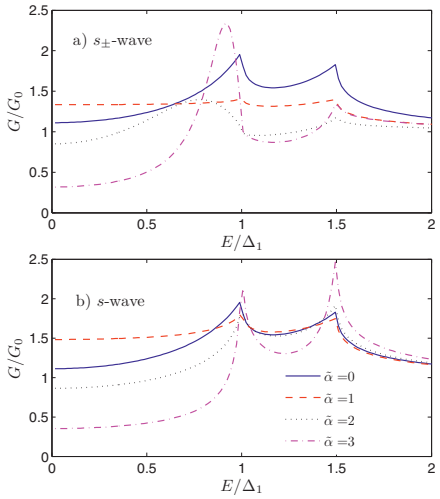

FIG. 3. (Color online) (a) Conductance for a N$|s_{\pm}$-wave junction and (b) a two-band N$|s$-wave junction for various strengths of interband coupling $\tilde{\alpha}$ normalized on its normal-state value, where we have set $Z=1$ and $r_{\Delta}=1.5$.

B. Crossed Andreev reflection

One of the most attractive prospects of CAR is as a realization of nonlocally correlated electron states, see, e.g., Ref. 42. The CAR process is however often masked by the competing process of elastic cotunneling (EC) and it is therefore interesting to search for situations in which CAR dominates. In this section, we investigate how the internal phase difference of the $s_{\pm}$-wave state alters the nonlocal conductance.

For the left-hand side lead ($x<0$), we will use the same normal region wave function ($\psi_N \to \psi_L$) as in Eq. (7) and for the right-hand side ($x>L$) lead we introduce

$$\psi_R = t_1[1,0,0,0]e^{ikx} + t_1^A[0,1,0,0]e^{-ikx} + t_2[0,0,1,0]e^{ikx} + t_2^A[0,0,0,1]e^{-ikx}. \tag{11}$$

For the superconducting interlayer ($0<x<L$), we now have to rewrite the wave function of Eq. (9) into

$$\begin{aligned}\psi_S = {} & (s_1 e^{iq_1^+ x} + s_2 e^{-iq_1^+ x})[u_1, v_1, 0, 0] \\ & + (s_3 e^{iq_1^- x} + s_4 e^{-iq_1^- x})[v_1, u_1, 0, 0] \\ & + (p_1 e^{iq_2^+ x} + p_2 e^{-iq_2^+ x})[0, 0, u_2, \delta v_2] \\ & + (p_3 e^{iq_2^- x} + p_4 e^{-iq_2^- x})[0, 0, \delta v_2, u_2],\end{aligned} \tag{12}$$

where we have introduced the wave vectors

$$q_{\lambda}^{\pm} = k_F\sqrt{1 \pm \sqrt{E^2 - \Delta_{\lambda}^2}/E_F}, \tag{13}$$

for electronlike and holelike quasiparticles, respectively. In the normal-metal regions we can to a good approximation assume equal and constant wave vectors $k=k_F$. In our calculations we have defined the Fermi energy by the value $E_F/\Delta_1=10^4$. We then apply the boundary conditions of Eq. (8) to the two interfaces at $x=0$ and $x=L$, which results in 16 equations in the variables $\{r_{\lambda}, r_{\lambda}^A, t_{\lambda}, t_{\lambda}^A, s_i, p_i\}$, which are solved numerically.

Since it would have no physical meaning to measure the signal for the (virtual) normal-metal bands λ' separately, we choose to consider the average process probabilities

$$P_{EC} = \frac{1}{2}\sum_{\lambda'}(|t_1|^2 + |t_2|^2), \tag{14}$$

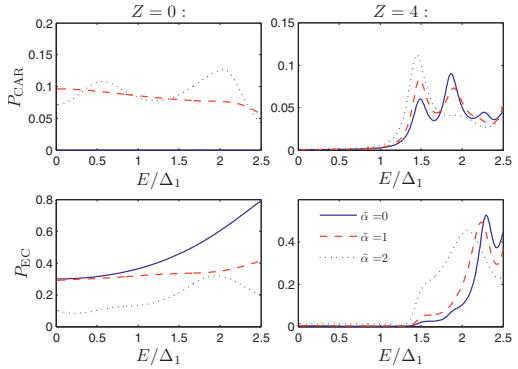

FIG. 4. (Color online) Nonlocal conductance through a N|$s_{\pm}$-wave|N junction for a relatively thin superconducting interlayer, $L=2\times10^4k_F^{-1}$, and for $r_\Delta=1.5$. The upper panels show the probability measure for crossed Andreev reflection while the lower panels show for elastic cotunneling. We have used barrier strengths $Z=0$ (left) and $Z=4$ (right), and a number of values for the interband coupling $\tilde{\alpha}$.

$$P_{\mathrm{CAR}} = \frac{1}{2}\sum_{\lambda'}(|t_1^A|^2 + |t_2^A|^2), \tag{15}$$

as the measure of nonlocal conductance, where $\Sigma_{\lambda'}$ again denotes summing over incoming electron bands.

The nonlocal conductance is then proportional to $P_{\mathrm{EC}} - P_{\mathrm{CAR}}$ and we show the result for its separate contributions in Figs. 4 and 5. As is expected for the components to the nonlocal conductance, it exhibits oscillations both as a function of energy and of the lead separation L, with decaying subgap contributions for increasing L.

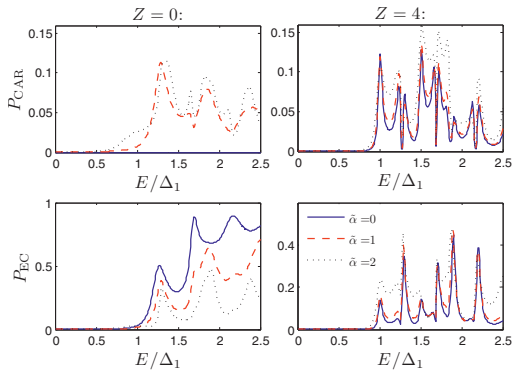

FIG. 5. (Color online) Nonlocal conductance through a N|$s_{\pm}$-wave|N junction for a relatively thick superconducting interlayer, $L=8\times10^4k_F^{-1}$, and for $r_\Delta=1.5$. The upper panels show the probability for crossed Andreev reflection while the lower panels show the probability for elastic cotunneling. We have used barrier strengths $Z=0$ (left) and $Z=4$ (right), and a number of values for the interband coupling $\tilde{\alpha}$.

It is seen that for high transparency, interband coupling facilitates the CAR process with respect to EC, a result which may be readily explained, since the coupling acts as an effective scattering barrier. Recall that for zero interface resistance (and no FWVM or spin polarization), the CAR process is completely absent. This result seems to be somewhat stronger for a $s_{\pm}$-wave superconductor than for a two-band s-wave superconductor (not shown) but P_{CAR} is never significantly larger than P_{EC}. All in all, there are only minor qualitative differences to be found for the $s_{\pm}$-wave state when compared to a more conventional s-wave state and we have therefore not included results for the latter here.

C. Josephson current

We now turn our attention to the Josephson coupling between two superconductors in a S|I|S junction with multiple bands. Below, we shall first consider the case where the right superconductor is $s_{\pm}$ wave while the left superconductor is single-band s wave, with order parameter $\Delta_s=|\Delta_s|\exp\phi_s$. The strategy is to calculate analytically the Andreev bound states at the interface, which carry the Josephson current. These states are found by using the boundary conditions Eq. (8) for the wave functions in each of the superconducting regions. However, since we will find that the interesting physics stems from allowing different band transmission, we let $V_0\ \mathrm{diag}(\hat{1},\hat{1}) \to \hat{V}=\mathrm{diag}(V_1,V_1,V_2,V_2)$. For later reference, we also define $r_Z=Z_2/Z_1=V_2/V_1$ as the ratio between the effective barrier strengths for the two bands; the motivation will be discussed in Sec. IV. Using an alternative parameterization to that in Sec. III A, we write the wave function for the left-hand side superconductor as

$$\begin{aligned}\psi_L = {} & s_1[1,e^{i\beta_s},0,0]e^{-ikx} + s_2[e^{i\beta_s},1,0,0]e^{ikx} \\ & + s_3[0,0,1,e^{i\beta_s}]e^{-ikx} + s_4[0,0,e^{i\beta_s},1]e^{ikx}\end{aligned} \tag{16}$$

while we for the right superconducting region have

$$\begin{aligned}\psi_R = {} & t_1[1,e^{i(\beta_1-\varphi)},0,0]e^{ikx} + t_2[e^{i(\beta_1+\varphi)},1,0,0]e^{-ikx} \\ & + t_3[0,0,1,\delta e^{i(\beta_2-\varphi)}]e^{ikx} + t_4[0,0,\delta e^{i(\beta_2+\varphi)},1]e^{-ikx},\end{aligned} \tag{17}$$

where $\beta_s=\arccos(E/|\Delta_s|)$ and $\beta_\lambda=\arccos(E/|\Delta_\lambda|)$. The gauge-invariant phase difference between the two superconductors has been defined as $\varphi=\phi_1-\phi_s$.

Setting up the boundary conditions of Eq. (8) yields a system of equations on the form

$$\Lambda\mathbf{t} = \mathbf{0}, \tag{18}$$

where $\mathbf{t}=\{s_1^L,t_1^L,s_2^L,t_2^L,s_1^R,t_1^R,s_2^R,t_2^R\}$ and Λ is a 8×8 matrix. The Andreev bound states are found by requiring a nontrivial solution for the system, $\det(\Lambda)=0$, which in general results in four energy states $E_\lambda^{\pm}(\varphi)$. The Josephson current is found in the ordinary way by[43]

$$I = 2e\sum_{i=1}^{4}\frac{\partial E_i}{\partial\varphi}f(E_i), \tag{19}$$

where E_i denotes the four ABS and $f(E)$ is the Fermi-Dirac distribution function. We will define the critical current I_c as

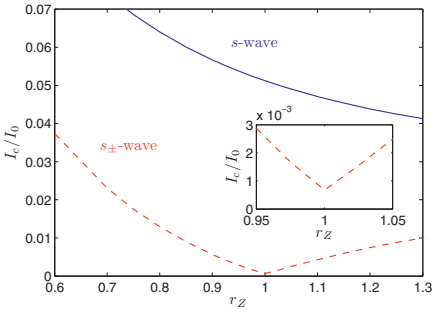

FIG. 6. (Color online) Critical current for a s-wave$|\mathrm{I}|s_{\pm}$-wave Josephson junction as a function of the ratio r_Z between the effective barrier strength of band 2 and band 1. There is no interband coupling ($\tilde{\alpha}=0$) and we have set $Z_1=6$ and $T=0$. Also shown is the critical current in the case that the right-hand side is a (two-band) s-wave superconductor.

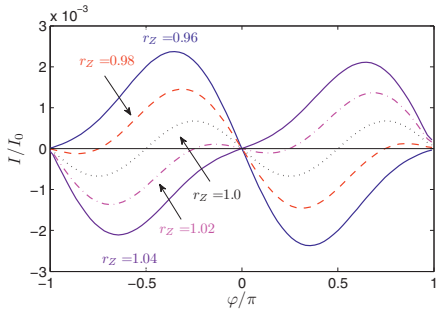

FIG. 7. (Color online) Current-phase relation for a s-wave$|\mathrm{I}|s_{\pm}$-wave Josephson junction with zero interband coupling ($\tilde{\alpha}=0$), with $Z=6$ and $T=0$.

the maximal current allowed by the current-phase relation for a given set of parameters, $I_c=\max\{I(\varphi)\}$. We also introduce the quantity $I_0=2e|\Delta_1|$ used for normalization of the current.

1. 0-π phase shifts for varying barrier strengths: The case of equal gap magnitudes

Before investigating the temperature dependence of the critical current, we will consider the limit $T\to 0$. Our main results in this section is the observation of a 0-π transition in the Josephson current for varying the barrier strength ratio r_Z, as shown in Fig. 6. For a s-wave$|\mathrm{I}|s_{\pm}$-wave Josephson junction this can be understood in a very simple manner as the competition between the $\lambda=1$ and the $\lambda=2$ band components of the current; the band with order parameter $\Delta_1=|\Delta|e^{i\phi_1}$ will favor the conventional 0 junction whereas at the same time the other band with $\Delta_2=-|\Delta|e^{i\phi_1}$ will favor a π junction. Here, we have for simplicity assumed that $|\Delta_\lambda|=|\Delta_s|\equiv|\Delta|$. To show this mechanism explicitly we proceed analytically in the limit of $\tilde{\alpha}=0$ and this minimal model also serves as a review of the basic physics involved in a ballistic Josephson junction. Now, the solutions for Eq. (18) can be shown to be

$$E_1^{\pm} = \pm|\Delta|\sqrt{1-D_1\sin^2(\varphi/2)},$$

$$E_2^{\pm} = \pm|\Delta|\sqrt{1-D_2\cos^2(\varphi/2)}, \tag{20}$$

where $D_\lambda=4/(4+Z_\lambda^2)$. $E_1^{\pm}$ are the well-known solutions for a one-band s-wave$|\mathrm{I}|s$-wave junction[43] while $E_2^{\pm}$ are the corresponding solutions for the negative-gap band. Expanding to first order in D_λ and inserting in Eq. (19) yields the Josephson current

$$I = I_1\sin\varphi, \tag{21}$$

where $I_1=(D_1-D_2)I_0/4$. It is obvious that for $Z_2<Z_1$ one will have $D_2>D_1$ and $I_1<0$, i.e., the system being in the π state. As shown in Fig. 6, the crossover point above which the $\lambda=1$ contribution dominates instead is $r_Z=1$. However, inspection shows that the current does not vanish entirely at the crossover point, a fact which is readily explained by going to the second-order expansion of Eq. (20). In the limit $Z_2\to Z_1$ partial cancellation of the two first-order terms then reduces the current to

$$I = I_2\sin(2\varphi), \tag{22}$$

where $I_2=-I_0D_\lambda^2/16$. In other words, the second-harmonic component to the current appears and is dominating close to the transition point. The general nonsinusoidality of the current-phase relation close to the transition point is illustrated in Fig. 7.

Before proceeding, it will be instructive for the subsequent discussion to analyze this current-phase relation a little further. In a region close to $r_Z=1$ (and for relatively large Z), we may write out the approximate Josephson current to be given by the expression

$$I/I_0 = \frac{D_1-D_2}{4}\sin\varphi - \frac{(D_1+D_2)^2}{64}\sin(2\varphi). \tag{23}$$

For a Josephson junction containing a second-harmonic component in the current-phase relation, the ground state needs neither to be a 0 state nor a π state but may instead be a φ state[44,45] with a general equilibrium phase difference φ_0. This ground-state phase can for our case be found as[46]

$$\varphi_0 = \arccos\left[\frac{8(D_1-D_2)}{(D_1+D_2)^2}\right]. \tag{24}$$

This phase value evolves smoothly from $\varphi_0=\pi$ for $r_Z\ll 1$ to $\varphi_0=0$ for $r_Z\gg 1$, passing $\varphi_0=\pi/2$ at $r_Z=1$. For the case of $Z=6$, our model system is a φ junction for an approximate region $r_Z\in(0.97,1.028)$ and we have verified numerically that Eq. (23) is qualitatively a very good approximation also well outside this region. The phase difference which supports the critical current will on the other hand be denoted as φ^* and can in a similar manner be found to evolve from to $-\pi/2$ for the π state at $r_Z\ll 1$ to $\varphi^*=-\pi/4$ for $r_Z=1^-$, where it jumps discontinuously to $\varphi^*=3\pi/4$ for $r_Z=1^+$, from which it again evolves smoothly toward $\pi/2$ for the limiting sinu-

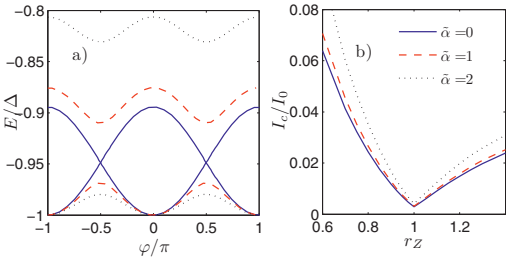

FIG. 8. (Color online) Josephson coupling for a s-wave|I|$s_{\pm}$-wave Josephson junction for various values of interband coupling strength $\tilde{\alpha}$, with (a) dispersion of the two Andreev bound states with $E<0$ shown to the left and (b) critical current as a function of barrier strength ratio r_Z shown to the right. Both results are given for intermediate barrier strength $Z=4$.

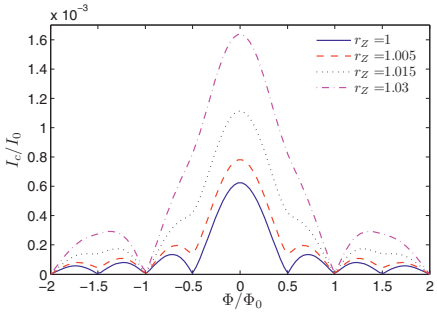

FIG. 9. (Color online) Fraunhofer-type magnetic diffraction pattern for a s-wave|I|$s_{\pm}$-wave junction in an external magnetic field for various values of barrier strength ratio. We have used the parameter values $Z=6$ and $\tilde{\alpha}=0$.

soidal current-phase relation. This phase-shift mechanism will be instrumental to the findings presented in Sec. III C 3.

Next we investigate the general case with nonzero interband coupling. The (numerical) solution for the two lower ABS energies at zero temperature is shown in panel (a) of Fig. 8 for different values of $\tilde{\alpha}$. While the energy states cross each other according to Eq. (20) for $\tilde{\alpha}=0$, they repel each other for nonzero interband coupling, forming a gap in the ABS energy spectrum which increases for increasing $\tilde{\alpha}$. As a trivial observation, this can be understood as a hybridization of the two formerly independent bands, as a finite hopping term introduces off-diagonal matrix elements in λ space. The general properties of the current-phase relation remains the same in spite of the explicit π periodicity of the ABS dispersion and also here this is explained by the partial cancellation of the two ABS contributions. As can be seen from panel (b) of Fig. 8, $\tilde{\alpha}>0$ does not change the behavior of the Josephson current in any dramatic way and neither does the interband coupling influence the position of the 0-π transition point; it remains at $r_Z=1$ for all values of $\tilde{\alpha}$. This motivates us to suppress the interband coupling $\tilde{\alpha}$ in what follows to be able to obtain analytically tractable results.

2. Magnetic field dependence of the critical current

As a simple application of the model described in the preceding section, we now calculate the dependence of the critical current I_c on an external magnetic field H, i.e., the magnetic diffraction pattern. This quantity is experimentally very interesting and experimental results for $I_c(H)$ have recently been presented for iron-based superconductors.[47–49] For our model, we are interested in studying how the magnetic diffraction patterns depend on the relative barrier strength of the two bands, as r_Z is seen as the primary parameter determining the behavior of the system.

In order to include an external magnetic field to our model system, we must define a width W along the z axis and an effective length d_J around $x=0$ over which the magnetic field H along the y axis penetrates the junction. The magnetic flux through the junction is then given by $\Phi=HWd_J$ and we let Φ_0 denote the magnetic-flux quantum. Using the approximation of Eq. (23) for the current-phase relation, we can study our system in the framework of Ref. 46, from which we straightforwardly find the expression

$$I_c(\Phi)=\left[\frac{D_1-D_2}{4}\sin\left(\frac{\pi\Phi}{\Phi_0}\right)\sin\varphi - \frac{(D_1+D_2)^2}{128}\sin\left(\frac{2\pi\Phi}{\Phi_0}\right)\sin(2\varphi)\right]\Big/\left[\frac{\pi\Phi}{\Phi_0}\right]. \quad (25)$$

Evaluating the above expression for the phase difference $\varphi=\varphi^*$ giving the maximum current for the respective r_Z, we obtain the Fraunhofer-type diffraction patterns shown in Fig. 9. The effect of the second harmonic component to the current is evident as a half-integer flux quantum modulation of the critical current which grows more pronounced as $r_Z\to 1$ but whose contribution is vanishing outside the φ-junction region. Although results for $r_Z<1$ are not shown here, these are largely symmetric with respect to $r_Z=1$. We may also note that similar results for the magnetic diffraction were presented Ref. 44, albeit for a completely different system.

3. Temperature dependence of the Josephson current: The case of different gap magnitudes

Motivated by the indications in Ref. 38 that different gap magnitudes are necessary for the occurrence of thermally induced 0-π transitions, we now consider a system for the general case of $\Delta_s\neq\Delta_1\neq|\Delta_2|$. As we showed in Sec. III C 1, interband coupling did not affect the 0-π transitions as a function of r_Z qualitatively, so we will assume in the following that $\alpha=0$, an approximation which moreover makes an analytical approach feasible. Solving the 8×8 system as two decoupled 4×4 systems, we obtain the analytical solution as given by Eqs. (B2) and (B3) in Appendix B. We also refer to this appendix for some more information regarding validity, existence, and uniqueness of this solution.

We will assume BCS-type temperature dependence of the gaps, with the s-wave gap of the left superconductor closing at a temperature $T_{c,s}=\Delta_s(T=0)/1.76$ while both gaps of two-band superconductor on the right-hand sides close simultaneously at $T_{c,\lambda}\equiv T_c=\Delta_1(T=0)/1.76$. We will parameterize

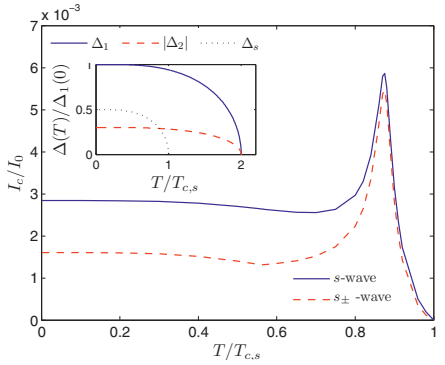

FIG. 10. (Color online) Temperature dependence of the critical current for the parameters $r_s=0.5$ and $r_\Delta=0.3$ with $Z=6$ and $r_Z=1$. Both the results for a two-gap s-wave and a $s_\pm$-wave superconductor are shown. Inset: temperature dependence of gap magnitudes for the same parameter set.

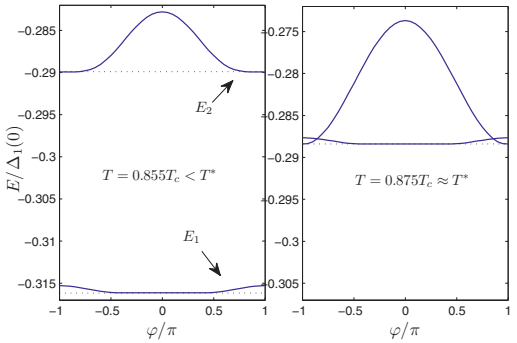

FIG. 11. (Color online) Energy of Andreev bound states E_λ^- for two temperatures close to the point where $|\Delta_2(T)|=\Delta_s(T)$ for $r_s=0.5$ and $r_\Delta=0.3$. Other parameters are $Z=6$ and $r_Z=1$. Shown with dotted lines are the relevant gap edges which the energy states track.

the difference in gap magnitudes by $r_s=\Delta_s/\Delta_1$ and $r_\Delta=|\Delta_2|/\Delta_1$, and will in most of what follows restrict ourselves to $r_s=0.5$ and $r_\Delta=0.3$ as a representative set of gap ratios, although we stress that our results are valid in a much larger portion of parameter space. The resulting temperature dependence of the three superconducting gaps is illustrated in the inset of Fig. 10.

First, we compare the temperature dependence of the critical current both for a $s_\pm$-wave and a two-gap s-wave superconductors in Fig. 10. The most distinctive feature for both these cases is the sharp peak at high temperature. This is exactly the temperature $T=T^*$ for which two of the gaps cross, i.e., $|\Delta_2(T^*)|=\Delta_s(T^*)$ and although this peak is not a signature of the $s_\pm$ state as such since it is present irrespective of the phase difference between the two right-hand side gaps, it would be interesting to disclose the mechanism behind this feature. We turn therefore to the energy dispersion of the ABSs, as shown in Fig. 11 for two temperatures close to the peak in the critical current. First, this illustrate how E_2 tracks the gap edge of $|\Delta_2(T)|$ and E_1 the gap edge of $\Delta_s(T)<\Delta_1(T)$ as the temperature is increased, whereas for $T>T^*$ both states track the smallest of the gaps, i.e., $\Delta_s(T)$. Second, we observe that the energy states are nondispersive for a phase interval centered around $\varphi=0$ and $\varphi=\pm\pi$ for E_1 and E_2, respectively (cf. the discussion in Appendix B) so that in these regions the current contributions of the states vanish. Third, we also observe that the dispersion of E_2 is strongly enhanced at $T=T^*$. This last observation can be understood by glancing at the expression for E_2 in Eq. (B3) for a given T, from which we realize, e.g., by setting $\cos(\varphi/2)=1$ that the bandwidth of the energy state is at its maximum for $\Delta_s=|\Delta_\lambda|$. This is of course exactly the case for $T=T^*$. Moreover, since the contribution from E_1 vanishes for a large φ interval for this temperature, whereas it is nonvanishing for E_2 for all φ in this limiting case of equal gap magnitudes, one does not get the effect of partial cancellation of the two current contributions that was present for lower temperatures and for $\Delta_s=\Delta_1=|\Delta_2|$. We note that although the peak strength for these gap ratios is somewhat extreme, we have verified that similar peaks or bumps persists in a major part of parameter space.

We have concluded that a peak in the critical current cannot be taken as a signature of $s_\pm$ pairing since it results from the energy gap crossing of the right-hand and left-hand superconductors in general. We therefore return to our investigation into possible thermally induced 0-π phase shifts as an unambiguous sign of $s_\pm$-wave pairing, although apparently no such phase shift is present in our results. However, we remember from the analysis of the current-phase relation in Sec. III C 1 that in the presence of a second-harmonic component to the current, a prospective 0-π transition was smeared out into a φ-state region for which the critical current remains nonzero. We therefore consider the current-phase relation for the junction with different gap magnitudes in Fig. 12 for two intermediate temperature values. It is evident that the second-harmonic component dominates, a fact which can be traced back to the vanishing of the ABS contributions for complementary phase intervals as discussed

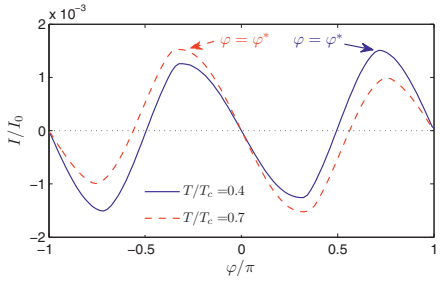

FIG. 12. (Color online) Current-phase relation for a system slightly below $(T/T_c=0.4)$ and slightly above $(T/T_c=0.7)$ the thermally induced phase shift appearing in the Josephson junction with gap ratios $r_s=0.5$ and $r_\Delta=0.3$ with $Z=6$ and $r_Z=1$. The arrows indicate the phase difference supporting the critical current $(I>0)$ for the two temperatures.

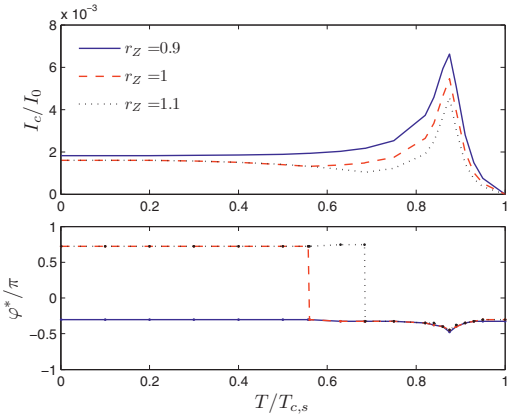

FIG. 13. (Color online) The upper panel shows the temperature dependence of the critical current for the parameters $r_s=0.5$, $r_\Delta=0.3$, and $Z=6$, similarly as in Fig. 10 but for various values of barrier strength ratios r_Z. The lower panel shows the phase difference φ^* supporting the critical current as a function of temperature for the same parameter set as above, illustrating the effect of the (discontinuous) phase shift from $\varphi^*>0$ to $\varphi^*<0$.

above. A related result is that the two maxima shown in Fig. 12 originate predominantly from one of the energy states each. Furthermore, we have seen that the contribution from an ABS is larger the closer the values of the gap magnitudes $\Delta_s(T)$ and $|\Delta_\lambda(T)|$, and as $T\to T^*$, $\Delta_s(T)$, and $|\Delta_2(T)|$ are closing in on each other whereas $\Delta_s(T)$ and $\Delta_1(T)$ are moving apart. Thus the difference in the rate at which the gaps decrease causes the E_1 state to lose dominance to E_2 for increasing temperature. (Since Δ_1 is by far the largest of the gaps, the corresponding ABS dominates for $T=0$ even though Δ_1 is further from Δ_s than is $|\Delta_2|$.)

In Fig. 12 we have also indicated the phase difference φ^* in the current-phase relation that supports the critical current for each of the two temperatures. We now understand that as the dominant contribution to the current changes from E_1 to E_2 with increasing temperature, there must be a jump in this phase value from $\varphi^*>0$ to $\varphi^*<0$ and this jump needs to happen discontinuously at the temperature $T=T_\varphi$ where the two contributions balance [cf. our discussion of $I_c(r_Z)$ in Sec. III C 1]. This is our main result in this section: Although the Josephson junction is at no point in a 0 state or a π state, the system may nevertheless exhibit discernible phase shifts when residing in the φ state. We illustrate this phenomenon for different parameters in Fig. 13 and note that similar behavior was observed for a large set of different gap ratios as long as $r_s\neq 1$ and $r_\Delta\neq 1$, the basic mechanism behind it being different temperature dependence of the different gaps. For the case of a two-gap s-wave state, a phase shift is of course not possible, as the two contributions to the current are then acting cooperatively at all times.

IV. DISCUSSION

Comparing the three systems considered in the previous section, it is easy to see that role played by interband scattering differs fundamentally. On the one hand, tunneling spectroscopy and nonlocal conductance in the absence of interband coupling are not dependent on the relative phase difference of the two $s_{\pm}$-wave order parameters, being merely the sum the contribution from two decoupled s-wave states. On the other hand, phase information enters explicitly into the calculation of the Josephson current so that the interplay between the phases of the two order parameters is evident also for zero interband coupling. Furthermore, it seems that the behavior observed for the Josephson current remains qualitatively unaltered also for finite α. This explains how it seems much more appealing to obtain phase information from multiband superconductors by the use of Josephson junctions than by tunneling spectroscopy and why we will focus our discussion on this experimental probe.

To be able to compare our results for the ballistic limit with our previously obtained results for the diffusive limit in Ref. 38, we now briefly recapitulate this work. Here we employed the quasiclassical Usadel equation[50] to study Josephson coupling in a s-wave|N|$s_{\pm}$-wave junction in the limit of weak proximity effect, an approximation which is warranted for low-transparency interfaces. We showed that for this case, 0-π transitions were observed both as a function of barrier transparency ratio (for arbitrary gap ratios r_s and r_Δ) and as a function of temperature (for some values of the gap ratios). Here, the obtained current-phase relation was purely sinusoidal irrespective of parameter values, a result which can be explained by the fact that the linear Usadel equation corresponds to only a first order approximation in the interface resistance so that no second harmonic terms will appear. Our present results, on the other hand, are valid for arbitrary interface resistance and we see that in this model the second harmonic term plays a crucial role in the behavior of the Josephson junction, which we will discuss more below. We should also remark here on the difference between the diffusive and the ballistic model in that the former in contrast to the latter has a interlayer with finite thickness, which was needed to justify the assumption of weak proximity effect.

The importance of a prospective second harmonic contribution to the Josephson current is natural when we are concerned with 0-π transitions, as this component may dominate when the first harmonic component vanishes close to the transition point. This fact, and the φ-junction behavior that follows, has been pointed out several times in the context of S|F|S junctions.[43,51,52] For our model, the influence of the second harmonic is seen to be particularly prevalent in the case of different gap magnitudes and/or high interface transparency. Before discussing its implication on the thermal phase-shift effect observed here, we consider the case of more conventional 0-π transitions. Most often when establishing 0-π transitions in a Josephson junction, one looks for a sharp cusp in the critical current as a function of the parameter in question, although this method cannot discern which side of the transition represents the 0 state and which represents the π state. By using a rf superconducting quantum interference device (SQUID) configuration[43] one may however measure the jump in the critical phase difference across the junction, which for a sinusoidal current-phase relation would be from $\varphi^*=\pi/2$ to $\varphi^*=-\pi/2$ or vice versa. (Note that it is crucial to this argument that one considers a

current-biased experiment in which a current $I>0$ is forced through the junction, letting the phase difference adjust accordingly.) In the presence of higher harmonics in the current-phase relation the jump from $\varphi^*>0$ to $\varphi^*<0$ or vice versa will in general be different, cf. the transition for varying r_Z, but the principle remains the same. This also holds when the sinusoidal component to the current-phase relation is subdominant for all parameter values, such as for the thermal transitions reported here so that the critical current is not even close to zero at the transition point. Inspecting Fig. 13, one sees that the critical current does in fact reach a minimum at $T=T_\varphi$. Hence this phase-shift effect can be regarded as a degenerate form of 0-π transition which can only be established by SQUID measurement of the critical phase difference. Alternatively, one could of course demonstrate the transition by using SQUID to map out the entire current-phase relation[53] but observing a single phase shift of the critical phase φ^* may be simpler experimentally.

Considering then the peak phenomenon described for the temperature dependence of the critical current, as pointed out earlier, it does not pertain to the $s_\pm$ state per se but is a general result in this framework of two gaps crossing at a certain temperature. In fact, this even holds when none of the two superconductors are multiband superconductors. Experimentally, this can however be understood to be a somewhat artificial situation, as the phenomenon would not occur for a junction consisting of two conventional superconductors with different zero-temperature gap magnitudes because of the universal ratio $2\Delta(0)/T_c=1.76$ for BCS superconductors. And, e.g., high-T_c cuprates, for which the corresponding ratio is larger, the value of $\Delta(0)$ is typically much larger than for any conventional superconductor as well. So although multiband superconductors are not necessary as such, the described situation can occur here much more easily because the superconducting pairing for both bands typically vanish at the same critical temperature, whereas the gap ratio $r_\Delta \neq 1$. This is the situation for the conventional multiband superconductor MgB_2 (Ref. 54) and also seems to be the case for the iron-based superconductors.[32] We should note that similar behavior was not found in the diffusive case[38] but that a finite temperature maximum in the critical current for multiband superconductors was predicted in Ref. 29. In that case, the effect was however ascribed to thermal effects combined with different sign of the two order parameters and is not related to gap crossing irrespective of the order-parameter sign as in our case. Furthermore, in Ref. 29 as well as in our results for the diffusive case, the current-phase relation was implicitly assumed to be purely sinusoidal, which may explain some of the differences with our present results for the ballistic case.

As the dependence of various observable quantities on the barrier strength ratio r_Z was considered frequently throughout Sec. III C, we would now like to present a more thorough rationale for this parameterization. First, we note that although our model assumes the same Fermi wave vector k_F for all bands in all regions of our setups, any FWVM between the different regions is equivalent with an increase in the barrier strength Z. And for different Fermi wave vectors $k_{F,s}$ and $k_{F,\lambda}$ for the s-wave superconductor on the left-hand side and bands 1 and 2 of the $s_\pm$-wave superconductor on the right-hand side in the Josephson junction, respectively, this gives rise to different effective barrier strengths $Z_{1,2}$ for the two bands. This line of thought is illustrated in Fig. 14. The idea of tailoring the experimental setup by the use of materials with appropriate Fermi surfaces was first proposed in Ref. 19 and as we discussed in Ref. 38, it might be possible to produce a series of junction samples with different barrier strength ratios r_Z by varying the doping level in the non-$s_\pm$-wave region of the junction. In this manner, it is conceivable that a 0-π transition can be observed for varying doping level, analogously as to how 0-π transitions are observed S|F|S junctions for varying interlayer thickness. The preceding argument naturally raises the question whether it might be more appropriate with a parameterization in which increased transmittance through the barrier for one of the bands was accompanied by decreased transmittance for the other band. We did nevertheless define r_Z as simply the effective barrier strength ratio because it is hard to tell exactly how the relative transmittance will change with doping level. This does probably also make it quite challenging to experimentally produce the right series of samples to observe 0-π transitions, which is what makes possible observable signatures for varying temperature all the more appealing.

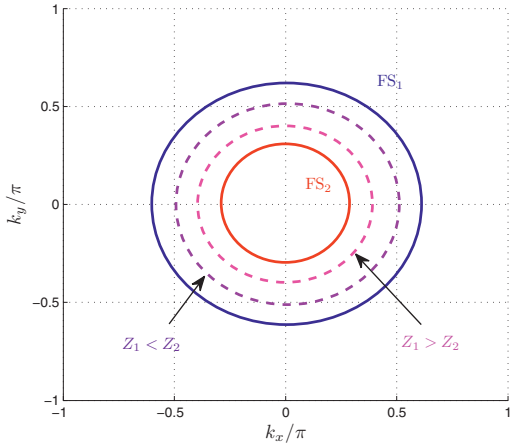

FIG. 14. (Color online) Illustration of the physical interpretation of the barrier strength ratio r_Z. The outer circle represents the Fermi surface of band 1 of the $s_\pm$-wave superconductor and the inner circle represents band 2. The two dashed circles in between represent the Fermi surface of the s-wave superconductor on the left-hand side of the junction for two situations: largest FWVM with respect to band 1 ($Z_1>Z_2$) and largest FWVM with respect to band 2 ($Z_1<Z_2$).

Finally, we discuss our model in context of the recently discovered iron-based superconductors. It should be stressed that our model is to be taken as a minimal model describing the generic behavior of transport phenomena in a two-band $s_\pm$ superconductor but we would like to point out how a more realistic model should take into account the specifics of the iron-based superconductors. First, the BTK approach does not incorporate any details of the band structure and spherical Fermi surfaces are assumed. Second, ours is a two-

band model whereas it has been argued that at least four bands, two holelike (h) and two electronlike (e), should be included to capture the physics behind the superconductivity in these materials.[55] The main effect of their inclusion from the point of view of transport would be the possibility of e-e and h-h interband scattering between nearly degenerate electron and hole bands, respectively. Since these scattering processes would involve no internal phase shift, we expect that the result would be qualitatively similar to the two-band case. This assumption can also be justified by the fact that h-h and e-e scattering processes should be weak in iron-based superconductors compared to the spin-density-wave-enhanced e-h interband processes[56] so that we to a good approximation can consider degenerate e and h bands. Generalization to a nondegenerate four-band model could nevertheless be made in our theory by a straightforward extension of Eqs. (1) and (2), with the inclusion of h-h and e-e interface scattering terms in Eq. (5), although an analytical treatment in that case would be a daunting task. Furthermore, one might have gap magnitudes that were momentum dependent but the approximation of constant s-wave gaps on each of the Fermi surfaces should be reasonable. (The possibility of a d-wave gap or other pairing symmetries with nodes on the Fermi surface is left out of the question in this work since the majority of experiments so far seem to indicate a nodeless gap on the Fermi surface.) Another extension would be to include interband scattering in the bulk of the $s_{\pm}$ superconductor, and not only near the interfaces as in our case, or even more sophisticated models, e.g., including momentum dependence in α.

Regarding the magnetic field dependence of the critical Josephson current described in Sec. III C 2, we may compare our results with the experimental results for iron-based superconductors available at the moment. Inspecting the diffraction pattern in Fig. 3 of Ref. 48, we note an intriguing similarity with ours for $r_Z \gtrsim 1$ in that the critical current is nonvanishing between the diffraction maxima. This may however just as well be the combined result of nonuniform current distribution, trapped flux, and deviation from the small junction limit[57] so that we cannot with any certainty interpret this observation as evidence for a nonsinusoidal current-phase relation nor would nonsinusoidality necessarily imply $s_{\pm}$-wave pairing. (The diffraction patterns obtained in Refs. 47 and 49 can on the other hand not be compared with our results at all, as the experimental situations for those works are different.) It should also be noted that our modeling of the flux threading the junction is rather simplified and does not include effects that may be present in real samples.[57] More importantly, assuming isotropic order parameters and Fermi surfaces, our model is insensitive to how the junction geometry is chosen. We therefore cannot capture the directionality of the electronlike Fermi surfaces in the folded Brillouin zone of iron-based superconductors, which is essential in other proposals for phase-sensitive corner junctions[26,27] and related geometries.

It would also be very interesting to see how robust the results presented here are to the introduction of material impurities. The iron-based superconductors are mostly expected to reside in some intermediate regime of impurity concentration,[2] thereby making neither the ballistic nor the diffusive limit a completely accurate description. In fact, a number of theoretical works[15–18,58,59] depend on a significant influence of impurities to explain the experimental results or to induce experimentally observable bound states. Our study in Ref. 38 was motivated by the fact that the diffusive regime is often the experimentally relevant one. Although taking the diffusive limit may not be strictly valid in this case, the results found might nevertheless capture important features of the real materials. In light of this, it would be very interesting to compare the results obtained in the diffusive and the ballistic limit with calculations performed using the quasiclassical Eilenberger equation,[60] which allows for arbitrary impurity concentration. This would require a multiband extension of the Zaitsev boundary conditions[61] and such a theory has only very recently been developed (see Ref. 62).

V. CONCLUSION

Possible signatures of $s_{\pm}$-wave pairing in tunneling spectroscopy stem mainly from the multigap nature of the superconductor but also from interference effects when the interband coupling is strong relative to the barrier strength. This may lead to subgap peaks in the conductance spectra not present for a corresponding s-wave model, although the appearance of these are relatively sensitive to the parameter values used. Similarly for the nonlocal conductance, it is found to be very difficult to discriminate qualitatively the interference effects of a $s_{\pm}$-wave state from those of a two-band s-wave state. Josephson coupling is on the other hand an intrinsically phase-dependent phenomenon, so it is natural that it is here that we find the most promising signatures of $s_{\pm}$-wave pairing, namely, 0-π transitions or similar phase shifts in a s-wave|I|$s_{\pm}$-wave junction. These are neither dependent on nor considerably affected by the presence of interband coupling. As in the diffusive case,[38] we find 0-π phase shifts as a function of the relative interface transparency, an effect whose detection is possible, in principle, but difficult in practice. We have also shown that a phase-shift effect is present as a function of temperature and although this effect is not as robust as the one reported for the diffusive case, it may nevertheless be possible to observe using a SQUID setup. For both cases, we have shown how the phase shifts can be ascribed to the competition between Andreev bound states for the two bands and how the nonsinusoidality of the Josephson current is essential in the description of the phase shifts. We have also pointed out that this second harmonic component in the current-phase relation may induce half-integer quantum flux modulations in the magnetic diffraction pattern of the Josephson junction. In addition, we found a peak feature in the temperature dependence of the critical current for the case of different gap magnitudes, an effect ascribed to the crossing of two gaps. Although it is hard to tell how relevant the signatures reported in this simplified model are for possible experimental realizations of the $s_{\pm}$-wave pairing state, our results shed more light on the basic mechanisms of transport and their implications in such systems.

ACKNOWLEDGMENTS

J.L. and A.S. were supported by the Research Council of Norway under Grants No. 158518/431 and No. 158547/431 (NANOMAT), and Grant No. 167498/V30 (STORFORSK). A.S. thanks A. Balatsky and Z. Tesanovic for discussions, and acknowledges the hospitality of the Aspen Center for Physics.

APPENDIX A: REFLECTION AND TRANSMISSION COEFFICIENTS FOR THE N$|s_{\pm}$-WAVE JUNCTION

In this section, we give the analytical solution for the reflection and transmission coefficients. We have to consider the two cases $\lambda'=1,2$ for the incoming electron band independently but will use the same symbols for the coefficients to simplify notation. First considering $\lambda'=1$, we have the transmission coefficients given by

$$s_1 = \frac{2iR_2}{\Gamma}, \tag{A1}$$

$$t_1 = \frac{-2iR_1}{\Gamma}, \tag{A2}$$

$$s_2 = \frac{2i\tilde{\alpha}}{\Gamma}\frac{X_{11}R_2 - X_{12}R_1}{\gamma_2}, \tag{A3}$$

$$t_2 = \frac{2i\tilde{\alpha}}{\Gamma}\frac{X_{21}R_2 - X_{22}R_1}{\gamma_2}. \tag{A4}$$

For the case of $\lambda'=2$, the corresponding expressions read

$$s_1 = \frac{2i\tilde{\alpha}}{\Gamma}\frac{X_{11}P_2 - X_{12}P_1}{\gamma_1}, \tag{A5}$$

$$t_1 = \frac{2i\tilde{\alpha}}{\Gamma}\frac{X_{21}P_2 - X_{22}P_1}{\gamma_1}, \tag{A6}$$

$$s_2 = \frac{2iP_2}{\Gamma}, \tag{A7}$$

$$t_2 = \frac{-2iP_1}{\Gamma}. \tag{A8}$$

The reflection coefficients are then found for both cases by insertion into

$$r_1 = -\delta_{\lambda',1} + u_1 s_1 + v_1 t_1, \tag{A9}$$

$$r_1^A = v_1 s_1 + u_1 t_1, \tag{A10}$$

$$r_2 = -\delta_{\lambda',2} + u_2 s_2 + \delta v_2 t_2, \tag{A11}$$

$$r_2^A = \delta v_2 s_2 + u_2 t_2, \tag{A12}$$

where $\delta_{\lambda',i}$ is the Kronecker delta.

The auxiliary quantities used for $\lambda'=1,2$ are given by

$$\Gamma = \gamma_2\gamma_1 + 2\tilde{\alpha}^2(4u_1u_2A - Z^2C_2C_1) + \tilde{\alpha}^4C_1C_2, \tag{A13}$$

$$X_{11} = ZA + 2iu_1u_2, \tag{A14}$$

$$X_{22} = ZA - 2iu_1u_2, \tag{A15}$$

$$X_{12} = ZB + 2iu_2v_1, \tag{A16}$$

$$X_{21} = ZB - 2iu_2v_1, \tag{A17}$$

$$Y_{12} = -ZB + 2\delta iu_1v_2, \tag{A18}$$

$$Y_{21} = -ZB - 2\delta iu_1v_2, \tag{A19}$$

$$R_1 = -Zv_1\gamma_2 + \tilde{\alpha}^2(\delta v_2X_{11} + u_2X_{21}), \tag{A20}$$

$$R_2 = -(2i+Z)u_1\gamma_2 + \tilde{\alpha}^2(\delta v_2X_{12} + u_2X_{22}), \tag{A21}$$

$$P_1 = -\delta Zv_2\gamma_1 + \tilde{\alpha}^2(v_1X_{11} + u_1Y_{21}), \tag{A22}$$

$$P_2 = -(2i+Z)u_2\gamma_1 + \tilde{\alpha}^2(v_1Y_{12} + u_1X_{22}), \tag{A23}$$

where

$$A = u_1u_2 - \delta v_1v_2, \tag{A24}$$

$$B = v_1u_2 - \delta u_1v_2, \tag{A25}$$

$$C_\lambda = v_\lambda^2 - u_\lambda^2, \tag{A26}$$

$$\gamma_\lambda = 4u_\lambda^2 - C_\lambda Z^2. \tag{A27}$$

The expressions above are valid both the $s_{\pm}$-wave and the coupled s-wave cases, where $s_{\pm}$ wave is found by setting $\delta=-1$ and s wave by $\delta=1$.

APPENDIX B: SOLUTION FOR THE ABS ENERGIES FOR DIFFERENT GAP MAGNITUDES

The coefficient matrix Λ for each of the uncoupled bands in the general case of different gap magnitudes yield after some manipulation the equation

$$\Im\mathrm{m}|\Lambda_\lambda| = (4+Z_\lambda^2)\sin(2\beta_s + 2\beta_\lambda) - Z_\lambda^2[\sin 2\beta_s + \sin 2\beta_\lambda] - 8\delta_\lambda \sin(\beta_s+\beta_\lambda)\cos\varphi = 0, \tag{B1}$$

with $\delta_1=1$ and $\delta_2=-1$ for a $s_{\pm}$-wave superconductor. Using that $\cos\beta_\lambda = E/|\Delta_\lambda|$ and $\cos\beta_s = |\Delta_\lambda|/\Delta_s\cos\beta_\lambda$ we can solve the equation for $\cos^2\beta_\lambda$, which produces the solutions

$$E_1^{\pm} = \pm \frac{Z_1^2+2}{Z_1}\sqrt{\frac{A_1\sin^2(\varphi/2)+B_1-\sqrt{C_1\sin^4(\varphi/2)+D_1\sin^2(\varphi/2)+F_1}}{2(Z_1^2+4)}}, \tag{B2}$$

$$E_2^{\pm} = \pm \frac{Z_2^2+2}{Z_2}\sqrt{\frac{A_2\cos^2(\varphi/2)+B_2-\sqrt{C_2\cos^4(\varphi/2)+D_2\cos^2(\varphi/2)+F_2}}{2(Z_2^2+4)}}, \tag{B3}$$

in addition to several other unphysical solutions. The auxiliary quantities here are given by

$$A_\lambda = 2K_\lambda, \tag{B4}$$

$$B_\lambda = \Delta_s^2 + |\Delta_\lambda|^2 - K_\lambda, \tag{B5}$$

$$C_\lambda = 8K_\lambda\Delta_s|\Delta_\lambda|, \tag{B6}$$

$$D_\lambda = 4(\Delta_s - |\Delta_\lambda|)^2K_\lambda, \tag{B7}$$

$$F_\lambda = (\Delta_s - \Delta_\lambda^2)^2, \tag{B8}$$

$$K_\lambda = 8\Delta_s|\Delta_\lambda|/(Z_\lambda^2+2)^2. \tag{B9}$$

To justify that the given solutions are the only solutions and are also in fact valid for all parameters, we have verified numerically that $\mathrm{Re}|\Lambda_\lambda|=\Im\mathrm{m}|\Lambda_\lambda|=0$ for all solutions of $E_\lambda^{\pm}$ used in this work. However, as can be seen by comparing with Fig. 11 and the accompanying discussion, evaluating $E_\lambda(\varphi)$ for around $\varphi\approx 0$ for Eq. (B2) or around $\varphi\approx\pm\pi$ for Eq. (B3) does not produce a valid result for $|\Delta_\lambda|\neq\Delta_s$. The explanation is that the physical Andreev bound states simply vanish in these regions and we have again confirmed numerically that $|\Lambda_\lambda|=0$ have no real solution for E here. In fact, solving only for the imaginary part of the determinant yields (clearly unphysical) solutions $|E_\lambda|>\min\{\Delta_s,|\Delta_\lambda|\}$, which furthermore result in complex factors $\sin\beta_\lambda$, rendering Eq. (B1) invalid as an expression for the imaginary part of the determinant. In the results presented above, we have handled this numerically by setting the bound-state energy equal to the gap value when vanishing so that it does not contribute to the current (since the energy states vanish at the gap edge with zero slope), although the energy states strictly speaking do not exist at all in these regions.

[1] Y. Kamihara, T. Watanabe, M. Hirano, and H. Hosono, J. Am. Chem. Soc. **130**, 3296 (2008).
[2] I. Mazin and J. Schmalian, Physica C **469**, 614 (2009).
[3] K. Ishida, Y. Nakai, and H. Hosono, J. Phys. Soc. Jpn. **78**, 062001 (2009).
[4] I. I. Mazin, D. J. Singh, M. D. Johannes, and M. H. Du, Phys. Rev. Lett. **101**, 057003 (2008).
[5] A. A. Golubov and I. I. Mazin, Physica C **243**, 153 (1995).
[6] D. Wang, Y. Wan, and Q.-H. Wang, Phys. Rev. Lett. **102**, 197004 (2009).
[7] Y. Nagai and N. Hayashi, Phys. Rev. B **79**, 224508 (2009).
[8] X.-Y. Feng and T.-K. Ng, Phys. Rev. B **79**, 184503 (2009).
[9] A. A. Golubov, A. Brinkman, Y. Tanaka, I. I. Mazin, and O. V. Dolgov, Phys. Rev. Lett. **103**, 077003 (2009).
[10] M. A. N. Araujo and P. D. Sacramento, Phys. Rev. B **79**, 174529 (2009).
[11] J. Linder and A. Sudbø, Phys. Rev. B **79**, 020501(R) (2009).
[12] S. Onari and Y. Tanaka, Phys. Rev. B **79**, 174526 (2009).
[13] H.-Y. Choi and Y. Bang, arXiv:0807.4604 (unpublished).
[14] P. Ghaemi, F. Wang, and A. Vishwanath, Phys. Rev. Lett. **102**, 157002 (2009).
[15] W.-F. Tsai, Y.-Y. Zhang, C. Fang, and J. Hu, Phys. Rev. B **80**, 064513 (2009).
[16] T. Zhou, X. Hu, J.-X. Zhu, and C. S. Ting, arXiv:0904.4273 (unpublished).
[17] M. Matsumoto, M. Koga, and H. Kusunose, J. Phys. Soc. Jpn. **78**, 084718 (2009).
[18] T. K. Ng and Y. Avishai, Phys. Rev. B **80**, 104504 (2009).
[19] W.-F. Tsai, D.-X. Yao, B. A. Bernevig, and J. P. Hu, Phys. Rev. B **80**, 012511(R) (2009).
[20] Y. Ota, M. Machida, T. Koyama, and H. Matsumoto, Phys. Rev. Lett. **102**, 237003 (2009).
[21] Y. Ota, M. Machida, T. Koyama, and H. Matsumoto, arXiv:0907.0277 (unpublished).
[22] T. K. Ng and N. Nagaosa, EPL **87**, 17003 (2009).
[23] Y. Ota, M. Machida, and T. Koyama, J. Phys. Soc. Jpn. **78**, 103701 (2009).
[24] W.-Q. Chen, F. Ma, Z.-Y. Lu, and F.-C. Zhang, arXiv:0906.0169 (unpublished).
[25] C. T. Chen, C. C. Tsuei, M. B. Ketchen, Z. A. Ren, and Z. X. Zhao, arXiv:0905.3571 (unpublished).
[26] J. Wu and P. Phillips, Phys. Rev. B **79**, 092502 (2009).
[27] D. Parker and I. I. Mazin, Phys. Rev. Lett. **102**, 227007 (2009).
[28] D. Inotani and Y. Ohashi, Phys. Rev. B **79**, 224527 (2009).
[29] D. F. Agterberg, E. Demler, and B. Janko, Phys. Rev. B **66**, 214507 (2002).
[30] I. I. Mazin, A. A. Golubov, and A. D. Zaikin, Phys. Rev. Lett. **75**, 2574 (1995).
[31] T. Chen, S. Huang, Z. Tesanovic, R. Liu, X. Chen, and C. Chien, Physica C **469**, 521 (2009).
[32] R. Gonnelli, D. Daghero, M. Tortello, G. Ummarino, V. Stepanov, R. Kremer, J. Kim, N. Zhigadlo, and J. Karpinski,

Physica C **469**, 512 (2009).
[33] G. E. Blonder, M. Tinkham, and T. M. Klapwijk, Phys. Rev. B **25**, 4515 (1982).
[34] G. Deutscher and D. Feinberg, Appl. Phys. Lett. **76**, 487 (2000).
[35] J. M. Byers and M. E. Flatté, Phys. Rev. Lett. **74**, 306 (1995).
[36] C. Benjamin, Phys. Rev. B **74**, 180503(R) (2006).
[37] S. Fujimoto, Phys. Rev. B **79**, 220506(R) (2009).
[38] J. Linder, I. B. Sperstad, and A. Sudbø, Phys. Rev. B **80**, 020503(R) (2009).
[39] V. V. Ryazanov, V. A. Oboznov, A. Y. Rusanov, A. V. Veretennikov, A. A. Golubov, and J. Aarts, Phys. Rev. Lett. **86**, 2427 (2001).
[40] A. I. Buzdin, Rev. Mod. Phys. **77**, 935 (2005).
[41] Y. Avishai and T. K. Ng, arXiv:0905.0625 (unpublished).
[42] G. Falci, D. Feinberg, and F. W. J. Hekking, Europhys. Lett. **54**, 255 (2001).
[43] A. A. Golubov, M. Y. Kupriyanov, and E. Ilichev, Rev. Mod. Phys. **76**, 411 (2004).
[44] A. Buzdin and A. E. Koshelev, Phys. Rev. B **67**, 220504(R) (2003).
[45] A. Buzdin, Phys. Rev. B **72**, 100501(R) (2005).
[46] E. Goldobin, D. Koelle, R. Kleiner, and A. Buzdin, Phys. Rev. B **76**, 224523 (2007).
[47] Y.-R. Zhou, Y.-R. Li, J.-W. Zuo, R.-Y. Liu, S.-K. Su, G. F. Chen, J. L. Lu, N. L. Wang, and Y.-P. Wang, arXiv:0812.3295 (unpublished).
[48] X. Zhang, Y. S. Oh, Y. Liu, L. Yan, K. H. Kim, R. L. Greene, and I. Takeuchi, Phys. Rev. Lett. **102**, 147002 (2009).
[49] X. Zhang, S. R. Saha, N. P. Butch, K. Kirshenbaum, J. Paglione, R. L. Greene, Y. Liu, L. Yan, Y. S. Oh, K. H. Kim, and I. Takeuchi, Appl. Phys. Lett. **95**, 062510 (2009).
[50] K. D. Usadel, Phys. Rev. Lett. **25**, 507 (1970).
[51] F. Konschelle, J. Cayssol, and A. I. Buzdin, Phys. Rev. B **78**, 134505 (2008).
[52] G. Mohammadkhani and M. Zareyan, Phys. Rev. B **73**, 134503 (2006).
[53] S. M. Frolov, D. J. Van Harlingen, V. A. Oboznov, V. V. Bolginov, and V. V. Ryazanov, Phys. Rev. B **70**, 144505 (2004).
[54] A. Brinkman, A. A. Golubov, H. Rogalla, O. V. Dolgov, J. Kortus, Y. Kong, O. Jepsen, and O. K. Andersen, Phys. Rev. B **65**, 180517(R) (2002).
[55] V. Cvetkovic and Z. Tesanovic, EPL **85**, 37002 (2009).
[56] V. Cvetkovic and Z. Tesanovic, Phys. Rev. B **80**, 024512 (2009).
[57] D. J. Van Harlingen, Rev. Mod. Phys. **67**, 515 (1995).
[58] Y. Bang, H.-Y. Choi, and H. Won, Phys. Rev. B **79**, 054529 (2009).
[59] O. V. Dolgov, A. A. Golubov, and D. Parker, New J. Phys. **11**, 075012 (2009).
[60] G. Eilenberger, Z. Phys. **214**, 195 (1968).
[61] A. V. Zaitsev, Sov. Phys. JETP **59**, 1163 (1984).
[62] M. Eschrig, arXiv:0907.2345 (unpublished).